Enzyme Models of Chloroperoxidase and Catalase.

Inaugural Dissertation

Zur

Erlangerung der Würde

eines Doktors der Philosophie

Vorgelegt der

Philosophisch-naturwissenschaftlichen Fakultät

der

Universität Basel

Von

Cécile CLAUDE

geboren in Rillieux La Pape (Frankreich)

Basel 2001.

Genehmigt von der Philosophisch-Naturwissenschaftlichen Fakultät auf Antrag von:

Prof. Dr. Wolf-Dietrich Woggon

Prof. Dr. Thomas Kaden

Basel, den 10. April 2001

Prof. Dr. Andreas D. Zuberbühler (Dekan)

In memory of my grand-father Paul Claude (1913-1998)
and rear grand-father Emile Bouveyron (1896-1988).
For my parents and grand-mother and all of them who
encouraged me during this work.

Ce n' est pas parce que les choses sont dificiles que nous n' osons pas,
c' est parce que nous n' osons pas qu' elles sont difficiles.

Sénèque.

Table of contents

A.2. Synthesis of the CPO model 32 and catalase model 33

INTRODUCTION

Introduction:

1. Historical background.

As early as the 17$^{\underline{th}}$ century it was recognized that one component in air is essential for life. This extremely simple molecule later known as dioxygen or commonly oxygen was discovered by Joseph Priestley and Carl Wilhelm in 1771-72 by thermal decomposition of mercury oxide and potassium nitrate respectively. During the next three years Lavoisier worked on the characterization of the new element composing dioxygen. In 1775 he named it oxygen due to its presence in numerous acids (oxy = acid, gen = generate). Lavoisier also established the role of dioxygen in the respiratory process. The fundamental equation dioxygen=life was formulated for aerobic systems.

Nearly two centuries later, in 1929, the electronic structure of dioxygen was solved by Linus Pauling using the theory of molecular orbitals. Pauling could explain the paramagnetism of dioxygen (χ_M=0.994 T^{-1}) as well as the interatomic distance (d=1.207Å) and the dissociation energy (E$_{diss}$=117.36 kcal mol^{-1}) which were until then poorly understood by chemists. This state is defined as the triplet state and depicted in term of molecular orbital in *figure 1*.
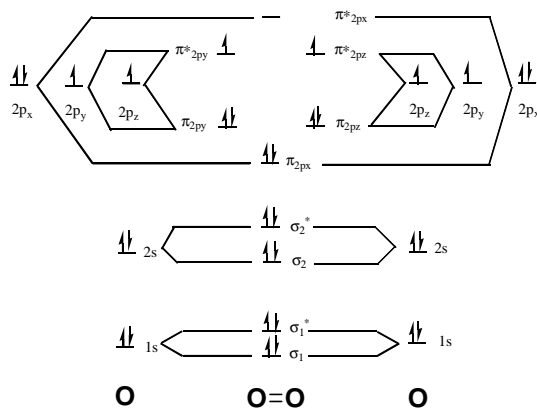
Figure 1: Molecular orbital diagram of triplet dioxygen.

The pioneering theory of Pauling could also predict the two metastable states of dioxygen where the molecule becomes diamagnetic. Both states are known as Δ and Σ singlet states (*figure 2*) and differ from the orbitals filling: the $^1\Sigma_y^+$ state has the two electrons paired in the π^*_{2py} orbital whereas the $^1\Delta_y$ has still on electron in each π^* orbital but with reversed spin. The latter state has a life time of 45 Min. and an O-O bond distance of 1.223Å.

$$
\begin{array}{cccc}
\text{—} \ \pi^*_{2px} & & & \text{—} \ \pi^*_{2px} \\
\pi^*_{2py} \ \uparrow\downarrow & \text{—} \ \pi^*_{2pz} & \pi^*_{2py} \ \uparrow & \uparrow \ \pi^*_{2pz} \\
\\
\pi_{2py} \ \uparrow\downarrow & \uparrow\downarrow \ \pi_{2pz} & \pi_{2py} \ \uparrow\downarrow & \uparrow\downarrow \ \pi_{2pz} \\
& \uparrow\downarrow \ \pi_{2px} & & \uparrow\downarrow \ \pi_{2px} \\
\\
& \uparrow\downarrow \ \sigma_2^* & & \uparrow\downarrow \ \sigma_2^* \\
& \uparrow\downarrow \ \sigma_2 & & \uparrow\downarrow \ \sigma_2 \\
\end{array}
$$
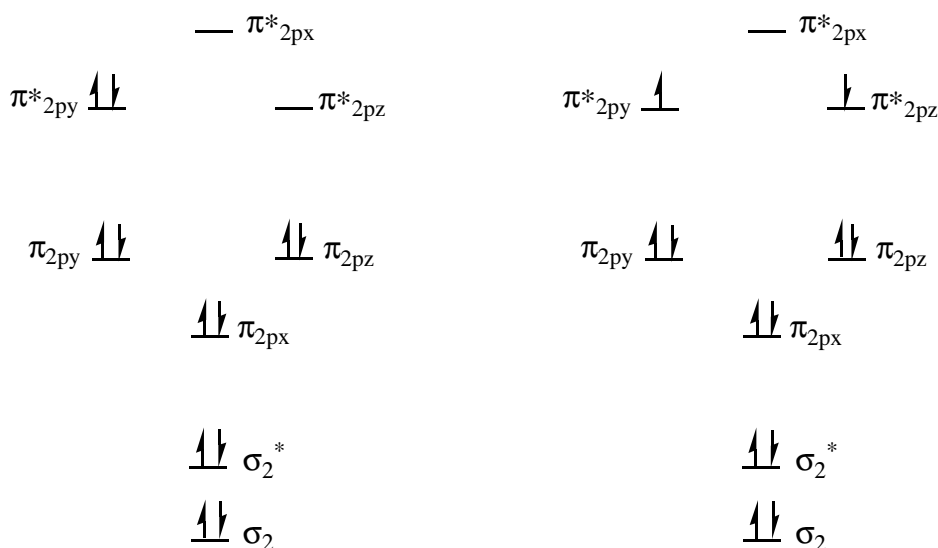
Figure 2: The singlet states 𝔻 and 𝕊 of dioxygen.

These singlet states are important for the reactivity of dioxygen in particular in the generation of ozone and radical species. These radicals are responsible for the formation of hydrogen peroxide, a highly oxidizing substance discovered by Thenard in 1818. Accumulation of hydrogen peroxide in the cell is extremely dangerous as it destroys the protein structure. The relationship between oxygen, hydrogen peroxide and the respiratory processes has been more deeply understood during the 20th century. For example, myoglobin which binds oxygen was the first protein of which the structure was solved by X-Ray diffraction in 1960 [1]. This is showing the interests and efforts developed to establish how dioxygen is used by aerobic organisms.

2. Biological relevance of dioxygen and derivatives.

In the second part of the 20th century the progress of medicine and biology has provided a better understanding of the importance of dioxygen and led to the discovery of numerous enzymes which are related to dioxygen.

Although dioxygen is the basic source of energy for aerobic systems, its consumption produces radicals such as superoxide ion (O_2^-) in cells. This highly reactive radical is very toxic and implied in numerous pathologies. Fortunately a "dioxygen cycle" (*figure 3*) exists by which oxygen [$^3O_2$] can be activated or recycled such that toxicity problems are prevented.
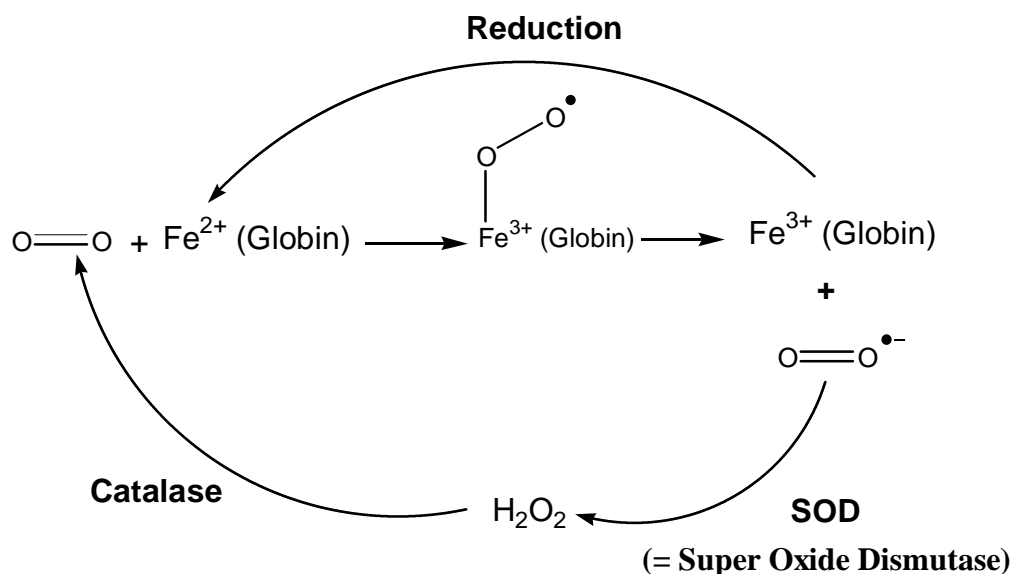
Figure 3: Oxygen and hydrogen peroxide interdependency.

The close dependency of hydrogen peroxide (H_2O_2) and dioxygen reflects the complexity of the nature despite the use of very simple molecule for ensuring life. Moreover, hydrogen peroxide which is known as a cell killer due to its high oxidizing power is required as a substrate for many enzymes. A real paradox exists: hydrogen peroxide and the superoxide ion have to be present in living organisms but their concentration has to be controlled accurately so that they are only short living in cells.

3. The enzymes in the "dioxygen cycle".

It was recognized early that metal containing species, in particular iron complexes, were involved in these processes. Rapidly the idea was accepted that a relatively simple unit is responsible for the transport and activation of dioxygen. Küster postulated a tetrapyrrolic structure [2] termed porphyrin. Its synthesis by Hans Fischer [3] established that its iron complex known as heme was able to bind dioxygen. Such heme units were shown to be essential for activating oxygen for oxidation reactions.

There are now seven hemes known which differ from each other by the nature of the substituents on the β-pyrrole positions. The most common heme is **heme *b*** or **hematin** (*figure 4*):
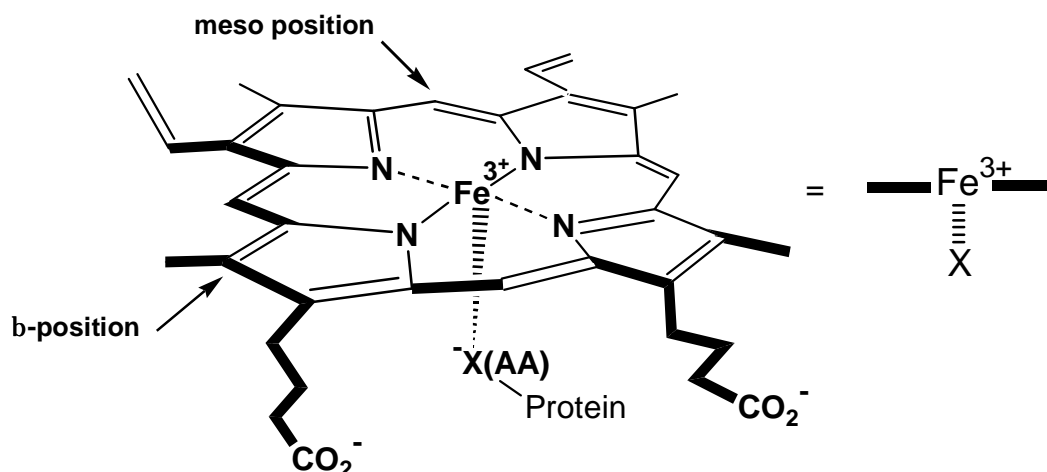
Figure 4: Heme *b*.

Several hundreds of heme *b* proteins are nowadays known which have different functions such as electron transfer, oxygen or nitric oxide transport or oxidation as shown in *table 1*. As all these proteins share exactly the same metal complex, it has been pointed out that the protein environment around heme *b* plays a decisive role in determining the function of the protein:

1) The amino acid residues maintain the heme unit bound to the protein

2) One amino acid residue coordinates axially to the iron in all heme proteins.

The nature of this axial coordination is thought to be the most important factor which determines the enzyme's activity. Therefore heme proteins are often classified according to the nature of the axial ligand (*table 1*). Finally the hydrophobic or polar character of the amino acid residues on the side opposite to the axial ligand (= distal side) tunes the specificity for a particular substrates and aids the formation of catalytic intermediates.

Axial Ligand	Protein Class	Function
(His)N	Cytochrome b	e^- transport
	Nitrophorin	NO transport
	Hemoglobin, myoglobin	O_2 transport
	Peroxidases	Oxidation by H_2O_2
(Tyr)O^-	Catalases	Dismutation of H_2O_2
(Cys)S^-	Chloroperoxidase (CPO)	Oxidative Halogenation by H_2O_2 ,Cl^- and H^+
	P-450	Oxidation by O_2
	Nitric Oxide Synthases (NOS)	NO synthesis by oxidation of Arg with O_2

Table 1: Heme *b* proteins classified by axial ligation.

The best known heme proteins are the globins, hemoglobin and myoglobin which are essential blood constituents. Peroxidases have also been the centre of intense studies as they were using hydrogen peroxide for oxidation in living organisms and have the same axial ligand, the nitrogen from histidine, as the globins. Less attention has been paid to Catalases which have a tyrosinate axial, similar to peroxidases. Finally heme-thiolate proteins are subject of special attention due to the unusual presence of a thiolate coordinating to the iron.

PREVIOUS KNOWLEDGES

I. Heme-thiolate proteins.

I.1. Classification and general features.

Heme-thiolate proteins have raised the interest of chemists and biologists for more than 30 years. The presence of an axial thiolate ligand for heme was unexpected with enzymes using molecular oxygen or even hydrogen peroxide as reagent. Namely thiolate functionality has always been claimed to be highly sensitive to oxidation in the presence of oxygen or peroxides.

Heme-thiolate proteins are divided into three classes so far: the cytochromes P450 (P450s), chloroperoxidases (CPO) and nitric oxide synthases (NOSs). P450s display a very large repertoire of oxidation reactions of unactivated X-H bonds such as the stereospecific hydroxylation of camphor **1** or the N-hydroxylation of amines (*figure 5*). They also catalyse demethylation, dehydration, reduction, aromatisation or isomerisation reactions [4]. CPO catalyses the oxidative halogenation of (1,3) cyclopentadione **3** into caldariomycin **5**, a dichlorinated natural product [5]. NOSs are responsible for the mammalian production of nitric oxide (•**NO**) which is a radical gas (*figure 5*). This radical, long disclaimed as a major air pollutant, is indeed a very important neuromediator at controlled concentrations. An overproduction of •**NO** results in pathologies such as toxic shock. A too low •**NO** concentration in turn is responsible for neurologic diseases such as Alzheimer for example [6].

P450s and NOSs in contrast to CPO use molecular oxygen and require an external source of electron to effect catalysis (*figure 5*). The electrons are delivered by either an external protein system or by two cofactors being tightly bound to the enzymes (*figure 6*).

a) P450$_{cam}$ reaction:
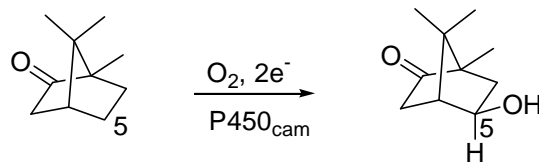
1: Camphor

2: 5-*exo*-Hydroxycamphor

b) CPO reaction:
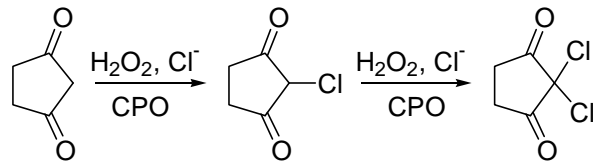
3

4

5: Caldariomycin

c) NOSs reaction:
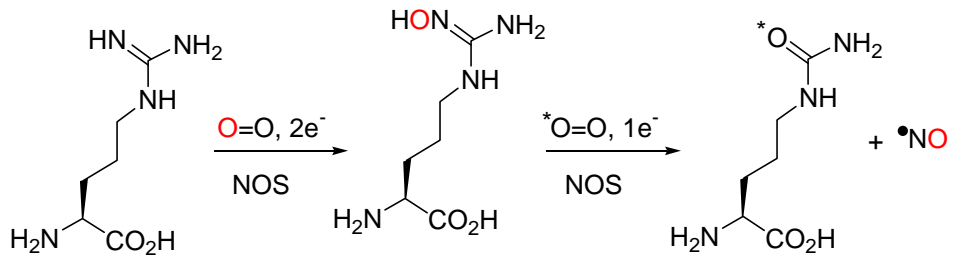
6: L-Arginine

7: N-Hydroxyarginine

8: L-Citrulline

Figure 5: Reactions catalysed by a) P450$_{cam}$, b) CPO and c) NOSs.
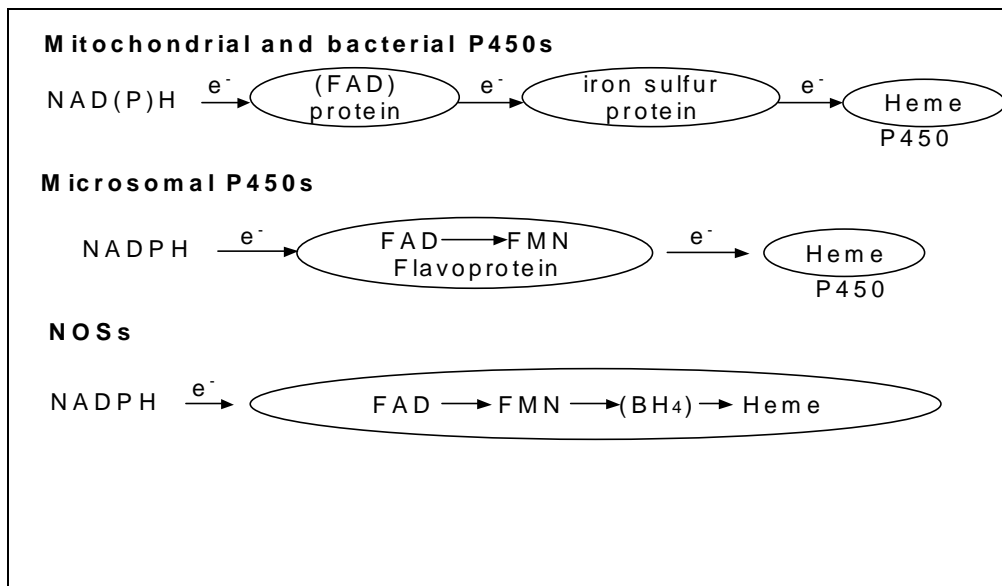
Figure 6: Electron transport systems for heme-thiolate proteins.

Abbreviations: BH$_4$: tetrahydrobiopterin; e$^-$: electron; FAD: Flavine adenine dinucleotide; FMN: Flavine adenine mononucleotide; NAD(P)H: Nicotineamide adenine dinucleotide (phosphate).

Heme-thiolate proteins are not only different by their electron delivery system but also by their general structure (*table 2*). If P450s and CPO are monomeric proteins [7, 8] NOSs are dimeric proteins [9] where each subunit contains an oxygenase and reductase domain.

The binding of heme differs from one enzyme subfamily to the other. P450s and NOSs heme are bound to the apoprotein via hydrogen bonds to arginine or histidine residues. For CPO the binding is ensured by hydrogen bonds to polar amino acid residues of the apoprotein and by an aqua manganese complex. The manganese atom is in turn bound to the apoprotein via the participation of amino acid residues [10].

Protein family	NAD(P)H required	Cofactors or redox proteins associated	Overall structure
P450s	yes	Flavoprotein + iron sulphur protein **or** FAD-FMN reductase	monomer
NOSs	yes	FAD, FMN, BH_4, Calcium-calmodulin	dimer
CPO	no	none	monomer

Table 2: Main characteristics of heme-thiolate proteins.

I.2. Crystal structures.

The progress of X-ray crystallography and molecular biology have permitted to obtain total or partial crystal structures for P450s, CPO and NOSs providing milestones to the understanding of their respective catalytic activities. The first X-ray structure of $P450_{cam}$, a heme-thiolate protein, has been solved by *Poulos et al.* in 1985 [11]. Since then the structure of five other P450s [12-15], of CPO [10] and of the oxygenase domain of one NOSs [16] have been elucidated.

I.2.1. $P450_{cam}$ and P450s structures [17].

Although the identity of the amino acids sequence for P450s is less than 10% the overall folding of the proteins is quite similar. The proteins exhibit a two domain structure composed of a β-sheet-containing domain and an α-helix-rich domain. The dominant element is helix I that traverses the entire protein and participate with three other helices in defining the heme binding region and the substrate oxidation pocket. Two important amino acid sequences are highly conserved in P450s and are essential for heme and O_2 binding.

First, the **central part of helix I** which forms an O_2 binding pocket in P450$_{cam}$ (*figure7)* is highly conserved. It creates a localized distortion and widening of Helix I in P450$_{cam}$ which has the sequence:

Gly/Ala-Gly-Xaa-Asp/Glu-Thr

(Xaa = variable amino acid).

The conserved threonine residue stabilizes the Fe(II)-O_2 adduct [18] and has been proposed to facilitate the heterolytic cleavage of the O-O bond after its one electron reduction (*see* I.3.1). At the three positions preceding that sequence hydrophobic amino acid residues are always found. Otherwise helix I is rich in polar amino acid residues in the vinicity of the heme on the distal side. These polar amino acid residues have been proposed to create an electric field which could be important in tuning the electron repartition (spin state tuning) in the iron d orbitals. The determination of the spin state is an important factor controlling the redox potential and thereby the ability of the protein to accept electron from NAD(P)H. Further these polar residues could stabilize the catalytic intermediates via H-bonds formation. One of them, a tyrosine residue, permits the binding of the substrate camphor **1** to the protein via a single hydrogen bond in P450$_{cam}$. **1** is thereby positioned in the vinicity of the heme above the pyrrole rings bearing the propionate side chains. This places the position 5 of **1** which is hydroxylated within bonding distance to the oxygen of the iron-oxo species formed during catalysis (*figure 5*).

Second, the **axial cysteinate** which coordinates to the iron of the heme belongs to a heme binding **decapeptide** sequence which contains five highly conserved amino acid residues. This sequence is:

Phe-Gly/Ser-Xaa**-Gly-**Xaa**-His/Arg-**Xaa**-Cys-**Xhy**-Gly**

(Xaa represents a variable amino acid and Xhy an hydrophobic residue).

This decapeptide sequence forms a loop where the cysteine proximal ligand is found at the N terminal end. The first amino acid of this loop is a phenylalanine whose phenyl group seems to protect the cysteinate ligand from oxidation. The second amino acid residue is either a glycine or a serine which probably also protects the cysteinate. The fourth amino acid is always a glycine which initiates the hairpin turn of the loop. The sixth amino acid which is a positively charged arginine or histidine is involved in an ionic or hydrogen bond with the heme carboxylates of the propionate side-chains. Finally the tenth amino acid residue is always a glycine which is in close contact to the heme.

Moreover the amide NH bonds of the fifth and sixth amino acid residues have also been postulated – in analogy to CPO from *Caldariomyces fumago* (*see* I.2.2)- to form hydrogen

bonds to the cysteinate [19]. The hydrogen bonds could ensure the permanent deprotonation of the sulphur and are an important feature of heme-thiolate proteins.
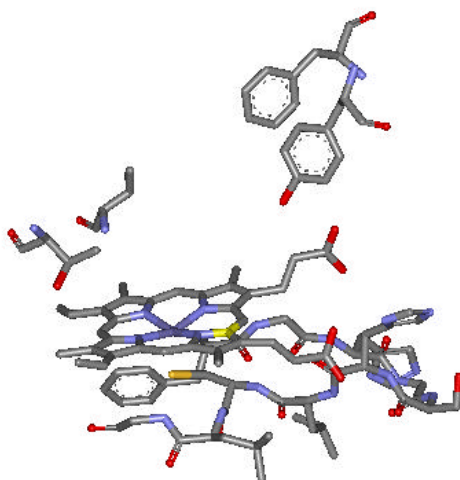
Figure 7: P450$_{cam}$ active site.

I.2.2. CPO crystal structure.

CPO share no markant amino acid sequence similarity with P450s. The crystal structure of CPO which has been solved recently [10] has provided a better comparison with P450s. CPO has been found to be 50% helical as P450s but the tertiary structure is completely different. Indeed CPO appears as a novel tertiary structure being a hybrid between P450s and peroxidases.

CPO comprises eight α helices, three short 3_{10} helices and a short antiparalell β sheet pair. Like P450s the heme environment comprises a proximal and a distal helix that provide the axial ligand and residues essential for the catalysis.

On the distal side three polar amino acid residues have been found to be essential for catalysis [20]. These are **His105**, **Asp106**, and **Glu183**. The presence of polar amino acids residues is not found in P450s in the proximity of the heme. However the presence of a distal histidine in the vinicity of heme is a pattern found in both peroxidases and catalases [21, 22]. In these enzymes the role of the histidine is:

1. to deprotonate the hydrogen peroxide which binds to the iron,
2. to assist the heterolytic cleavage of the O-O bound of the iron peroxide complex to yield the so-called compound I and water.

On the proximal side the thiolate ligand is found in a sequence of polar amino acid residues. The comparison with the decapeptide sequence of P450s reveals no amino acid identity. The sequence is the following:

Pro-Thr-Asp-Ser-Arg-Ala-**Pro-**Cys-**Pro-**Ala.

Nevertheless the amino acid sequence provides a rigid scaffolding for the iron-sulphur interaction. The presence of two proline residues before and after the axial cysteine results in a very similar geometry pattern as found for the Xaa-Cys-Xhy sequence of P450s. Two clear hydrogen bonds are stabilizing the cysteine ligand. They originate from the amide NH from the Pro-Cys bound and from the Pro-Ala bound (*figure 8).
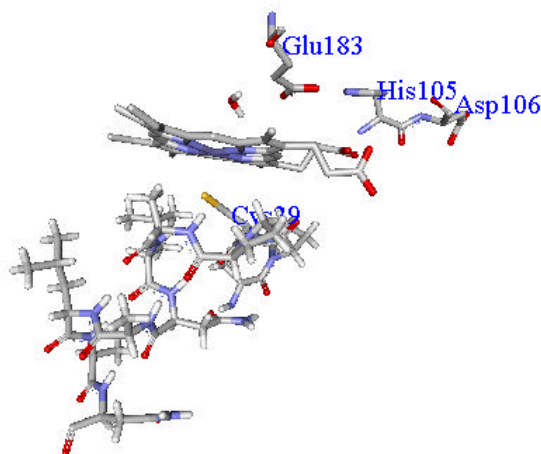
Figure 8: CPO active site.

I.2.3. NOSs crystal structure.

Contrary to CPO and P450s enzymes NOSs are the only heme-thiolate proteins which have a dimeric structure. Each monomeric unit is divided into an oxygenase and a reductase domain. NOSs are distinctive from any other heme-proteins as they require five cofactors to work. The dimers are hold together by the presence tetrahydrobiopterin (BH_4) which role is probably further to serve as an electron reservoir during catalysis. The presence of calcium/calmodulin (CaM) units also maintain the dimeric structure as shown in *figure 9*.
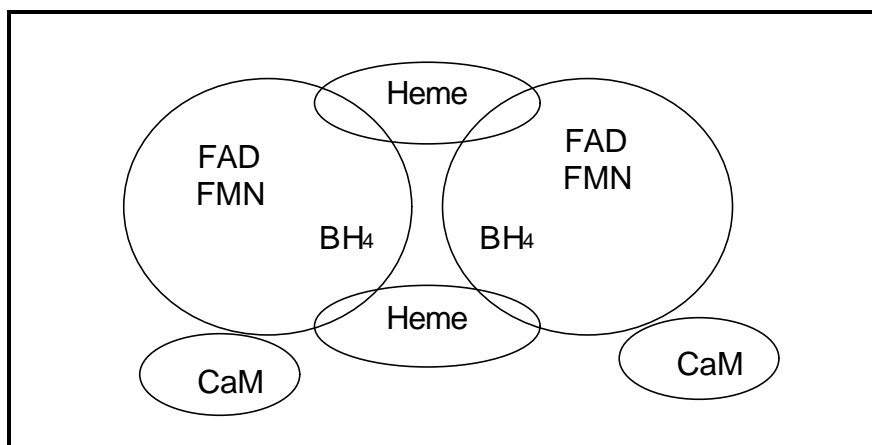
Figure 9: Schematic representation of NOSs dimeric structure

(Abbreviations according to *figure 6*).

The oxygenase domain is located in the N-terminal part whereas the reductase domain is found in the C-terminal part of the amino acid sequence. BH_4 binds in the oxygenase domain very close to the heme. The primary structure (oxygenase + reductase domain) is indeed very similar to the sequence of P450 BM3. Nevertheless the cloning of the oxygenase domain of NOSs has shown that no significant amino acid sequence homology to P450s exists.

Recently the crystal structure of *i*NOS from murine macrophage has been solved by *Tainer et al.* [16]. The structure of the protein is unique. Contrary to P450s and CPO the heme binding domain is composed of β sheet and β wings.

The sequence which contains the distal cysteinate residue in NOSs is a highly conserved nonapeptide sequence:

Trp-Arg-Asn-**Ala**-Pro/Ser-**Arg-Cys**-Ile/Val-**Gly**.

If one makes abstraction of the missing amino acid which would fit in the 7th position, a troubling sequence similarity to P450s does appear.

A molecular modelling attempt of the nonapetide *vs.* the P450s decapeptide has indicated that despite the deletion of one amino acid the conformation of the nonapeptide is very similar to the decapeptide one [17]. Therefore by analogy to P450s decapeptide the tryptophane is proposed to protect the cysteinate as a tryptophane replaces also phenylalanine in two P450s [17]. Further the arginines of the sequence are placed so that they probably interact with the heme carboxylates as is the case for histidine (n-2) in P450s. The hairpin turn is initiated by an alanine (Ala 4 in the sequence) instead of a glycine in NOSs *vs.* P450s. As in CPO or P450s the cysteinate is stabilized by two hydrogen bonds from the peptide nitrogen at position (n+3) from cysteine and from the

indole of tryptophane. Finally the sequence is terminated by a glycine and the amino acid following cysteine is always an hydrophobic one.

On the proximal side the amino acid residues are largely hydrophobic but the presence of a glutamic acid residue has been found to be essential for catalysis [23]. The role of this residue is to place the amino guanidino nitrogen of L-arginine **6** close to the heme iron. A tryptophane residue further stabilizes **6** by a second hydrogen bond to the carboxylate functionality of **6** and methionine and glycine residues further complete the hydrogen bond network which holds the substrate near the heme (*figure 10*). This high degree of stabilization is also an unique feature of NOSs compared to other heme-thiolate proteins. The high stabilization of substrate in NOSs may be related to the open distal pocket. In P450s the pocket is buried which provides a more rigid environment for the substrate.

These unique characteristics may permit the better stabilization of the iron peroxo complex via hydrogen bonds. The absence of a structured water molecule network in NOSs, and of polar amino acid residues may also render the scission of O-O bond more difficult thereby favourising the iron peroxo complex as a catalytic intermediate as discussed in I.3.2.
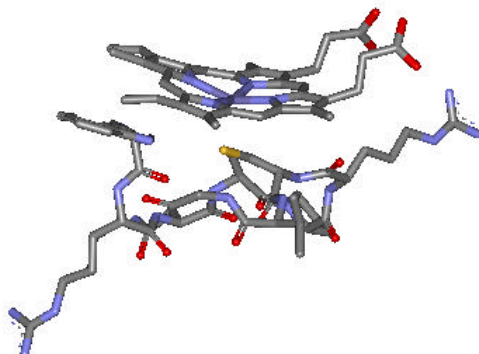
Figure 10: Active site of iNOS.

I.2.4. Summary.

The heme-thiolate proteins which are closely related to P450s oxygenase show very similar catalytic activities despite less than 10% overall sequence similarity. The only common point between all these proteins is the active site which contains an heme-thiolate complex. Nevertheless a very similar proximal environment for the heme is observed. A stabilization of the thiolate ligand is always achieved via a peptide loop and further by two hydrogen bonds. This pattern, unique to heme-thiolate proteins could be responsible for their close

reaction similarities (*table 3*). For example CPO is also able to catalyse P450 like reactions such as epoxidation and in turn P450s are able to use hydrogen peroxide to effect catalysis.

P450s	**Phe**-	Gly/Ser-	Xaa-	Gly-	Xaa-	His/Arg-	Xaa-	**Cys-**	Xhy-	**Gly-**
CPO	Pro-	Thr-	Asp-	Ser-	Arg-	Ala-	Pro-	**Cys-**	Pro-	Ala-
NOSs	**Trp-**	Arg-	Asn-	Ala-	Pro/Ser-	Arg-	…	**Cys-**	Ile-	**Gly-**

Table 3: Comparison of the peptide sequence containing the proximal cysteine ligand.

I.3. Catalytic cycle of heme-thiolate proteins.

I.3.1. P450s oxygenases.

$P450_{cam}$ is the first non membrane bound P450 enzyme which has been purified and therefore the most studied heme-thiolate protein. The importance of P450s in the metabolism of xenobiotics has motivated an intense research on the mechanism of these enzymes. The catalytic cycle is still not fully characterized but the essential features have been agreed now for some time. The essential steps for catalysis involve (*figure 11*):

(1) Binding of the substrate which in $P450_{cam}$ results in the displacement of a water molecule from the iron of the heme. This binding is also accompanied by a change of the spin state from low spin ferric six coordinated to high spin ferric five coordinated. This change in the spin state is also responsible for a anodic shift in the redox potential from –300 mV to –170 mV.

(2) A reduction of the iron (III) to its ferrous form as the redox potential is now close to the potential of the redox protein.

(3) Binding of oxygen to give the ferrous P450-dioxygen complex which has been recently characterized by X-Ray diffraction [18]. The remaining water molecules in the oxygen binding pocket enable together with the distal threonine a stabilization of this complex via hydrogen bonds.

(4) A second electron transfer to give a peroxo iron (III) species

(5) The protonation and cleavage of the O-O bond with the concomitant formation of a water molecule and of the reactive iron-oxo species or **compound I**.

(6) The incorporation of the oxygen atom of the iron-oxo complex into the substrate molecule.

(7) The release of the product and rebinding of water to give back the resting state.

Whereas the three first steps have been observed and characterized spectroscopically and by X-Ray diffraction the last steps of the process occur to rapidly to have been observed yet. Therefore the identity of the iron-oxo complex has been postulated based on the analogy with the so-called **compound I** of the peroxidases and model studies. Evidence for a **compound I** analogue has also been provided by the use of the so-called "peroxide-shunt" pathway (*figure 11*). Upon addition of peroxide the same intermediate is obtained and is catalytically active. The mechanism of oxygen insertion has also been the subject of numerous studies which gave raise to several theories. A concerted mechanism was first proposed [24] but the stereochemistry of the product obtained was inconsistent with this pathway. A radical mechanism has then been proposed [25] but the use of radical clocks and the measurement of isotope kinetic effects gave no consistent results which would support this mechanism. The concept was refined with the theory of the "low spin high spin" surface developed by *Shaik et al.* [26, 27]. Therefore an ionic intermediate involving a carbocation is proposed by *Newcomb et al.* [28]. Despites all these efforts none of the theories fully accounts for the stereochemistry and kinetic data which have been measured.

Figure 11: Postulated catalytic cycle of P450s oxygenases.

I.3.2 The special case of NOSs.

Contrary to P450s NOSs are catalysing the five electron reduction of L-arginine to produce L-citrulline and NO. The mechanism by which this unusual odd 5e⁻ oxidation occurs is the object of intense investigations. Although NOSs are known only since 1985 the efforts developed by biochemists have permitted to establish the fundaments of the catalytic cycle. First it has been demonstrated that the catalytic cycle proceeds via two distinct phases [29]. The first phase is likely to be a classical P450 hydroxylation. A nitrogen of the guanidine functionality is hydroxylated to produce L-N-hydroxyarginine **7** (NHA) consuming one equivalent of NADPH and one molecule of oxygen. NHA **7** is an intermediate product in NOSs catalysis which is detected. The second phase involves the three electron reduction of NHA **7** to release L-citrulline **8** and NO. It consumes also one molecule of oxygen but only half an equivalent of NADPH. In both steps the oxygen incorporated to the guanidine resp. N-hydroxyguanidine functionality arises from molecular oxygen (*figure 5*).

Much attention has been paid to the second reaction as it is unprecedeed in heme-thiolate protein catalysis. It is now agreed that an iron peroxo complex is the catalytic species for this step [17]. The discussion arises on how this peroxo complex can be formed without further reacting with a second electron to form compound I. Two hypotheses are being intensively investigated and are (*figure 12*):

1. The iron peroxo complex is formed as in a classical P450 oxidation and NHA binds to this peroxo complex. In this scheme the radicals are so short living that they account for the absence of any detected radical during the second part of NOSs catalysis.

2. NHA **7** which redox potential would permit to reduce iron (III) to iron (II) is the electron donor. BH₄ acts as an electron donor to compound II which is formed upon deligation of NHA.
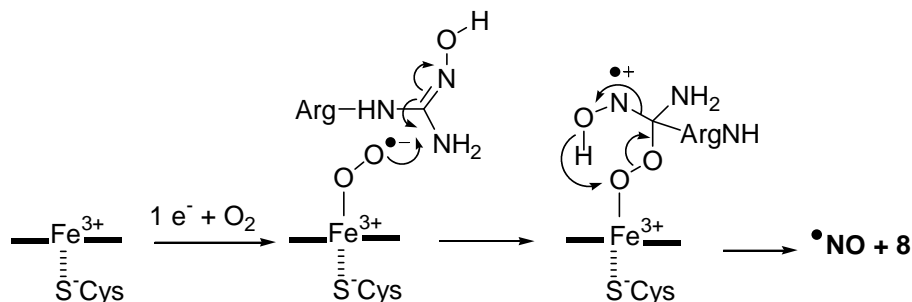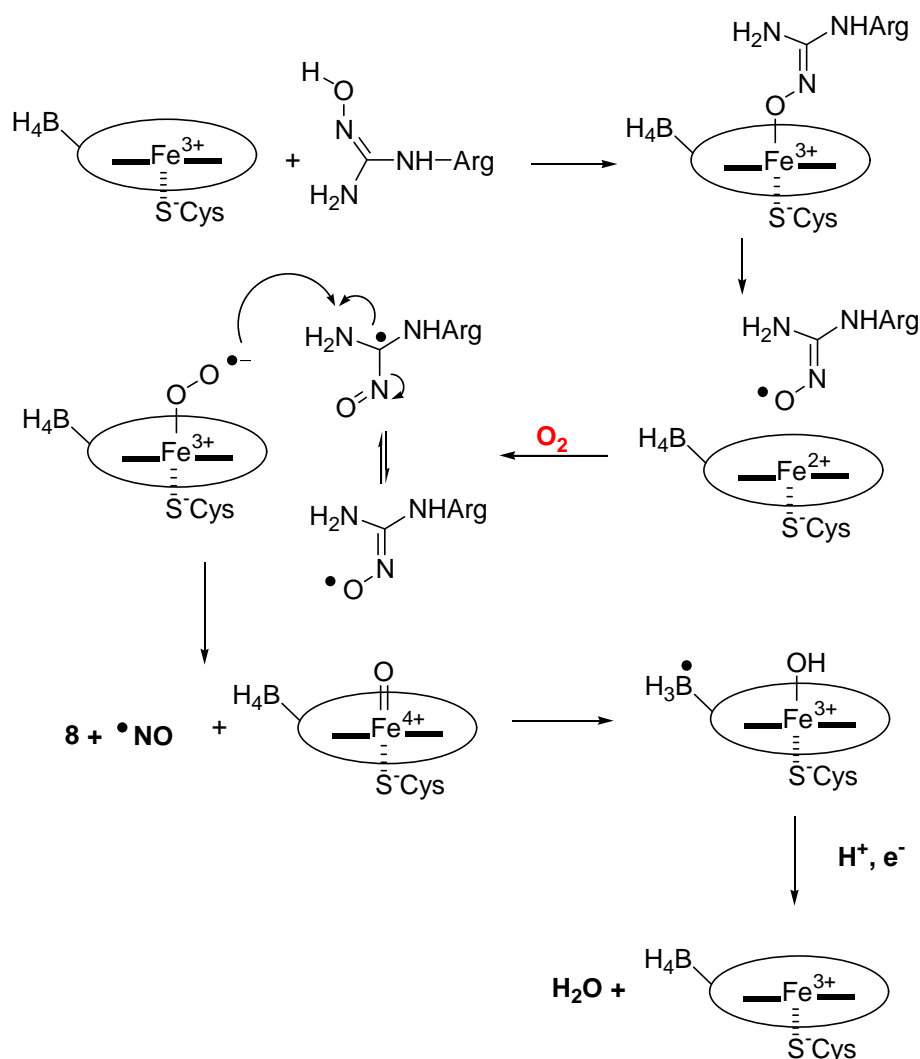
Figure 12: Proposed mechanisms for NOSs activity.

This second hypothesis has gained some experimental evidence very recently as the radical of BH_4 has been observed during NOSs catalysis [30]. Moreover the work of *Groves et al.* [31] with model and measurement of the redox potential of NHA **7** support this finding.

I.3.3. The CPO catalytic cycle.

Contrary to P450s and NOSs CPO is the only heme-thiolate protein so far which uses directly hydrogen peroxide to effect catalysis. Moreover CPO works at the unusually low pH of 2.75. As formally CPO catalyses the Cl^+ addition to the β-position of an α, γ diketone much attention has been paid to its mechanism. The studies on CPO itself have only established that the first steps in the catalytic cycle are similar to the steps observed in peroxidases and catalases. These are (*figure 13*):

1. The binding of hydrogen peroxide to form a peroxy-iron (III) complex
2. The protonation of the terminal oxygen of the peroxy to furnish a water molecule and an iron-oxo species.

After this step the way by which chloride binds to the active site was obscure. It has long been believed that free HOCl was the actual catalytic species in the reaction [30]. However the way HOCl could be produced from the established iron-oxo species was not rationalized. The crystal structure of CPO which has been published in 1995 by *Poulos et al.* [10] confirmed that a glutamine and a histidine residue are found near the heme on the proximal side. Modification of the enzyme on the histidine residues by *Wagenknecht and Woggon* [20] had demonstrated that one of these residues is essential for catalysis. This fact is already well established for peroxidase and catalase thereby apparently validating the first steps of the process. Namely in catalase and peroxidase an histidine residue assists the formation of compound I (*see I.2.2*). Contrary to catalase and peroxidase the essential histidine residue in CPO has been found not to be the final proton acceptor/deliver. But it is part of a sequence of three amino acid residues which forms a proton delivery system: the final residue in close proximity to the heme is a glutamic acid. With help of histidine it can be protonated and deprotonated. The protonation/deprotonation of histidine is favoured by an aspartic acid residue and assisted by a water molecule in the vinicity of heme.
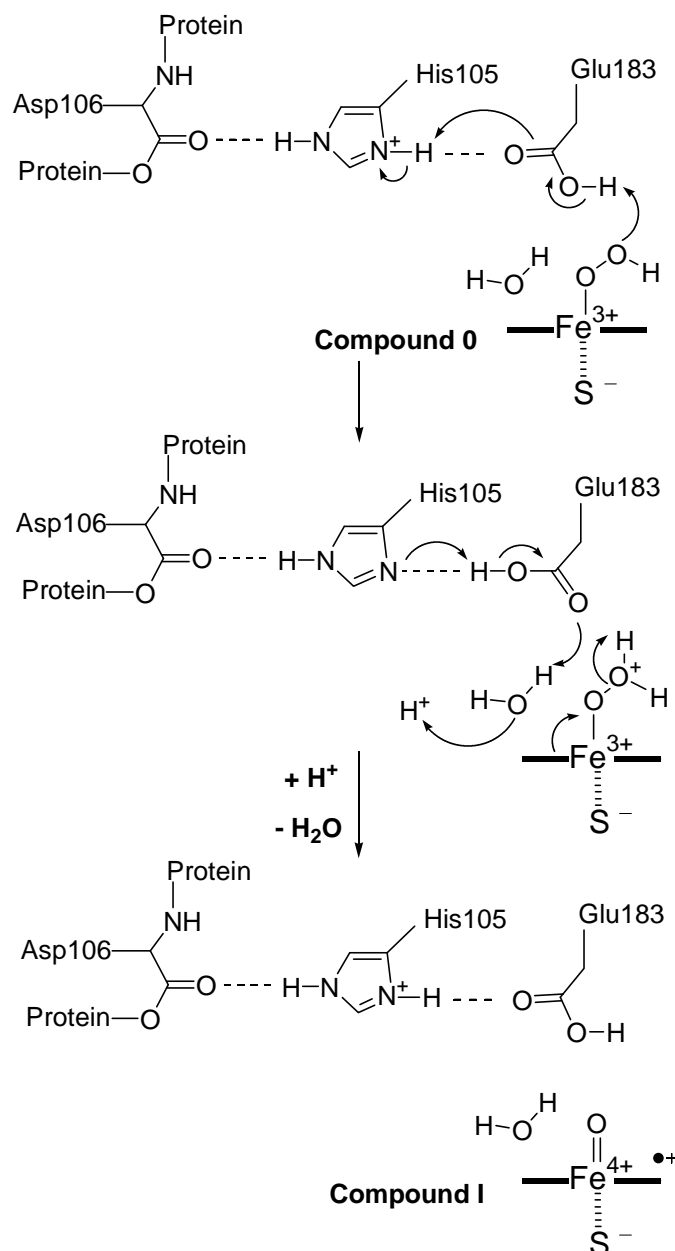
Figure 13: The proton delivery system in CPO and its role in compound I formation.

Based on model studies it could be established [20] that:

1. The formation of the OCl complex is necessary for catalysis.

2. The catalytic species is not the iron (III) OCl complex.

3. The protonation of the OCl complex is essential for catalysis.

4. Upon protonation an intermediate is formed that has the same UV-Vis properties than the native enzyme intermediate trapped under controlled pH=4.5 conditions.

5. This intermediate is the catalytic species and is an iron (III) HOCl complex.

Nevertheless despites these milestones a total physical characterization of the iron (III) HOCl complex for both the model and the native enzymes has not been done yet.

I.3.4. Which role for the thiolate axial ligand?

Although the catalytic cycles of heme-thiolate proteins are distinctive the central intermediate is always found to be the high-valent iron-oxo species which structural characterization is attempted for more than twenty years. For example the compound is always described as an iron (IV) porphyrin radical cation but calculations have supported the existence of a radical centered not on the porphyrin ring but on the sulphur [33] (*figure 14*).
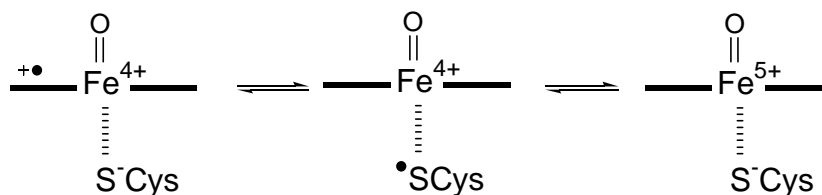
Figure 14: Different structural formulations of the high valent iron-oxo species for heme-thiolate proteins.

The "push-pull" effect proposed for peroxidase [34] would be replaced (*figure 15*) by the "push" effect of the thiolate ligand in heme thiolate proteins if the participation of sulphur as a radical could be confirmed.

heme-thiolate proteins　　　　**peroxidases**
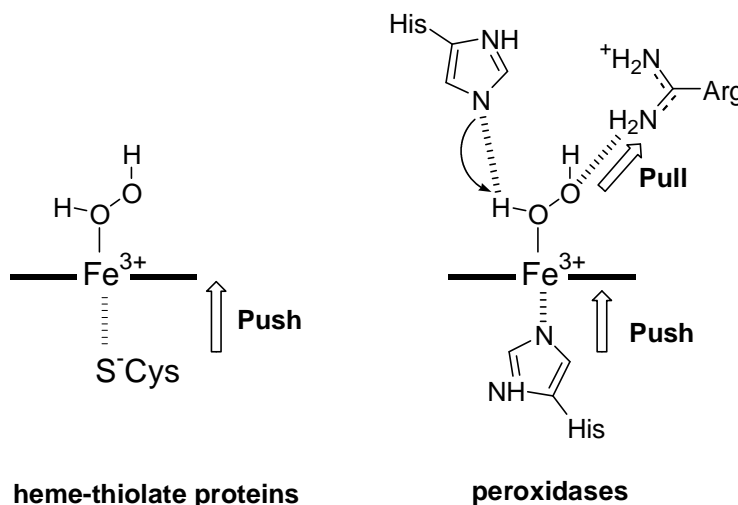
Figure 15: Push-pull effect *vs.* pull effect.

In peroxidase the distal histidine abstracts one proton. Departure of water is favoured by an arginine residue which protonates the terminal oxygen which is not binding to the iron atom. The distal histidine favours the process by enhancing the electron density of the iron as does the thiolate in heme-thiolate proteins which lack the distal arginine and histidine residues. The machinery which assists the heterolytic cleavage of compound 0 to compound I in peroxidase has no equivalency in P450s and NOSs. In P450s a water

molecule network is thought to assist weakly the push effect of the thiolate ligand whereas no feature is found in NOSs to facilitate the process.

These differences may responsible for the specific reactivity of each protein class.

II. Catalases in comparison to heme-thiolate proteins.

II.1. Reactivity and biological relevance.

Contrary to heme-thiolate proteins catalases have been studied since the beginning of the century. The isolation of catalase is possible from almost all mammalian and non mammalian cells containing a cytochrome system. The source of catalase for biological studies is nevertheless exclusively the mammalian liver or erythrocytes as the concentration of the enzyme is the highest in these tissues [35]. Despites this efforts in understanding catalases the full catalytic cycle is still not clear. The amino acid sequence and crystal structure are known for *Beef Liver Catalase* [36]. Two other crystal structures of *Penicillium vitale catalase* [37] and *lysodeikticus catalase* [38] have been solved recently.

Catalases are extraordinary efficent enzymes which have a turnover nearly at the rate of diffusion control. These are the only heme containing enzymes which catalyse exclusivly the disproportionation of H_2O_2 into molecular oxygen and water. This process is very important for the degradation of superoxide anion O_2^- which is released by the oxygen adduct of globins under oxidative stress for example. Superoxide anion is first reduced to hydrogen peroxide by SOD (*see* introduction). The only other known reaction of Catalases is the oxidation of low molecular weight alcohols such as ethanol at high hydrogen peroxide concentration [39]. This is referred to as peroxidatic activity of catalase. The degradation of ethanol by catalase is thought to be the main pathway of ethanol degradation in liver. It was suggested that this very high specificity is due to the presence of the phenolate axial ligand. Moreover catalases are not reduced by sodium dithionite [40] as is the case of all other heme proteins. This unique property of catalases may be explained by their low redox potential which has been estimated to be less than –500 mV. The difficult reducibility of catalase is of importance for the catalytic cycle which will be discussed in paragraph II.3.

II.2. Crystal structure.

Crystals of catalase were obtained as early as 1937 from *Beef Liver Catalase* [41] which is the most extensivly studied catalase. Nevertheless suitable crystals of catalases for a high resolution X-ray analysis were difficult to obtain. As a consequence the corresponding structure was only published in 1981 [36]. The preliminary crystal studies have established that the tetrameric protein is arranged with a high degree of symmetry [42]. This feature

resembles the structure of haemoglobin which has also four subunits [43] but has no markant similarities with heme-thiolate proteins. Each subunit of catalase is equivalent and contains one heme, working independently. One of them is even often inactive as the heme is degraded into bilverdin (= opened tetrapyrrole unit where two α pyrrole positions are oxidized and where the corresponding meso carbon is missing) [44].

The high resolution crystal structure obtained by *Murthy et al.* [36] reveals that the heme is bound in an hydrophobic part of the protein. Contrary to P450s or CPO the heme is found between a β sheet domain on its distal face and a "wrapping" domain on its proximal side.

Catalase is bound to the protein via salt-bridges between the propionate side chains and two arginine residues. This pattern is reminding of the globins and is not encountered in any other heme proteins. The heme appears to deviate from the mean plane by 1 Å which is an unusual high value for heme protein and adopts a domed structure [45]. Contrary to heme-thiolate protein where the pyrroles are nearly coplanar and where the iron atom is displaced down to the thiolate ligand, catalases show no significant displacement of the iron to the tyrosinate.

The proximal side of the heme is crowded thereby protecting the axial ligand from protonation. The proximal ligand, which has been identified as a tyrosine residue, interestingly has an adjacent proline residue in an α-helix chain. This pattern is reminding of the Pro-Cys-Pro sequence of CPO. The role of the proline is proposed to restrict the movement of the tyrosine [45]. The guanidinium group of the arginine residue found at position (n-4) respective to the tyrosine is proposed to be responsible for the ionisation of the hydroxy group of the tyrosine. The guanidinium group forms two hydrogen bonds to the tyrosinate oxygen.

Hydrophobic amino acid residues are dominantly found on the distal side. The binding of the substrate hydrogen peroxide is ensured by the presence of an histidine residue and an aspargine residue. A water molecule possibly forms a bridge between the aspargine and histidine but its role is not rationalized. The histidine residue has been found to be essential for catalysis and its N_δ is located 3.5 Å above the iron. This distance allows the hydrogen peroxide to bind to the iron and be deprotonated by the histidine. For the ethanol degradation pathway two hydrophobic amino acid residues, a phenylalanine and a valine enable the stereospecific abstraction of the pro-R hydrogen by compound I. These two residues also important in stabilizing the heme in the apoprotein via π stacking interactions between the phenylalanine residue and pyrrole ring II. The valine residue is also engaged

in a hydrophobic interaction with pyrrole IV (*figure 16*). This situation distinguishes also catalases from heme-thiolate proteins.
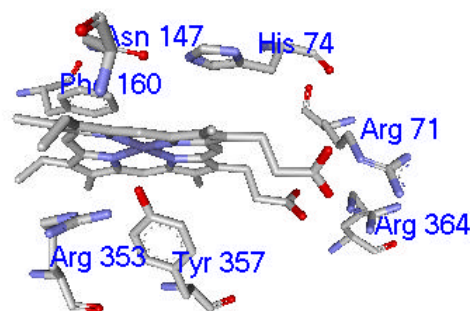
Figure 16: Active site of Beef Liver Catalase.

II.3. Catalytic cycle.

The catalytic cycle of catalases share similarities with the corresponding reactions of peroxidases which have an histidine axial ligand [46] and with CPO which has a thiolate ligand. The cycle starts from a five coordinated iron (III) heme complex. The hydrogen peroxide binds to the iron atom after deprotonation by the proximal histidine residue. The so-called **compound 0** is formed. On transfer of the hydrogen atom from the histidine to the terminal hydroxy group the heterolytic cleavage of the peroxy bond occurs to furnish a molecule of water and the high valent iron-oxo species. For the second step of the mechanism several hypotheses have been made (*figure 17*) [47] and will be discussed taking into account the following results:

1) alkyl or acyl hydroperoxides are not reductants of **compound I** [48]
2) only un-ionised donors interact with **compound I** but the substrate becomes ionised after binding to the reductant [49]
3) **compound II** which is the one electron reduced product of **compound I** inhibits catalase activity [47]
4) **compound II** can not be detected during the second step of catalase activity [47]
5) the hydrogen abstraction to alcohols proceed stereospecifically but the kinetic isotpe effects are variable [47].

First the possibility of the oxygen transfer of compound I to the reductant followed by a rearrangement has been formulated [47]. Second, an hydride transfer to compound I has

been suggested [50]. Finally a mechanism involving outer sphere electron exchange or inner sphere electron transfer has been invoked [51, 52]. All these mechanism are not satisfactory for the reasons exposed in the next discussion. They have been proposed as isotope studies with enriched $H_2^{18}O_2$ seemed to indicate that the oxygen arises from the second molecule of hydrogen peroxide [53].

Oxygen transfer mechanism:
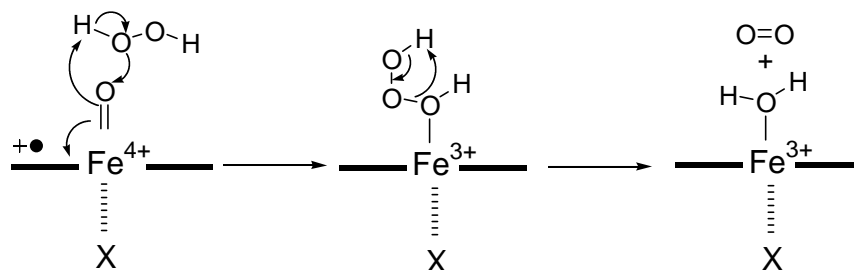
Hydride transfer mechanism:
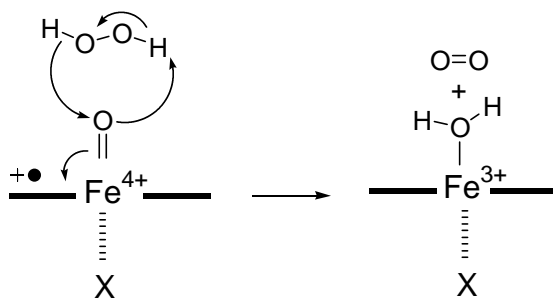
Electron sphere mechanism:
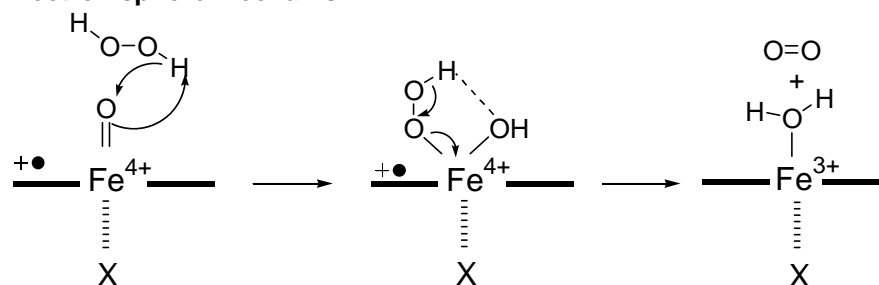
Figure 17: Different mechanisms postulated for catalase activity.

II.3.1. The "oxygen transfer" mechanism.

This first mechanism assumes a nucleophilic character of the oxygen atom of compound I on the second molecule of hydrogen peroxide. The nucleophilicity of compound I is not known but it would imply that compound I must be reduced by poor electron donor. It has been found that the reverse happens that is only hard donors such as ethanol rather than

polarizable substrates can reduce compound I. Therefore this mechanism has been abandoned.

II.3.2. The hydride transfer mechanism

The transfer of an hydride from hydrogen peroxide can be ruled out by measurement of kinetic isotope effect using deuterated hydrogen peroxide or alkyl peroxides after formation of compound I. A better answer to this mechanism is the use of chiral deuterated ethanol as ethanol is also oxidized efficiently by catalases. The results obtained by using chiral deuterated ethanol revealed that the oxidation of ethanol occurs specifically by the loss of the pro-R hydrogen. The measured kinetic isotope effect of 1.9 is too small for such a mechanism. Namely the isotope effect should be around 7 for a primary hydrogen atom abstraction process if it is rate determing.

If such a mechanism would be consistent this prerequisites that a **compound I** - reductant complex forms, an hypothesis which can be rationalized from the crystal structure [45]. The second molecule of hydrogen peroxide is proposed to bind to the histidine and aspargine distal residues. Thereby it places one hydrogen in the vinicity of the oxygen atom of **compound I**. The hydrogen is transferred to the iron-oxo complex generating the iron (III) hydroxy complex and oxygen, the remaining proton (*figure 18*) would be trapped by the histidine residue. This proton finally adds to the hydroxy complex to permit release of water and restore the resting state.
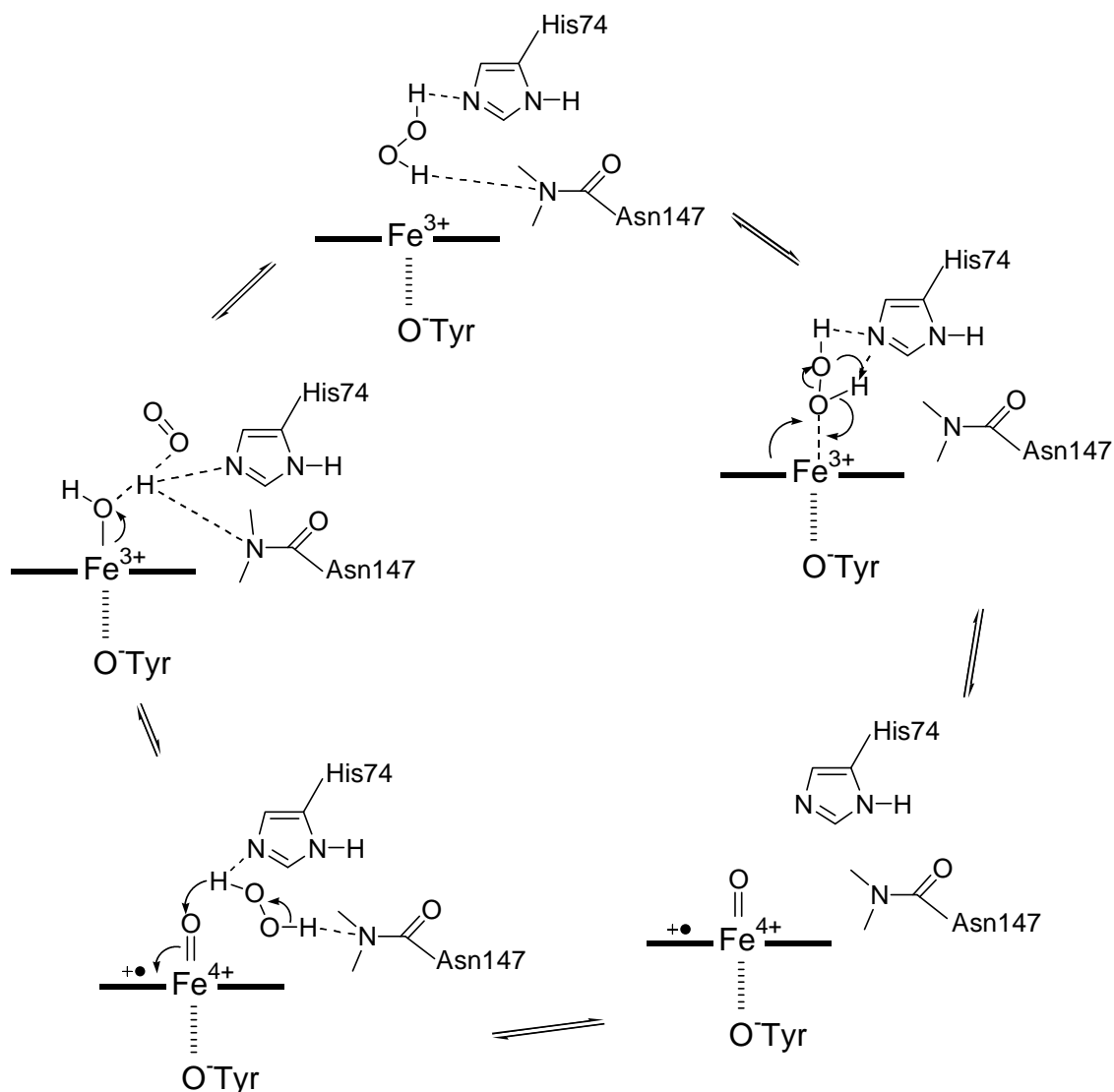
Figure 18: The hydride transfer mechanism.

II.3.3. The electron sphere mechanism.

The mechanisms which would involve an electron transfer process is favoured by *Schonbaum et al.* [47]. The hydrogen peroxide adds to the iron thereby reduces it formally to iron (III). The hydroxylated peroxide complex then rearranges to yield water and oxygen. Such a mechanism is rather unusual with iron complexes as it implies a seven coordinated iron atom or the loss of the phenolate coordination. Therefore this mechanism was not retained.

II.3.4. Proposed mechanism.

Based on the results obtained for CPO where the chloride acts as a nucleophile adding to compound I [54] one can propose that the mechanism of catalase could be the following. The second molecule of hydrogen peroxide is probably deprotonated by the distal histidine

residue. The peroxide then attacks the iron-oxo species to give an ozone-like intermediate (*figure 19*). Upon protonation of the oxygen bound to the iron oxygen evolves. As in the case of hydride transfer mechanism the iron hydroxy complex formed is protonated to its corresponding water complex and deligates from the heme to restore the resting state.
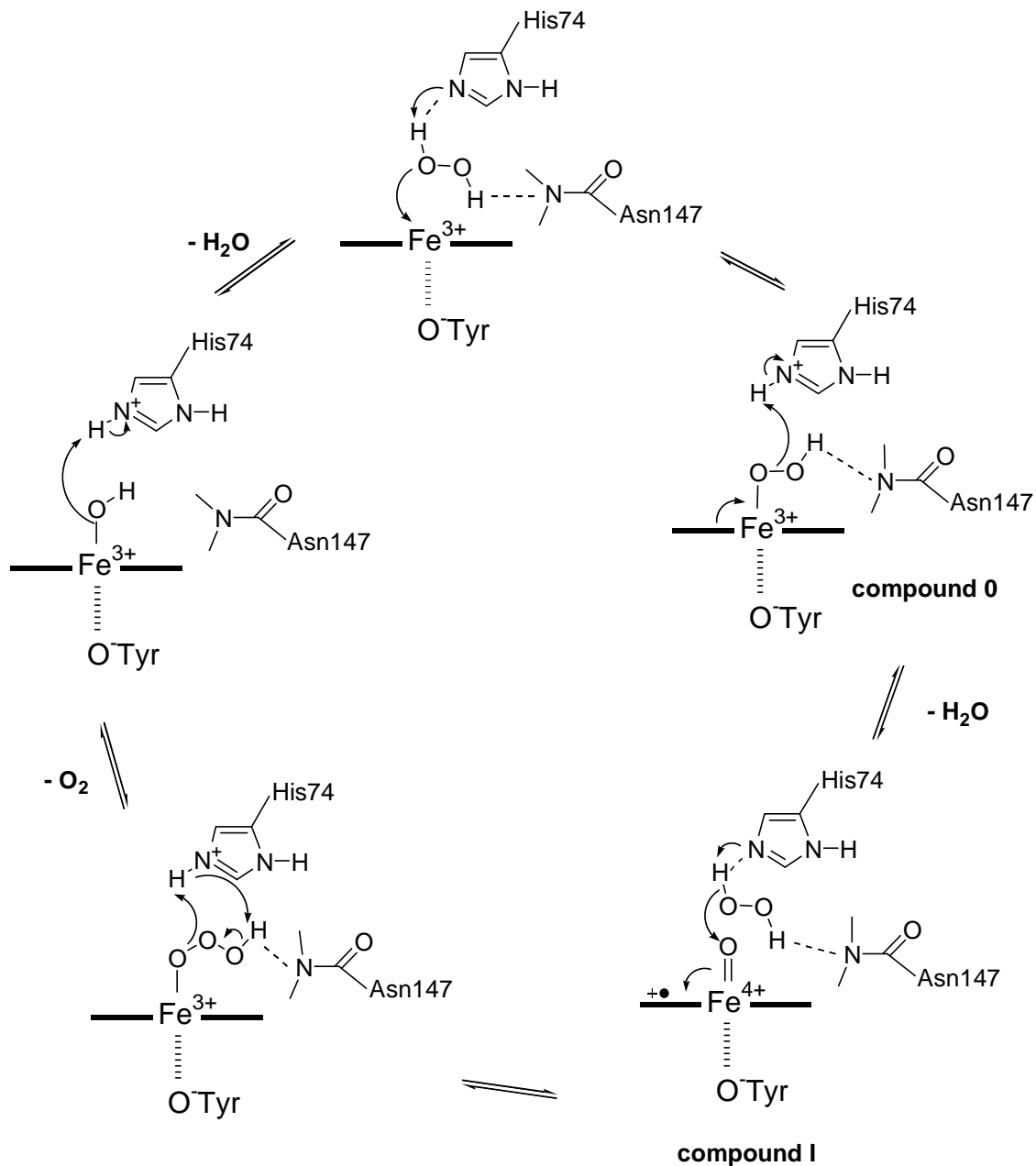
Figure 19: Proposed catalytic cycle of catalase.

The distinction between mechanisms **II.3.2)** and **II.3.4)** relies on:

1. the redox potential value of compound I which is unknown
2. the possibility of the formation of an ozone like iron porphyrin complex.

Since no conclusive experiments have been reported so far, the validity of both mechanisms is not established. Nevertheless if compound I of catalase would be reduced

by hydride from hydrogen peroxide it should also be the case for compound I of heme-thiolate proteins. Namely the redox potential value of compound I is, based on the value for the resting state, excepted to be more positive for heme-thiolate proteins than for catalase. Therefore the mechanism proposed in *figure 19* could be more consistent with the data collected as it implies a role of the distal amino acid residues also in the second step. Finally the main difference between catalases and heme-thiolate protein is the ability of the former to react with a second molecule of hydrogen peroxide in a two electron process.

III. Synthetic active site analogues.

To obtain high resolution X-Ray structures or satisfactory physical characterization of catalytic intermediates is not always possible with enzymes. Therefore the development of active site mimics is still a powerful tool in the elucidation of catalytic cycles. The advantage is even more evident for organic chemist who can use an efficient active site analogue as catalyst for chemical reactions which are only feasible under drastic conditions. The mimic is namely often soluble in organic solvents contrary to proteins.

Among other the analytical physical methods which are now routinely used for proteins could not have been developed if models had not been synthesized to validate and optimise the parameters. Also the identification of short living intermediates is due to the existence of models e.g. CPO models.

The design of models has primarily been devoted to models for haemoglobin and myoglobin with the hope to create in hand "artificial blood". Therefore more attention has been paid on the stabilization of the diogygen adduct of heme models rather than to the specificity of the axial ligand. With the discovery of heme-thiolate proteins models have been developed to rationalize the effect of axial ligation during catalysis.

Porphyrins which are active site analogues of heme proteins can be divided into several classes (*figure 20*):

- The simple **meso tetraaryl porphyrins** which have the main advantage to be generally robust for catalysis [55].

- Also widely used are the **octaalkylporphyrins** being only substituted on the β-pyrrole positions [55].

For both models, the synthesis is short and high yielding. These models have been widely used to characterize postulated intermediates such as the iron oxo complex or compound I; they suffer, however, from disregarding the axial ligation.

- The more elaborated **"tailed-porphyrins"** [56]. They are usually diaryl or tetraaryl porphyrin where on one aryl an "arm" is anchored to introduce a fifth axial ligand. If they have the advantage to take into account the axial ligand, the binding of the latter often suffers from "on-off". Dimeric or polymeric species can be obtained if the tail binds to another porphyrin molecule which is a severe limitation. These models for heme-thiolate proteins suffer moreover from the insufficient protection of the sulphur towards oxidation [57].

- The **"strapped porphyrins"** are similar to the tailed one. The axial ligand is introduced via a bridge between two meso or β-pyrrole positions. The advantage is to hold the axial ligand in the vinicity of the central metal. Usually the meso positions bear substituted phenyl rings which are properly functionalised [55]. The synthesis is dependant on the yield obtained for the bridging step which is usually not very high.

- The elaborated **"capped porphyrins"** protect one of the porphyrin face and thereby form a binding cavity for reagents and substrates [55]. Their synthesis is often tedious and yields are poor.

- The combination of the "capped" and "tailed" concepts has given raise to **"pocket porphyrins"** which allow to study the influence of the axial ligand on the binding of reagents or substrate [55].

- The **"picket fence porphyrins"** developed by Collman are very popular as they have revealed good binding ability *vs.* dioxygen [55]. They are characterized by meso aryl moieties which carry in the ortho position a bulky e.g. amide group, usually a pivaloyl moiety (= picket).

The concepts mentioned above can be varied to give raise to "picket pocket" [55], "gyroscope" [58] or "basket handle" [58] porphyrins among others.

As the enantiomeric excess in catalytic reactions still gains more interest chiral porphyrins have also been developed such as "chiral basket" or "twin-coronets" [59] porphyrins. Increasing the complexity and size of the substituents of the porphyrin macrocycle suffer from the drawback of poor overall yields of the synthesis.
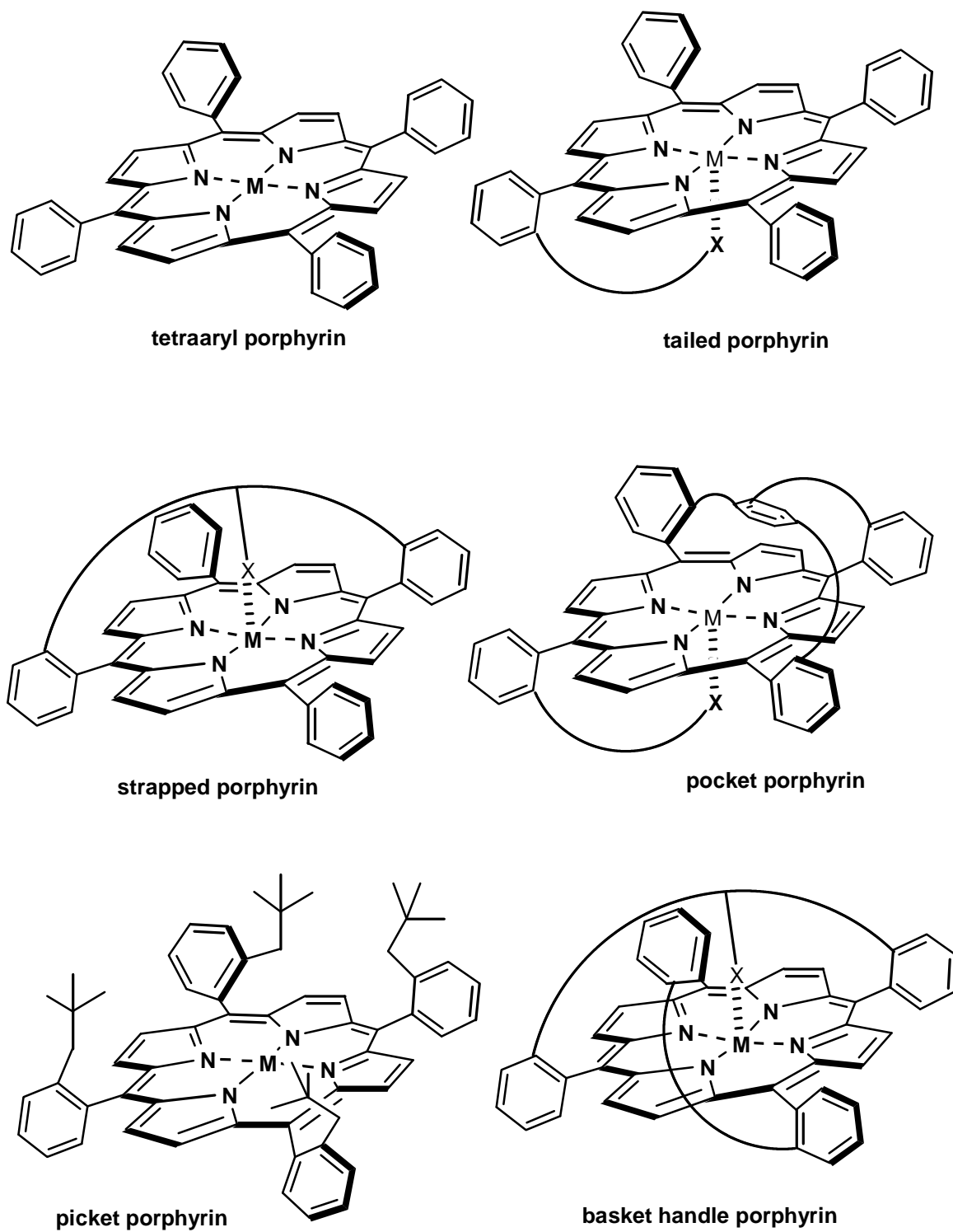
Figure 20: Some of the most used porphyrin classes as active site analogues.

IV. Problem to be addressed.

The progress of enzymology and biochemistry permits to work directly with the proteins themselves to obtain a certain degree of information on possible intermediates of the catalytic cycle. Nevertheless this approach still suffers from approximations and requires much more time in data collection and analysis than with a simplified model.

In particular the recent cryogenic X-ray studies on $P450_{cam}$ have not permitted to solve the structure of the iron-oxo species [18]. Neither is the mechanism of oxygen insertion solved. And finally none of the studies P450 enzymes accounts for the specificity of the axial ligand in the formation of intermediates.

Therefore the aim of this work was to develop iron porphyrin complexes as model compounds which would permit to rationalize the specificity of the axial ligand. In a first part the synthesis and characterization of a CPO model designed by *Wagenknecht and Woggon.* had to be verified carefully to improve the purity of the iron complex. As catalase is very close to CPO it was decided to prepare two models suitable for the investigation of the thiolate *vs.* phenolate axial ligation to iron porphyrins. The models for the resting state should be investigated by UV-Vis, NMR, EPR and ENDOR techniques to have a complete characterization.

A study on the generation of the postulated intermediates of CPO should then be undertaken to fully characterize the HOCl complex as a key intermediate and to confirm the conclusion by *Wagenknecht and Woggon.*[20]. Finally it was anticipated that models of compound I could be prepared to gain information on their electronic nature for heme-thiolate proteins and catalase.

**RESULTS AND
DISCUSSION**

V. Design and Synthesis of Models.

V.1. Design.

V.1.1. Criteria for a suitable model.

Although numerous heme models have been published, the necessity of improving them is a challenging task for the organic chemist. Most of the models do not respond to the elegant definition of *Bruice et al.* [60] for the ideal active site mimic. The structural characteristics of the ideal analogue implies to have:

1. a domain that holds the catalytic functional groups at the active site in a geometry that mimics the active site structure of the enzyme,

2. a binding domain for the substrate and

3. a structure that protects the catalytic functional groups from side reactions with species other than the substrate.

According to this definition the model should respond to the following criteria:

4. the original ligands from the active site have to be conserved. In our case an iron porphyrin with a thiolate or an oxygen coordinating axially to the iron atom is required.

5. easily observable spectroscopic properties close to the one of the enzymes.

6. at least a stochiometric reaction (single turnover) between the catalytic intermediate and the substrate. Ideally the turnover should be near the value obtained for the enzymes.

Most of the compounds synthesized as heme-thiolate models or as catalase analogues until now do not respond to point **1.** above as they do not retain the proper axial ligand.

The models where a free thiolate or phenolate ligand mimics the sulphur respectively oxygen ligation and the tailed-models suffer from an "on-off" equilibrium (*see* chapter III). Moreover in protic solvents the protonation of the oxygen or sulphur has been reported [61].

Models with a tight coordination of the axial ligand are in general not good catalysts as the thiolate and/or the porphyrin is rapidly oxidized in the presence of oxidants [62].

Good catalysts for P450 like activity are known but the central metal is not iron [63] and all of them do not retain the sulphur ligation. The work of *Wagenknecht et al.* [64] describes for the first time an efficient iron porphyrin catalyst with an axial thiolate ligation but the model did not permit the complete characterization of the P450 like catalytic species.

For catalases only two iron porphyrin models **9** and **10** (*figure 21* and *table 4*) are known having phenolate ligation [65, 66] but their pendant thiolate analogues have not been studied until now.
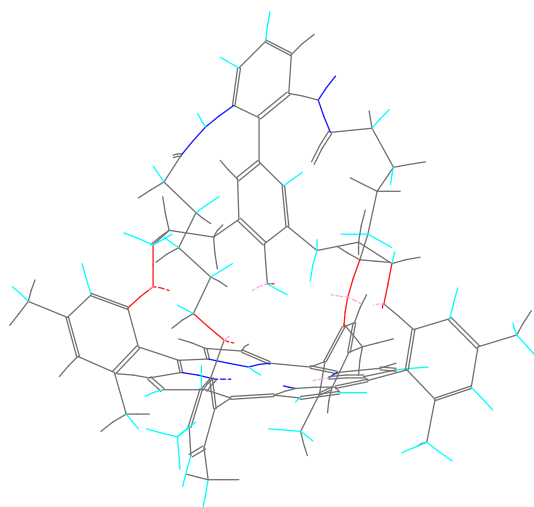
9: *Bruice et al.*
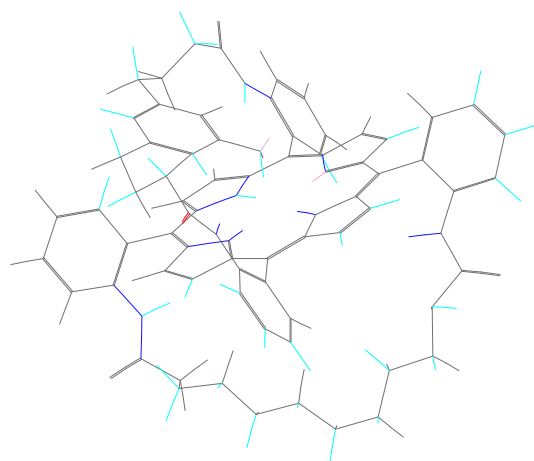
10: *Meunier et al.*

Figure 21: Models 9 and 10 for Catalase with phenolate ligation.

	9 (*Bruice et al*)	10 (*Meunier et al.*)
UV-Vis (λ in nm)	325, **420** (Soret), 490, 552, 608, 653 in chloroform	**420** (Soret), 509, 580, 657 in toluene
NMR (δ in ppm)	122.4 (meta-phenol H), 83 (β-pyrrole), 13.1, 13.4, 11.9, 11.6 (H meta from meso phenyl)	**n/a**
EPR	**n/a**	**n/a**
Redox potential	**n/a**	**n/a**
Catalase activity	**n/a**	**TO: 71, or 21% yield of dioxygen**

Table 4: Available analytical data for catalase models 9 and 10 taken from ref. [65] and [66].

Clearly if the axial ligation is recognized as a determining factor in the catalytic activity no study has been undertaken to correlate the phenolate (O⁻) versus the thiolate (S⁻) ligation to the difference between catalases and heme-thiolate proteins.

V.1.2. Choice of the models.

Since several analogues which meet most of the criteria mentioned in *V.1.1.* have been characterized [57, 67, 68], we decided to pursue the development of a promising mimic of CPO [69]. *Figure 22* summarizes the features of our targets which respond almost completely to the definition of *Bruice et al.*:

Bulky amide substituents to prevent μoxo dimer formation and provide a substrate cavity

alkyl substituent to protect pyrrole from oxidative degradation and increase solubility in organic solvents

Thiophenolate or phenolate to mimic the axial ligand of CPO and catalase

tert-Butyl group to ensure a permanent sulfur/oxygen coordination and prevent μoxo dimer generation

11: X=S⁻ (CPO model)

12: X=O⁻ (catalase model)

Figure 22: Target molecules 11 and 12.

V.2. Synthetic approach.

V.2.1. Retrosynthesis.

The retrosynthesis (*scheme 1*) relies on three building blocks which are provided by the disconnection of the ether bond of the axial "bridge" moiety **16** or **15** and by the Mac Donald's porphyrin synthesis. This step requires an aldehyde **14** and a dipyrrylmethane unit **13** which are condensed under acid catalysis.

Scheme 1: Retrosynthesis.

The dipyrrylmethane unit **13** has been synthesized according to the procedure described by *Aissaoui and Woggon.* [68] and the aldehyde **14** via an ortho-directed lithiation of the N-pivaloyl activated *m*-anisidine [20]. The bridge **15** is synthesized by a modified literature procedure [70] and bridge **16** by an adaptation of it (*see* V.4.1.).

V.2.2. Porphyrin synthesis.

Although the CPO model **11** has been already described, several open questions required a more careful characterization. Particularly the facts that:

a) Atropisomers were never separated and could not be distinguished by any spectroscopic or chromatographic method. This case was unpreceded in the literature.

b) The introduction of the bridge moiety was not accompanied by a red shift of the Soret band in UV-Vis spectroscopy as is the case for similar molecules [68].

c) The NMR data of the metal free precursors of **11**, compounds **21** and **22** (see *scheme 5*), were badly resolved suggesting a mixture of conformers or possibly a mixture of several compounds.

d) The mass spectra (MS) has not be obtained despite the use of several MS techniques.

e) The ESR data of the resting state were indicative of several species.

Moreover as NMR spectroscopy is nowadays a tool of choice for the structural determination in solution we wanted to determine the conformation of our compounds by this method as it would help refining the structure for improving our model if necessary. The understanding of the factors influencing binding constants could also be gained from this structural elucidation combined to other spectroscopic methods.

The first step of the synthesis (*scheme 2*) is the Mac Donald's condensation of **13** and **14**. This step was examined in details as the separation and characterization of atropisomers had not been solved previously.

1) *p*-TsOH, MeCN, RT, 18 hr

2) *o*-chloranil, THF, 30 Min, RT.

>100%

17a

17b

79% Zn(OAc)₂, MeOH,CH₂Cl₂, Δ, 10 Min
Zinc insertion

18a: a,a isomer

18b: a,b isomer

Ratio 15:85

80% HCl 37% , CH₂Cl₂

80% HCl 18%, CH₂Cl₂

17a: 9% overall from **13** and **14**

17b: 55% overall from **13+14**
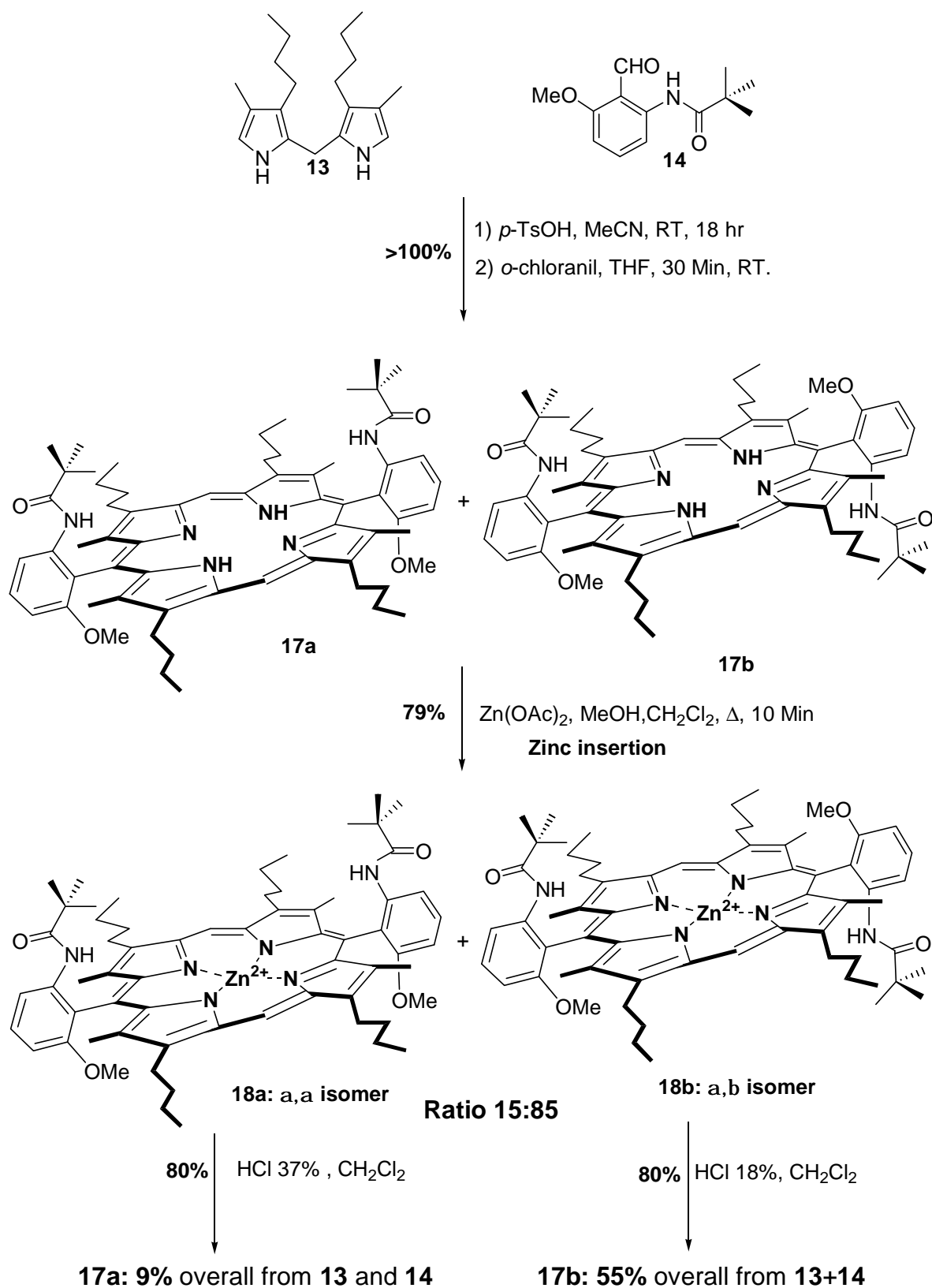
Scheme 2: Synthesis of the porphyrin macrocycle.

V.2.3. Separation and structure of atropisomers.

V.2.3.1. Definition.

The existence of isomers in meso substituted porphyrins having functionalised aromatic substituents has been pointed out in 1969 [71]. The existence of atropisomers is due to an hindered rotation of the aryl-porphyrin bond. The energy barrier required for rotation is known to increase with a more rigid porphyrin nucleus. The transition state goes namely through a highly distored porphyrin ring [72]. If sterically hindering groups are close enough this process could be impossible even at 200°C.

In our case we can only have, assuming a symmetry in the spatial arrangement of the butyl side-chains, two isomers. The first isomer is the one where the same substituents of the aryl are facing on the same side of the porphyrin plane. As it is reminding of a **cis** conformation in alkenes the isomer is defined as the α,α isomer. The second isomer is the α,β isomer. It corresponds to a **trans** geometry where the same substituents of the aryl are on opposite sides of the porphyrin plane (*figure 23*).

18b: a,b isomer

18a: a,a isomer
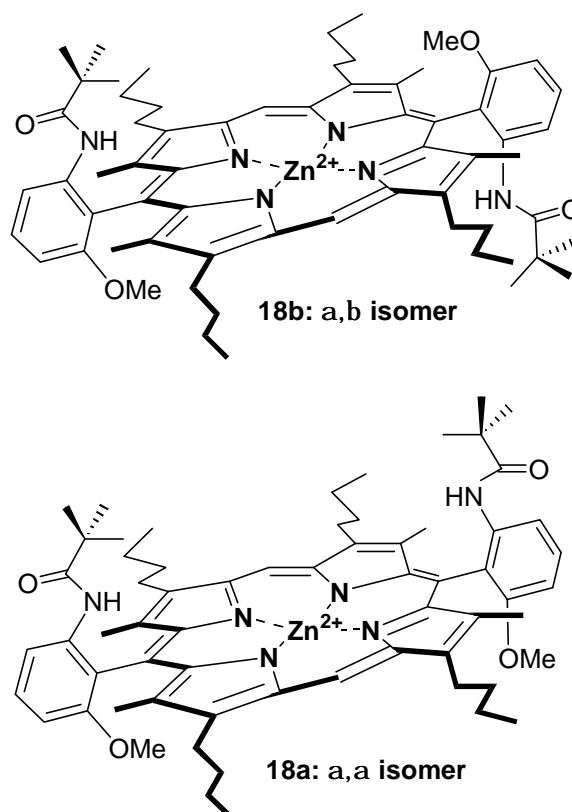
Figure 23: Atropisomers.

V.2.3.2. Separation of atropisomers.

Since the first report on isolated atropisomers [73] it has been only few cases where the latter have not been separated directly by chromatography and where a proper derivatization was necessary. Until the design of our target the absence of distinction between geometrical isomers of porphyrins has not been reported. Moreover tetraarylporphyrins having ortho pivaloyl groups on the aryl moiety are cases where the separation is most documented and where the spectroscopic properties also allowed the attribution of the proper structure [74-76]. (5, 15) diaryloctaalkylporphyrins were even used as model compounds for atropisomer's characterization as the latter are thermally stable [20].

From these various reported data and given the intriguing behaviour of the "bridged" species we have postulated that atropisomers **18a** and **18b** are not interconvertible. Probably the desired isomer **18a** has been previously discarded during purification.

To verify this working hypothesis we turned to a more careful TLC control of the reaction. From the crude mixture after zinc insertion we were finally able to well distinguish two spots on TLC for 1**8a** and **18b** having the proper mass (*figure 24*).

TLC on silica gel. Eluent: Hexane:
Ethylacetate (5:1) + 1%vol triethylamine.
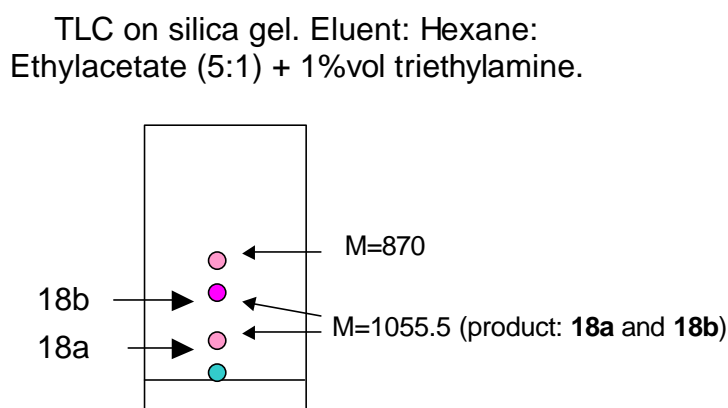
Figure 24: TLC of the crude reaction mixture after zinc insertion.

These spots corresponding to **18a** and **18b** gave also two distinct peaks on the HPLC by using a reverse phase C-18 column at 50°C and a gradient of a MeCN: H_2O mixture as eluent (see experimental part). The HPLC ratio has been calculated to be 8:2. Most likely **18b** which is the most apolar and the most abundant compound was the compound that has been isolated previously by *Wagenknecht and Woggon*. and that was used to finally obtain the CPO model.

As it is known that usually the most polar compound is the α,α isomer it was necessary to first characterize completely and unambiguously both products **18a** and **18b** and then find out why such a selectivity appeared.

V.2.3.3. Characterization by NMR spectroscopy and derivatization.

After separation by column chromatography and removal of zinc both compounds **17a** and **17b** were analysed by proton and carbon NMR spectroscopy. The chemical shifts which were assigned by using 1D- and 2D- NMR spectra (*see* experimental part) differ principally for the Butyl, NHPiv and OMe substituents as summarized in the *table 5*.

Proton[a]	$\delta_{a,a \text{ isomer}}$ (18a)/ppm	$\delta_{a,b \text{ isomer}}$ (18b)/ppm	$\Delta(\delta)_{(18a/18b):}$
10,20 (meso H's)	10.20	10.20	0.00
5'	8.45	8.45	0.00
4'	7.78	7.79	0.01
3'	7.08	7.11	0.03
N$\underline{\text{H}}$Piv	7.06	6.90	0.16
$CH_{2\alpha}$	4.02-3.91	4.05-3.91	0.00
OMe	3.54	3.62	-0.08
Me Pyrrole	2.59	2.57	0.02
$CH_{2\beta}$	2.16	2.15	0.01
$CH_{2\gamma}$	1.75	1.70	0.05
$CH_{3\delta}$	1.1	1.06	0.04
NH$\underline{\text{Piv}}$ (*tert*-Bu)	-0.05	-0.13	0.08
N$\underline{\text{H}}_{\text{porphyrin}}$	-2.21	-2.24	0.03

Table 5: ^{1}H-NMR chemical shifts for both isomers.
a): Numbering according to *figure 22*, Conditions: 2 mM porphyrin in CDCl$_3$, 295 K.

The largest difference in chemical shift is observed for the proton of the OMe group and for the N-pivaloyl functionality. This reflects that the placement of the aryl regarding the porphyrin plane is not the same. From studies on di- and tetra- aryl porphyrins it is known that the aryl substituents can adopt the two following conformations:

1. be perpendicular to the porphyrin plane
2. be tilted from the above mentioned plane

The tilting is more important when sterically hindering substituents are found on the aryl moieties [78]. Nevertheless the shifts difference is not a decisive argument to assign the configuration. Namely the difference could also be rationalized by a different geometry of the porphyrin macrocycle. Porphyrin ring systems are not always planar [79] and can deform to adopt:

1. a domed conformation

2. a ruffled conformation

3. a saddle conformation

4. a waved conformation

5. a propelled conformation

Since there is little knowledge on NMR data of one or the other conformation the chemical shifts are not a decisive argument in the assignment of the structure of atropisomers. However the analysis of the carbon chemical shifts in iron porphyrin complexes gives an indication on the degree of ruffling [80]. Finally the question addressed is a geometrical problem in relation with spatial distances and symmetry. Therefore the measurement of Nuclear Overhauser Enhancement (NOE) in proton NMR spectroscopy is the most reliable technique for determining spatial configuration in solution.

Prerequisite for observation of NOE effects is that the protons of interest are close enough in space and resonate at different frequencies. In the case of the α,β isomer **17b** such a NOE effect may likely to be observed between the proton of the CH_3 from the pivaloyl and the CH_3 from the OMe substituents. Unfortunately the actual distance which has been ruled out from molecular modelling was too large (> 5 Å) to give a positive result. As a consequence no corresponding NOE was observed in the NMR spectra. The methyl ether functionality was therefore subsequently replaced by a larger protecting group of the hydroxy function. A *p*-nitrophenylester was synthesized as the presence of a phenyl ring could induce a π stacking stabilization of the phenyl moiety above the porphyrin plane. Thereby the proton of the phenyl ester should lie very close to the pivaloyl moiety (*figure 25*).
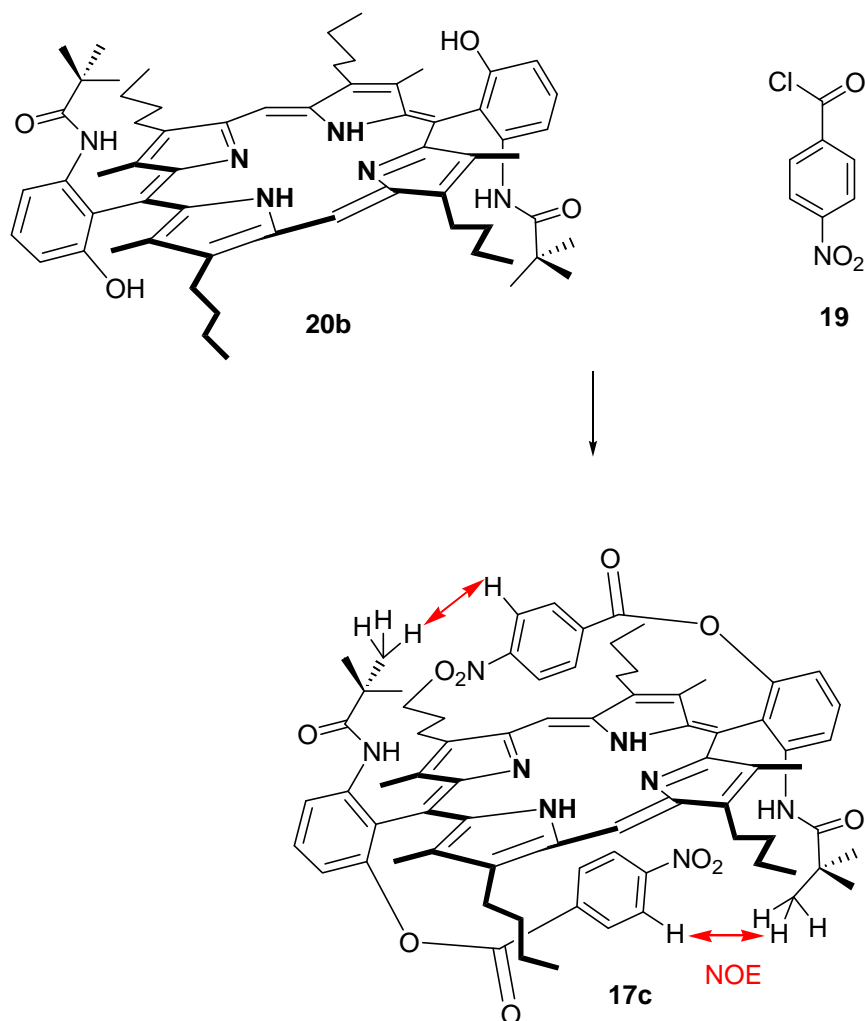
Figure 25: Derivatization and expected NOE effects.

As expected a strong NOE effect was observed between the pivaloyl protons and the protons of the nitrophenylester. Thereby the most apolar compound **17b** was unambiguously attributed to the α,β isomer whereas the other isomer **17a** was determined as the α,α one.

The question of the ratio (85:15) obtained has to be answered because such a selectivity is unprecedeed in porphyrin synthesis. For example *Aissaoui and Woggon* have reported with similar structures a ratio of 60:40 in favour of their corresponding α,β isomer [67].

V.2.3.4. Why such a ratio and no interconversion?

Compared to porphyrins which have been published in the literature our models indeed combine the steric hindrance of the "picket fence porphyrins" of Collmann and of the "octaalkyl" porphyrins.

Atropisomerization has long been recognized to be slowed down by the presence of bulky substituents on the meso aryl groups. The increase of the steric hindrance results in a higher energy barrier for atropisomerization [81]. This is related to the necessity for the porphyrin

macrocycle to distore during the transition state. This distorsion allows the substituted phenyl ring to pass above the β-pyrrole positions. If the latter are also substituted the distortion required is again increased [73].

In our case we have not only one but two ortho substituents which can come in contact with the pyrrole rings during atropisomerization. Such a situation generates a conflict for the direction in which the pyrrole ring has to be deformed to enable a rotation of the C_{aryl}-C_{meso} bond (*figure 26*).

direction of distorsion for the aryl for the OMe group to allow atropisomerization

direction of distorsion for the aryl for the NHPiv group to allow atropisomerization

pyrroles have to move in the vertical plane

NHPiv groups prohibit the atropisomerization

OMe group prohibits the atropisomerization
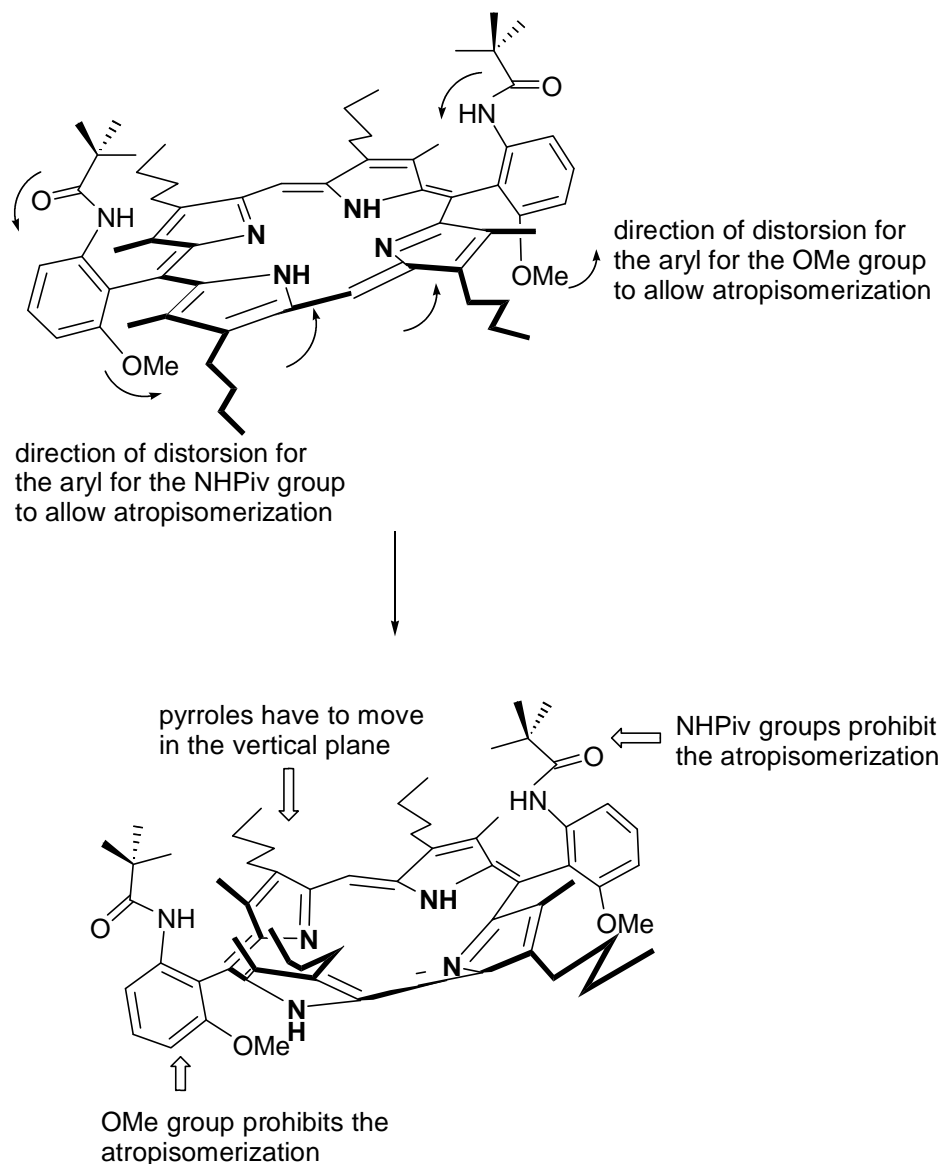
Figure 26: Schematic representation of the required distortions for isomerization.

Several attempts to interconvert the isomers failed (*table 6*). A prolonged heating only results in the destruction of the porphyrin.

Method:	Result:
Heating, 60°C, DMF	No interconvertion
Heating, (120°C), DMF	No interconvertion
Heating, (160°C), DMSO	degradation
Heating, 200°C, decaline	degradation

Table 6: Attempts for atropisomerization.

This result was first surprising because porphyrins having (ortho, meta, para) substituted aryl groups were isomerisable at 90°C [82]. Nevertheless it appears that the presence of two ortho substituents on the aryl groups is the reason of the thermal stability of these isomers as confirmed by the synthesis of analogues [83].

V.2.3.5. NMR solution structure of 17a and 17b.

Taking advantage of the thermal stability of the compounds we have pursued the three dimensional characterization of our intermediates **17a** and **17b** by NMR spectroscopy. The first question to be addressed is the geometry of the aryl substituents. For the ortho substituents (position 3' and 6' on the aryl moieties) the C_{aryl}-X-$C_{substituent}$ bond can adopt a cis or trans configuration. Moreover the amide substituent can also adopt a cis or trans configuration for the N_{amide}-C_{amide} bond. Therefore eight ($2^3 = 8$) structures are possible (*figure 27*). These structures can be distinguished from each other by the NOE effects measured.
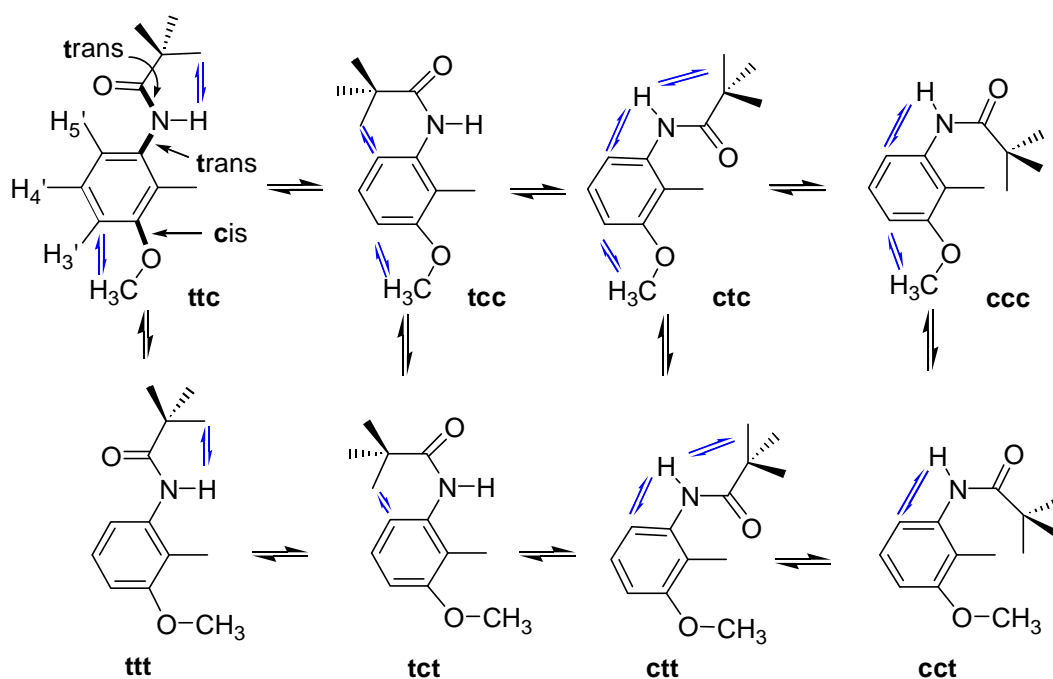
Figure 27: Conformation of the aryl moiety and expected NOE effects.
(The coloured arrows represent the NOE effects).

The NOE which are observed are summarized in *table 7*:

NOE between:	$H_{3'}$	$H_{5'}$	OMe	N<u>H</u>Piv	NH<u>Piv</u>	Me pyrrole
$H_{3'}$		-	**s**	-	-	-
$H_{5'}$	-			**w**	-	-
OMe	**s**	-		-	-	**m**
N<u>H</u>Piv	-	**w**	-		**s**	**m**
NH<u>Piv</u>	-	-	-	**s**		**m**
Me pyrrole	-	-	**m**	**m**	**m**	-

Table 7: NOE effects observed in the ROESY and NOESY spectra of 17a or 17b.
<u>Abbreviations:</u> w: weak, m: medium, s: strong.

As the NOE between the OMe group and $H_{3'}$ is strong the C_{aryl}-C_{ether} bond geometry is cis and the structures **ttt** to **cct** can be excluded. For the amide substituent the absence of NOE between the N<u>H</u>Piv proton and $H_{5'}$ implies a trans conformation of the C_{aryl}-N_{amide} bond. Thereby only structures **ttc** or **tcc** are dominant. Last the NOE effect between the NH and the *tert*-butyl group of the NH<u>Piv</u> moiety indicates that the N_{amide}-C_{amide} bond is also in a trans configuration.

ttc in *figure 27* is thereby the preferred conformation at the aryl moieties. Moreover the relatively high field shifted chemical shift of the amide proton N<u>H</u> which is found at 6.9 ppm and the shift of the *tert*-butyl substituent around 0 ppm also supports this conformation. The shielding effect can namely not originate from the phenyl ring as the entity is planar. Therefore it can arise only from the porphyrin ring current [58].

The planarity of the amide moiety and its coplanarity with the phenyl ring can be determined from the ^{15}N-H coupling constant. It is namely established with peptide models that the value of this coupling constant reflects the sp^2 hybridisation degree of the nitrogen atom in the amide bond [84]. In our compounds the value measured from the ^{15}N satellites peaks of the NH signal in the proton NMR spectra was of 90 Hz. This implies that the sp^2 character of the nitrogen is about 100%. The sp^2 character of the nitrogen atom results in a partial double bond character of the O=<u>C-N</u> bond. Hence is the amide bond planar. Due to this double bond character a conjugation of the N-Phenyl bond with the O=C-N bond occurs. It results in a planar structure for the whole system Phenyl-N-C=O (*figure 28*).

= porphyrin ring system
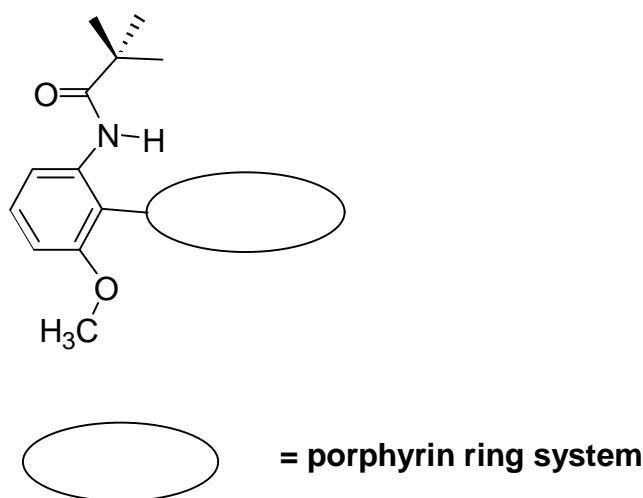
Figure 28: Conformation of the aryl substituents.

The structure of the aryl moiety obtained from the NOE observed is in good agreement with the crystal structure data of Collmann [85] for its (5,10,15,20) [tetra-(o-N-aminopivaloyl)-phenyl] porphyrinato iron (II) model (TPivPP) which binds dioxygen.

Finally the degree of tilting from the vertical plane passing through the 5, 15 positions can also be appreciated from NOE effect. If the phenyl rings would be perfectly perpendicular to the porphyrin ring the NOE effects observed for the *tert*-butyl groups of the pivaloyl substituents to the butyl side chains should be quasi inexistent. As a medium to strong effect is observed even to the butyl protons, the titling of the phenyl substituents is probably

relatively important. Moreover the detection of a NOE effect to the butyl side chains raises the question of the spatial arrangement of the butyl side-chains.

Until now it was assumed that the β-butyl groups are more or less lying in the plane of the porphyrin. The NOE observed are inconsistent with this assumption. For example the NOE effect from the $CH_{2\alpha}$ to the neighbouring meso proton is not strong as well as the one to the β-methyl groups. Further the $CH_{2\alpha}$ protons are splitted in a complex multiplet which at higher field proved to be a set of two multiplets. In other words either the protons are diastereotopic and the $C_{pyrrole}$-C_α rotation is blocked or the butyl side-chains are distributed on each side of the porphyrin plane in a symmetric manner. With help of molecular modelling and based on the published crystal structure of octaethylporphyrin we propose that the butyl chains are arranged in an "up-down" conformation [86]. This minimizes the steric interactions between two chains and an overall C_2 symmetry is conserved.

Last point to be discussed is the planarity of the porphyrin core. The splitting of the $CH_{2\alpha}$ signal in a complex multiplet is an indication that probably the porphyrin core is not completely planar. Moreover the UV-Vis spectra of **17a** or **17b** show a maximum of absorption at 408 nm. This value is less than the value obtained for tetraphenylporphyrins which are known to be ruffled. However this does not exclude the possibility of a saddle conformation. The saddle conformation would limit the interaction between the adjacent butyl chains. Nevertheless as no crystal structure has been done the degree of deviation from planarity can not be judged.

The NOE effects observed and a force field calculation using the MM2 method [87] led to the model structures depicted in *figure 29*.
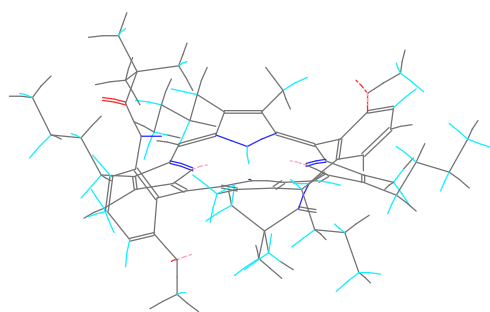
17b
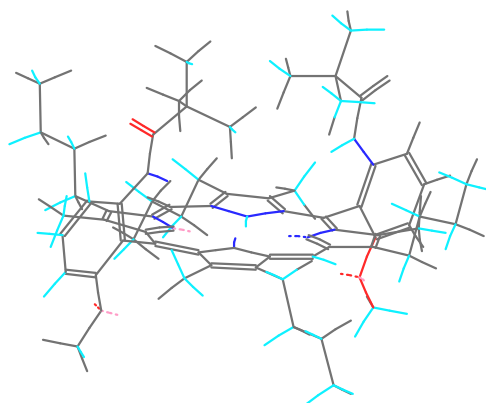
17a

Figure 29: Proposed structure of both isomers.

V.2.4. Synthesis of the bridged porphyrins 21 and 22.

The methoxy ether, the protecting group for the phenol, was subsequently deprotected (*scheme 3*). Two methods were considered: the use of concentrated HBr at reflux [88] and Lewis acids such as BBr$_3$ at low temperature [89]. Both methods, however cleave also the pivaloyl group, even faster than the methyl ether. Accordingly a milder Lewis acid with a nucleophilic co-solvent [90] seemed suitable. Indeed the Lewis acid aluminium chloride in the presence of an excess of ethanethiol selectively cleaved the methyl ether bond in 75% yield for **17a** and 97% yield for **17b** (*scheme 3*).

17a $\xrightarrow[\text{CH}_2\text{Cl}_2, \text{RT, 14hr}]{\text{AlCl}_3, \text{EtSH}}$

20a: 75% from 17a
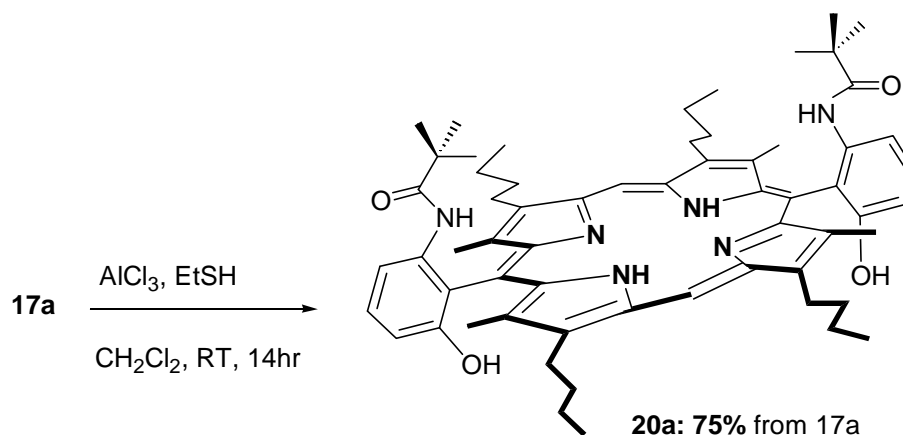
20b: 98% from 17b by the same reaction

Scheme 3: Deprotection of the methyl ether.

The isomers **20a** and **20b** were found to be not interconvertible. As for **17a** and **17b** their NMR and TLC behaviours of **20a** and **20b** are distinct. For example under the purification conditions initially used for **20b** by column chromatography, **20a** remains on the column. As **20b** can not be interconverted into **20a** the target **11** can not be obtained from the isolation of **18b**.

V.2.4.1. Bridging.

The further confirmation of the non conversion of atropisomers into each other was next established by the introduction of the bridge **15**. If the α,β isomer **20b** is used one can obtain:

1. a tailed monomer having one or two bridges hanging
2. an oligomeric porphyrin array or oligomeric cyclic structure (*figure 30*)
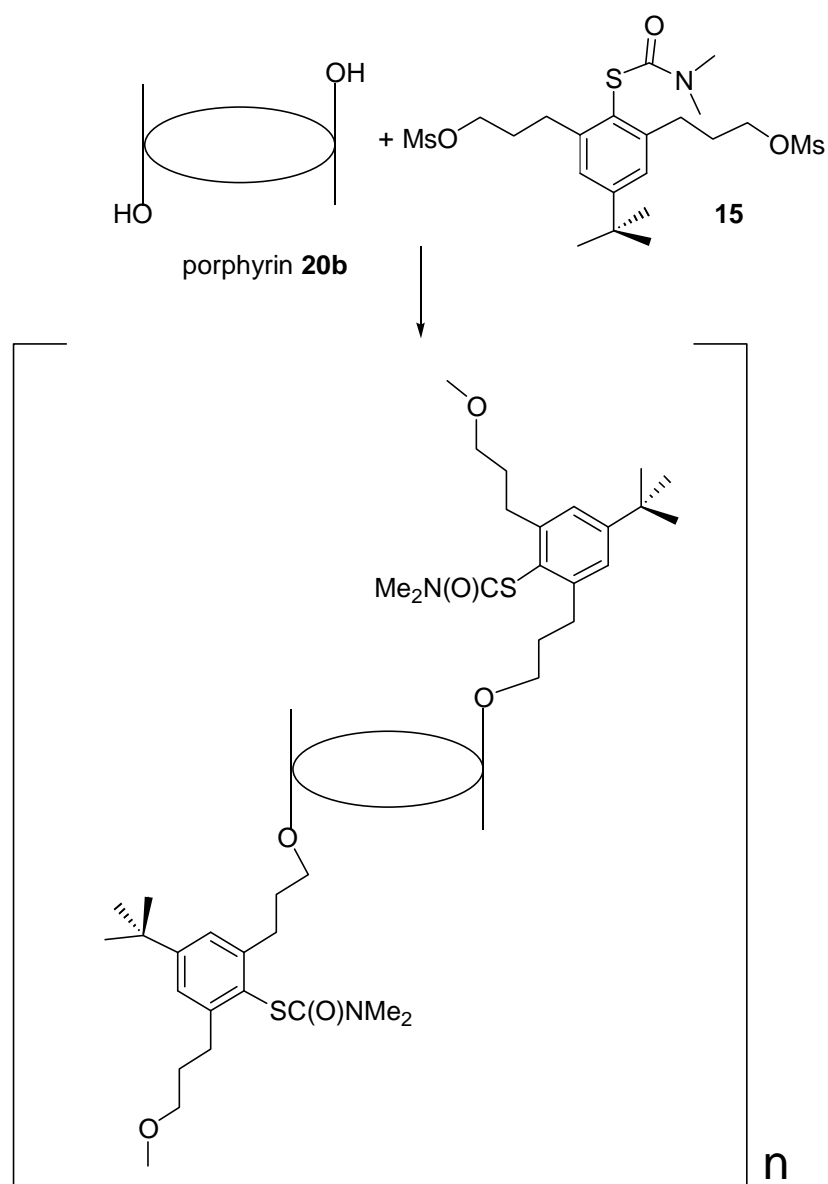
Figure 30: Formation of polymeric species upon bridging with the a,b isomer 20b.

The α,α isomer **20a** is the only isomer which can yield the desired bridged structure. Nevertheless oligomers can also be obtained from **20a** as the step involves the reaction of bifunctional compounds. The reaction conditions have therefore to be carefully optimised to minimize the formation of polymeric species.

The experience in "supramolecular" chemistry with polyfunctionalized compounds has shown that bridging is favoured under high dilution conditions. The presence of one of the reagents in a controlled low concentration during the reaction also favours the ring closure process over the reaction with a second molecule of reagent [57].

Therefore we have achieved the bridging step (*scheme 4*) by typically working with porphyrin solution having a concentration of 1 mg ml^{-1} (approximately 1 mM). The bridge was added over 3 hours at a concentration around 6 mM.
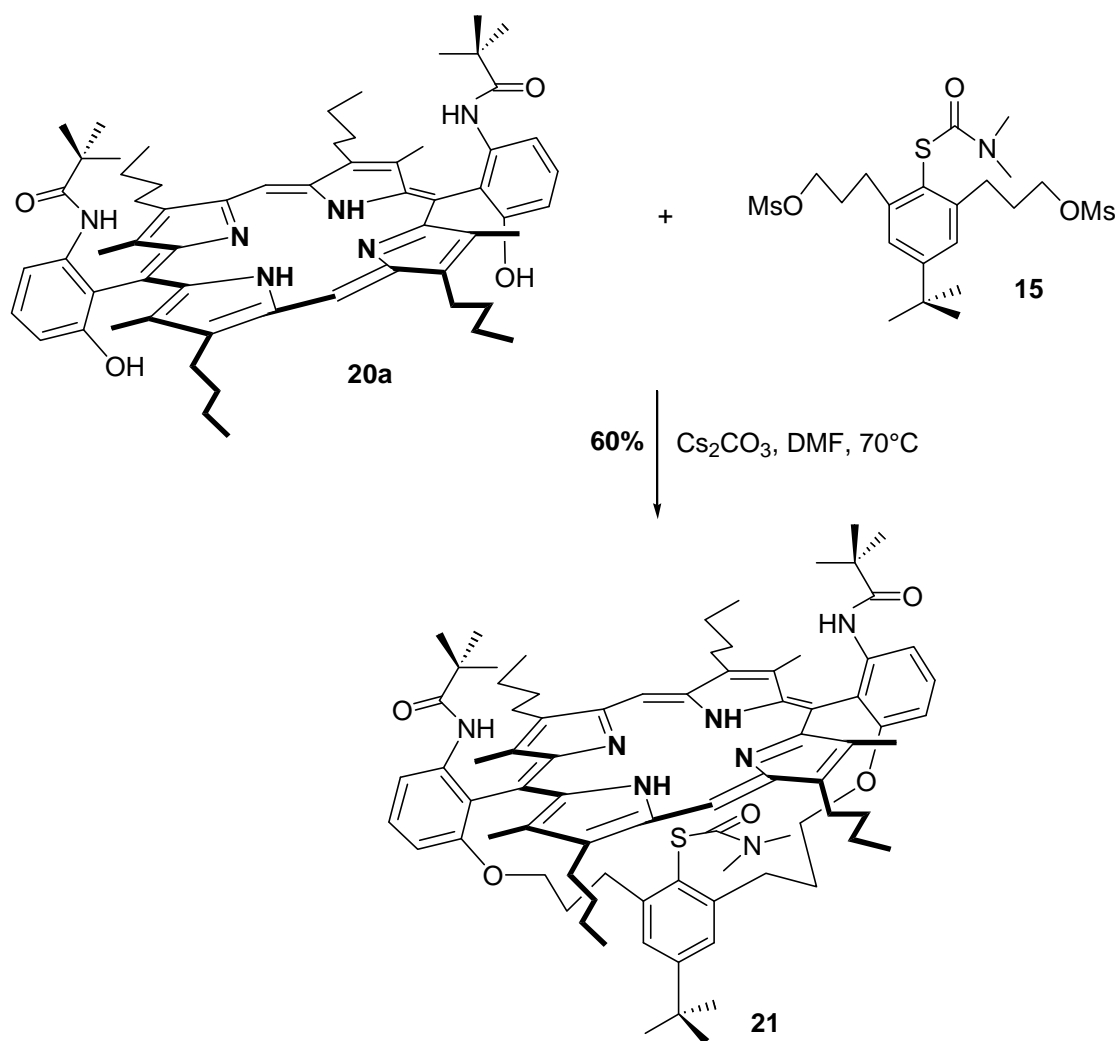
Scheme 4: Bridging step.
Note: the real conformation of the amide moiety is shown in figures 31 and 32

With **20a** we obtained from the crude reaction mixture a mass spectra composed of two peaks by MALDI-TOF: the M$^+$ peak and a peak with [M+133]$^+$ corresponding to the cesium complex of the   desired porphyrin. The cesium was removed by an acidic work-up to furnish the S-protected bridged porphyrin **21** in 60% yield.

When **20b** was used the product mixture could not be directly analysed by MS. Upon repeated column chromatography purification using a mixture of toluene: methylene chloride and methanol (1:1+10% V/V) and addition of a matrix for MALDI-TOF we were able to obtain peaks with masses corresponding to: two porphyrins + two bridges, three porphyrins + three bridges. This result demonstrates that the mimic obtained with the α,β isomer **20b** is a mixture of porphyrin oligomers.

V.2.4.2. Characterization of the bridged porphyrin 21.

V.2.4.2.1. Differences upon bridging attempts.

The bridged compound was compared to the compounds obtained by working with the α,β isomer **20b**. The first markant difference is the TLC behaviour: whereas the desired compound runs with a retention factor of 0.3 in a system hexane: ethyl acetate: triethylamine (5:1+1% V/V) the products obtained in the second case stay on the baseline.

Second the UV-Vis spectra are different: the maximum of absorption (Soret band) is found at 414 nm for **21** and at 408 nm for the oligomers' mixture. This represents a 6 nm red-shifted for the bridged compound compared to the oligomers' mixture obtained from **20b**. The red shift which is observed after bridging could relate the increase of electron density on the porphyrin macrocycle. This could be the consequence of an interaction of the phenyl ring from the bridge via π interactions. If this hypothesis is correct the phenyl ring should be almost parallel to the porphyrin plane and relatively close to it. The second explanation for this shift could be a change in the geometry of the porphyrin macrocycle. It is known that the introduction of nitro groups or of further phenyl groups at the meso positions also induces a red shift which has been rationalized by a more distorted structure of the porphyrin core [91]. Therefore the shift could indicate that from the proposed saddled conformation of **20a** the core becomes either domed or ruffled. A second proposal, based on a study with tetraphenylporphyrins where the degree of phenyl substitution was increased, relates the red shift to a more important tilting of the phenyl substituents and not to an increased distorsion of the macrocycle [92]. In the case of **21** probably both factors, a more ruffled porphyrin core and a more important tilting of the phenyl groups accounts for this results as further indicated by NMR studies and force field calculation (see V.2.4.2.2.).

Next the NMR spectra are not superimposable: the bridged compound **21** gives a well resolved set of signals (*table 8*) whereas the oligomers' mixture gives raise to broad overlapping signals. The presence of the desired compound in the mixture can be excluded as signals found in the bridged compound **21** are absent in the spectra of oligomers.

Proton[a)]	δ/ ppm for 21 (obtained with pure 20a)	δ/ppm for the oligomers (obtained with pure 20b)
20	10.11	10.15-10.11
10	9.72	
5'	8.61	8.45 and 8.40
4'	7.77	7.77 and 7.71
3'	6.95	7.12 and 6.96
NHPiv	8.42	7.00 and 6.96
3", 5"	6.37	6.57 and 6.30
$CH_{2\alpha}$	3.92-3.82 and 3.62-3.52	3.98-3.81
$CH_{2\alpha'}$	4.17-4.04 and 3.98-3.85	3.98-3.81
$CH_{3pyrrole}$	2.72 and 2.55	2.62 and 2.55
$CH_{2\beta'}$	2.22	2.09-1.99
$CH_{2\gamma'}$	1.82-1.72	1.75-1.59
$CH_{2\beta}$	1.97-1.87 and 1.82-1.72	2.09-1.99
$CH_{2\gamma}$	1.72-1.62	2.09-1.99
$CH_{3\delta}$	1.145 and 1.135	1.75-1.59
2''' (*tert*-Butyl$_{bridge}$)	1.09	1.34-1.21
NHPiv (*tert*-butyl)	0.52	-0.03 to -0.28
$N(CH_3)_2$	1.72 and –1.32	0.9
NH$_{porphyrin}$	-2.0	-2.20—2.26

Table 8: ^{1}H-NMR shifts for the bridged/oligomer compounds.
a) see *figure 22* **for numeration. Conditions: 2 mM in CDCl$_3$ at 280K.**

V.2.4.2.2. Solution structure of the bridged compound 21.

As the structure in solution is important for the future metal insertion we have pursued our studies by NMR spectroscopy taking advantage of NOE effects and the possibility of working in two dimensions. The NOE peaks which are relevant in the determination of the predominant conformation of **21** are summarized in *table 9*.

NOE between	H$_{3'}$	H$_{5'}$	N$\underline{H}$Piv	NH$\underline{Piv}$	OCH$_{2\alpha'}$	Me pyrrole	N(CH$_3$)$_2$	N$\underline{H}$porphyrin	H$_{3'',5''}$
H$_{3'}$		-	-	-	w	-	-	-	-
H$_{5'}$	-		s	m	-	-	-	-	-
N$\underline{H}$Piv	-	s		s	-	-	-	-	-
NH$\underline{Piv}$	-	m	s		-	m	-	-	-
OCH$_{2\alpha'}$	w	-	-	-		m to s	-	-	-
Me pyrrole	-	-	-	m	m to s		-	-	m
N(CH$_3$)$_2$	-	-	-	-	-	-	s	m	-
N$\underline{H}$porphyrin	-	-	-	-	-	-	m		-
H$_{3'',5''}$	-	-	-	-	-	m	-	-	

Table 9: Selected NOE signals observed for 21.

The first conclusion from these data is a change in the conformation discussed for the aryl substituents in **V.2.3.5.**. The weak NOE which is observed between H$_{3'}$ and OCH$_{2\alpha'}$ indicates that the C$_{aryl}$-O$_{ether}$ bond is now in a trans conformation i.e. the structures which can represent it are **ttt** to **cct** (*figure 27*). This change is accompanied by a modification of the conformation of the C$_{aryl}$-N$_{amide}$ bond. The strong NOE observed between H$_{5'}$ and N$\underline{H}$Piv excludes a trans conformation of the C$_{aryl}$-N$_{amide}$ bond. The change to a cis conformation is further confirmed by the low field displacement of the resonance position of N$\underline{H}$Piv from 6.9 ppm to 8.5 ppm. So only structures **ctt** or **cct** can represents the proper conformation. Finally the medium NOE from H$_{5'}$ to NH$\underline{Piv}$ eliminates structure **cct**. The trans character of the N$_{amide}$-C$_{carbonyl}$ is also ruled out from the low field displacement of the NH$\underline{Piv}$ resonance signal from 0.01 ppm to 0.55 ppm. Therefore only structure **ctt** can represent the proper conformer as illustrated by *figure 31*.

From the ^{15}N satellites of the NH signal in the 1H-NMR spectra a coupling constant of 90 Hz was obtained. Based on that coupling constant the nitrogen atom was found to have a sp^2 character of almost 100% as for **17a** and **17b**. According to this result the N-C=O bond has a partial double bond character which induces the planarity of the amide group. The double bond character also induces a conjugation of the N-C=O with the phenyl group . This again implies that the aryl substituent are planar (*figure 31*).
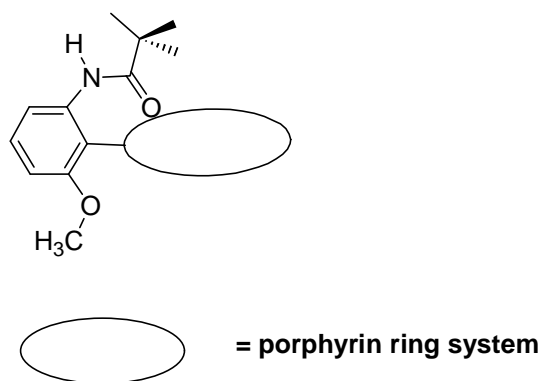
Figure 31: Conformation of the meso aryl substituents in 21 determined from the NOE effects.

This determined conformation is very surprising as the inversion of the geometry of the C_{aryl}-N_{amide} bond demands energy (around 40 kcal mol^{-1}) and contrasts with the known crystal structures obtained by Collmann for aryl substituents in TPivPP iron complex [85].

Further changes are obvious. The meso proton are splitted in a set of two singulets as are the β-methyl from the pyrrole. The butyl chains are also splitted in a set of two signals which are in part resonating at the same frequencies. This implies that the pyrrole rings from the porphyrin are differentiated. This differentiation is due to the bulk induced by the bridge and more particularly by the protecting group of the sulphur. This symmetry distortion implies that the bridge is nearly parallel under two of the pyrrole rings (*figure 32*). The molecule **21** is sterically constrained as confirmed by the diastereotopy of the $OCH_{2\alpha'}$ groups. In other words little flexibility may be possible in the structure.

The proximity of the sulphur to the centre of the porphyrin ring is the next important point to verify. Namely the sulphur has to point in the direction of the porphyrin ring to enable a future coordination to the central iron atom which will be inserted. From the NMR spectra we have a clear indication that the sulphur is in the proper position. First the NCH_3 signals are splitted into two broad singulets, one of which is found at very high field (δ= -1.32 ppm). This shielding can only result from the porphyrin ring current as it is established from the NOE observed that the phenyl ring is under two pyrrole rings. Second NOE peaks are observed between the NCH_3 of the sulphur protecting group and the NH signals from the porphyrin.

The subsequent force field calculation of the structure gives the following picture (*figure 32*).
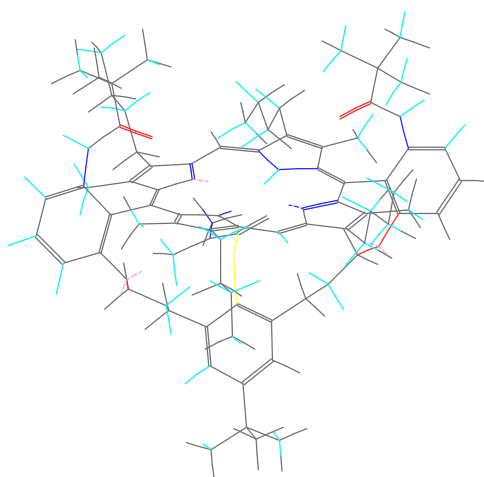
Figure 32: Structure of 21 based on NMR data after force field optimisation.

V.2.4.3. The free thiol porphyrin 22.

The metal free complex was next obtained by deprotection of the thiocarbamate group. As thiocarbamoyl groups are known to be cleaved by either reductive conditions [93] or strong bases [94], both methods were tried to find optimal conditions (*table 10*).

Method:	Conditions:	Result:
reduction	100 eq. NaH, THF, reflux	No reaction
reduction	1000 eq. NaBH$_4$, THF, reflux, 48 hr.	No reaction
reduction	Me$_3$OBF$_4$, then NaBH$_4$, THF, RT	No reaction
reduction	1000 eq. LiAlH$_4$, THF, reflux 24 hr.	Aluminium insertion into porphyrin
reduction	500 eq. LiAlH$_4$, 500 eq. AlCl$_3$, THF, reflux	No reaction
basic deprotection	100 eq. KOMe, MeOH, reflux	No reaction
basic deprotection	100 eq. KOMe, dioxane, reflux	95% yield

Table 10: Deprotection of the thiocarbamate.

The deprotection only proceeded under strong basic conditions using 100 eq. of KOMe in dioxan at 100°C (*scheme 5*). The yield obtained was nearly quantitative and the thiol function is surprisingly little sensitive to oxidation: leaving the compound in air for more than one day did not reveal any oxidation as proved by the clean NMR and mass spectra obtained.
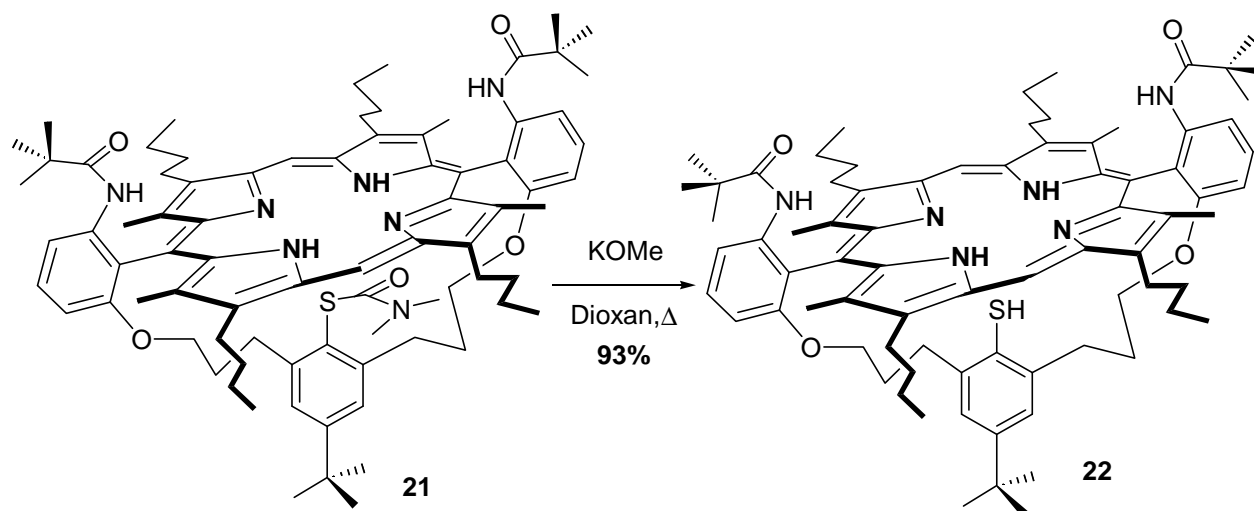
Scheme 5: Deprotection of the thiocarbamate.

As for the other steps the solution structure was determined by NMR. The conformation of the aryl substituents of **22** remain identical to the one of **21** as the same NOEs are observed. Upon heating the conformation of the aryl moiety did not change. The meso protons, the methyl on the pyrrole and the butyl side chains are now giving for each distinct group of proton a single resonance signal (*table 11*). This means that the symmetry of the pyrroles has been recovered upon deprotection. Such a situation is induced by a change in the placement of the bridge relative to the porphyrin macrocycle. It lies now more perpendicular respective to the tetrapyrrolic macrocycle probably to maximize a possible hydrogen bond between the SH and nitrogen from the pyrrole. This assumption is confirmed by the exchange peak between the NH of the porphyrin and the SH. It is particularly strong whereas the exchange peak with water for both the SH and the $NH_{porphyrin}$ signal is very weak. The chemical shift of the SH which is found at the very high field value of –3 ppm for a thiol group (typical shift for SH: 2 to 6 ppm) reveals that the thiol functionality is located in the vinicity of the centre of the porphyrin ring. Thereby the sulphur atom will be ideally placed for a future coordination with the iron atom.

Proton[a)]	δ/ppm
$H_{10,\,20}$	10.12
$H_{5'}$	8.64
NHPiv	8.46
$H_{4'}$	7.77
$H_{3'}$	6.94
$H_{3'',\,5''}$	6.2
$CH_{2\alpha}$	4.05-4.02 and 3.94-3.9
$CH_{2\alpha''}$	3.62
$Me_{pyrrole}$	2.62
$CH_{2\beta}$	2.12
$CH_{2\gamma}$	1.67
$CH_{3\delta}$	1.05
$H_{2'''}$ (*tert*-butyl$_{bridge}$)	0.87
$CH_{2\gamma'}$	0.67
NH<u>Piv</u> (*tert*-butyl)	0.55
$CH_{2\underline{b}'}$	0.47
N<u>H</u>$_{porphyrin}$	-2.13
S<u>H</u>	-3.01

Table 11: NMR chemical shifts for 22
a) see *figure 22* for numbering, Conditions: 2 mM in CDCl$_3$ at RT.

The force field calculation illustrates the structure proposed in solution (*figure 33*).
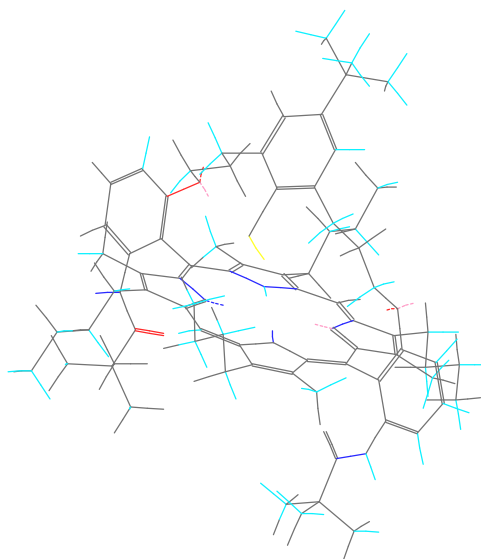
Figure 33: Force field molecular modelling of the thiol porphyrin 22.

V.2.4.4. The iron insertion.

Finally the iron was inserted to obtain the target molecule. This step revealed difficulties to obtain pure compounds using standard procedures (*table 12*).

Method:	Conditions:	Results:
Iron (III) salt, solvent	FeCl$_3$ hydrate, toluene, reflux	No insertion
Iron (II) salt, base, solvent	30 eq. FeBr$_2$, 2,6 lutidine 60 eq., toluene, reflux	100% insertion **< 10%** pure **11**
Iron (II) salt, base, solvent	10 eq. FeBr$_2$, 20 eq. Et$_3$N, toluene, reflux	100% insertion, **75%** pure **11**

Table 12: Iron insertion methods.

We postulated that the use of a functionalised pyridine counter base- 2,6 lutidine, led to the formation of pyridine oxides. The latter are generated by the trace of oxygen which remain despites working in a glove-box (O$_2$ level about 0.1 ppm) or with Schlenk tubes. They are responsible for porphyrin oxidation probably via the formation of an high valent iron-oxo species (*scheme 6*).
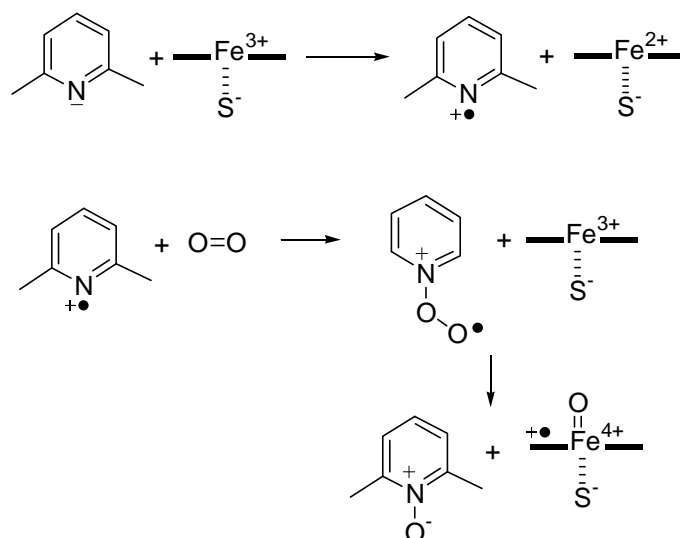
Scheme 6: Possible degradation of the porphyrin in the presence of N-oxides

To circumvent this problem we used triethylamine (*scheme 7*) as other iron insertion methods did not work with an analogue bridged species [95].

Actually the use of triethylamine prevents porphyrin oxidation thereby increasing the yield in pure product up to 75% (*scheme 7*). The purification could be achieved simply under an argon or nitrogen atmosphere as the iron complex turned out to be stable even after prolonged exposure to air.

22

75% | FeBr$_2$, Et$_3$N, Toluene, Δ

11
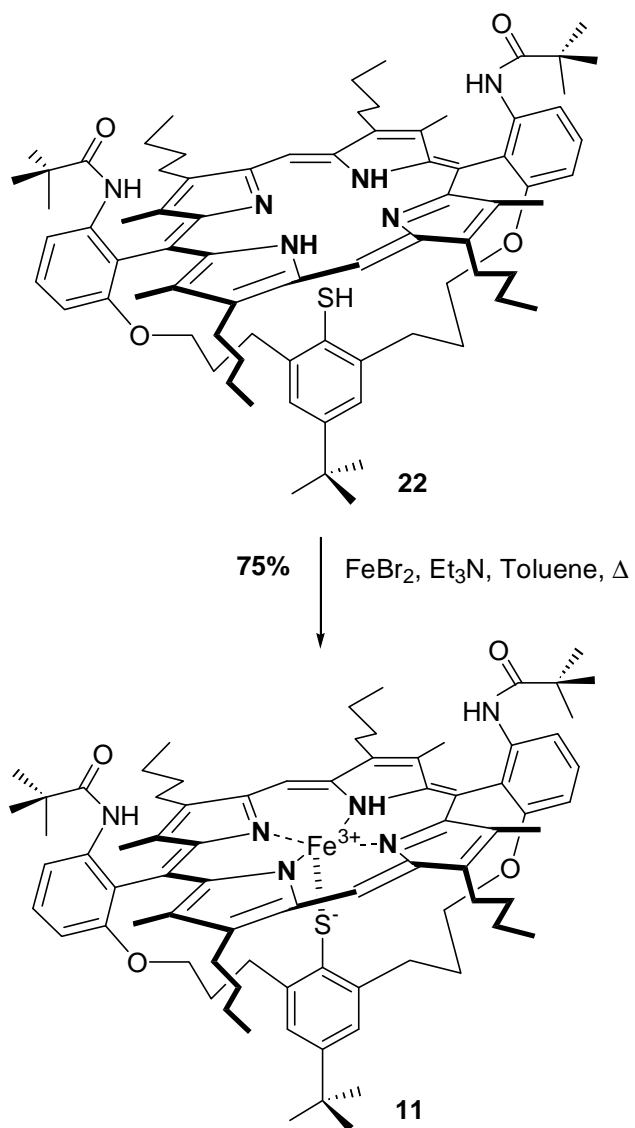
Scheme 7: Iron insertion.

V.2.5. Synthesis of the catalase mimic 12.

The target structure **12** is the following (*figure 34*). The synthesis relies on the same retrosynthesis as for the CPO model **11** (*scheme 1*).
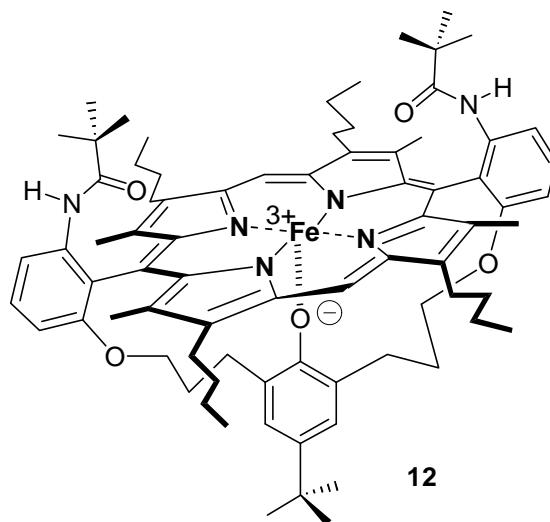
Figure 34: Target catalase model 12.

V.2.5.1. Synthesis of the bridge moiety 16.

The synthesis of the proper bridge **16** shown in *scheme 8* for obtaining the desired structure **12** is similar to the synthesis used for the sulfo bridge **15**.
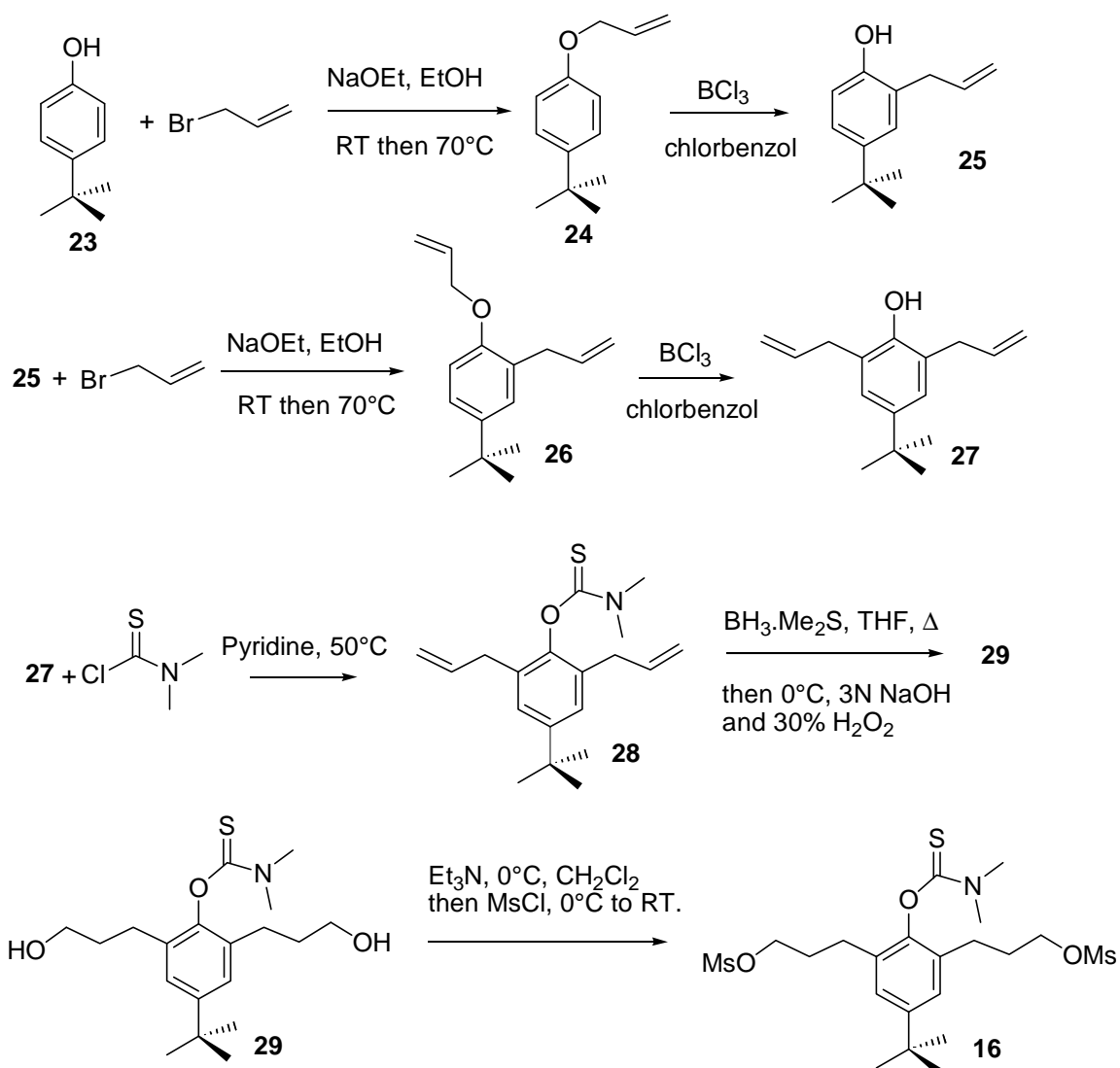
Scheme 8: Synthesis of bridge 16.

Upon two successive allylether formation and Claisen rearrangement the tetra substituted phenol **27** obtained is protected as thiocarbamate. Subsequently the double bounds are hydroborated and the alcohol functionalities are subsequently transformed to the corresponding mesylate.

For the sulfo bridge **15** used for the obtainment of the CPO model **11**, a Newmann-Kwart rearrangement is done before the hydroboration step which yields **26**.

V.2.5.2. Bridged porphyrins 30 and 31.

As for **21** the bridge **16** was coupled to pure **20a** under dilute conditions and slow addition of it to yield the protected phenolate analogue **30** of **21** (*scheme 9*).

19a + 16

60% | Cs$_2$CO$_3$, DMF, 70°C
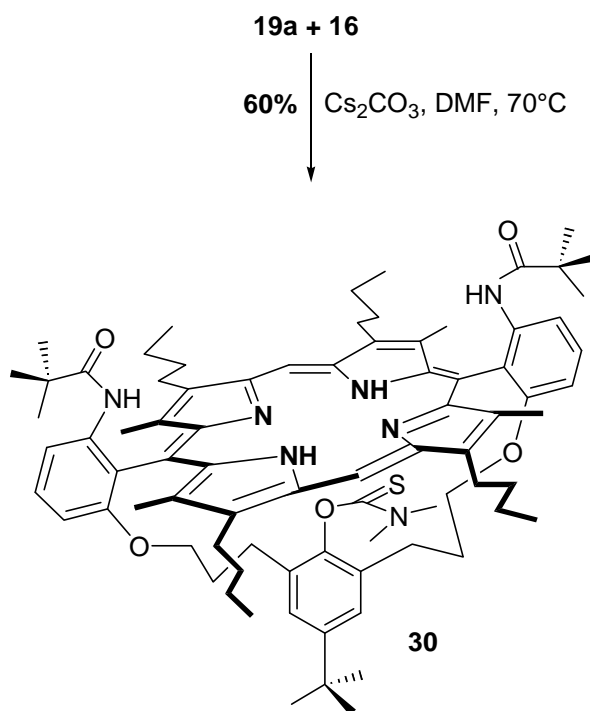
Scheme 9: Synthesis of 30.

If the UV-Vis spectrum of **30** is not different from the one obtained for **21** the NMR reveals slight shifts indicative of a different conformation for the bridge moiety of **30** compared to **21** (*table 13*).

Proton[a)]	δ/ ppm for 30	Δ(δ)/ppm from 21
20	10.10	-0.01
10	9.71	-0.01
5'	8.59	-0.02
4'	7.77	0
3'	6.98	+0.03
NHPiv	**8.29**	**-0.13**
3", 5"	6.33	-0.04
$CH_{2\alpha}$	4.15-3.6	0.2
$CH_{2\alpha'}$	4.15-3.6	0.02
$CH_{3pyrrole}$	2.69 and 2.55	-0.03 and 0
$CH_{2b'}$	**0.1**	**-2.12**
$CH_{2g'}$	**0.03**	**-1.57**
$CH_{2\beta}$	2.2	-0.02
$CH_{2\gamma}$	1.75	0
$CH_{3\delta}$	1.14 and 1.12	0 and –0.01
tert-butyl bridge	**1.26**	**+0.17**
NHPiv (*tert*-butyl)	0.47	-0.05
$N(CH_3)_2$	**2.1 and –2.17**	**+0.38 and –0.85**
$NH_{porphyrin}$	**-2.2**	**-0.2**

Table 13: NMR chemical shifts for 30 compared to 21.

The NOE effects which are essentially identical to the one observed for **21** and the 2D-NMR spectra lead to the following proposed structure (*figure 35*).
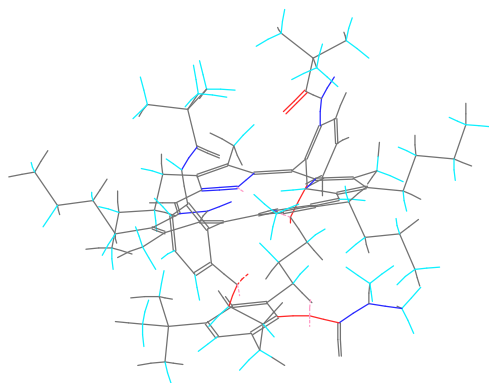
Figure 35: Solution structure of 30.

In the next step (*scheme 10*) the thiocarbamate was deprotected under milder conditions as only 60 eq. of KOMe were necessary to obtain pure **31** with 95% yield.
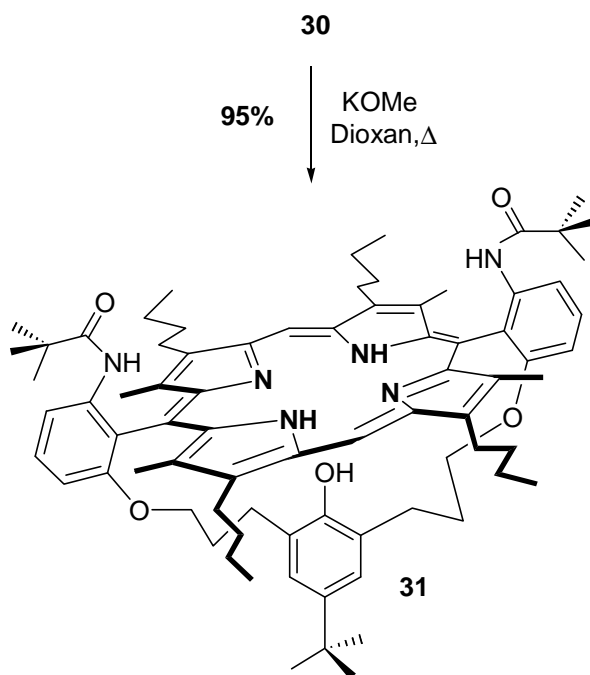
Scheme 10: Synthesis of 31.

As for **30** the same NOE signals are comparable to the data obtained for **22**. But they are for some signals of the bridge moiety stronger. The chemical shifts of the signals which are attributed to the bridge moiety are also slightly different (*table 14*).

Proton[a]	δ/ppm for **31**	$\Delta(\delta)$/ppm **from 22**
$H_{10,\,20}$	10.14	0.02
N$\underline{H}$Piv	**8.36**	**0.10**
$H_{3",5"}$	6.11	0.09
$CH_{2\alpha}$	3.94	0.2 for one set of **21**[b]
$CH_{2\alpha"}$	3.65	0.03
CH_3 pyrrole	2.65	0.03
$CH_{2\beta}$	2.06	0.06
$CH_{2\gamma}$	1.71	0.06
$H_{2""}$ (tert-butyl)	**0.89**	**0.22**
NH$\underline{Piv}$ (*tert*-butyl)	0.53	0.02
$CH_{2\beta"}$	0.5	0.03
$CH_{2\gamma"}$	0.08	**-0.79**
O$\underline{H}$	**-2.15**	**+0.85**
N$\underline{H}_{porphyrin}$	**-2.29**	**-0.16**

Table 14: Selected chemical shifts of 31 compared to 22.
a) see *figure 22* for numbering, b) in 22 the corresponding protons are splitted in two multiplets (table 11), Conditions: 2 mM 31 , 300 MHz, CDCl₃, RT.

Taken together these observations indicates that the phenolate is closer to the porphyrin core than is the thiolate. The perpendicularity of the bridge respective to the porphyrin plane is also increased as confirmed by force field calculations (*figure 36*).
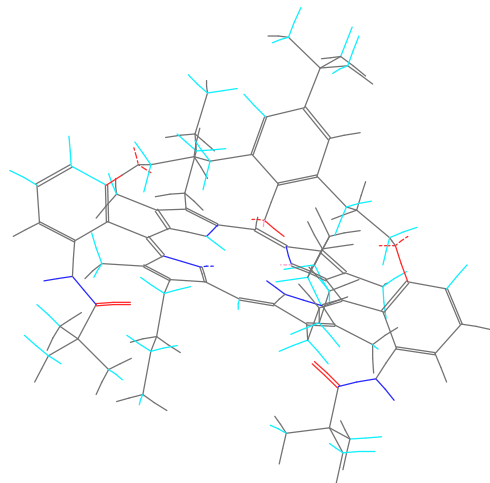
31

Figure 36: Solution structure for free phenol porphyrin 31.

The conformational analysis based on the NOE effects reveals that the change of geometry obtained for the C_{aryl}-C_{amide} bond in comparison with **18a** and **20a** in the bridged structure **21**, **22** (precursors of CPO model **11**) and **30**, **31** (precursors of catalase model **12**) is a unique feature due to bridging.

Finally the catalase mimic **12** was obtained from metal free precursor in 90% yield using the same iron insertion procedure as for **11**. Noteworthy the time which was necessary for the iron insertion increased from 1 hr. to 12 hr. probably reflecting the difference in the geometry between both models and a difference in the redox potential between **22** and **31**.

VI. Resting State studies.

VI.1. UV-Vis spectroscopy.

UV-Vis spectroscopy is widely used for the characterisation of porphyrins as it requires very small quantities (nanomoles) of product. For iron porphyrin complexes it is a powerful method to characterize:

1. the oxidation state of the iron,
2. the nature of axial ligation and
3. the number of ligands.

The spectra of porphyrins are known since 1883 when Soret [96] identified the most intense absorption band of porphyrins. The spectra are reflecting two types of electronic transitions which give raise to two distinct types of absorption bands:

1. a very strong band known as the Soret band and
2. 10 to 100 times less intense satellite bands in the visible region (500 to 800 nm).

The number of distinct satellite bands depends i.a. on the presence or absence of a metal. Usually the metal free porphyrins are characterized by four absorption bands in the visible region whereas metal containing one only have two bands. The absorption bands are due to a π-π* electronic transitions. For metal containing porphyrin complexes the absorption bands corresponding to d-d transitions of the metal are not observed as their intensity is very low.

The classification of porphyrin spectra has been established by Gouterman et al. [97]. Three type of spectra are encountered with porphyrins. These are:

1. normal absorption spectra,
2. hyper absorption spectra and
3. hypso absorption spectra.

In normal absorption spectra the Soret band corresponds to a π electron transition from an $a_{1u}(\pi)$ or $a_{2u}(\pi)$ orbital to an $e_g(\pi)$ orbital. The a_{1u} or a_{2u} orbitals are the HOMO orbitals of the porphyrin ring system whereas the e_g orbital usually corresponds to the LUMO orbital of the porphyrin.

In hypsoporphyrin spectra the influence of the metal d orbitals induces a blue shift of the Soret band respective to the metal free precursor. This is due to the presence of a filled e_g (d_π) orbital of the metal which modifies the energy level of the HOMO and HUMO of the porphyrin.

With thiolate ligation a third type of spectra is encountered: the hyperporphyrin spectra. This is the case for the iron (II) spectrum upon binding of CO (carbon monoxide) and it is the signature of the thiolate ligation. Namely only with thiolate as a fifth ligand such a spectrum is obtained with hemes upon CO binding. The Soret band is red shifted compared to the metal free one and the Soret band is accompanied by new strong absorption bands which are not attributed to the HOMO/LUMO transitions. They are due to strong interactions of the metal d electrons with the porphyrin orbitals which creates charge transfer interactions. Among these spectra the most current case is the presence of a "split Soret" band. One Soret band is found blue shifted compared to normal porphyrin spectra between 350 and 390 nm whereas the second one is found red shifted between 440 and 480 nm. The origin of the splitting of the Soret band is complex in the case of heme thiolate complexes and can not be explained only by charge transfer interactions between the ring and the metal. It is probably due to the transition of a π electron of the thiolate to the LUMO of the porphyrin [98].

VI.1.1. The CPO model 11.

The UV-Vis spectra obtained with the CPO model **11** reveal some solvent dependence regarding the shape of the absorption bands. The Soret band is more broadened in methylene chloride than in toluene. The use of MeCN, DMSO or DMF which can potentially coordinate to the iron results in contrary to a less broadened band but no shift of the absorption maxima are observed. This indicates that DMF, DMSO or MeCN probably do not coordinate to **11** as upon coordination a change in the geometry and electron density would happen. This would cause a change in the value of the Soret band.

The results suggests that the CPO model **11** is a five coordinated complex. Namely if **11** would be a six coordinated complex this would imply that the sixth ligand is a stronger ligand than DMSO, DMF or MeCN. But from the synthetic procedure the ligands which can occupy the sixth axial position can only be bromide (from the iron dibromide) or water (present in the solvents and silica gel used for chromatography). Both ligands are known to be weaker ligand than DMSO or DMF which strongly supports the five coordinated state for **11**.

The spectrum in toluene (*figure 37*) is characterized by a broadened Soret band at 406 nm with a slight shoulder at 380 nm. After protonation with strong acids such as HCl or HBr the Soret band shifts to 390 nm and the shoulder disappears. The modification of the spectra upon acid addition indicates that the sulphur is fully deprotonated upon iron

insertion. We propose that the shoulder is a contribution of the thiophenolate ring to the UV-Vis spectrum.

In the visible region the spectrum is rather featureless. Only broad bands having maxima at 512 nm and 580 nm are observed. This pattern is typical of high spin iron (III) complexes.

The iron oxidation state was also checked by addition of reductants. Upon addition of potassium superoxide, tretraethylammonium cyanide or sodium borohydride the Soret band is shifted to 418 nm and is less broadened. This 10 nm red shift is typical of a reduction process centered on the iron.

VI.1.2. The catalase model 12.

The UV-Vis spectra of the catalase model **12** are solvent independent with the exception of acetonitrile which causes a 2 nm blue shift of the Soret band. The visible region is composed of broad bands centered at 485 and 600 nm. As discussed for the CPO model **11** the absence of solvent effect on the Soret band indicates that **12** is most probably a five coordinated iron (III) complex. The shift in MeCN could nevertheless suggest a coordination of the solvent to the iron.

Contrary to **11** the Soret band is clearly separated from a shoulder at 354 nm (*figure 37*). As is the case with **11** the shoulder disappears upon addition of acid and the spectra obtained are characterized by a broadened Soret band at 390 nm. The shoulder, based on the native protein spectra, is attributed to the phenolate ring [35].
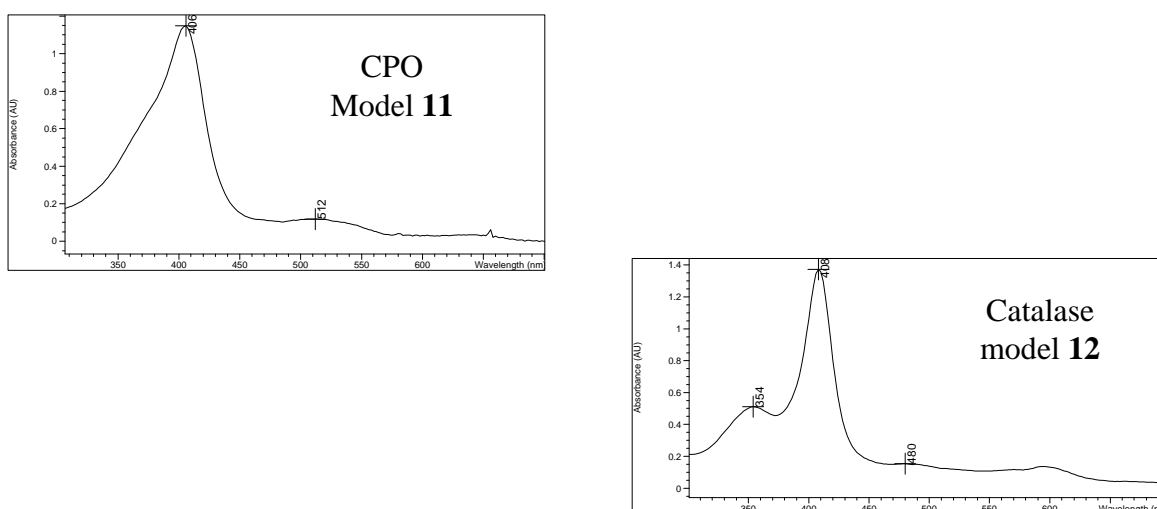
Figure 37: UV-Vis spectra of complexes **11** and **12** in toluene at RT.

VI.2. NMR spectroscopy.

The use of NMR spectroscopy in paramagnetic species is of great interest since many structural informations can be deduced from the spectra of heme proteins.

VI.2.1. Paramagnetic NMR.

To describe the interaction of a spin system **I**, **S** in a magnetic field in liquids one can start with the time independent Schrödinger equation:

$$\mathcal{H}\,\psi = E\,\psi\,. \quad \text{eq. (1)}$$

Where $\mathcal{H}$ is the spin Hamiltonian operator, E the corresponding observable energy and ψ the eigen function. This is the same formalism as the one used for electrons in a molecule. The Hamiltonian for paramagnetic NMR have three terms:

$$\mathcal{H} = \mathcal{H}_{\text{Zeeman}} + \mathcal{H}_{\text{S}} + \mathcal{H}_{\text{paramagnetic}}. \quad \text{eq. (2)}$$

The scalar spin spin coupling Hamiltonian $\mathcal{H}_{\text{S}}$ which is important for the EPR spectroscopy will be discussed later in VI.2.3. The first term, the spin Zeeman Hamiltonian, describes for one spin the energy of the interaction of the magnetic moment **m**, which is proportional to the spin of the nucleus $\mathbf{m} = \hbar\,\gamma\,\mathbf{I}$ and the magnetic field B_0. $\mathcal{H}_{\text{Zeeman}}$ becomes:

$$\mathcal{H}_{\text{Zeeman}} = -\,\hbar\,\gamma\,B_0\,\mathbf{I_z} = -\,\hbar\,\omega_0\,\mathbf{I_z.} \quad \text{eq. (3)}$$

Where $\hbar$ is the reduced Plank's constant, ω_0 the rotation frequency and γ the gyromagnetic ratio. For a nucleus with a spin number ½ the energy difference for the observable transition is then given by:

$$\Delta E = \hbar\,\gamma\,B_0 = \hbar\,\omega_0. \quad \text{eq. (4)}$$

In the nature the nuclei are not isolated, but are part of a molecule. Due to interaction with the electronic shells of other atoms of the molecule and with other molecules the effective field B' seen is reduced and the transition energy becomes:

$$\Delta E = \hbar\,\gamma\,B_0\,(1 - \sigma) = \hbar\,\gamma\,(B_0 - B_{\text{diamagnetic}}) \quad \text{eq. (5)}$$

where the correcting factor σ is known as the isotropic shielding constant.

The third term in eq. 2, the so-called isotropic or paramagnetic Hamiltonian, now represents the interaction of the nucleus with the paramagnetic moment, normally an unpaired electron, **S** and has itself two parts:

$$\mathcal{H}_{\text{paramagnetic}} = \mathcal{H}_{\text{dipolar}} + \mathcal{H}_{\text{contact}} \quad \text{eq. (6)}$$

The first term in eq. 6 is the classical dipole dipole Hamiltonian $\mathcal{H}_{\text{dipolar}}$ and represents the interaction between the dipolar moment of the nucleus observed and the paramagnetic

center. The Fermi contact Hamiltonian $\mathscr{H}_{contact}$ is the result of a finite quantity of electron spin density on the place of the nucleus being observed.

To discuss the paramagnetic effect it is common to use the ratio of the relative change in the field and the external field B_0:

$$(\Delta B/B_0)_{isotropic} = (\Delta B/B_0)_{dipolar} + (\Delta B/B_0)_{contact} \quad \text{eq. (7)}$$

For discussion of paramagnetic effects we eliminate the also observed diamagnetic part according to eq. (5) by subtraction of that part to get the isotropic (or paramagnetic) shift:

$$(\Delta B/B_0)_{isotropic} = (\Delta B_{obs} - \Delta B_{diamagnetic}) / B_0. \quad \text{eq. (8)}$$

Both the Fermi contact shift and the pseudocontact shift can be calculated if some geometrical data are known or if the components of the magnetization in the x, y and z directions are known. Most formula used for determining the value of these shifts relies on oversimplifying hypotheses so that they only apply in cases where the symmetry of the complex is very high. Thereby their use is quite limited.

However the numerous studies on heme by NMR have permitted to establish guidelines for the attribution of the resonance signals and for determining the predominant origin of the paramagnetic shift. As we will deal principally with iron (III) complexes we will next develop in VI.2.2. the principles which have been established in this case.

Additionally the relaxation is important in the understanding of the NMR spectroscopy of paramagnetic compounds. By applying radio frequency (RF) pulses to a spin system in a magnetic field it is brought into a none equilibrium state. Relaxation is the process by which the spins return to their equilibrium state. The spin spin or transverse relaxation time T_2 directly influences the observed free induction decay (FID) after a RF pulse. A fast decay results in a short T_2 and after a Fourier transformation (FT) of the time domain signal to the frequency domain in broad lines in the spectra. In contrary if T_2 is long the lines become sharp. The longitudinal relaxation time T_1 also influences the NMR spectra, mainly the intensity of the observed lines. It is also called spin lattice relaxation time, because the spin exchanges energy with the environment. Important for paramagnetic NMR is that T_2 can always be only equal or lower than T_1.

VI.2.2. The ^{1}H-NMR of iron (III) porphyrin complexes.

The results obtained for iron (III) porphyrin complexes are first depending on the spin state of the complex. The two most common spin states encountered for iron (III) are the low spin (S=1/2) and the high spin (S=5/2) state. Both spin states are easily distinguished by NMR spectroscopy as in the high spin state the relaxation rate ($T_2 = 10^{-12} - 10^{-11}$ s^{-1}) is 10

times higher than for the low spin complexes ($T_2 = 10^{-11} - 10^{-10}$ s^{-1}). The short T_2 for high spin iron (III) heme complexes results in broadened signals. As the value of T_2 is smaller for iron (III) high spin species than for iron (III) low spin species the NMR spectra of high spin complexes are characterized by more broadened signals- typically the line width is over 300 Hz and up to 1,000 Hz- than for low spin systems where the line width ranges from around 100 Hz to 400 Hz. The second difference between both spin states is the range of chemical shifts observed. Whereas for high spin species a signal range of over 100 ppm is observed, the low spin complexes signals range from –20 to +20 ppm (40 ppm range) [99].

Most high spin iron (III) complexes which have been studied until now are five coordinated complexes as the presence of a sixth ligand usually induces a spin state change from high spin to low spin. The estimation of the dipolar and contact shift has been done for several TPP iron complexes [100] and for octaalkyl porphyrins [99] as well as for natural heme [101]. From these studies the following conclusions appear:

1. For the meso phenyl substituents the origin of the paramagnetic shift is approximately equally distributed between dipolar and contact shifts and is found in a range of ±6 ppm. Usually it is found positive for the ortho and para positions and negative for the meta position.

2. For the β pyrrole substituents the isotropic shift is essentially of contact origin and is strongly negative. It results in a very large isotropic shift of –30 to –60 ppm for the H, CH_3 or $CH_{2\alpha}$ at the β pyrrole position. The origin of the negative contact shift is the σ spin density at the pyrrole positions. A strong σ donation of the nitrogen lone pair in the Fe-N bond may increase this effect. The further CH_2 of the alkyl chains at β pyrrole position are practically not affected by the paramagnetic shift.

3. For the meso protons the origin is also essentially the contact shift. This shift is found to be very important and is usually positive. This results from a π spin density at the meso position which is consistent with the unpaired spin electron delocalisation from the d_{xy}, d_{yz} orbitals to the LUMO e_g orbital of the porphyrin ring system or to π back bonding (charge transfer).

4. However it has been pointed out that the sign of the contact shift for the meso position is dependent on the coordination number of iron. In five coordinated complexes the fifth ligand induces an out of plane displacement of the iron which results in a less important spin delocalisation to the porphyrin ring. In six

coordinated iron complexes the metal is in the "plane" of the porphyrin which results in a maximal spin delocalisation [102]. Consequently a positive isotropic shift for five coordinated iron (III) complexes and a negative isotropic shift for six coordinated iron (III) complexes is observed.

Accordingly the NMR spectra of high spin iron (III) porphyrin complexes are an essential tool for determining the coordination number of the iron.

VI.2.3. NMR spectra of the complexes.

In order to gain information on the coordination of an eventual sixth ligand to the iron and to determine the spin state of the complexes we have recorded their NMR spectra at different temperatures. The first point which was decisive was the choice of the solvent. Namely most of polar organic and protic solvents can coordinate to the iron. Thus the solvents which remain are: toluene or eventually chloroform. Toluene was used first as the characterization of catalytic intermediates was done in this solvent. The spectra obtained in toluene are characterized by broad lines ranging from –60 to +140 ppm at 295 K. The line width measured was up to 1,000 Hz. This is a first indication for an iron (III) high spin complex for **11**.

In order to assign the signals which are arising from the bridge moiety the spectra of the iron complex of **17b** has also been recorded. The later looks like the combined spectra of octaalkyl iron (III) porphyrins and of tetraphenyl iron (III) porphyrins. Hence the signals of the methyl pyrrole protons, $CH_{2\alpha}$ protons and of the aryl substituents were assigned by comparison.

The important signals for the CPO model **11** (*table 15*) were assigned according to the data obtained with the iron complex of **17b**. The signal at 90 ppm was assigned to the $H_{3",5"}$ protons of the thiophenolate moiety as the value is in good agreement with the value reported for free thiophenolate iron porphyrin complexes [103]. Moreover this signal is not detected in the non bridged complex.

Proton[a]	δ /ppm[b] d_8-toluene	δ/ppm (literature):
10, 20	-57.1	~ -50 [100]
3'	13.17	[100]
4'	10.61	11-13 [100]
5'	8.30	[100]
Me pyrrole	38.00	35-70[c] [99] [104]
$CH_{2\alpha}$	39.44 and 35.92	30-50 [99]
3", 5"	85.33	60 [103]
2''' (*tert*-butyl) or $CH_{2\alpha'}$[d]	5.37 and -1.57	d)

Table 15: ^{1}H-NMR of the CPO model 11 at 295 K.
a): numbering according to *figure 22*; b) relative to TMS; c) for natural hemes the methyl groups give a set of four resonance where two signals are found at 35-45 ppm and two at 55-70 ppm; d) the literature could not permit to attribute the signal unambiguously.

The temperature dependence of the spectra in d_8-toluene has been obtained in the range of –30°C to RT. The Curie plot (δ= f(T) where δ is the chemical shift and T the temperature) of chosen signals are presented in *figure 38*. The reference is always the true chemical shift uncorrected from the diamagnetic contribution.
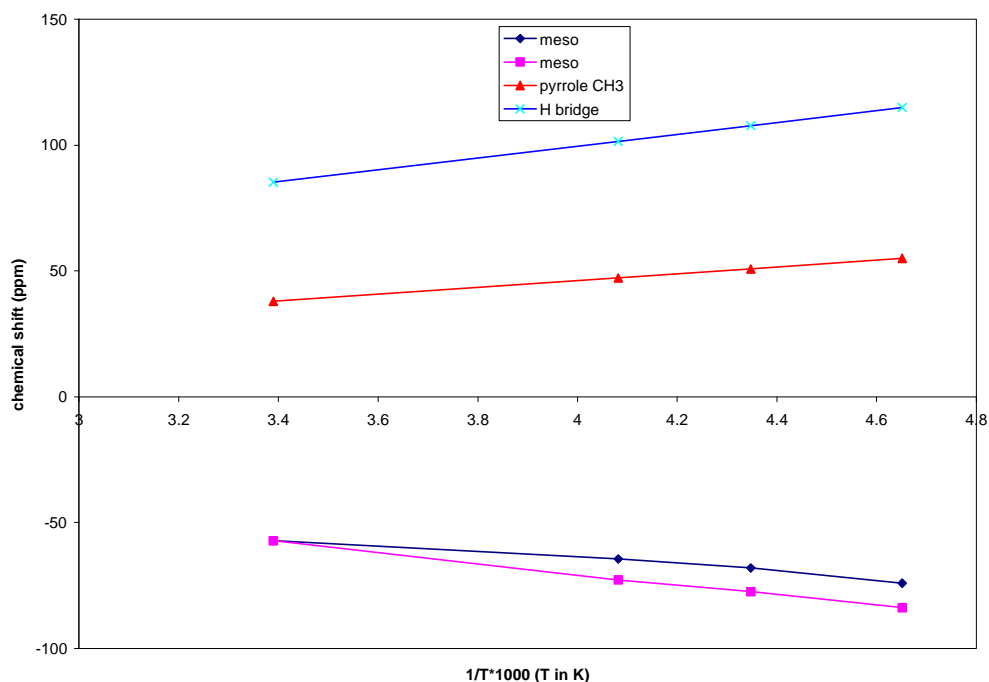
Figure 38: Curie plot of selected signals for 11 in toluene-d$_8$.

The results obtained, a quasi linear dependence of the chemical shift δ vs. the inverse of the temperature T, demonstrate that the porphyrin has a Curie behaviour i.e. no secondary Zeeman interactions occur. The splitting of the meso signals by lowering the temperature suggests that either several conformations are frozen out or that the complex is not symmetric. This finding suggests that the shape of the EPR spectra could be unusual and may confirm this result.

VI.3. EPR spectroscopy.

The use of EPR spectroscopy in the determination of the spin state of iron complexes is a preferred method for physical chemists. EPR spectroscopy and NMR are complementary to each other. Whereas the NMR gives geometrical information on the molecule the EPR deals with the electron repartition in the d orbitals of the iron. Both techniques give the spin state but the symmetry around the iron can only be ruled out from the EPR. Nowadays the combination of both techniques has led to the development of ENDOR (electron nuclear double resonance) spectroscopy.

VI.3.1. EPR spectroscopy [105].

To interpret the EPR spectra of unpaired electrons we can use the same formalism as for NMR spectroscopy. The Zeeman Hamiltonian of eq. 2 becomes for an isolated electron **S** in analogy with eq. 3:

$$\mathcal{H}_{Zeeman} = - g \, \boldsymbol{b} \, B_0 \, S_z = - \hbar \, \omega_0 \, S_z \quad eq. (9)$$

where $\hbar$ is the reduced Plank's constant, $\boldsymbol{b}$ the Bohr magneton and B_0 the magnetic field.

The g factor is the most widely used information extracted from an EPR spectrum. The energy difference is according to eq. 4:

$$\Delta E = g \, \boldsymbol{b} \, B_0 = \hbar \, \omega_0. \quad Eq. (10)$$

Usually it is denominated g_{eff} as it is the value calculated from the B_{eff} value where the resonance occurs.

To describe additionally the interaction with nucleus spins **I** the spin spin coupling Hamiltonian $\mathcal{H}_S$ is necessary and g becomes a tensor quantity:

$$\mathcal{H}_S = g \, \boldsymbol{I} \, \boldsymbol{S} \quad eq. (11)$$

where is *S* the electron spin tensor and *I* the nucleus spin tensor.

The hyperfine interaction between *S* and *I* gives important information on the environment of the paramagnetic center.

In EPR spectroscopy the continuous wave (CW) technique is still widely used and the first derivative of the absorption signal registered is plotted *vs.* the magnetic field.

For heme protein the Hamiltonian is usually expressed in function of the projection of **S** and **I** in the x, y, z directions. And has the following expression:

$$\mathcal{H} = g \, \boldsymbol{b} \, B \, S + D \, [S_z^2 - 1/3 \, S(S + 1)] + E \, (S_x^2 - S_y^2] \quad eq. (12)$$

where E is the rhombic component and D the tetragonal component.

VI.3.2. ENDOR spectroscopy (electron nuclear double resonance) [106].

CW-ESR only reflects the spin state and the geometry around the iron but is insufficient to reveal the number of ligands coordinated to the iron. NMR on the other hand permits to see ligands which possess a nucleus spin suitable for NMR. This situation is fortunately the case for many ligands encountered with porphyrins. Therefore since twenty years scientists are developing methods which combine the power of both EPR and NMR. The combination of both method has led to the ENDOR spectroscopy.

The value of the coupling constant between the electron spin of the metal and the nuclear spin of the nucleus observed by NMR is the most useful piece of information extracted

from an ENDOR spectra. It permits to determine the local geometry around the paramagnetic center.

VI.3.3. Results for the CPO model 11.

The EPR spectra of the thiolate complex **11** recorded at 100 K and 5 K do not show any temperature dependence of the spin state (*figure 39*). This results is in contrast with the known spin state change of CPO upon lowering the temperature [107].
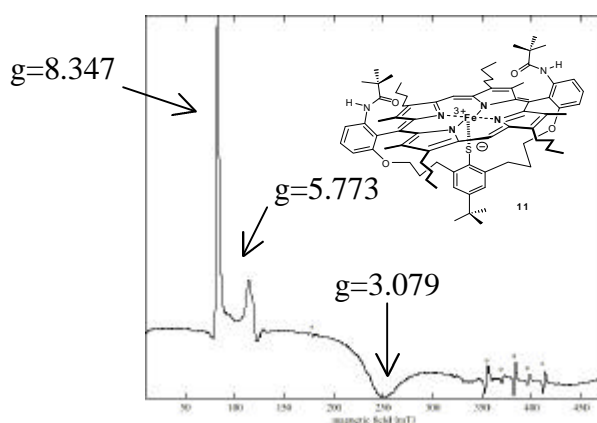
*: the signals are artefacts from the machine

Figure 39: CW-EPR spectrum at 5K of 11.

The position of the EPR lines which are found at g_{eff}= 8.35, 5.77 3.07 and 2.00 are indicative of an high spin configuration. These values are usually obtained for the resting state of heme-thiolate proteins at RT or for the heme-substrate complex of them. The additional sharp absorption-like line at g_{eff}=8.35 and the broad line at g_{eff}= 3.07 strongly contrast with the previous results obtained by *Aissaoui et al.* with an aqua complex [108]. The aqua complex was namely characterized by sharp first derivative like lines at g_{eff}= 5.67 and at g_{eff}=2.00. Nevertheless the spectrum obtained with the CPO model **11** is in good agreement with the water free complex of them [109] where no sixth ligand is found. The shape of the spectra and the g_{eff} values are usually attributed to a rhombic symmetry around the iron. This kind of symmetry is also found in native CPO [107], P450$_{cam}$ substrate bound [110] and NOS [111]. In as much as the symmetry is concerned the CPO model **11** is an excellent mimic of the CPO resting state at higher temperature. The lack of spin crossover may be related to the lack of binding a sixth ligand in toluene. Namely the change of spin state could be related to the coordination of an additional ligand upon freezing the protein structure in CPO. For example the proximal water molecule [10] may upon lowering the temperature change its spatial position and coordinate to the iron at the

vacant sixth position. This hypothesis is supported by the predominantly low spin character of $P450_{cam}$ without substrate where it has been proved by X-Ray diffraction that a water molecule coordinates to the iron [112].

However the recent progress in simulation of EPR spectra questions the validity of the rhombic symmetry explanation for the signals. Namely if one assumes a pure rhombic symmetry then $E/D=1/3$ and the g_{eff} values should be 4.3 and 2 approximatively. Therefore some authors have proposed that the local symmetry around the iron atom is still axial but that the influence of the additional parameters a and F in the description of the spin Hamiltonian (see eq. (12)) is not any more negligictable [113]. Accordingly the Hamiltonian $\mathscr{H}_S$ becomes:

$$\mathscr{H}_S = g\, \boldsymbol{b}\, B\, S + D\, [S_z^2 - 1/3\, S\, (S+1)] + E\, (S_x^2 - S_y^2] + a/6\, [S_z^4 + S_y^4 + S_x^4 - 1/5\, S\, (S+1)\, (3S^2 + 3S-1) + F/160\, [35\, S_z^4 - 30\, S\, (S+1)\, S_z^2 + 25\, S_z^2 - 6\, S\, (S+1) + 3\, S^2\, (S+1)^2] \text{ eq. (13)}.$$

The second proposal which is advanced is that the interactions between the g_{eff} factors is strong and negative (i.e. $g_\perp > g_\parallel$) [113, 114].

A distinction between the two last theses is not possible as the experiments do not permit to evaluate the parameters a and F.

However other possibilities can be enviewed. The first one which would account for the broad signal at $g_{eff}= 3.07$ and relies on the degree of flexibility of the CPO model **11**. The EPR simulations suggest that the signal at $g_{eff}=3.07$ is essentially due to a contribution of the sulphur from the bridge. As the sulphur is linked to the porphyrin via a "bridge" a certain degree of freedom for the placement of the bridge moiety respective to the porphyrin plane is possible. This freedom could generate several crystalline forms of **11**. This hypothesis is also supported by the temperature dependent NMR measurements which have revealed a splitting of the meso resonance signals upon lowering temperature.

The second possibility would be the role of the solvent used in defining the crystal network. Sharp line arise in EPR spectra when the paramagnetic centers are distributed randomly respective to the axis of the magnetic field. With toluene there is a tendency to form an oriented crystal network. This results in a non random distribution of the complex **11** in the EPR probe which could be the origin of the broadened signals as well. Moreover intermolecular interactions could occur and also yield to a broadening of the line by spin-spin coupling.

The last hypothesis is that a large amount of electron spin from the iron is delocalised to the sulphur via the σ-bond interaction. This would be also accompanied by a large out plane displacement of the iron i.e. by a large rhombic distortion.

Probably all hypotheses taken together contribute to the shape of the spectra obtained for **11** and further experiments are required to judge the most adequate proposal discussed above.

VI.3.4. Results for the catalase model 12.

The EPR spectra of the catalase model **12** (*figure 40*) show marked difference to the spectra of the thiolate complex **11** (*figure 39*). First the signal intensity for **12** at the same concentration is greater than for **11**. Such a result can be explained by a longer relaxation time for **12** than for **11**.

Second the spectra are characterized by two sharp signals at g_{eff}=5.83 and g_{eff}=2.00. Its shape is corresponding to classical first derivative signals in EPR spectroscopy. Whereas the spectra of thiolate complex **11** were rather indicative of a rhombic symmetry, the phenolate complex **12** presents an axial symmetry with a very weak rhombic distortion (indicated by the small shoulder in the g_{eff}=5.83 signal). For **12** the simulations [114] fit with the experimental spectra. The $g_∥$ factor which corresponds to g_{eff}= 5.83 represents the amount of spin in the z direction (i.e. parallel to the static magnetic field) and the $g_⊥$ which is g_{eff}=2.00 the amount of spin in the (x, y) plane. Such a spectrum is typical of a pure high spin iron (III) complex [115] and fits with the spectra of *Beef Liver Catalase* obtained by *Jung et al.* at neutral pH [116].
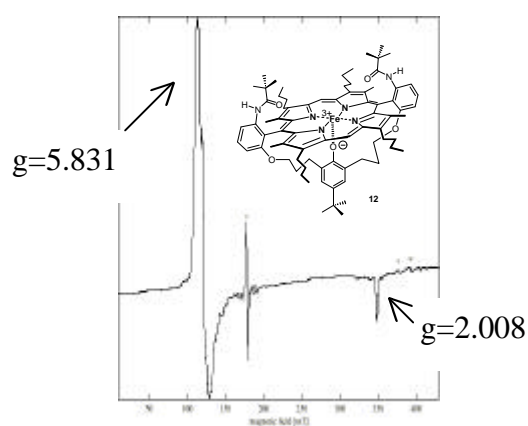
*: the signals are artefacts from the machine

Figure 40: CW-EPR spectrum at 5K of 12.

Attempts to detect an eventual sixth ligand by ENDOR spectroscopy did not reveal any nucleus coupling to the iron thereby confirming the NMR conclusions on a five coordinated high spin iron (III) complex for **12**. There are several proposals to explain the different shapes of the EPR spectra of **11** and **12**.

First in the case of the catalase model **12** a π back bonding interaction between the oxygen and the iron is not possible as the oxygen atom does not possess d orbitals. As the electronegativity of the oxygen is greater than the one of the sulphur, the σ bond between the oxygen and the iron in **12** is not as strong as in the case of the sulphur in complex **11**. This means that both the iron and oxygen conserve their spin density in **12** whereas in **11** the spin density of the iron is displaced to the sulphur.

Second the geometric characteristics (*table 16*) of the sulphur iron bond and the oxygen iron bond can also account for the results. The iron sulphur bond is longer than the iron oxygen bond when the crystallographic data of heme-thiolate proteins are compared to catalase (*table16*). This may also favour the out plane displacement of the iron in **11** compared to **12**. Also the angle of the phenyl-sulphur-iron and of the phenyl-oxygen-iron should be smaller for the CPO model **11** than for the catalase model **12**. These geometrical data implies that the geometrical flexibility for the complex **12** is lower than for complex **11**. Thereby there could be a single crystalline form obtained for **12** upon crystallisation which could contribute to sharper ESR signals.

Enzyme	Fe-S resp. Fe-O (in Å)	Angle (Fe-S-C) resp. Fe-O-C) (in °)
P450$_{cam}$	2.31	105.2
NOS	2.3	105.7
CPO	2.35	107.5
BLC	1.98	132.5

Table 16: X-Ray data for heme-thiolate proteins and catalase [117].

VI.4. Electrochemistry.

VI.4.1. Principle of the method: cyclic voltammetry.

The complete characterization of the resting state requires the estimation of the redox potential. The redox potential is a very important characteristic of the heme proteins as it

determines their ability to be reduced by NAD(P)H or a reductase enzyme. The ease of reduction is also linked to the ability to bind oxygen.

The factors controlling the redox potential are complex. Among them the nature of axial ligand, the presence of electron withdrawing/donating groups on the porphyrin skeleton, the nature of the substituents and the solvent are important factors that determine the value of the redox potential.

To estimate the redox potential the complexes were submitted to cyclic voltammetry. Cyclic voltammetry is a versatile method to study electroactive species. The principle is extremely simple: the potential of a working electrode is cycled and the resulting current is recorded. The electron exchange is achieved at the surface of the electrode. The parameters influencing the results are the scanning range of the potential, the scan speed, the salt and the solvent. The choice of the scan range is important to ensure a reversible process. The scan speed has also to be carefully chosen to avoid non diffusion controlled processes. It also depends on the stability or half-life time of the reduced species which is generated during the measurement.

VI.4.2. Results.

The cyclic voltammograms of both complexes **11** and **12** are typical of a reversible process which is a metal centered, one electron transfer to the electrode (*figure 41*). The difference between the anodic peak potential and the cathodic peak potential is 80 to 90 mV, a value characteristic of iron porphyrin complexes. Interestingly the value of the redox potential are very close from one to the other suggesting a minor role of the axial ligand in the determination of the redox potential (*table 17*).

Catalase model **12**

CPO model **11**
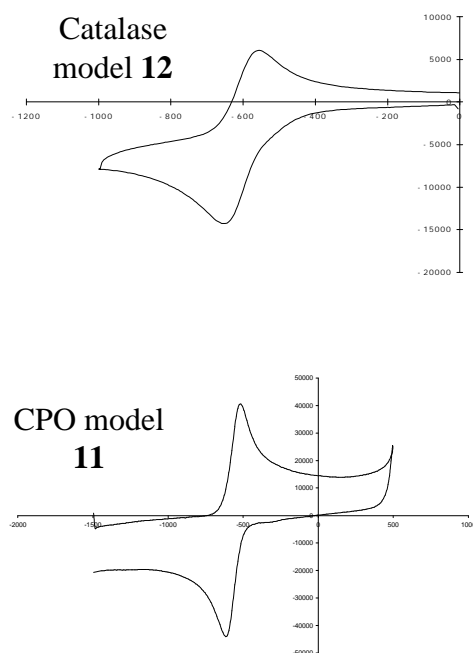
Figure 41: Cyclic voltammograms of 11 and 12.
Conditions: 2.3 mM **11** or **12** in 0.1M LiClO$_4$ DMF solution saturated with LiBr, scan
speed 100 mV s^{-1}.

Compound:	E$_{red}$ (mV):	E$_{ox}$ (mV):	DE (mV):	E^0 (mV):
11	-605	-525	80	**-565**
12	-640	-550	90	**-600**

Table 17: Values of the redox waves measured by cyclic voltammetry.

This finding is in strong contrast with the influence of the peripherical substituents. For comparison the replacement of the N-pivaloyl groups by an amide furan functionality shifts the potential positively of 250 mV [118]. This suggests that the protein environment is significant for controlling the redox potential and not the nature of the fifth axial ligand for a given spin state. More particularly the strong negative values obtained supports that the presence of hydrogen bond to the thiolate resp. phenolate is an essential factor in tuning the redox potential as demonstrated by *Morishima et al.* with P450$_{cam}$ mutants [119]. Recently *Ueyama et al.* have also shown that each hydrogen bond to the thiolate sulphur results in a positive shift of the redox potential of 250 to 300 mV [120-122].

The results with **11** and **12** also support that the thiolate resp. the phenolate strongly donates electron density to the iron in the absence of hydrogen bond.

VI.5. Summary.

The complete characterization of complex **11** and **12** has revealed that both species are high spin five coordinated iron (III) complexes. Therefore, as the data are comparable to the literature reports on the native enzymes, both **11** and **12** are good mimic of CPO and *Beef Liver Catalase* respectively.

The differences observed between **11** and **12** reflects that the axial coordination differ between thiolate and phenolate. On the base of NMR data, craft field modelling and published X-Ray structures of heme-thiolate proteins and catalase [117] we suggest that the angle between the thiolate ligand and the z-axis is smaller than for the phenolate and that the iron sulphur distance is greater than the iron oxygen distance. In other words the phenolate ring is more perpendicular to the porphyrin plane than is the thiophenolate ring. The sulphur has also a stronger σ bond to the iron which is reinforced by a π back bonding interaction. This results in the displacement of the electron spin of the iron to the sulphur. Such a situation does not occur with the oxygen phenolate.

VII. Characterization of catalytic intermediates.

After the characterization of the resting state the next problem was to determine the ability of **11** and **12** to form stable complexes with ligands. This investigation requires to find ligands with good binding constants and find conditions to minimise side-reactions such as porphyrin degradation.

VII.1. Preliminary studies with water.

As mentioned in VI.3.3. CPO induces a spin state change when the temperature is lowered [107]. We have postulated that the binding of a water molecule upon freezing could be the reason of this spin crossover phenomenon. In order to verify this assumption we have examined the possibility of obtaining a water complex of **11** and **12**. Therefore we have attempted to detect water binding under several conditions summarized in *table 18*:

Solvent:	Water (% vol):	Time:	Result:
Toluene	3% (toluene saturation)	24 hr	No binding
Toluene	50% (biphasic system)	48 hr	No binding
MTHF[a]	MTHF saturated with water	48 hr	No binding

Table 18: Attempts to form water complex of 11 and 12.
a) MTHF= 2-methyltetrahydrofuran.

The conditions chosen took into account the requirement of the EPR and ENDOR techniques which limit the choice of solvent to obtain good results i.e. a good matrix [123]. The formation of a water complex was followed by UV-Vis spectroscopy. If water would bind to the five coordinated complex a red shift of the Soret band is expected to occur as the electron density around the iron is increased.

Despites several experiments varying the reaction time no change in the UV-Vis spectra of both the CPO model **11** and the catalase model **12** were detected. This suggests that water does not bind at the sixth axial position of iron.

To verify this assumption NMR and EPR spectra were also recorded for **11** and **12**. The NMR spectra remained unmodified with the meso signals being still detected at –50 ppm indicating that no coordination of a water molecule to the iron happened at RT either with the CPO model **11** or the catalase model **12**.

The freezing of the probes for EPR experiment could give raise to water coordination upon geometrical changes when crystallization occurs. The EPR spectra which were obtained after the saturation of the solutions with water did reveal minor changes.

For CPO model **11** solely the signals at g_{eff}= 5.79 and g_{eff}= 2.00 which were a minor contribution of an high spin iron (III) complex with axial symmetry disappeared. This finding indicates that the symmetry of the iron complex became more rhombic. Such a fact is *per se* indicative of a non coordination of water. If water would coordinate a displacement of the iron atom back to the porphyrin plane would be expected. Such a geometrical modification corresponds to a change from a rhombic to an axial symmetry (*figure 42*).

out of plane displacement   in plane iron
(rhombic distortion)   (axial symmetry)

━━ ━━ represents the porphyrin plane
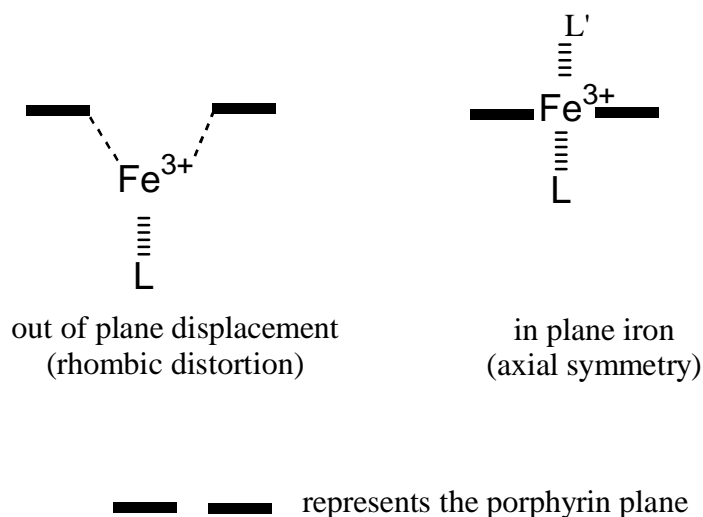
Figure 42: Schematic representation of the geometry of five and sixth coordinated iron porphyrin complexes.

The ENDOR spectra of **11** after water addition also did not reveal a coupling between water protons and iron. This result indicates that water was not coordinated to the iron, at least up to 5 K.

For the catalase model **12** no change was obtained in the EPR spectra and an ENDOR experiment could not reveal the presence of water protons in the vinicity of the iron. Hence we also concluded that the water did not bind to **12** as well.

These results for **11** and **12** suggest two explanations. First water which is known as a weak field ligand has a too low binding affinity to the complex. Second sterically demanding pivaloyl groups could prevent the binding of a sixth ligand. To get more information on the possibility of binding ligands we used a second approach.

VII.2. Binding of strong field ligands.

In this second approach to evaluate the affinity of our models for a sixth axial ligand we have used so-called strong field ligands which are know to bind strongly to the iron. Such ligands are e.g. imidazoles, and cyanide. These ligands would induce a change from high

spin to low spin system. Hence their binding would be easier to detect by NMR and EPR spectroscopy (*see* VI.2).

VII.2.1. Binding of Imidazole and Imidazole derivatives.

We first tried to bind imidazole to the CPO model **11** and to the catalase model **12**. The use of toluene where the solubility of imidazole is poor did not permit to obtain the desired complex. Therefore we changed to methylene chloride with the same result and finally to DMF where imidazole has a greater solubility. Even then and despite the use of up to 1,000 equivalents of imidazole no formation of an imidazole complex has been detected for **11** or **12** either by UV-Vis or EPR spectroscopy. Therefore we used 2-Methyl-Imidazole and finally 4-Phenyl-Imidazole which is soluble in toluene and 2-Methyltetrahydrofuran. For both derivatives the results were the same as for imidazole.

The unability of the complexes to coordinate imidazole indicates that the binding constant are very low. There could be two reasons for this.

The first one is the steric hindrance induced by the pivaloyl substituents and the butyl side chains which also prevent to some extent the access to the iron atom. They are namely found in a plane perpendicular to the porphyrin core. Thereby the binding of a sixth ligand could only be possible if the ligand is small enough or flexible enough to diffuse between the porphyrin plane, the butyl side chains and the "cap" formed by the pivaloyl substituents. If this hypothesis is correct the binding of cyanide should be possible.

The second reason could be the presence of the bromide counter ion or of another species in the porphyrin sphere (*figure 43*).
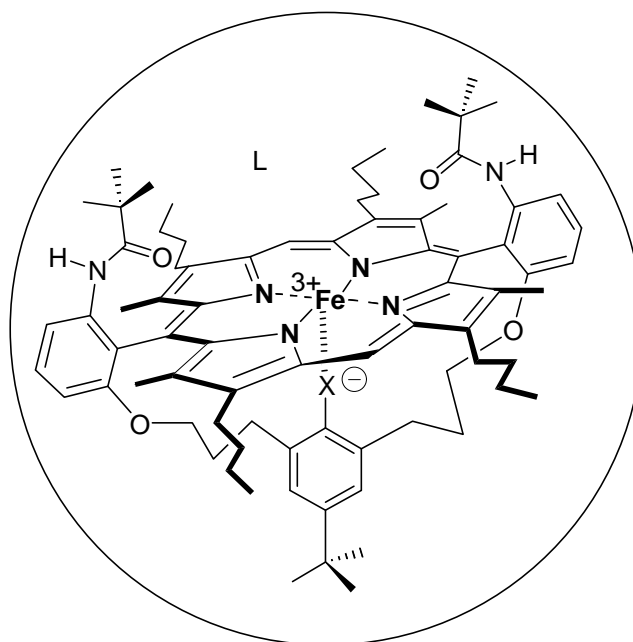
L: Ligand; the circle is a schematic
representation of the ligand sphere

Figure 43: Presence of molecules in the ligand sphere of a porphyrin.

Although it has been established by both NMR and EPR analysis that the bromide doesn't coordinate, it could still be present in the ligand sphere of the porphyrin thereby reducing the accessibility of another ligand. The detection of this counter ion is neither possible by the NMR nor by the EPR methods used.

Further due to the use of triethylamine as a base in the reaction this molecule could also interact with the porphyrin in the ligand sphere. As diamagnetic molecule it should be detectable by NMR spectroscopy. Unfortunately in the region where the signals of triethylamine usually appear they are likely to be masked by the presence of the paramagnetic signals arising from the iron porphyrin itself. To verify this hypothesis only the use of a ligand able to displace species from the porphyrin ligand sphere would allow a change in the characteristics of the complex.

VII.2.2. Binding of cyanide.

The binding of cyanide was then tested with the CPO model **11** in toluene by adding tetraethylammonium cyanide. The first process which has been observed is not the primary binding of the cyanide to the iron but a redox process. Cyanide is namely also a known reductant of iron porphyrin complexes [124]. As a consequence the UV-Vis spectrum is found to be the sum of the corresponding iron (II) porphyrin complex with a maxima of the Soret band at 418 nm and of the iron (III) cyanide porphyrin complex characterized by a

maxima of the Soret band at 412 nm. The recording of the corresponding NMR spectra confirmed:

1. the reduction from iron (III) to iron (II) which is then in a low spin configuration as revealed by the diamagnetic NMR signals obtained.

2. The binding of cyanide to iron (III) to give a low spin iron (III) complex which NMR spectrum ranges from –10 to + 25 ppm.

The preparation of the low spin complex of **11** with cyanide confirms that the very low binding constants found for imidazole could be due to steric hindrance or to the presence of a species in the porphyrin ligand sphere. Unfortunately this experiment can not determine which of the hypothesis is the most appropriate.

These results demonstrate that **11** and **12** could be good mimics to stabilize catalytic intermediate provided the affinity for the ligand is high enough. These requirements may also explain why halides in particular the bromide ion from iron dibromide used for iron insertion does not remain coordinated to **11** and **12**.

VII.3. Formation of the ⁻OCl complex.

Given the possibility of binding small ligands we have pursued the characterization of the catalytic intermediates proposed for CPO. The first intermediate proposed is the ⁻OCl complex which is obviously not the true catalytic species.

Formation of such a complex in organic solvents can be achieved by two routes (*figure 44*) [20]:

1. the direct formation via an hypochlorite salt which is soluble in organic solvent

2. the indirect formation via the preliminary formation of compound I (oxo complex) as postulated for the native enzyme.
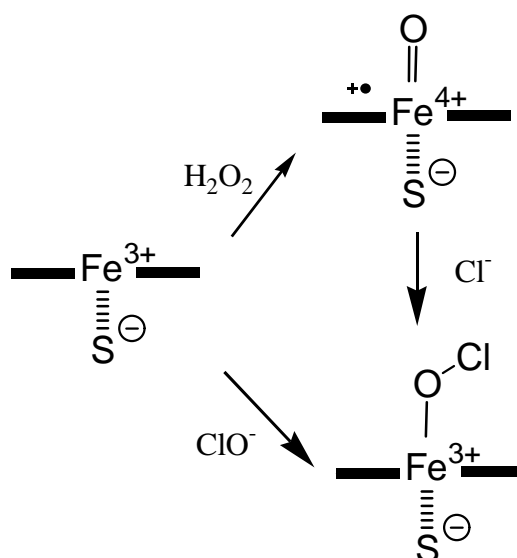
Figure 44: Formation of ClO⁻ complex.

We chose to use method **1.** in a first approach as method **2.** requires to first characterise compound I which is known to decay rapidly.

VII.3.1. UV-Vis studies.

The hypochlorite ion is commercially available as natrium hypochlorite aqueous solutions. As such aqueous solution are very little soluble in organic solvents they are not suitable for quantitative studies but can be used for qualitative comparisons. Therefore using a phase transfer catalyst, benzyltriethylammonium chloride, we have prepared methylene chloride solution containing hypochlorite [20]. After concentration of the solution the resulting salt obtained was a solid. This permits the exact quantification of the amount of hypochlorite added. The characterization of the hypochlorite complex of the CPO model **11** and the catalase model **12** was undertaken in methylene chloride first as the hypochlorite salt was prepared in this solvent.

For the CPO model **11** the slow disappearance of the Soret band indicated that undesired side reactions such as oxidative degradation of the porphyrin core has occurred. The use of only 100 equivalent with **11** did not led to this reaction but no changes were observed.

For the catalase model **12** the addition of up to 1000 equivalents of hypochlorite did not led to significant changes except a dilution effect.

To check the influence of the solvent upon the formation of the ClO⁻ complex we changed to toluene. In this solvent hypochlorite is known to be sparingly soluble via the formation of a charge transfer complex.

For the CPO model **11** the Soret band slowly shifted to 414 nm i.e. a 6-8 nm red shift compared the resting state upon addition of 100 equivalents of hypochlorite. This result indicates a probable binding of the hypochlorite ion to the iron. As for water the binding of hypochlorite results in an increased electron density around the iron, hence an expected red shift in the UV-Vis spectra.

To confirm that the binding species was actually hypochlorite we repeated the experiment by using a biphasic system: 10% vol of an aqueous NaOCl solution were stirred with a toluene solution of **11** for 30 Min. After phase separation the UV-Vis spectrum obtained was identical to the one obtained with the benzyltriethylammonium salt procedure.

However the results obtained do not permit to eliminate a second hypothesis. It is namely reported in the literature [125] that upon addition of hypochlorite to iron porphyrin complexes the so-called compound I is formed. Fortunately the UV-Vis, ESR and NMR spectra should make it possible to distinguish between the two proposed complexes.

For the catalase model **12** no changes were detected independent of the quantity of hypochlorite added apart from dilution effects. This results seems to indicate that **12** doesn't bind hypochlorite and should be confirmed by using other methods.

VII.3.2. EPR studies.

The binding of ClO$^-$ should induce a change in the geometry of the complex and thereby in its symmetry. As discussed for water the symmetry should change to a more axial symmetry. Consequently the EPR spectra should be modified.

For the CPO model **11** no changes were observed in methylene chloride indicating that obviously no coordination occurred in this solvent.

When the solvent was changed to toluene the spectra were modified. The signals observed before in the region of g_{eff}=6-8 and 2.9 disappeared and led to a new single broad signal around g=2. As the signals lacks the typical three lines splitting of low spin iron (III) porphyrin complexes we propose that the iron is still in a high spin iron (III) state.

When catalase mimic **12** was used a little change in the g_{eff} values were observed both in methylene chloride and toluene. This shift could suggest that a coordination had occurred. If so it has no influence on the spin state and symmetry of the complex and should be confirmed by the formation of HOCl complex which is expected to give a split Soret band and permits to use ENDOR spectroscopy which would detect the proton of the HOCl ligand.

VII.3.3. NMR of 11-⁻OCl.

To confirm the presence of a sixth ligand which can be judged from the chemical shift of the meso protons the NMR spectra of **11-⁻OCl** was recorded at RT in toluene d_8. The signal at -50 ppm disappeared and a new signal around 40 ppm was observed. Accompanying this change the signals attributed to the β-methyl and β-CH$_2$ were even more positively shifted. These changes clearly indicate that the sixth position is now occupied.

VII.4. The HOCl complex.

As the results obtained with the ⁻OCl addition are not clear for the catalase **12** as the UV-Vis spectra and EPR spectra do not see clear changes, the characterization of the protonated form of the models **11** and **12** was undertaken. Namely the protonation of the ClO⁻ complexes of **11** and **12** is expected to give a split Soret band according to the results of *Wagenknecht and Woggon.*[20].

VII.4.1. UV-Vis characterization.

First the catalase model **12** in the presence of ⁻OCl was submitted to protonation with acetic acid (AcOH) in both methylene chloride and toluene as the EPR and UV-Vis spectra of **12-ClO⁻** did not display clear changes.

The choice of AcOH as source of proton is justified by the nearly neutral pH of hypochlorite (pH= 7.2) and by the necessity of using a weak acid to avoid protonation of the amide functionalities. Upon addition a clear splitted Soret band appeared as well in methylene chloride as in toluene thereby indirectly confirming that **12-⁻OCl** had been obtained before (*figure 45*). The possible formation upon AcOH addition of a mixture of **12-OAc** and **12** was checked by addition of acetic acid before hypochlorite. The resulting spectra showed that the corresponding Soret band in presence of AcOH was at 408 nm as for **12** or **12-⁻OCl**.
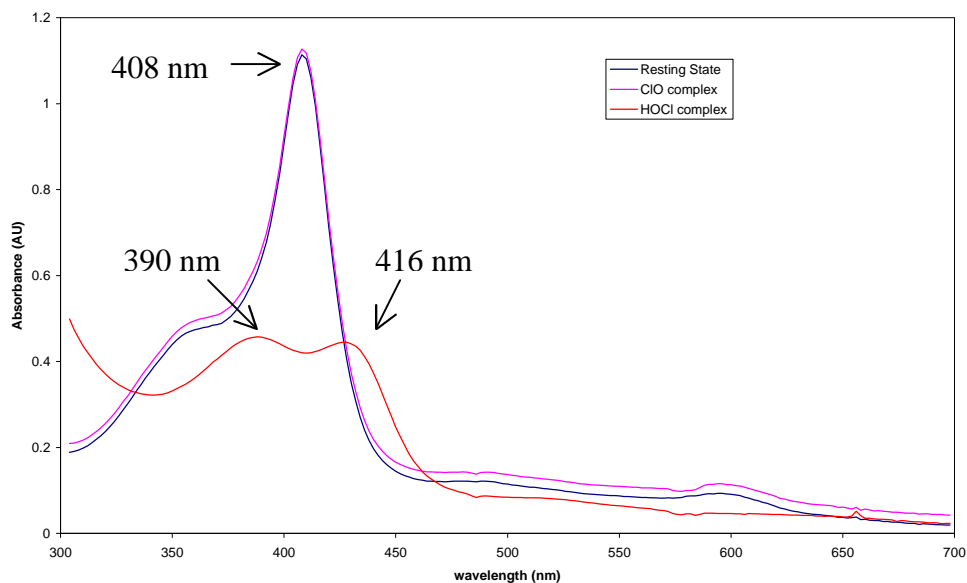
Figure 45: UV-Vis changes upon 12-HOCl formation.

As the changes are more significant in UV-Vis spectroscopy when the formation of the HOCl complex is attempted we turned to the same procedure for having a confirmation of our results with the CPO model **11** where there are evidence for the formation of the ClO⁻ complex. Contrary to **12** upon addition of acetic acid to **11-⁻OCl** no further changes have been observed in the UV-Vis spectra in both methylene chloride and toluene. The reason for this behaviour is not understood as the EPR spectrum in toluene changed drastically.

VII.4.2. EPR studies.

Next the EPR spectra of **12-HOCl** and **11-HOCl** were recorded at 100K.

For the catalase model **12** the g_{eff} values were slightly modified but the shape of the spectra is intact. This would tend to indicate that the coordination of HOCl did not happened which contradicts the results of the UV-Vis investigation.

For the CPO model **11-HOCl** the EPR spectra changed to a typical axial symmetrical spectrum of an iron (III) high spin complex in toluene (*figure 46*) with g_{eff} at 5.79 and 2.00.
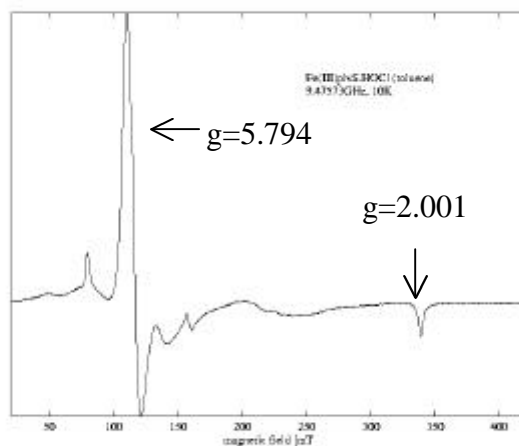
Figure 46: EPR spectrum of 11-HOCl at 5K.

The formation of the HOCl complex of **11** is only detectable in toluene and not by the techniques used in methylene chloride. The reason for this solvent dependency is not yet understood.

VII.4.3. Catalytic activity essays.

In order to check if a catalytic activity, despites the absence of detectable formation of **11-HOCl** in methylene chloride, with the system **11+⁻OCl+AcOH+CH₂Cl₂** we have tested the system in the presence of monochlorodimedone. This check was important to compare the results obtained by *Wagenknecht and Woggon.* [20].

Using their conditions we could calculate a turnover of 38. The fact that attempts to produce the HOCl complex of **11** gave no change in UV-Vis, NMR and EPR spectroscopy in methylene chloride as compared to the resting state of **11** seemingly contradicts the results of the catalytic chlorination of monochlorodimedone.

It may be that either free HOCl acts as the chlorinated species and is liberated from **11** or the complex **HOCl-11** is produced in amounts escaping the detection limits of the methods used to characterize it.

VII.5. Formation of compound I.

The next species to characterize is compound I analogue of **11** and **12**. First it would permit to exclude that upon addition of hypochlorite ion the complex formed from **11** and **12** are compound I analogues. Second upon addition of chloride it would confirm the formation of **11-⁻OCl** and **12-⁻OCl**. The subsequent addition of acid to these complexes would furnish the corresponding HOCl complexes. Third it could eventually allow to

determine which of the proposed structures for compound I analogues (*figure 47*) is the most appropriate.
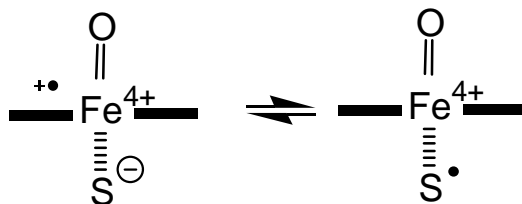
Figure 47: Structures proposed for compound I analogues with a thiolate ligand.

VII.5.1. Generation of iron oxo species and their characterization.

The generation of compound I analogues for peroxidase and P450 enzymes has been long investigated by chemists. Several methods have been developed with tetraarylporphyrins as models as the former proved to be robust against oxidative degradation [126].

The methods use different oxygen donors which usually primary forms a peroxy like adduct with the iron (*figure 48*):

1. hydrogen peroxide [61]
2. peracids such as *meta* chloroperoxybenzoic acid (*m*CPBA) [127]
3. iodozylbenzene [128]
4. dioxiranes [129]
5. ozone [130]

For **1.** and **2.** the use of a protic solvent such as methanol is usually necessary to facilitate the departure of the corresponding acid (*figure 48*). The use of dioxirane permits also to determine whether the cleavage of the peroxo bond is heterolytic or homolytic [131].
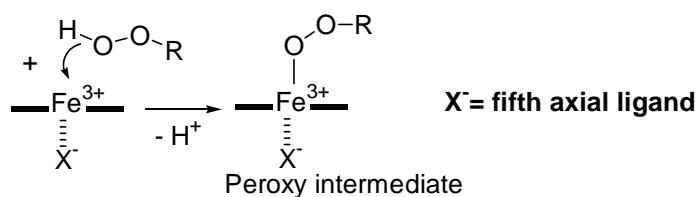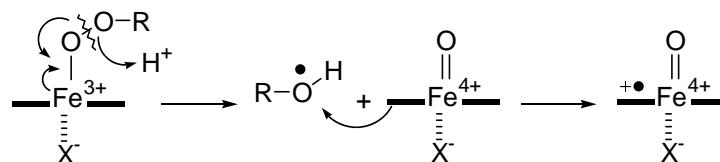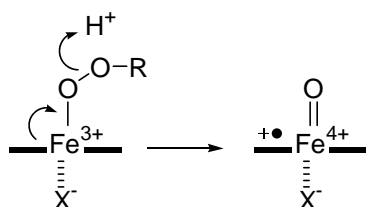
Figure 48: Formation of compound I analogues.

After generation of the iron oxo species the questions which have to be addressed are:

1. The oxidation state of iron

2. If the iron is found in the iron (IV) state: Is the radical centered on the porphyrin or on the fifth axial ligand?

3. For the radical species the type of orbital which contains the radical.

The characterization of iron oxo species relies on the pioneering work of Dolphin who was the first to propose a formulation as an iron (IV) coupled to a radical cation on the porphyrin [132]. The best characterized compound I among the enzymes is compound I of Horseradisch Peroxidase (HRP). For HRP compound I was characterized by UV-Vis [132], resonance Raman [133], Mössbauer [134] and more recently by EXFAS (extended X-Ray spectroscopy) [135] spectroscopy. The UV-Vis spectra has a Soret band which maxima is the same as for the resting state but which intensity is around the half. In the visible region new peaks appear at 650 nm. The Mössbauer spectra are consistent with an iron (IV) species in the high spin state as indicated by the Q value. Finally EXFAS reveals an iron oxygen bond of 1.64 Å which is consistent with a formulation as an iron oxygen double bound.

All works which have been done with models seems also to indicate that the iron is found in the oxidation state (IV) although most of the studies relies only on the UV-Vis characterization.

VII.5.2. UV-Vis characterization attempts.

To generate compound I analogues of **11** and **12** we used hydrogen peroxide or *m*CPBA in methylene chloride or toluene (*table 19*).

Complex:	Solvent:	Oxidant:	Eq.:	Soret initial (nm):	Final Soret (nm):
11	CH_2Cl_2	H_2O_2	Excess [a)]	408	**406**
12	CH_2Cl_2	H_2O_2	Excess [a)]	408	408
11	CH_2Cl_2	*m*CPBA	2.5	408	**406**
12	CH_2Cl_2	*m*CPBA	2.5	408	408
11	Toluene	H_2O_2	Excess [a)]	408	**410**
12	Toluene	H_2O_2	Excess [a)]	408	408
11	Toluene	*m*CPBA	2.5	408	**410**
12	Toluene	*m*CPBA	2.5 to 10	408	408

Table 19: Formation of compound I.

a) Conditions: 0.2 ml 30% H_2O_2 solution was added (10% vol resp. to toluene):the exact amount of H_2O_2 can not be estimated as the partition coefficient of H_2O_2 is not known.

In methylene chloride with H_2O_2 as oxidant the changes observed for the CPO model **11** were a steady diminution of the intensity of the Soret band which was accompanied by a broadening and a slight blue shift to 406 nm. The expected changes in the visible region which is usually the appearance of bands in the 650-670 nm region was not detected. The changes observed are rather indicative of a degradation of the complex **11** with time (steady loss of intensity).

Upon addition of methanol which could assist compound I formation the decay of the Soret band and the destruction of the porphyrin was accelerated but apparently did not help the formation of the desired complex.

For the catalase model **12** under the same conditions the intensity of the Soret band did not diminish so rapidly which could be related to a catalase like activity of the complex.

For the CPO model **11** the use of *m*CPBA as oxygen donor gave comparable results as with H_2O_2 as oxidant. Moreover *m*CPBA appears to be a more aggressive oxidant as only 10 eq. are necessary to destroy the porphyrin within 5 minutes.

For the catalase model **12** the use of as much as 100 eq. of *m*CPBA results only in a partial destruction of **12** immediately after the addition. Afterwards and within 48 hrs the complex **12** did not show any further degradation suggesting that a catalase like activity took place. When the solvent was toluene the results were different.

For the CPO model **11** by both the use of hydrogen peroxide or *m*CPBA as oxidant the Soret band shifts to 410 nm and exhibits a shoulder around 370 nm. This red shift is usually typical for compound II formation [136] or for a radical centered on the axial ligand and not on the porphyrin or for peroxy like complexes[137]. A peroxy complex (*figure 15*) would result from the non cleavage of the O-O bond.

For the catalase model **12** the results obtained were also comparable to the data with H_2O_2 as oxygen donor again suggesting a catalase like activity of the complex.

Taken all together these data suggest that:

1. The process of formation of compound I is solvent dependent. In solvents which can liberate a proton the radical could be centered on the porphyrin ring as indicated by the absence of change in the position of the absorption maxima. In neutral solvents the radical could be centered on the fifth ligand as suggested by the red shift observed for the Soret band or more likely the peroxy complex would be a stable intermediate.

2. The presence of an oxygen rather than an sulphur at the fifth coordination enhances the stability of the porphyrin. In the case of a phenolate coordination a catalase like activity seems to take place whereas this is not the case with a thiophenolate ligation.

VII.5.3. EPR characterization.

As the UV-Vis spectra in toluene show a red shift for the CPO model **11** we repeated the experiment in the ESR where the concentration is much higher (from µM to mM). Upon addition of 5 equivalents of *m*CPBA to **11** a mixed spin system appeared composed of:

1. the *m*CPBA adduct of the iron porphyrin which is characterized by an high spin iron (III) axial spectra with g_{eff}= 5.79 and g_{eff}=2.001

2. a contribution of the well known "rhombic iron" at g=4.26 and g=2.

The addition of further 5 eq. results in the disappearance of the contribution of the *m*CPBA adduct and leaves only the "rhombic iron".

When the catalase model **12** was used the spectra changed directly to a line at g=4.26 and g=2. This results combined to the absence of a typical decolouration of the solution indicates that the spin system related to g=4.26 and g=2 may be a characteristic trace of the peroxy complex as stable catalytic intermediate. Namely such spectra have been reported by several groups for its formation with synthetic iron porphyrins [138].

Given the hypothesis that the spectra does corresponds to the compound I analogue it would mean that the overall spin of the system is 3/2. Such a value can only arise from an high spin iron (IV) (S=1) which is ferromagnetically coupled to a radical (S=1/2). As practically no EPR characterization of compound I analogues exists and more particularly no characterization of models which have a thiolate or phenolate fifth axial ligand the data can not be compared to any previous work. Nevertheless combined with the UV-Vis spectroscopical data the results suggest that the axial ligand would be involved as a radical in compound I analogue. The presence of the signal at g_{eff}= 4.26 and g_{eff}=2 may be the result of a tight coupling between the radical and the iron (IV). This strong coupling could be explained by the spanned structures of our models: this is not the case in enzymes where the coupling are weak.

If the complexes obtained would not be compound I analogues but peroxy like complexes this would imply that neither the sulphur from the thiophenolate nor the oxygen from the phenolate have a strong enough "push" effect to weaken the O-O peroxo bound for a cleavage. As a consequence this suggests that the protein environment which is missing in our models is essential to assist this cleavage. In turn this means that a "pull" effect is also necessary in heme-thiolate proteins to generate compound I or as suggested by new results on $P450_{Cam}$ that the catalytic species in heme thiolate protein may be the peroxy complex [139].

VII.6. Peroxo complex.

In order to check the role of a peroxo complex in the catalytic cycle of NOSs we next have attempted its characterization. Peroxo complex can be formed by:

1. the use of superoxide ion with iron (III) [140] or
2. the use of a reductant and the addition of oxygen to the iron (II) complex [141].

As the first method is more accessible we used it to characterize the peroxo complex. The inconvenient is that the solvents which can be used are polar solvents such as DMSO or MeCN. They can thereby also coordinate to the iron at the sixth position. For **11** and **12** we could notice that the formation proceeds in two steps as mentioned by previous publication [141]. First one equivalent of superperoxide reduces the iron (III) to iron (II) and thereby generates dioxygen. Probably the iron dioxygen complexes is formed. In a second reaction which is very fast the second equivalent of superoxide reduces the complex to form the peroxo complex (*scheme 11*).
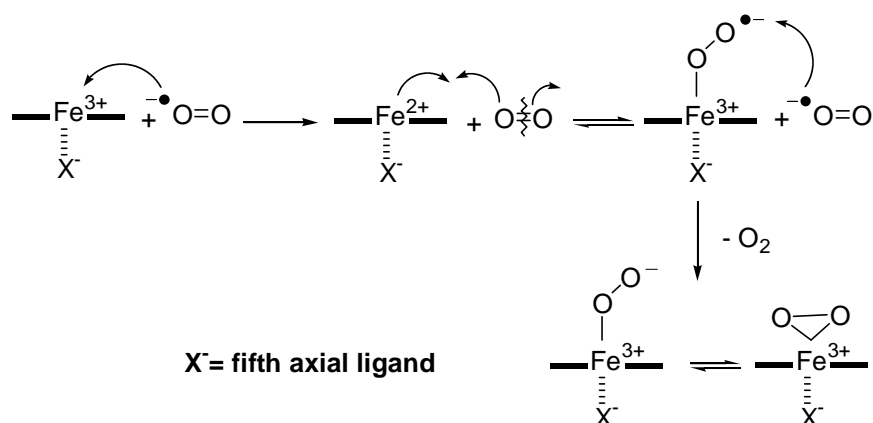
Scheme 11: Formation of iron peroxo complex.

The UV-Vis spectra was indicative of reversible processes: upon addition of potassium superoxide the Soret band slowly shifted to 418 nm which corresponds to the reduced iron (II) complex. At the same time the iron (II) reacted with the second molecule of superoxide to give the desired complex which was characterized by a Soret band at 428 nm, a value in good agreement with the data found in the literature [142]. With time the Soret band returned to 414 nm and finally to 408 nm. This suggests that there is a competition in the ligation of superoxide with the solvent. Traces of water could also be responsible for the destruction of the peroxo complex upon protonation to furnish in a first step the iron (III) water complex (*scheme 12*).
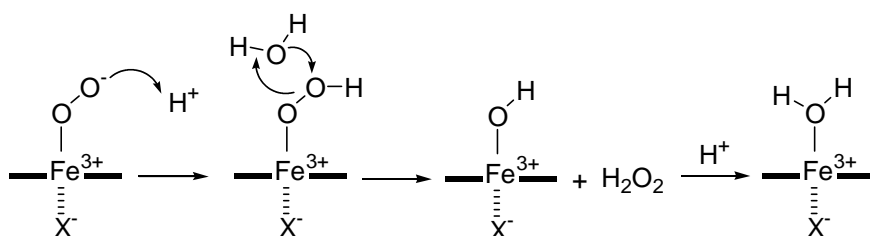
Scheme 12: Possible degradation of the peroxo complex.

The UV-Vis characterization of the peroxo complex excludes that the complexes which have been obtained in the formation of compound I analogues are peroxo complexes. Thereby it supports that the EPR set of signals at g=4.26 and g=2 do characterize the so-called compound I of **11** and **12**.

VII.7. Summary.

The CPO model **11** and the catalase model **12** can react only with small ligand molecules and show low binding affinity for ligands at the sixth axial position in general. This could be explained by the bulk induced by the amide functionalities on the aryl substituents or by the presence of a species in the ligand sphere of these complexes.

The spectroscopic parameters of the CPO model **11** are not completely in agreement with earlier data. Nevertheless a catalytic chlorination activity was observed in one case. Thus further investigations are required towards a complete understanding of the CPO catalytic chlorinations.

For catalase model **12** seems to have a catalase like activity as the degradation of the porphyrin core under oxidative conditions is much less important as for the CPO model **11**.

VIII. Improvement of the models.

The data obtained for the CPO model **11** and for the catalase model **12** suggest that steric hindrance is a problem for having a good binding to iron for ligands at the sixth position. Moreover oxygen binding studies with the oligomeric mixture obtained from **20b** [143] have indicated that a secondary reaction process occurs upon oxygen binding to iron (II). This second reaction is postulated to be the hydroxylation of the N-H bond of the amide by the following reaction path (*figure 49*):
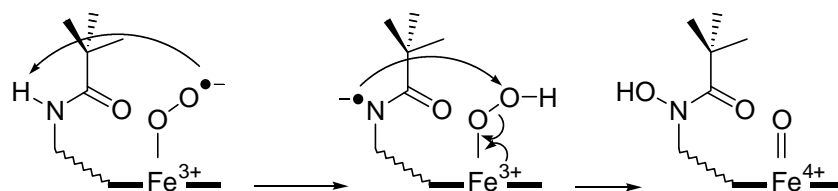
Figure 49: Hydroxylation of the amide N-H.

Taking into account:

1. the necessity to check the reactivity of the N-H bond in the presence of oxidant bound to the iron and

2. the steric bulk induced by the pivaloyl which could prohibit ligand binding

we have designed three further models which also respond to the definition of *Bruice et al.* of an ideal enzyme mimic (*see* V.1.1).

The CPO model **32** and the catalase model **33** (*figure 50*) were synthesized to replace the amide functionality as face protecting groups. The naphthyl substitution at the meso position has been introduced to avoid the formation of μ-oxo dimers in the presence of oxygen.

The CPO models **34** and **35** (*figure 50*) are tailed models starting from **20b**. They were presumed to be good models as the oligomeric mixture obtained from **20b** showed better binding affinity for a sixth ligand to the heme iron. Moreover, based on the results obtained by *Mukaiama et al.* [120, 123], the sulphur could be stabilized by the presence of the amide group in its vinicity via the formation of an hydrogen bond. The formation of an hydrogen bond could also favour the coordination of the sulphur to the iron. The steric bulk of the amide group would also protect it from oxidation. **34** and **35** shall also be candidates to compare the effect of a thiophenolate *vs.* an alkyl thiolate axial ligation to the heme iron. Hence the CPO model **35** is expected to be a closer model to CPO. The amino acid cystein is namely an aliphatic thiol compound.
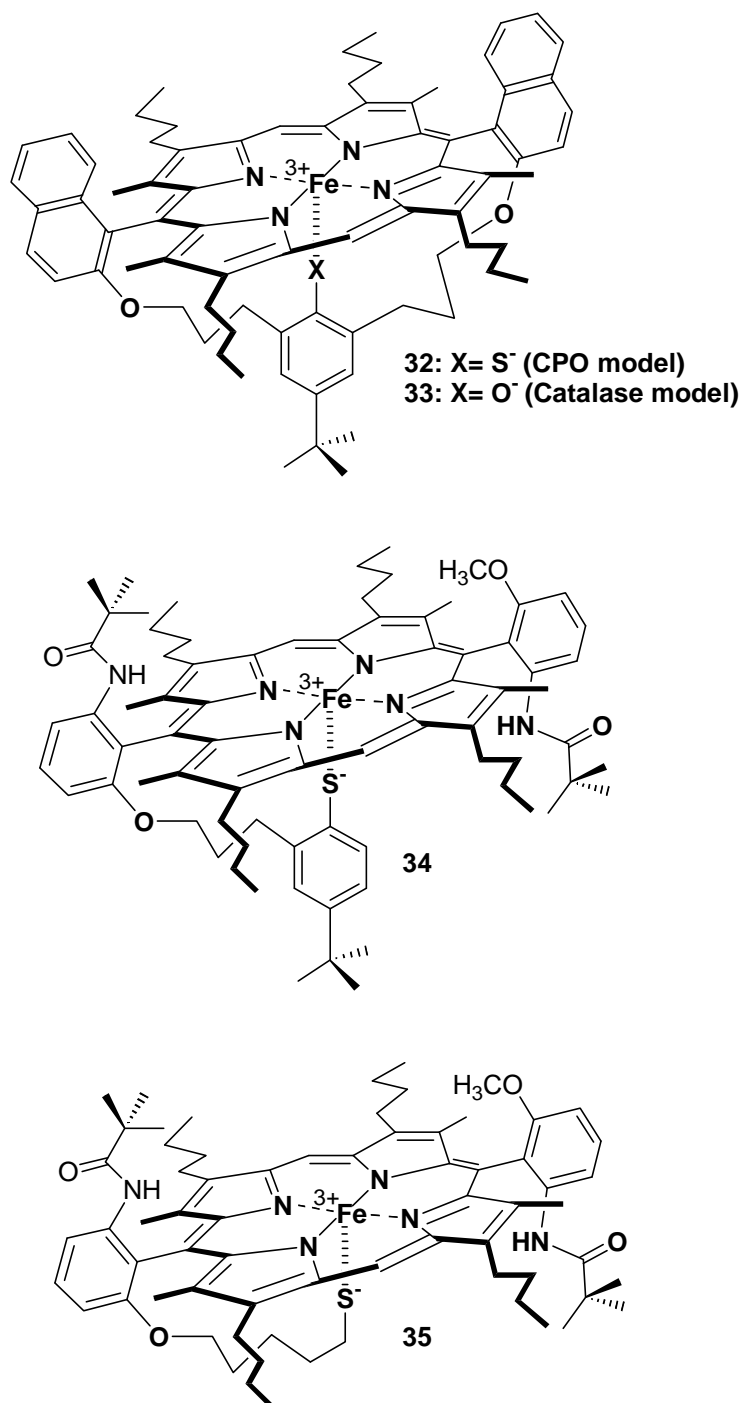
Figure 50: The new models.

VIII.1. Synthesis and characterization of the naphthyl models 32 and 33.

The synthesis of the models relies on the same procedure used for the CPO model **11** and the catalase model **12** (*scheme 13*).

11 +

CHO
OMe

36

pTsOH, MeCN, RT then Zn(OAc)$_2$ then H$^+$

+ a,b isomers 37b and 37b

Atropisomers' Ratio: 1:1

OMe

M=Zn^{2+}: **37a**
M=2H: **38a**

OMe

BBr$_3$, RT
OMe ⟶ OH

39

Cs$_2$CO$_3$, **15** or **16**, DMF, 60°C

NH

N

NH

O

XPr

O

40: XPr= SC(O)NMe$_2$

41: XPr: OC(S)NMe$_2$

KOMe, dioxan, Δ

NH

N

NH

N

O

XH

O

⟶ **32 or 33**

42: X= S

43: X=O
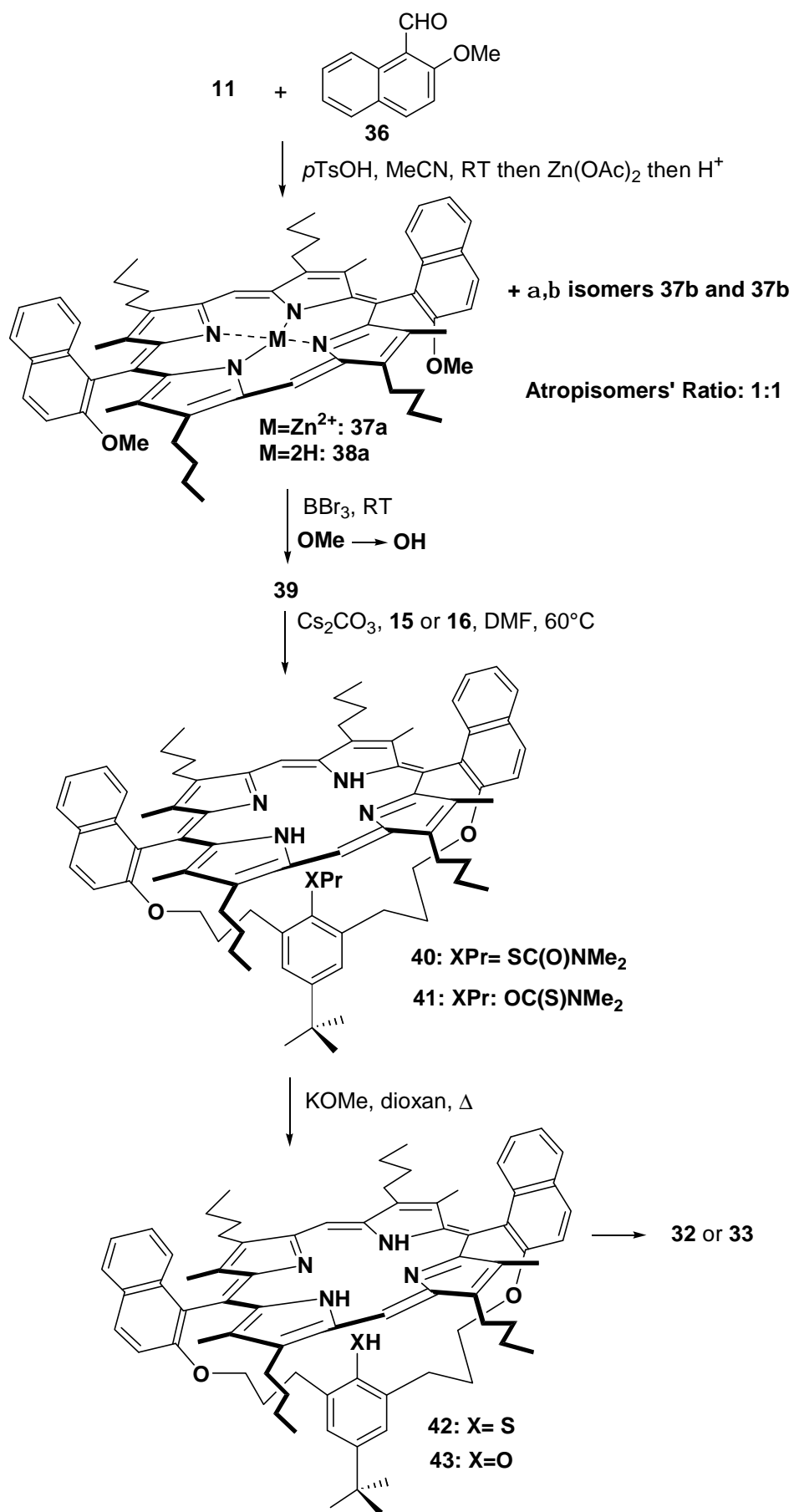
Scheme 13: Synthesis of 32 and 33.

The first step was the porphyrin condensation which proceeds in 70% yield.

The marked difference compared to the synthesis of **11** or **12** is the ratio for the atropisomers which in the present case is about **1:1**. This results clearly confirms that steric bulk above the porphyrin plane is the reason for the high selectivity obtained during the synthesis of the pivaloyl models **11** and **12** in favour of the α,β isomer **17b** (85:15).

As it was the case for **17a** and **17b** the atropisomerisation of **38a** and **38b** was also not possible under 200°C due to the high energy barrier for the C_{aryl}-C_{meso} bond rotation.

The deprotection of the methyl ether functionality was subsequently successfully achieved with the use of BBr_3 at RT to give **39**.

The coupling of **39** with the bridge **15** under high dilution proceeds in 60% yield to give pure **40**. The deprotection of the sulphur to yield the metal free compound **42** was done under the same conditions (KOMe in dioxane) as for the synthesis of **22**.

For the catalase model **33** the bridging of **39** with **16** occurs with 65% yield to give **41**. The deprotection of **41** with KOMe in dioxane proceeds in 95% yield to **43**.

As for the metal free precursor **22** of the CPO model **11** and for the metal free precursor **31** of the catalase model **12** we used NMR spectroscopy to refine a craft field minimisation of both structures **42** and **43** (*figure 51*). The comparison of the chemical shifts obtained for the bridge protons and for the SH resp. OH of the bridge suggests a different porphyrin core geometry compared to **22** and **31** (*table 20*). First the upfield shift of the bridge aromatic protons 3" and 5" probably results in a smaller distance of the bridge moiety from the porphyrin core. Second the upfield shift of the methyl pyrrole and $CH_{2\alpha}$ implies that the geometry of the porphyrin core is not the same as for the models **22** and **31**. We propose that the core is more planar which results in an increased π density on the pyrrole substituent hence the upfield shift.

Proton[a)]:	δ in ppm for **42**	Δ(δ) (22-42) in ppm:	δ in ppm for **43**	Δ(δ) (43-31):
10, 20	10.10	-0.02	10.17	+0.03
CH$_3$ pyrrole	2.19	-0.43	2.21	-0.44
CH$_{2\alpha}$	4.05	0 and 0.2	3.92 and 3.84	-0.02 and – 0.10
CH$_{2\gamma'}$	0.5	-0.17	-0.4	-0.32
H$_{3",5"}$	6.13	-0.07	5.95	-0.16
H$_{2'''}$ (*tert*-butyl bridge)	0.88	0.01	0.79	-0.10
S<u>H</u> or O<u>H</u>	-3.01	0.00	-2.19	+0.10
N<u>H</u>$_{porphyrin}$	-2.03	+0.10	-2.19	+0.10

Table 20: Selected NMR chemical shifts for 42 and 43 compared to 22 and 31.
a) Numbering see *figure 22*.
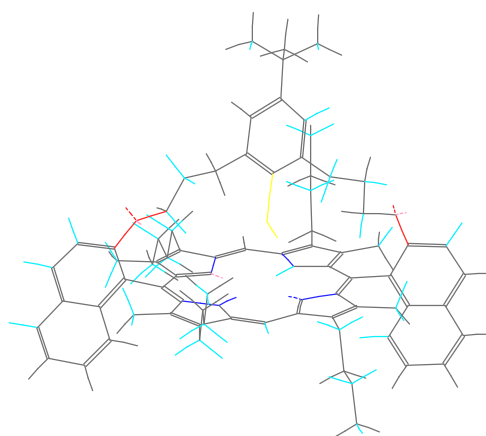
42
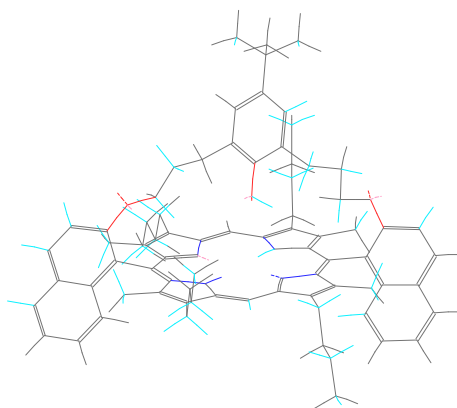
43

Figure 51: Force field modellisation of 42 and 43.

Finally the iron insertion using the FeBr$_2$/Et$_3$N method in toluene gave pure CPO model **32** and pure catalase model **33** in 75% and 90% yield respectively.

VIII.2. Characterization of the resting state of 32 and 33.

VIII.2.1. UV-Vis characterization.

As for the CPO model **11** and for the catalase **12** the full spectroscopic characterisation of CPO model **32** and catalase model **33** was undertaken.

The UV-Vis spectra were nearly identical to the one obtained for **11** and **12** (*figure 52*).

For the CPO model **32** the Soret band was found at 408 nm as for model **11** and it was also broadened compared to the metal free precursor **42**. In the visible part of the spectrum a broad band was observed at 512 nm and at 580 nm. This indicates that the CPO model **32** is an iron (III) five coordinated species.

Contrary to the CPO model **11** the reduction of **32** was not total with the use of natrium bohrohydride or natrium hydride as reductant. This suggests that the redox potential of **32** is more negative than the redox potential of **11**.

For the catalase model **33** the Soret band was found at 410 nm which represents a 2 nm blue shift compared to model **12**. The visible part of the spectrum is as for **12** showing a broad absorption band centered at 520 nm and at 580 nm. The characteristic shoulder attributed to the iron phenolate ligation in model **12** was found at 356 nm in **33** instead of 354 nm in **12**. All these observations suggests that catalase model **33** is also an iron (III) five coordinated species.

The reduction of **33** with hydrides was also not complete, suggesting a lower redox potential for the catalase model **33** compared to catalase model **12**.
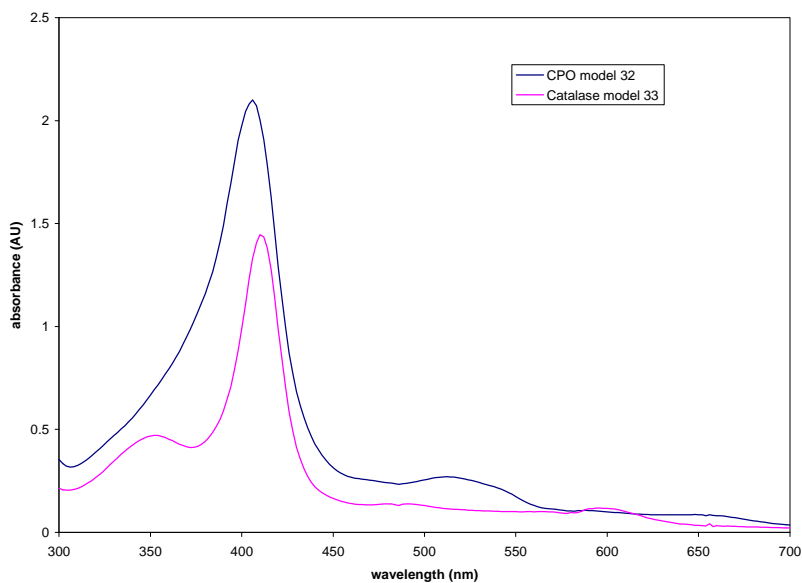
Figure 52: UV-Vis spectra in toluene at RT of 32 and 33.

VIII.2.2. EPR characterization

The EPR characterization of the CPO model **32** and of the catalase model **33** (*figure 53*) proved to be analogue to the results obtained with the previous models **11** and **12**.

The EPR spectra of the CPO model **32** is characterized by absorption lines found at g_{eff}= 8.391, 5.884, 3.005 and 2.007. This spectra can be interpreted with the same proposals as for CPO model **11**. The CPO model **32** is probably characterized by a strong σ bond between the iron and the sulphur and the electron spin density would be delocated from the iron to the sulphur. The strong σ bond is most probably strengthened by the π back bonding interaction between the sulphur and the iron.
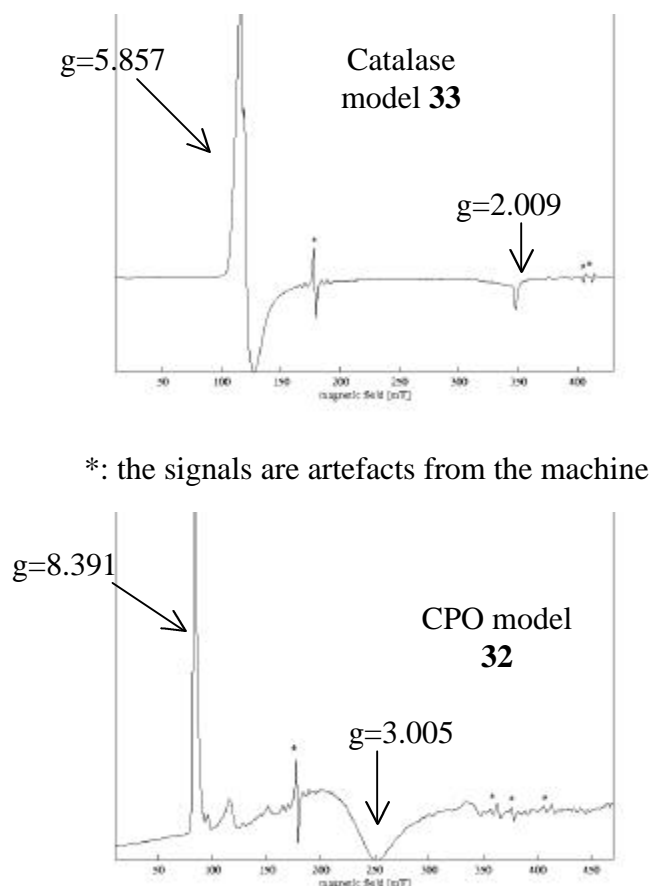
*: the signals are artefacts from the machine

Figure 53: EPR spectra at 5K in toluene of models 32 and 33.

For the catalase model **33** the g_{eff} values are found at 5.857 and 2.009 respectively. Contrary to the previous catalase model **12** the small rhombic distortion indicated in **12** by a shoulder in the g_{eff} signal at 5.857 totally disappeared. The absence of a shoulder indicates that the axial symmetry of the naphthyl model **33** is higher than for the model **12**. The higher degree of symmetry could be related to a more planar porphyrin core in catalase model **33** compared to catalase model **12**.

VIII.2.3. NMR characterization.

Next the NMR spectra were recorded in toluene at RT.

For the CPO model **32** the spectra ranged from –62 to +82 ppm. The line width of the signals were found to be up to 1,000 Hz for the signal at –62 ppm which is attributed to the meso protons. These data confirm that the CPO model **32** is as CPO model **11** a high spin iron (III) five coordinated species.

For the catalase model **33** the spectra ranged from –59 ppm to 130 ppm. The line width was also found to be up to 1,000 Hz for the meso proton signals found at –59ppm. These

data support that the catalase model **33** is also a high spin iron (III) five coordinated complex.

VIII.2.4. Electrochemistry.

Finally the cyclic voltammetry experiments in DMF with LiClO$_4$ as electrolyte gave redox potential values of –660 mV for the CPO model **32** and –680 mV for the catalase model **33** (*table 21*). The value which are around 100 mV more negative than for the corresponding models **11** and **12** supports the difficult reduction of **32** and **33** in the presence of sodium borhydride or natrium hydride as the difference in redox potential between the oxidant and reductant is increased.

Compound:	E$_{ox}$ (mV):	E$_{ox}$ (mV):	DE (mV):	E^0 (mV):
32	-610	-710	100	-660
33	-780	-635	145	-710

Table 21: Cyclic voltammetry.
Conditions: 2.3 mM **32** or **33** in 0.1M LiClO$_4$ DMF solution; Scan speed. 500 mV s^{-1}.

Further the data comparison suggests that the porphyrin environment and thereby the overall geometry of the complex is the decisive factor controlling the redox potential and probably not the nature of the axial ligand.

VIII.3. Characterization of catalytic intermediates.

VIII.3.1. The ClO⁻/HOCl complexes.

VIII.3.1.1 UV-Vis characterization.

Using the same procedures as for the CPO model **11** and the catalase model **12** we first have tried to generate the potential ClO⁻ complexes of CPO model **32** and of catalase model **33**. The UV-Vis characterization (*table 22*) using either benzyltriethylammonium hypochlorite (= salt in *table* 22) led to comparable results as obtained with **11** and **12**. for the shifts of the Soret band's value.

However the models **32** and **33** were found to be more sensitive to oxidative degradation than the parent pivaloyl substituted complexes.

Compound:	Method:	Solvent:	Soret initial (nm):	Soret final (nm):
32	10% NaOCl	CH_2Cl_2	410	410
32	salt	CH_2Cl_2	410	410
33	10% NaOCl	CH_2Cl_2	410	410
33	salt	CH_2Cl_2	410	410
32	10% NaOCl	Toluene	410	**412**
32	salt	Toluene	410	**414**
33	10% NaOCl	Toluene	410	410
33	salt	Toluene	410	**412**
32	10% NaOCl then AcOH	CH_2Cl_2	410	**destruction**
33	10% NaOCl AcOH	CH_2Cl_2	410	**destruction**
32	Salt then AcOH	CH_2Cl_2	410	410
33	Salt then AcOH	CH_2Cl_2	410	**396**
32	10% NaOCl then AcOH	Toluene	410	**destruction**
33	10% NaOCl then AcOH	Toluene	410	**390+416**
32	Salt then AcOH	Toluene	410	**414**
33	Salt then AcOH	Toluene	410	**392+416**

Table 22: UV-vis characterization of the ⁻OCl complexes for 32 and 33.

VIII.3.1.2 EPR characterization.

The EPR characterization of the complexes in toluene did not led to the same results as for models **11** and **12**.

For the CPO model **32** we did not get a single broad signal at g_{eff}=2 for the spectra as found for the parent CPO model **11.** Instead the spectra suggests the existence of two spin systems. The first spin system corresponds to a typical axial high spin iron (III) complex with g_{eff}=5.78 and g_{eff}=2. The second spin system corresponds to the "rhombic iron" with g_{eff}=4.26 and g_{eff}=2. These results indicate that in the case of the naphthyl substituted models **32** the addition of hypochlorite led to the probable formation of the corresponding oxo complex rather than to the formation of the desired $^-$OCl complex. The addition of acid should confirm this results as acid assists the cleavage of the O-Cl bond of the peroxy complex to yield the oxo complex and HCl.

When acetic acid was added to the system **32+ ClO$^-$** in toluene, the spectra obtained was the spectra of the pure "rhombic iron" having g_{eff} values at 4.26 and 2.00. These results suggests that contrary to our proposal for the CPO model **11** the spectra characterized by g_{eff} values at 4.26 and 2.001 could be characteristic for the oxo complex and not for a peroxy complex.

For the catalase model **33** the EPR experiments gave the spectra of the "rhombic iron" with g_{eff} values at 4.26 and 2.001 upon addition of ClO$^-$ and upon addition of ClO$^-$ and acetic acid. These data also indicate that the oxo complex rather than the desired ClO$^-$ and HOCl complexes is formed upon addition of hypochlorite to the catalase model **32**. Further it is also not consistent with the interpretation proposed for the catalase complex **12** where we have proposed the formation of peroxy complex rather than compound I analogue upon addition of peroxides.

The reason of these different behaviour upon modification of the meso substituents is yet not understood and requires further experiments to establish whether the compound I analogues do have the same EPR spectra as their corresponding peroxy intermediates.

In conclusion the naphthyl models are not suitable models for CPO catalytic intermediates. From these results it appears that the amide substituents are essential for obtaining $^-$OCl complexes of synthetic iron porphyrins.

VIII.3.2. Oxo complex.

To confirm our findings that the complexes obtained upon addition of hypochlorite are actually compound I analogues we used H_2O_2 and *m*CPBA to generate the oxo complexes

of the CPO model **32**. The UV-Vis characterization (*table 23*) confirmed that the complexes obtained previously with hypochlorite are potentially compound I analogues.

Compound:	Method:	Solvent:	Soret initial (nm):	Soret final (nm):
32	10% vol of a 30% aqueous H_2O_2 solution	CH_2Cl_2	406	400
32	2.5 eq. *m*CPBA	CH_2Cl_2	406	412
32	10% vol of a 30% aqueous H_2O_2 solution	Toluene	406	414
32	2.5 eq. *m*CPBA	Toluene	406	414

Table 23: UV-Vis characterization of compound I formation for 32.

Next the EPR spectra are also identical to the spectra obtained previously upon addition of hypochlorite and acid to **32**. They are characterized by $g_{eff}=4.26$ and $g_{eff}=2$.

These results also suggest that the complex obtained with **11** and **12** are not peroxy complex but are actually compound I analogues. If this proposal is correct the porphyrin environment do not play an essential role on the structure of compound I analogues as the EPR signals are identical for the four models synthesized.

VIII.4. Summary.

The results obtained with the naphthyl models of CPO and catalase show that the pivaloyl substituents are more efficient protecting groups respective to an oxidative degradation of the porphyrin ring in the presence of oxidants. The better accessibility of the sixth position of the iron atom is not advantageous as it led to a higher sensitivity towards oxidative degradation.

A second aspect which would reduce the ligand affinity of models **32** and **33** is the hydrophobic character of the complexes. The affinity for polar ligand such as hypochlorite is reduced due to hydrophobic repulsion of polar ligands.

These proposal suggests that residues which have hydrogen bond donors or acceptors and are hence polar or polarizable are essential for having good mimics of the CPO and catalase enzymes.

VIII.5. Synthesis of the tailed models 34 and 35.

VIII.5.1. Synthesis and solution structure of species tailed with a protected sulphur.

Based on the comparison between the naphthyl and pivaloyl substituted models for CPO we turned to new models of CPO which would combine:

1. the necessity to keep pivaloyl substituents and
2. the necessity of an opened distal side.

As mentioned in the introduction of this chapter we decided to synthesize tailed models **34** and **35**.

The synthesis of the CPO model **34** started with the synthesis of the corresponding "tailed" bridge moiety **47** by a procedure analogous to the synthesis of bridge **15** (*scheme 14*).
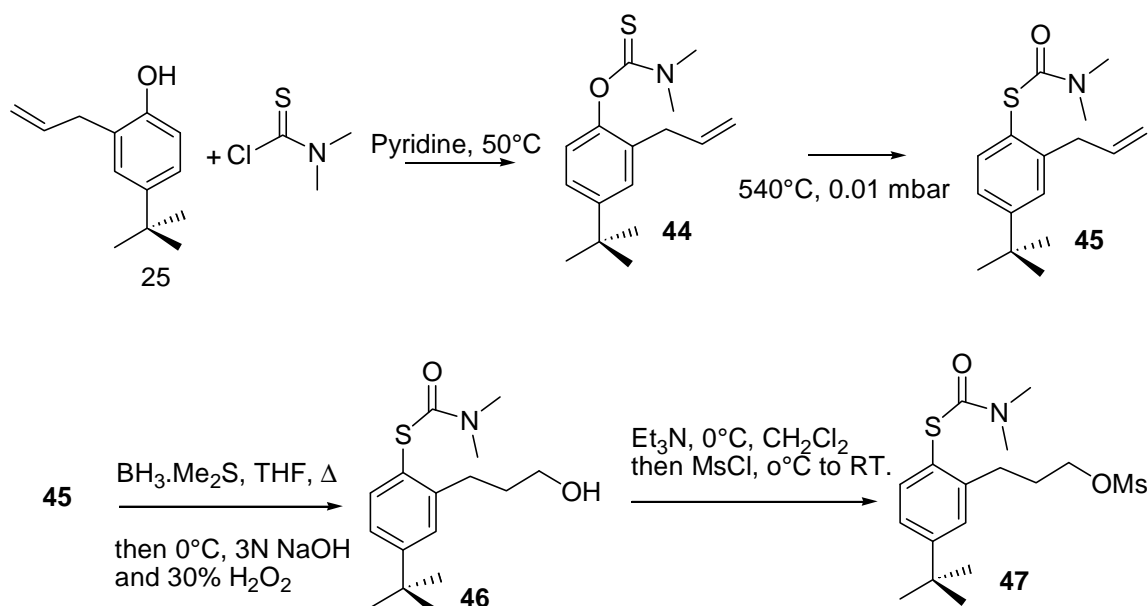
Scheme 14: Synthesis of the tailed bridge 47.

Then starting from **20b** a mono protection of one hydroxy group using iodo methane was achieved to give **48** (*scheme 15*) in 33% yield. This yield was expected from a statistic addition of the methyl group to both hydroxy functions, one hydroxy function or none of them in **20b**. The tailed bridge **47** was coupled to **48** under normal dilution conditions to yield the protected sulphur tailed compound **49** (*scheme 15*). High dilution is not necessary in this case as polymerisation is not possible. The introduction of the tailed bridge **47** was not accompanied by a red shift of the Soret as for the bridge compounds.

This result supports that the red shift upon bridging is due to the introduction of the bridging moiety. Then this shift is a characteristic feature which is useful to control the course of the bridging reaction.

20b

33% | Cs$_2$CO$_3$, DMF, 60°C
then 1eq. MeI, RT

48

Cs$_2$CO$_3$, DMF, 60°C then 43

49
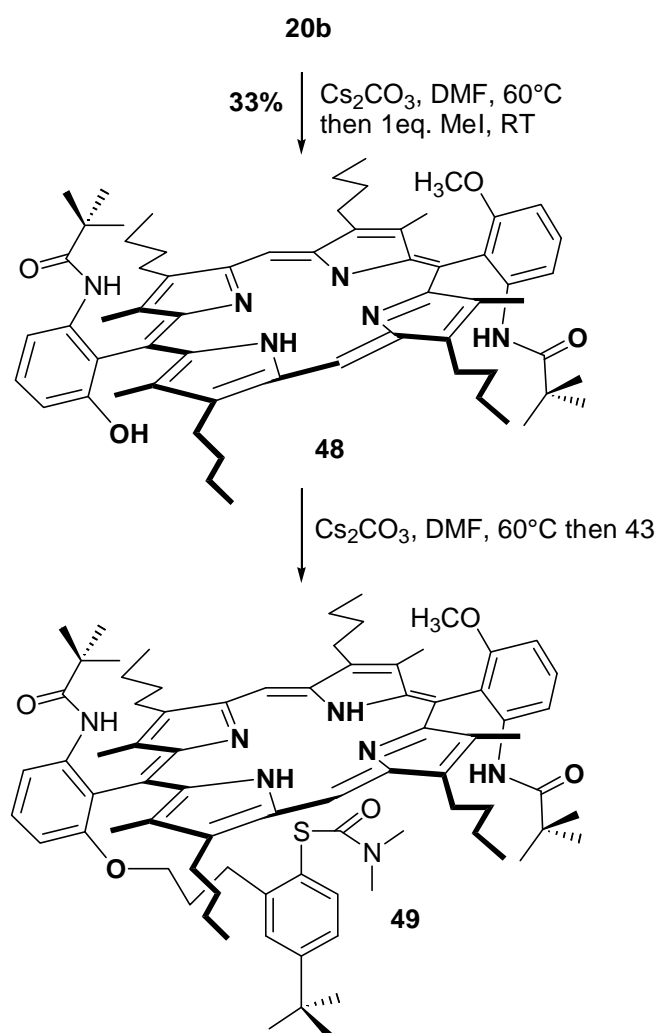
Scheme 15: Synthesis of the protected tailed precursor 49.

To check if the sulphur is in position to subsequently coordinate to the iron the structure in solution was determined by NMR spectroscopy using the chemical shifts and the NOE effects.

The first question addressed was the conformation of the amide bond and the related meso aryl substituents. For both meso aryl substituents the NOE effects observed between the NH amide proton and the neighbouring proton 5' of the aryl moiety is inexistent. According to *figure 27* this implies that only structures **ttt**, **tct**, **tcc** and **ttc** are possible. The NOE observed between the *tert*-butyl substituent and the amide NH proton is strong. The amide bond is therefore trans which eliminates structures **tcc** and **tct** as shown in *figure 54*.

For the aryl moiety bearing at position 2' the OMe group a strong NOE effect is observed between the proton of the OMe and proton 3'. Therefore the predominant middle conformation of the meso aryl substituent is **ttc**.

For the aryl substituent where the bridge is attached a strong NOE effect is also observed between the $CH_{2\alpha'}$ of the bridge and proton 3'. Therefore the preferred conformation for the corresponding aryl moiety is also **ttc** as shown in *figure 54*.

= porphyrin ring system
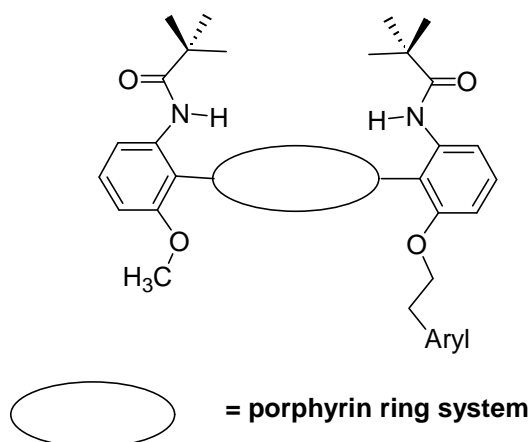
Figure 54: Conformation of the meso aryl substituents in 49.

The conformation obtained with the non bridged strucutre **49** is now comparable to the X-Ray structure of Collmann [85] for its TPivPP iron complex. These findings also supports that only bridging induces a change in the conformation of the ortho amide moiety on the meso aryl substituents.

The second question was to verify that the proximity of the sulphur to the center of the porphyrin core. This feature is essential to favour the coordination of the sulphur to the iron after iron insertion.

To answer this problem a first indication is the chemical shift of the N-methyl groups of the thiocarbamate protecting group. The N-methyl groups are connected to a nitrogen engaged in an amide bound. As the nitrogen has a strong sp^2 character the methyl group are coplanar and can be distinguished as cis and trans methyl groups provided the environment is magnetically not equivalent. Accordingly they give raise to a set of two singulets.

In the precursor **21** of the CPO model **11** they are found at 1.72 ppm and –1.3 ppm whereas in the bridge precursor **15** they are found at 3.3 ppm and 3.2 ppm respectively.

In **49** the signals were found at 2.47 ppm and 1.6 ppm respectively. Compared to the precursors **46** and **47** where the corresponding signals are found around 3.0 ppm (resp. 3.05 and 2.9 ppm) the shifts observed indicate that the sulphur is in the vinicity of a group which has a shielding effect.

However compared to **21** the shielding effect is by far less important which means that the sulphur is further away from the porphyrin core.

To establish the origin of the shielding which could also be due to an intermolecular effect between two porphyrin molecules we have examined the NOE effects observed for the protons of the bridge's arm.

The $CH_{2\gamma'}$ protons show a medium NOE to the NH amide proton of the other meso aryl substituent. A medium NOE effect is also found from the $CH_{2\beta'}$ to the $CH_{2\beta}$ protons. These data suggest that the phenyl group of the tail is lying to some extent under the porphyrin core but the sulphur is not in the immediate vinicity of the centre of the porphyrin core. Nevertheless the strong affinity of sulphur for iron could be sufficient to permit the coordination of the sulphur after iron insertion.

The force field modellisation which takes into account the NOE effects and chemical shifts gives the following structure (*figure 55*).
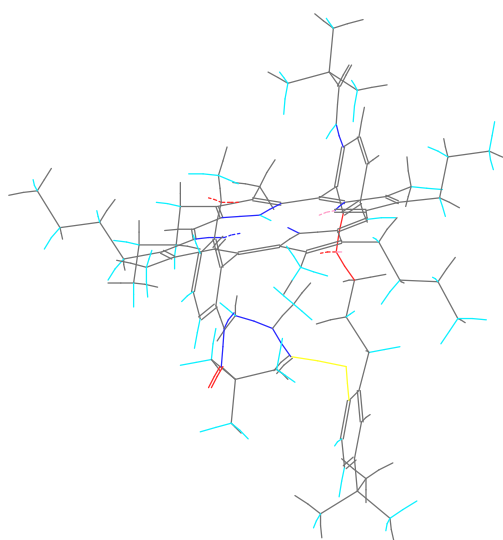

Figure 55: Craft field modellisation of 49.

The second tailed model **35** with an alkyl bridge was also synthesized by using the same strategy. The tailed alkyl bridge **54** was synthesized from commercially available δ-bromo valeric acid **50** (*scheme 16*).
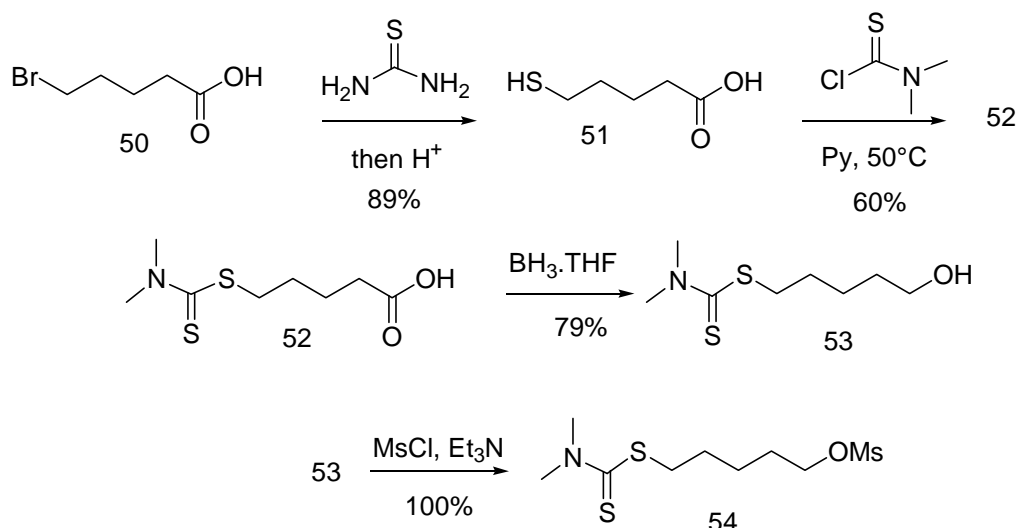
Scheme 16: Synthesis of the alkyl bridge 54.

As for the thiophenolate analogue **49** the bridge **53** was coupled to porphyrin **48** (*scheme 17*) to yield **55**. As for **49** the UV-Vis spectrum did not show a red shift of the Soret band upon bridging. This supports once again that the red shift is an indication that a bridging reaction takes place.
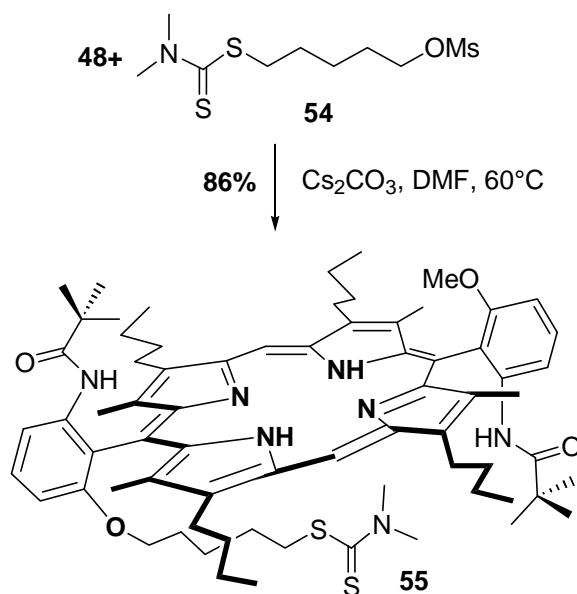
Scheme 17: Synthesis of 55.

The NMR data analysis for the conformation of the meso aryl substituent reveals that the same NOE effect are observed i.e. the conformation of the aryl substituents is the same as found by Collmann for its TPivPP iron complex.

The analysis of the conformation of the tail showed that the sulphur is probably not within bonding distance of the iron (*figure 56*). Namely no change for the chemical shifts of the N-methyl protons is observed upon bridging. Moreover the analysis of the NOE effects show that the protons from the alkyl bridge are not close to any proton of the β-pyrrole

substituents or more important to the $NH_{porphyrin}$ protons as is expected from the conformational study of **21**. These data are consistent with a tail hanging perpendicular to the porphyrin plane passing through the meso carbon 5 and 15 as showed by the molecular modelling minimization obtained (*figure 56*).
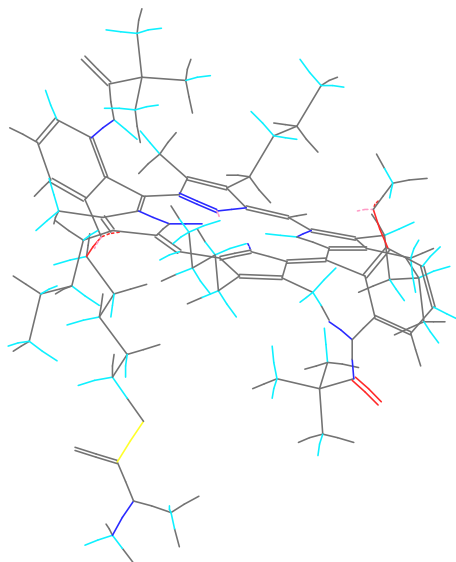

Figure 56: Craft field modellisation of 55.

The consequence after the iron insertion appears immediately: after deprotection and iron insertion the sulphur of a porphyrin molecule will coordinate to the iron atom of a second porphyrin molecule upon iron insertion. An oligomer array would be the resulting compound for the iron complex as no steric constraints can force the thiolate ligation to build monomers (*figure 57*).

Such a situation will probably not be the case for **34** as the phenyl ring induces steric hindrance. This hindrance prevents then the formation of oligomers and favours the coordination of the sulphur to the heme unit where it is anchored (*figure 57*). For these reasons we did only pursued the synthesis of model **35**.
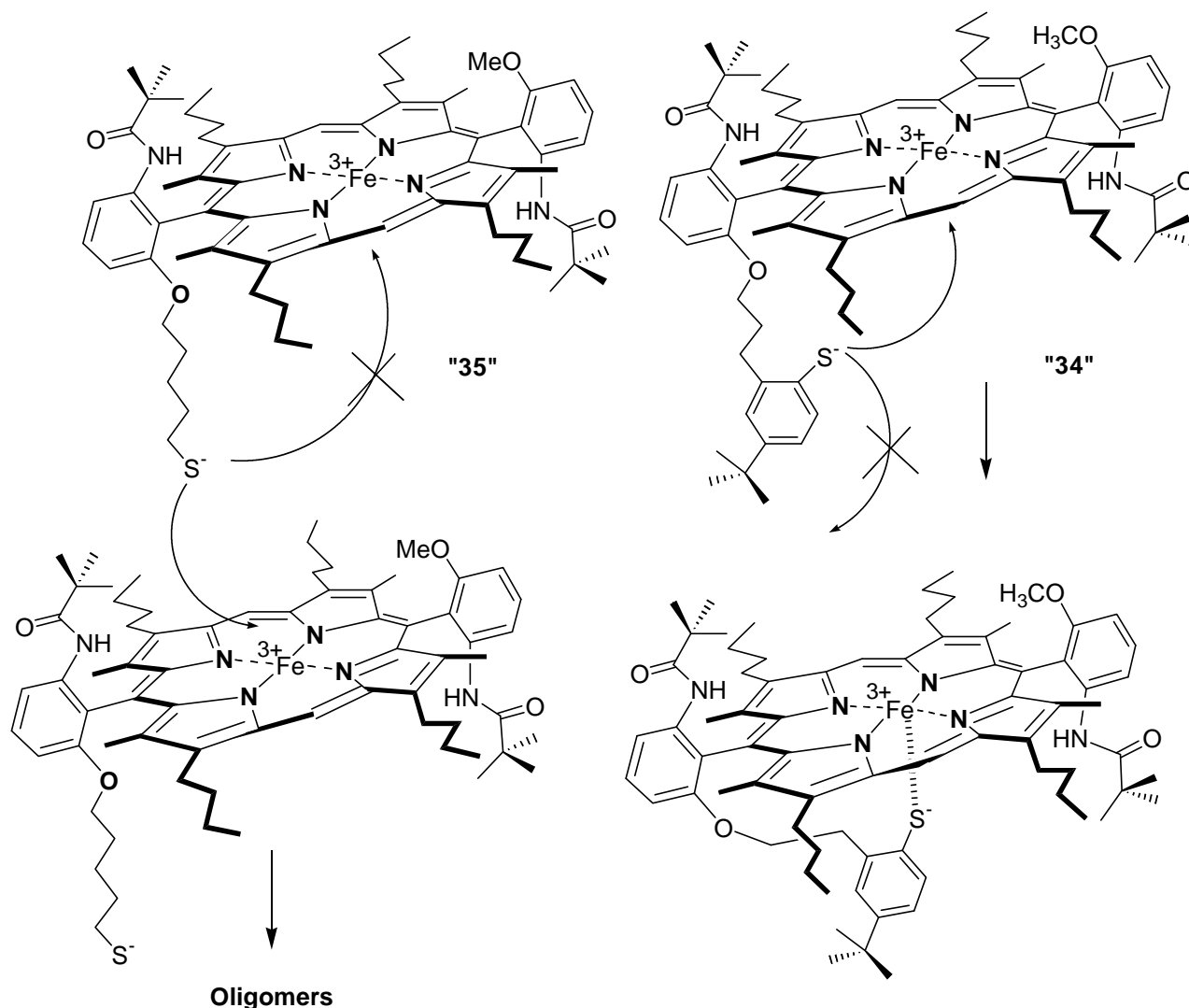
Figure 57: Formation of oligomers or monomer with 34 or 35.

VIII.5.2. Deprotection of the sulphur to get model 34.

The deprotection of the sulphur revealed difficulties as the compound first oxidized massively despites using a degassed reaction mixture for the thiophenolate model **49**. Second the part which was not oxidized was a mixture of two compounds which could not be separated as oxidation kept lowering the yields. Therefore the iron was first inserted into **49** and the deprotection was attempted (*scheme 18*). Unfortunately no satisfactory conditions were found to yield pure desired **33**.

FeBr$_2$, Et$_3$N, Toluene, Δ
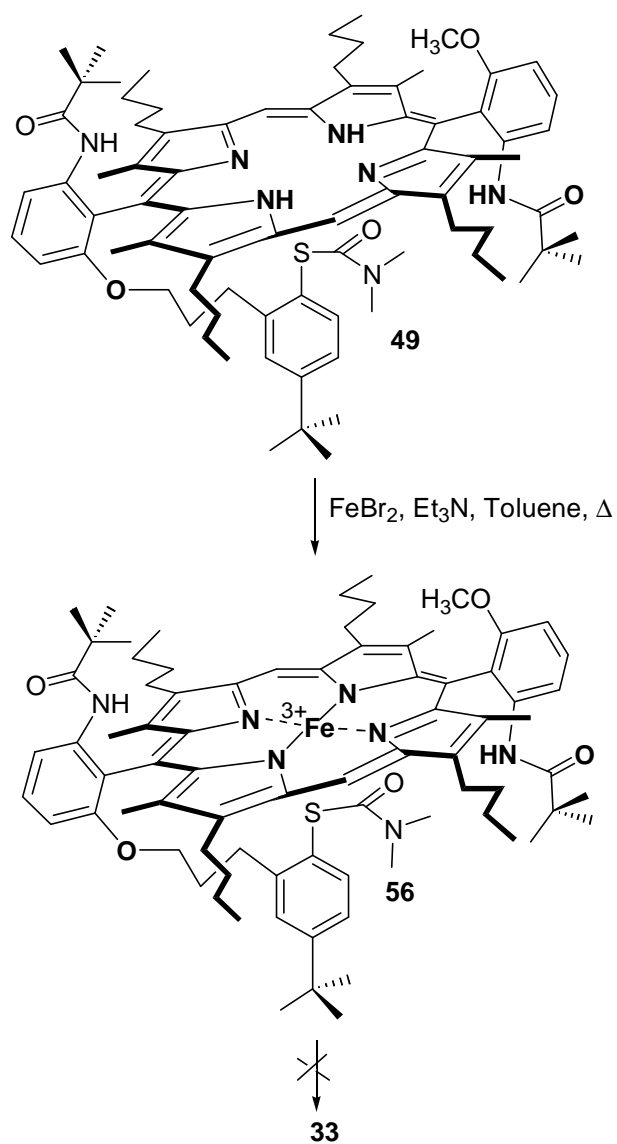
Scheme 18: Synthesis of 33 upon iron insertion and deprotection of the sulphur.

VIII.6. Summary and perspectives.

The attempts to obtain better models finally support the approach of bridged structures over tailed models. Contrary to the conclusion of *Nakamura et al.* with hydrogen bonded stabilized heme thiolate complex [122] we could not notice such an effect with the precursors **49** and **55**. Nevertheless the results obtained for metal free tailed porphyrin have permit to establish that upon bridging the UV-Vis spectra are red shifted and that the conformation of the ortho amide substituents on the meso aryl groups is changed.

For these reasons the future direction for having better binding constant is probably still to use an ortho amide function on the aryl moiety. But instead of having a bulky substituent directly linked to the carbonyl group of the amide this one should be anchored at a greater distance. For example the replacement of the *tert*-butyl group by a furan already improved the binding abilities of **11** [118].

EXPERIMENTAL PART

General remarks:

Solvents and reagents:

Solvents for reactions were of HPLC, purissime or purum quality. Solvents for water sensitive reactions were dried with the appropriate agent: calcium hydride for methylene chloride, sodium for toluene and sodium-benzophenone for ether and tetrahydrofurane. The dried solvents were used directly after distillation from the drying material.

Solvents for oxygen sensitive reactions carried out with Schlenk technique or in the Glove-box were dried and distilled before being degassed on high vacuum (3 purge-thaw cycles on high vacuum).

Solvents for chromatography were distilled on a Büchi rotatory evaporator before use.

Commercially available reagents were supplied by Fluka, Aldrich or Heraeus and used as received except otherwise indicated.

Apparatus and material:

For solvent distillation and removal, a Büchi rotatory evaporator RE 111 was used. Vacuum controlled was monitored by Vacuum controller 168 and supplied by a membrane pump MZ 2C from Vacuubrand. Cooling was achieved via a heat exchanger UWK 300 from Vacuubrand filled with isopropanol and temperature was maintained under 5°C.

For drying compounds, a high vacuum oil pump 2012 from Alcatel was used and vacuum was around 10^{-3} mbar.

Weighting was achieved with a Mettler AE 163 apparatus with a precision of $\pm$ 0.1 mg (>10 mg weighted product) or $\pm$ 0.01 mg (<10 mg weighted).

Glove-box were supplied by Mercaplex (model 2201) and oxygen and water content were monitored by a Teledyne analyser. The value were kept below 3 ppm for oxygen and 10 ppm for water. Degassing ante-chamber was done through a membrane pump MZ 2C from Vacuuband and solvents were removed via an oil pump Speedivac EV 50 from Edwards.

Purifications:

Column chromatography were carried out on silica gel 60 (40-63 μm) or on neutral alumina supplied by Merck. Packing was done as a slurry of silica or alumina under 0.4 bar pressure

(air or argon). Separations were achieved with a pressure of max. 0.2 bar. Probe deposing was achieved by dissolving the crude product in a minimum of the eluting mixture and deposing through a Pasteur pipette on the top of the column.

Size (diameter*length) of the column and eluant are given in the experimental section. Solvent mixture is indicated as V/V ratio.

Preparative plates 20 cm*20 cm*2 mm (Silica gel F_{260}) were purchased from Merck. After development, the product was recovered by stirring the silica band containing it with the appropriate solvent and filtration of silica gel followed by concentration on rotatory evaporator.

Reactions were followed on 5*10 cm thin layer silica gel F_{260} plates (0.25 mm) from Merck.

The UV active compounds were detected with a UV-lamp from Camag either at 254 nm or 366 nm.

UV inactive compounds or detection of aldehydes or double bonds were revealed by spraying the appropriate reagent. Aldehydes were sprayed with 0.4% DNPH in 2M HCl, double bonds were revealed by an ethanolic $KMnO_4$ solution and NH_2 functions by a 10% Ninhydrine ethanolic solution.

Spectroscopic methods:

UV-Vis spectra were recorded on a HP 8452A diode array spectrophotometer from Helwett-Packard and worked out with the software UV-Vis Chemstation A.02.04 from Hewlett-Packard. Precision of measurements is ± 2 nm (diode distance) and only the maxima are indicated. The percentages are calculated in reference to the most intense signal.

<u>Abbreviation:</u> UV-Vis (solvent): λ (nm) (relative absorption in %).

NMR spectra for routine analysis were recorded on a Gemini 300 apparatus from VARIAN or a BRUCKER DPX 400 with automatic sampler changer.

The frequency for ^{1}H NMR is 300 MHz and 75 MHz for ^{13}C NMR for the VARIAN apparatus and 400.13 resp. 101 MHz for the BRUCKER one.

Characterizations were done on a BRUCKER DRX 600 NMR-spectrometer with a frequency of 600.13 MHz for ^{1}H NMR and 150 MHz for ^{13}C.

All two dimensional experiments were also recorded on this apparatus.

Solvents for NMR measurements were purchased by Dr. Glaser AG, Basel.

Reference for ^{1}H is the TMS signal and for ^{13}C the solvent signal.

Spectra are reported as follow for proton spectroscopy: ^{1}H-NMR (frequency in MHz, solvent), δ: chemical shift in ppm, (multiplicity, coupling constant in Hz, signal attribution, integral value).

Multiplicity is indicated as follow: s = singlet, d = doublet, t = triplet, q: quadruplet, qui = quintuplet, sext= sextuplet, m = multiplet, br: broad signal.

For carbon spectra, the report is : ^{13}C-NMR (frequency, solvent): chemical shift in ppm, attribution.

ESR spectra were recorded on a BRUCKER CW-spectrometer in the X-band mode, 10 mW power at 100 K. The pulse ESR spectra and low temperature spectra were recorded at the Institute of Physical Chemistry of the ETH-Zürich.

Mass spectroscopy:

For the porphyrins a MALDI-TOF mass-spectrometer LaserTec from Vestec coupled to a double canal oscilloscope TDS 520 A from Tectronix were used. The spectra were worked out on a Gateway PC-computer using the software Voyager Biospectrometry (version 2.13).

FAB and EI mass spectrometry were recorded on a doubly focused spectrometer VG-70-250 from Varian. For EI the ionisation potential was 70 eV.

Cyclic voltammetry:

Measurements of redox potential were achieved with a polarograph Model 443 from Amel. The results were computed with the software Amel (version 5.6E) and EXCEL.

The working electrode is a glassy-carbon electrode (0.1 mm) which was polished on aluminium oxide pasta (0.05 μm) and washed with the solvent used for measurement before use. The three electrode configuration was achieved with a Pt-counter electrode and a NaCl-Calomel (SCE) reference electrode. The electrolyte is a 0.1M $LiClO_4$ DMF solution saturated with LiBr to avoid problems of ligand exchange during measurement.

Before measuring the solution was purged with argon for 15 Min and during the measure was maintained under an argon stream passing above the solution.

The results are indicated as E_0 value in mV uncorrected from the difference of +5 mV due to use of NaCl-SCE instead of KCl-SCE system. Precision is ±10 mV.

Part A: Porphyrin synthesis.

A.1. Synthesis of the CPO model 11 and the catalase model 12.

The synthesis of compound **13** and **14** were achieved according to literature procedure [20, 68]. The analysis (spectra and yields) were identical. Therefore their synthesis is not reported.

5,15-Bis-(6'-pivaloylamino-2'-methoxyphenyl)-3,7,13,17-tetrabutyl-2,8,12,18-tetramethyl-porphyrinato- zinc (II) (18a and 18b):

668.5 mg (2.84 mmol, 1 eq.) **14** in 50 ml acetonitrile were bubbled for 15 Min. with argon. 814 mg (2.84 mmol, 1 eq) **13** and 54 mg (0.284 mmol, 0.1 eq) *p*TsOH were added and the solution was stirred at RT. for 20 hr under light exclusion. Subsequently 1.047 g (4.28 mmol, 1.5 eq) *o*-chloranil were added in 20 ml THF and the reaction mixture was reacted for a further 30 Min. The dark-brown solution was evaporated and the residue was filtrated by column chromatography (silica gel, 6*20 cm, Hex:EE 3:1+1% Et_3N). The fractions containing the product were concentrated, redissolved in 125 ml dichloromethane and 25 ml methanol. To the red solution was added 1.3 g (7.1 mmol, 5 eq) zinc acetate and the reaction was refluxed 10 Min. until it turned pink. The solution was neutralized with 200 ml saturated $NaHCO_3$ solution, filtered over celite. The aqueous phase was extracted three times with 100 ml CH_2Cl_2. The combined organic layers were dried over Na_2SO_4, filtered and evaporated. The residue was further purified by column chromatography (silica gel, 6*35 cm, Hex:EE 5:1+ 1% Et_3N).

Finally 814.07 mg (53.8%) of the α,β-atropisomer **18b** and 174.1 mg (11.3%) of the α,α-atropisomer **18a** were recovered.

Analysis:

Yield: 65.1% (53.8% α,β-atropisomer and 11.3% α,α-atropisomer).

TLC (silica gel, Hex:EE 5:1+1% Et_3N)**:** R_f= 0.31 for **18b** and R_f= 0.17 for **18a**

HPLC (RP-18 250 mm, gradient $MeCN:H_2O$ 90 to 100% MeCN, 50°C)**:** Rt=10.48 Min. for **18a** and Rt=11.56 Min. for **18b**.

MALDI-TOF: M=1064.8 (M)$^+$.

UV-Vis (CH_2Cl_2+1% Et_3N): λ = 412 nm (100%), 576 nm (8%), 538 nm (7.9%).

NMR analysis:

18a:

^{1}**H-NMR** (600 MHz, CDCl$_3$, RT):

δ: 10.15 (s, H$_{10,20}$, 2H); 8.45 (d, J= 8.36, H$_{5'}$, 2H); 7.8 (t, J = 8.42, H$_{4'}$, 2H); 7.12(d, J = 8.46, H$_{3'}$, 2H); 6.91(s, N$\underline{H}$Piv, 2H); 4.03-3.87 (m, CH$_{2\alpha}$, 8H); 3.61 (s, OC$\underline{H}_3$, 6H); 2.58 (s, CH$_{3pyrrole}$, 12H); 2.17 (qui, J= 7.41, CH$_{2\beta}$, 8H); 1.74 (sext, J= 7.48, CH$_{2\gamma}$, 8H); 1.11 (t, J= 7.24, CH$_{3\delta}$, 12H); -0.18 (s, C(O)C(C$\underline{H}_3$)$_3$, 18H).

^{13}**C-NMR** (151 MHz, CDCl$_3$, RT): The signals were attributed with help of HETCOR, HMBC and HMQC experiments.

176.5: C=O; 159.4: C$_{2'}$; 147.8: C$_{4,6,14,16}$, 147.1: C$_{1,9,11,19}$; 144.1: C$_{2,8,12,18}$; 140.5: C$_{1'}$; 137.5: C; 130.6: C$_{4'}$; 121.7: C$_{6'}$; 113.7: C$_{5'}$; 108.1: C$_{5,15}$; 106.8: C$_{3'}$; 97.9: C$_{10,20}$; 55.9: OCH$_3$; 39.0: $\underline{C}$(CH$_3$)$_3$; 35.5: C$_\beta$; 26.3: C$_\alpha$and C($\underline{C}$H$_3$)3; 23.2: C$_\gamma$; 14.2: C$_\delta$; 14.0: CH$_{3pyrrole}$.

18b:

^{1}**H-NMR** (600 MHz, CDCl$_3$, RT):

δ: 10.21 (s, H$_{10,20}$, 2H); 8.5 (d, J= 7.69 , H$_{5'}$, 2H); 7.84 (t, J= 8.3, H$_{4'}$, 2H); 7.17 (d, J= 7.75, H$_{3'}$, 2H); 6.89, (s, N$\underline{H}$Piv, 2H); 4.05-3.95 (m, CH$_{2\alpha}$, 8 H); 3.69 (s, OC$\underline{H}_3$, 6H); 2.65 (s, C$\underline{H}_{3pyrrole}$, 12H); 2.17 (qui, J= 7.6, C$\underline{H}_{2\beta}$, 8H); 1.73 (sext, J= 7.5, C$\underline{H}_{2\gamma}$, 8H); 1.1 (t, J= 7.4, C$\underline{H}_{3\delta}$, 12H); -0.17 (s, C(O)C(C$\underline{H}_3$)$_3$, 18H).

^{13}**C-NMR** (151 MHz, CDCl$_3$, RT): The signals were attributed with help HETCOR, HMBC and HMQC experiments. 176.5: C=O; 159.4: C$_{2'}$; 147.8: C$_{4,6,14,16}$; 147.1: C$_{1,9,11,19}$; 144.1: C$_{2,8,12,18}$; 140.5: C$_{2,8,12,18}$; 137.5: C$_{3,7,17,13}$; 130.6: C$_{4'}$; 121.7: C$_{1'}$; 113.7: C$_{5'}$; 108.1. C$_{5,15}$, 106.8: C$_{3'}$; 97.9: C$_{10,20}$, 55.9: O$\underline{C}$H$_3$; 39.0: C($\underline{C}$H$_3$)$_3$; 35.5: C$_\beta$; 26.3. C$_\alpha$ and C(CH$_3$)3; 23.2: C$_\gamma$; 14.2: C$_\delta$; 14.0: $\underline{C}$H$_{3pyrrole}$.

a,a-[5,15-Bis-(6'-pivaloylamino-2'-methoxy-phenyl)-3,7,13,17-tetrabutyl-2,8,12,18-tetramethyl-porphyrin] (17a):

174.1 mg (16.31 mmol, 1 eq) **18a** were dissolved in 20 ml dichloromethane and 25 ml concentrated HCl. The green solution was stirred at RT. for 30 Min., the organic phase was separated and the aqueous phase extracted twice with dichloromethane. The combined organic layers were neutralized with a saturated aquous NaHCO$_3$ solution, separated, dried over sodium sulphate, filtered and concentrated. The red residue was purified by column chromatography (silica gel, 6*20 cm, Hex 3: EE 1+1% Et$_3$N) to yield 129.2 mg (78%) **17a** as a violet powder.

Analysis:

Yield: 78%.

TLC (silica gel, Hex:EE 3:1+1% Et$_3$N)**:** R$_f$= 0.20 (UV$^+$, Vis$^+$).

HPLC (CN 125 mm, Hex:CH$_2$Cl$_2$ 8:2, RT)**:** 3.8 Min.

MALDI-TOF: M=1001.5 (M)$^+$.

UV-Vis (CH$_2$Cl$_2$+1% Et$_3$N): λ = 408 nm (100%), 508 nm (8%), 542 nm (3%), 588 nm (1%)

^{1}H-NMR (300 MHz, CDCl$_3$, RT):

δ: 10.22 (s, H$_{10,20}$, 2H); 8.47 (d, J = 8.3, H$_{5'}$, 2H); 7.8 (t, J= 8.46, H$_{4'}$, 2H); 7.1 (d, J = 8.79, H$_{3'}$, 2H); 7.08 (s, N$\underline{H}$Piv, 2H); 4.04 - 3.93 (m, CH$_{2\alpha}$, 8H); 3.56 (s, OC$\underline{H}_3$, 6H); 2.61 (s, CH$_{3pyrrole}$, 12H); 2.18 (qui, J = 7.41, CH$_{2\beta}$, 8H); 1.77 (sext, J = 7.42, CH$_{2\gamma}$, 8H); 1.12 (t, J = 7.42, CH$_{3\delta}$, 12H); -0.03 (s, C(O)C(C$\underline{H}_3$)$_3$, 18H); -2.19 (br, N$\underline{H}_{porphyrin}$, 2H).

^{13}C-NMR (75 MHz, CDCl$_3$, RT.): the signal attribution was determined on the basis of the previous results for **17b**:

176.49: C=O: 159.24: C$_{2'}$;145.33: C$_{4,6,14,16}$; 143.71: C$_{1,9,11,19}$; 141.89: C$_{1'}$; 140.03: C$_{2,8,12,18}$: 135.79: C$_{3,7,13,17}$; 130.73: C$_{4'}$; 120.29: C$_{1'}$; 113.69: C$_{5'}$; 107.13: C$_{5,15}$; 106.99: C$_{3'}$; 97.06: C$_{10,20}$; 55.78: OCH_3; 39.08: $\underline{C}$(CH$_3$)$_3$: 35.50: C$_\beta$; 26.39:C$_\alpha$; 26.29: C($\underline{C}$H$_3$)$_3$; 23.25: C$_\gamma$; 14.18: C$_\delta$; 13.34: CH$_{3pyrrole}$.

a,b-[5,15-Bis-(6'-pivaloylamino-2'-methoxyphenyl)-3,7,13,17-tetrabutyl-2,8,12,18-tetramethyl-porphyrin] (17b):

1.13 g (1.06 mmol, 1 eq) **18b** were dissolved in 100 ml dichloromethane and 30 ml 18% HCl. The green solution was stirred for 10 Min. and the aqueous phase was extracted with dichloromethane. The organic layers were neutralized with an aqueous NaHCO$_3$ solution, separated, dried over sodium sulphate, filtered and evaporated. The residue was purified by column chromatography (silica gel, 6*25 cm, Hex:EE 2:1 +1% Et$_3$N) to yield 919.7 mg (86.5%) violet powder **17b**.

Analysis:

Yield: 86.5%.

TLC (silica gel, Hex:EE=5:1+1% Et$_3$N)**:** R$_f$=0.21 (UV$^+$, Vis$^+$).

HPLC (CN 125 mm, Hex:CH$_2$Cl$_2$ 8:2)**:** R$_t$ = 3 Min.

MALDI-TOF: M=1001.5 (M)$^+$.

UV-Vis (CH$_2$Cl$_2$+1% Et$_3$N): λ = 408 nm (100%), 508 nm (8%), 542 nm (3%), 588 nm (1%)

^{1}H-NMR (300 MHz, CDCl$_3$, RT):

δ: 10.22 (s, H$_{10,20}$, 2H); 8.47 (d, J = 8.3, H$_{5'}$, 2H); 7.81 (t, J = 7.9, H$_{4'}$, 2H); 7.13 (d, J= 8.5, H$_{3'}$, 2H); 6.93 (s, NHPiv, 2H); 4.07-3.93 (m, CH$_{2\alpha}$, 8H); 3.64 (s, OCH$_3$, 6H); 2.60 (s, CH$_{3pyrrole}$, 12H); 2.17 (qui, J = 7.48, CH$_{2\beta}$, 8H); 1.72 (sext, J = 7.26, CH$_{2\gamma}$, 8H); 1.08 (t, J = 7.42, CH$_{3\delta}$, 12H), -0.11 (s, C(O)C(CH$_3$)$_3$, 18H); -2.22 (br, NH$_{porphyrin}$, 2H).

^{13}C-NMR (101 MHz, CDCl$_3$, RT.): the signals were attributed from the results obtained for **17b.** and from a HETCOR spectrum. 176.6: C=O: 159.3: C$_{2'}$;145.2: C$_{4,6,14,16}$; 143.8: C$_{1,9,11,19}$; 142.2: C$_{1'}$; 140.03: C$_{2,8,12,18}$: 135.8: C$_{3,7,13,17}$; 130.8: C$_{4'}$; 120.5 C$_{1'}$; 113.7: C$_{5'}$; 107.1:C$_{5,15}$; 106.8: C$_{3'}$; 97.3: C$_{10,20}$; 55.8: OCH$_3$; 39.1: C(O)C(CH$_3$)$_3$; 35.50: C$_\beta$; 26.4: C$_\alpha$; 26.3: C(CH$_3$)$_3$; 23.2: C$_\gamma$; 14.2: C$_\delta$; 13.4: CH$_{3pyrrole}$.

a,a-[5,15-Bis(6'-pivaloylamino-2'-hydroxy-phenyl)-3,7,13,17-tetrabutyl-2,8,12,18-tetramethyl-porphyrin] (20a):

129.2 mg (0.13 mmol, 1 eq) **17a** were dissolved in 20 ml dichloromethane and 20 ml ethanethiol. 654 mg (4.9 mmol, 38 eq) aluminium chloride were added and the green solution was stirred overnight at RT. The solution was then diluted with water (100 ml), the product was recovered by extraction with dichloromethane. The combined organic layers were washed with a saturated sodium hydrogenocarbonate solution, separated, dried over sodium sulphate, filtered and evaporated. The residue was purified by column chromatography (silica gel, 5*25 cm, CH$_2$Cl$_2$:Hex 7:3 +0.5% MeOH +0.1% Et$_3$N) to yield 95 mg (75.6%) violet powder **20a**.

Analysis:

Yield: 75.6.

TLC(silica gel, CH$_2$Cl$_2$: Hex 7:3+ 0.5% MeOH + 0.1% Et$_3$N)**:** R$_f$= 0.4 (UV$^+$, Vis$^+$).

HPLC (CN 125 mm, Hex:EE 7:3+0.5% MeOH)**:** 3.1 Min.

MALDI-TOF: M=973.4 (M)$^+$.

UV-Vis (CH$_2$Cl$_2$+1% Et$_3$N): λ = 408 nm (100%), 510 nm (14%), 576 nm (11.4%), 540 nm (9.6%).

^{1}H-NMR (300 MHz, CDCl$_3$, RT): δ: 10.29 (s, H$_{10,20}$, 2H); 8.42 (d, J = 7.9, H$_{5'}$, 2H); 7.73 (t, J = 8.24, H$_{4'}$, 2H); 7.17 (s, NHPiv, 2H); 7.12 (d, J = 8.25, H$_{3'}$, 2H); 4.22 (s, br, OH, 2H); 4.05-3.9 (m, CH$_{2\alpha}$, 8H); 2.68 (s, CH$_{3pyrrole}$, 12H); 2.18 (qui, J = 7.42, CH$_{2\beta}$, 8H); 1.76 (sext,

J = 7.63, $CH_{2\gamma}$, 8H); 1.11 (t, J = 7.3, $CH_{3\delta}$, 12H); 0.11 (s, $C(O)C(C\underline{H}_3)_3$, 18H); -2.34 (br, $N\underline{H}_{porphyrin}$, 2H).

^{13}C-NMR (75 MHz, $CDCl_3$, RT): the signals were interpreted by comparison of the data obtained for **17a** and **18a**:176.40: C=O: 155.43: $C_{2'}$;145.75: $C_{4,6,14,16}$; 144.84: $C_{1,9,11,19}$; 142.67: $C_{2,8,12,18}$; 139.21: $C_{1'}$: 136.42: $C_{3,7,13,17}$; 131.37: $C_{4'}$; 117.66: $C_{6'}$; 113.28: $C_{5'}$; 111.67:$C_{3'}$; 103.66: $C_{10,20}$; 97.99: $C_{5,15}$; 39.08: $\underline{C}(CH_3)_3$: 35.48: C_β; 26.47: $C(\underline{C}H_3)_3$; 26.37: C_α; 23.27: C_γ; 14.14: C_δ; 13.21: $CH_{3pyrrole}$.

a,b-[5,15-Bis-(6'-pivaloylamino-2'-hydroxy-phenyl)-3,7,13,17-tetrabutyl-2,8,12,18-tetramethyl-porphyrin] (20b):

400.6 mg (0.4 mmol, 1 eq) **17b** were dissolved in 50 ml dichloromethane and 35 ml ethanethiol. 2.03 g (15.2 mmol, 33.5 eq) aluminium chloride were added and the green solution was stirred overnight at RT. The solution was then diluted with water (200 ml), the product was recovered by extraction with dichloromethane. The combined organic layers were washed with a saturated sodium hydrogenocarbonate solution, separated, dried over sodium sulphate, filtered and evaporated. The residue was purified by column chromatography (silica gel, 10*25 cm, Hex:EE 2:1+1% Et3N).) to yield 390 mg (100 %) violet powder **20b**.

Analysis:

Yield: 100% violet powder.

TLC (silica gel, Hex:EE 2:1+1% Et3N)**:** R_f= 0.48 (UV[+], Vis[+]).

HPLC (CN 125 mm, Hex:EE 8:2+0.5% MeOH, RT)**:** 2.6 Min.

MALDI-TOF: M=973.4 (M)[+].

UV-Vis (CH_2Cl_2+1% Et3N): λ = 408 nm (100%), 510 nm (14%), 576 nm (11%), 540 nm (9.6%)

^{1}H-NMR (300 MHz, $CDCl_3$, RT): δ: 10.32 (s, $H_{10,20}$, 2H); 8.43 (d, J = 7.9, $H_{5'}$, 2H); 7.77 (t, J = 8.24, $H_{4'}$, 2H); 7.16 (d, J = 8.24, $H_{3'}$, 2H); 6.92 (br, N$\underline{H}$Piv, 2H); 4.6 (s, O$\underline{H}$,2H); 4,12-4,02 (m, $CH_{2\alpha}$, 8H); 2.68 (s, $CH_{3pyrrole}$ 12H); 2.19 (qui, J = 7.42, $CH_{2\beta}$, 8H); 1.73 (sext, J = 7.48, $CH_{2\gamma}$, 8H); 1.09 (t, J = 7.1, $CH_{3\delta}$, 12H); -0.01 (s, $C(O)C(C\underline{H}_3)_3$, 18H), -2.22 (br, N$\underline{H}_{porphyrin}$, 2H).

^{13}C-NMR (101 MHz, $CDCl_3$, RT): the signals were attributed from a HETCOR spectra and comparison between **20a** and **20b**: δ: 176.8: C=O: 156.3: $C_{2'}$;145.0: $C_{4,6,14,16}$; 143.9: $C_{1,9,11,19}$; 141.9: $C_{2,8,12,18}$; 138.9: $C_{1'}$: 136.0: $C_{3,7,13,17}$; 130.7: $C_{4'}$; 118.4: $C_{6'}$; 112.5: $C_{5'}$;

111.9: $C_{3'}$; 102.6: $C_{5,15}$; 97.3: $C_{10,20}$; 38.7: $\underline{C}(CH_3)_3$: 35.1: C_β; 26.1: $C(\underline{C}H_3)_3$; 26.0: C_α; 22.9: C_γ; 13.7: C_δ; 12.8: $CH_{3pyrrole}$.

Derivatization of **17b** to its *para*-nitrophenylester **17c** gave the following NMR analysis:

^{1}H-NMR (600 MHz, CDCl$_3$, RT): δ: 10.11 (s, $H_{10,20}$, 2 H); 8.84 (d, J = 8.43, $H_{5'}$, 2H); 7.93 (t, J = 8.39, $H_{4'}$, 2H); 7.61 (s, N$\underline{H}$Piv, 2H); 7.55 (d, J = 8.21, $H_{3'}$, 2H); 6.64 (d, J= 8, $H_{3'',5''}$, 2H); 6.4 (d, J = 8.01, $H_{2'',6''}$, 2H); 3.98-3.91 (m, $CH_{2\alpha}$, 8H); 2.68 (s, $CH_{3pyrrole}$, 12H); 2.15 (qui, J = 7.69, $CH_{2\beta}$, 8H); 1.76 (sext, J = 7.48, $CH_{2\gamma}$, 8H); 1.12 (t, J = 7.35, $CH_{3\delta}$, 12H); 0.25 (s, C(O)C(C$\underline{H}$_3)_3, 18H); -2.48 (br, N$\underline{H}$_{porphyrin}, 2H).

A strong NOE effect is observed between the Pivaloyl H's and $H_{3'',5''}$ of the phenylester moiety, indicative of the (α,β) configuration.

MALDI-TOF: M=1270.9 (M-1)$^+$

UV-Vis (CDCl$_3$): λ= 410 nm (100%), 510 nm (8.5%), 580 nm (5.7%), 546 nm (4.2%).

5,15-{(6-pivaloylamino-[4-tert-butyl-2-N,N-dimethylthiocarbamoyl-1,3-phenylen)-bis-(trimethylenoxy)-di-2,1-phenylen]}-3,7,17,27-tetrabutyl-2,8,12,18-tetramethyl-porphyrin (21):

95 mg (80.09 mmol, 1 eq) **20a** were dissolved in 100 ml abs. DMF and 1.065 g (3.27 mmol, 33.5 eq) **cesium carbonate** were added. The solution was vigorously stirred at 60°C for 30 Min. and 59.7 mg (0.12 mmol, 1.2 eq) of **15** in 20 ml abs. DMF were added within 3 hr. The reaction was then stirred at 60°C for a further 45 Min.

The red solution was quenched with 250 ml aqueous 10% HCl solution, the aqueous phase was extracted with three times with 100 ml TBDME. The combined organic layers were neutralized with 300 ml of a saturated NaHCO$_3$ solution, separated, dried over Na$_2$SO$_4$, filtered and evaporated. The residue was purified by column chromatography (silica gel, 5*35 cm, Hex:EE 5:1+1% Et$_3$N) to yield 67.67 mg (53%) red powder **21**.

Analysis:

Yield: 53%.

TLC (silica gel, Hex:EE 2:1+ 1% Et$_3$N)**:** R$_f$= 0.45 (UV$^+$, Vis$^+$).

HPLC (CN 125 mm, Hex:EE 85:15+0.5% MeOH, RT)**:** 2.9 Min.

MALDI-TOF: M=1289.6 (M-1)$^+$.

UV-Vis (CH$_2$Cl$_2$): λ = 414 nm (100%), 510 nm (9.8%), 580 nm (5.7%), 546 nm (4.9%)

^{1}H-NMR (600 MHz, CDCl$_3$, 280K): the signal attribution was made with help of COSY, NOESY and ROESY spectra at low temperature. δ: 10.11 (s, H$_{10}$, 1H); 9.72 (s, H$_{20}$, 1H); 8.61 (d, J= 7.97, H$_{5'}$, 2H); 8.42 (s, N$\underline{H}$Piv, 2H); 7.77 (t, J = 8.37, H$_{4'}$, 2H); 6.95 (d, J = 7.69, H$_{3'}$, 2H); 6.37 (s, H$_{3'',5''}$, 2H); 4.17-4.04 and 3.98-3.85 (2*m, CH$_{2\alpha'}$, 2*2H); 3.92-3.82 and 3.62-3.52 (m, CH$_{2\alpha}$, 8 H); 2.72 and 2.55 (2*s, CH$_{3pyrrole}$, 2*6 H); 2.22 (qui, J = 7.42, CH$_{2\beta'}$, 4H); 1.82-1.72 (m, CH$_{2\gamma'}$, 4H); 1.97-1.87 and 1.72-1.82 (2*m: CH$_{2\beta}$, 2*4H); 1.72 (br, N(C$\underline{H}_3$)$_2$, 3H); 1.62-1.72 (2*m, CH$_{2\gamma}$, 2*4H); 1.15-1.13 (2*t, J = 7.2, C$\underline{H}_{3\delta}$, 12H); 1.09 (s, H$_{2'''}$, 9H); 0.52 (s, C(O)C(C$\underline{H}_3$)$_3$, 18H); -1.32 (br, N(C$\underline{H}_3$)$_3$, 3H); -2.00 (br, N$\underline{H}_{porphyrin}$, 2H).

To get a better resolution for NMR the thiocarbamate protecting group (i.e. (CH$_3$)$_2$N-C=O) was replaced by a thiothiocarbamate protecting group (i.e. ((CH$_3$)$_2$N-C=S)

Analysis:

TLC (silica gel, Hex:EE 7:1 +1% Et$_3$N)**:** R$_f$= 0.39 (UV$^+$, Vis$^+$).

MS (MALDI-TOF): M=1306 (M)$^+$.

^{1}H-NMR (600 MHz, CDCl$_3$, RT): 10.11 (s, H$_{20}$, 1 H); 9.69 (s, H$_{10}$, 1 H); 8.6 (td, ^1J = 8.06, ^2J = 0.6, H$_{5'}$, 2H), 8.32 (s, N$\underline{H}$Piv, 2H); 7.73 (t, J = 8.06 Hz, H$_{4'}$, 2 H); 6.97 (d, J = 7.57, H$_{3'}$, 2H); 6.41 (s, H$_{3'',5''}$, 2H); 4.08 (m, CH$_{2\alpha}$, 2H); 3.94 (m, CH$_{2\alpha}$, 2H); 3.84 (m, CH$_{2\alpha}$, 2H); 3.81 (m, CH$_{2\alpha}$, 2H); 3.65 (m, CH$_{2\alpha'}$; 2H); 3.62 (m, CH$_{2\alpha'}$, 2 H); 2.72 (s, CH$_{3pyrrole}$ attached to C$_{3,17}$, 6H); 2.54 (s, CH$_{3pyrrole}$ attached to C$_{7,13}$, 6H); 2.32 (s. N(C$\underline{H}_3$)$_2$, 3H); 2.22 (qui, J = 7.3, CH$_{2\beta}$, 4H); 2.00 (m, CH$_{2\beta'}$, 2H); 1.94 (m, CH$_{2\beta'}$, 2H); 1.805 (m, H$_\gamma$, 4 H); 1.72 (m, CH$_{2\gamma'}$, 4H); 1.16 (s, H$_{2'''}$, 9H); 1.155 (m, CH$_{3\delta}$, 6H); 1.151 (m, CH$_{3\delta}$, 6H); 0.7 (m, CH$_{2\beta'}$, 4H); 0.08 (t, J = 7.3, CH$_{2\gamma'}$, 2H); 0.07 (m, J=7.3 Hz, CH$_{2\gamma'}$, 2H); -0.98 (s, N(C$\underline{H}_3$)$_2$, 3H); -2.07 (br, N$\underline{H}_{porphyrin}$, 2H).

^{13}C-NMR (150 MHz, CDCl$_3$, RT): 197.4: C=S; 176.93: C=O; 160.0: C$_{2'}$; 151.46: C$_{4''}$; 145.83: C$_{6,14}$; 145.23: C$_{4,16}$; 144.5: C$_{1''}$; 143.87: C$_{1,19}$; 143.5: C$_{9,11}$; 141.68: C$_{2,18}$; 141.35: C$_{8,12}$; 139.19: C$_{1'}$; 135.88: C$_{3,17}$; 135.52: C$_{7,13}$; 130.88: C$_{4'}$; 126.45: C$_{2'',6''}$; 122.94: C$_{3'',5''}$; 120.63: C$_6$; 113.11: C$_5$; 109.85: C$_3$; 107.46: C$_{5,15}$; 97.16: C$_{10}$; 96.33: C$_{20}$; 70.07: C$_{\alpha''}$; 44.16: N$\underline{C}$H$_3$; 39.63: C(O)$\underline{C}$(CH$_3$)$_3$; 38.71: N$\underline{C}$H$_3$; 35.53: C$_\beta$; 35.14: C$_{\beta'}$; 34.2: C$_{1'''}$; 31.2: C$_{2'''}$; 30.34: C$_{\beta''}$; 28.68: C$_{\gamma'}$; 26.37: C$_\alpha$; 26.03: C$_\alpha$; 23.34: C$_\gamma$; 23.28: C$_\gamma$; 14.22: C$_\delta$; 14.03: C$_{\delta'}$; 13.69: CH$_{3pyrrole}$ attached to C$_{3,17}$; 13.22: $\underline{C}$H$_{3pyrrole}$ attached to C$_{7,13}$.

5,15-{(6-pivaloylamino-[4-tert-butyl-2-sulfhydryl-1,3-phenylen)-bis-(trimethylenoxy)-di-2,1-phenylen]}-3,7,17,27-tetrabutyl-2,8,12,18-tetramethyl-porphyrin (22):

67.67 mg (0.052 mmol, 1 eq) **21** were dissolved in 20 ml degassed dioxane and the solution was bubbled for 30 Min. with argon. 1.55 ml (5.2 mmol, 100 eq) KOMe (95% powder). The reaction mixture was heated up to 110°C and the green solution was stirred for 55 Min. The solution was neutralized after cooling to RT with 100 ml aquous saturated NH$_4$Cl solution under argon and the product was recovered by extraction with three times 50 ml TBDME. The combined organic layers were dried over Na$_2$SO$_4$, filtered and evaporated. The residue was purified by column chromatography under argon (silica gel, 3*25 cm, Hex:EE 4.5:1+1% Et$_3$N) to yield 58 mg (93%) red powder **19**.

Analysis:

Yield: 93%.

TLC (silica gel, Hex:EE 5:1+ 1% Et$_3$N).**:** R$_f$= 0.22 (UV$^+$, Vis$^+$).

HPLC (CN 125 mm, Hex:EE 95:5+0.5% MeOH, RT)**:** 3.8 Min.

MALDI-TOF: M=1218.9 (M-1)$^+$.

UV-Vis (CH$_2$Cl$_2$): λ = 414 nm (100%), 510 nm (12.6%), 580 nm (9.3%), 544 nm (3.9%)

^{1}H-NMR (600 MHz, CDCl$_3$, RT): the signal attribution was made with help of COSY, NOESY and ROESY spectra. δ: 10.12 (s, H$_{10,20}$, 2H); 8.64 (d, J = 8.24, H$_{5'}$, 2H); 8.46 (s, N$\underline{H}$Piv, 2H); 7.77 (t, J = 8.39, H$_{4'}$, 2H); 6.94 (d, J = 8.24, H$_{3'}$, 2H); 6.2 (s, H$_{3'',5''}$, 2H); 4.05-4.02 and 3.94-3.9 (2 m, CH$_{2\alpha}$, 2*4H); 3.62 (t, J = 7.42, CH$_{2\alpha'}$, 2*2H); 2.12 (qui, J = 7.42, CH$_{2\beta}$, 8H); 1.67 (sext, J = 7.38, CH$_{2\gamma}$, 8H); 1.05 (t, J = 7.3, CH$_{3\delta}$, 12H); 0.87 (s, H$_{2'''}$, 9H); 0.67 (m, CH$_{2\gamma'}$, 4H); 0.55 (s, C(O)C(C$\underline{H}_3$)$_3$, 18H); 0.47 (m, CH$_{2\beta'}$, 4H); -2.13 (br, N$\underline{H}$$_{porphyrin}$, 2H); -3.01 (s, S$\underline{H}$, 1H).

^{13}C-NMR (101 and 151 MHz, CDCl$_3$, RT): the interpretation was done with comparison with the corresponding phenolate moiety **31** and a HETCOR spectrum.

177.0: C=O; 159.34: C$_{2'}$; 146.37: C$_{1''}$; 145.34: C$_{4,6,14,16}$; 143.76: C$_{1,9,11,19}$; 141.72: C$_{2,8,12,18}$; 139.5: C$_{4''}$; 138.06: C$_{1'}$; 135.61: C$_{3,7,13,17}$; 130.67: C$_{4'}$; 129.30: C$_{4'',6''}$; 123.14: C$_{3'',5''}$; 120.60: C$_{6'}$; 113.13: C$_{5'}$; 108.16: C$_{3',10,20}$; 97.09: C$_{5,15}$; 68.34: C$_{\alpha'}$; 39.70: C(O)$\underline{C}$(CH$_3$)$_3$; 35.36: C$_\beta$; 33.6: C$_{1'''}$; 31.23: C$_{\beta'}$; 30.94: C$_{2'''}$; 29.06: C$_{\gamma'}$; 26.99: C(O)C($\underline{C}$H$_3$)$_3$; 26.32: C$_\alpha$; 23.13: C$_\gamma$; 14.17: C$_\delta$; 13.39: $\underline{C}$H$_{3pyrrole.}$

5,15-{(6-pivaloylamino-[4-tert-butyl-2-thiolato-1,3-phenylen)-bis-(trimethylenoxy)-di-2,1-phenylen]}-3,7,17,27-tetrabutyl-2,8,12,18-tetramethyl-porphyrinato iron (III) (11):

To 12.2 mg (10 µmol, 1 eq) **22** were added in a Schlenktube 21.57 mg (0.1 mmol, 10 eq) **iron (II) dibromide** and 27.9 µl (0.2 mmol, 20 eq) **triethylamine** and 3 ml of toluene. The mixture was degassed three times in the high vacuum and refluxed for one hour. Subsequently the reaction was filtered over celite and concentrated. The residue was further purified through column chromatography (silica gel, 2*20 cm, Hex:EE 8:1) under argon to yield 9.55 mg (75%) **11** as a brown solid.

Analysis:

Yield: 75 %.

TLC (silica gel, Hex:EE 7:1)**:** R_f= 0.39 (UV$^+$, Vis$^+$).

MS (MALDI-TOF): M=1272 (M)$^+$.

UV-Vis (toluene): λ = 408 nm (100%), 512 nm (br, 10%)

NMR (600 MHz, toluene-d$_8$, RT): -57.1 (br, H$_{10,20}$, 2H); 8.3 (H$_{5'}$, 2H); 10.6 (H$_{4'}$, 2H); 12.7 (N$\underline{H}$Piv, 2H); 13.17 (H$_{3'}$, 2H); 35.9 and 39.4 (CH$_{2\alpha,}$ 8H); 38 (CH$_{3pyrrole}$, 12H); 85.3 (H$_{3'',5''}$, 2H); all other signals between –10 and +10 ppm could not be assigned.

ESR (10K, toluene): $g_{//}$= 8.347 and $g_{\perp}$=3.079 (br) for five coordination state; $g_{//}$= 5.773 and $g_{\perp}$=2.00 for six coordination state.

Cyclic voltammetry (DMF, 0.1M LiClO$_4$, RT): E^0= -565 mV vs SCE.

Iron(II) complexes:

Iron(II) sulphate:

A UV sample solution of **11** in 2 ml THF was stirred in the glove-box with a large excess of sodium borhydride for 30 Min.

Analysis:

UV-Vis (THF): λ= 420 nm (100%), 484 nm (26%), 538 nm (14.9%), 570 nm (12.4%).

MALDI-TOF: M=1273 (M)$^+$.

The sample was not stable enough to allow a further characterization.

5,15-{(6-pivaloylamino-[4-tert-butyl-2-N,N-dimethyloxythiocarbamoyl-1,3-phenylen)-bis-(trimethylenoxy)-di-2,1-phenylen]}-3,7,17,27-tetrabutyl-2,8,12,18-tetramethyl-porphyrin (30):

To a solution of 52.2 mg (53.6 μmol, 1 eq) **20a** in 55 ml abs. DMF under argon was added 594.0 mg (2.09 mmol, 34 eq) **cesium carbonate** and the supension was stirred at 80°C (oil bath temperature) for 30 Min. Then 32.8 mg (73.84 μmol, 1.2 eq) **16** in 5 ml abs. DMF were added within 3 hours. After cooling the solution was diluted with 50 ml 10% HCl and extracted with four times with 30 ml TBME. The combined organic layers were then washed twice with 150 ml saturated aqueous solution of NaHCO$_3$, dried over sodium sulphate, filtered and evaporated. The residue was further purified by column chromatography (silica gel, 4*25 cm, Hex:EE 4:1+ 1% Et$_3$N) to afford 14.2 mg (55%) red solid **30**.

Analysis:

Yield: 55%.

TLC(silica gel, Hex :EE 4:1+1% Et$_3$N)**:** R$_f$= 0.33 (UV$^+$, Vis$^+$).

MS (MALDI-TOF): M=1291 (M)$^+$.

UV-Vis (CDCl$_3$): λ = 414 nm (100%), 510 (10.4%); 542 (5.9%).

^{1}H-NMR (300 MHz, CDCl$_3$, RT):

δ:10.1 (s, H$_{20}$, 1H); 9.71 (s, H$_{10}$, 1H); 8.59 (d, J= 8.26, H$_{5'}$, 2 H); 8.29 (s, N<u>H</u>Piv, 2H); 7.77 (t, J = 8.3, H$_{4'}$, 2H); 6.98 (d, J = 7.7, H$_{3'}$, 2H); 6.33 (s, H$_{3'',5''}$, 2H); 4.15-3.6 (m, H$_{α,α',α''}$, 12H); 2.69 (s, CH$_{3\text{pyrrole}}$ attached to C$_{3,17}$, 6H); 2.55 (s, CH$_{3\text{pyrrole}}$ attached to C$_{7,13}$, 6H); 2.2 (m, H$_{β,β'}$, 8H); 2.1 (s, N(C<u>H</u>$_3$)$_2$, 6H); 1.75 (m, H$_{γ,γ'}$, 8H); 1.26 (s, H$_{2'''}$, 9H); 1.14 (J = 7.2, H$_δ$, 6H); 1.12 (t, J = 7.2, H$_{δ'}$, 6H); 0.47 (s, NHC(O)C(C<u>H</u>$_3$)$_3$, 18H); 0.1 (td, ^1J = 15; ^2J = 3, H$_{β''}$, 4H); 0.03 (td, ^1J = 15; ^2J= 3, H$_{γ'''}$, 4H); -2.2 (br, N<u>H</u>$_{\text{porphyrin}}$, 2H).

^{13}C-NMR (151.0 MHz, CDCl$_3$, RT):

5,15-{(6-pivaloylamino-[4-tert-butyl-2-hydroxy-1,3-phenylen)-bis-(trimethylenoxy)-di-2,1-phenylen]}-3,7,17,19-tetrabutyl-2,8,12,18-tetramethyl-porphyrin (31):

To a solution of 14 mg (10.84 μmol, 1 eq) **30** in 3 ml abs. dioxane was added under argon 48 mg (650.8 mmol, 60 eq) **KOMe** (95% powder) and the solution was stirred at 90°C (oilbath temperature) for 3 hours.

After cooling the solution was diluted with 30 ml of a 10% HCl solution and extracted four times with TBME. The organic layers were then washed twice with an aqueous saturated NaHCO$_3$ solution, dried over sodium sulphate, filtered and concentrated. The residue was further purified by column chromatography (silica gel, Hex:EE 4:1+ 1% Et$_3$N) to yield 9.7 mg (74%) red solid **31**.

Analysis:

Yield: 74%.

TLC (silica gel, Hex:EE 1:1+1% Et$_3$N)**:** R$_f$= 0.5 (UV$^+$, Vis$^+$).

MS (MALDI-TOF): M=1203 (M)$^+$.

UV-Vis (CDCl$_3$): λ = 414 nm (100%), 512 (8.2%); 546 (4.2%); 572 (3.4%).

^{1}H-NMR (500 MHz, CDCl$_3$, RT): the signals were attributed by COSY and NOESY experiments. δ: 10.14 (s, H$_{10,20}$, 2H); 8.62 (dd, ^1J = 7.8, ^2J = 0.76, H$_{5'}$, 2H); 8.36 (s, N$\underline{H}$Piv, 2H); 7.77 (t, J = 8.3, H$_{4'}$, 2H); 6.95 (dd; ^1J = 7.5, ^2J = 0.82, H$_{3'}$, 2H); 6.11 (s, H$_{3'',5''}$, 2H); 3.94 (t, J = 7.7, H$_{α,α'}$, 8H); 3.65 (t, J= 4.9, H$_{α''}$, 4H); 2.65 (s, CH$_{3pyrrole}$, 12H); 2.06 (qui, J = 7.7, H$_{β,β'}$, 8H); 1.71 (sext, J = 7.7, H$_{γ,γ'}$, 8H); 1.06 (t, J = 7.7, H$_{δ,δ'}$, 12H); 0.89 (s, H$_{2'''}$, 9H); 0.53 (s, C(O)C(C$\underline{H}_3)_3$, 18H); 0.5 (m, H$_{β''}$, 4H); 0.08 (m, H$_{γ''}$, 4H); -2.15 (s, O$\underline{H}$, 1H); -2.29 (s, N$\underline{H}_{porphyrin}$, 2H).

^{13}C-NMR (125 MHz, CDCl$_3$, RT): the signals were attributed by HMQC, HMBC experiments.

176.99: C=O; 159.46: C$_{1'}$; 146.16: C$_{1''}$; 145.71: C$_{4,6,14,16}$; 143.99: C$_{1,9,11,19}$; 141.94: C$_{2,8,12,18}$; 139.59: C$_{4''}$; 139.16: C$_{2'}$; 135.81: C$_{3,7,13,17}$; 130.82: C$_{4'}$; 125.51: C$_{2'',6''}$; 122.84: C$_{3'',5''}$; 120.74: C$_{6'}$; 113.07: C$_{5'}$; 108.88: C$_{3'}$; 107.38: C$_{5,15}$; 97.45: C$_{10,20}$; 68.94: C$_{α''}$; 39.68: C(O)$\underline{C}$(CH$_3)_3$; 35.42: C$_{β,β'}$; 33.83: C$_{1'''}$; 31.24: C$_{2'''}$; 29.06: C$_{β''}$; 26.98: C(O)C($\underline{C}$H$_3)_3$; 26.36: C$_{α,α'}$; 24.93: C$_{γ''}$; 23.31: C$_{γ,γ'}$; 14.2: C$_{δ,δ'}$; 13.4: $\underline{C}$H$_{3pyrrole}$.

5,15-{(6-pivaloylamino-[4-tert-butyl-2-hydroxy-1,3-phenylen)-bis-(trimethylenoxy)-di-2,1-phenylen]}-3,7,17,27-tetrabutyl-2,8,12,18-tetramethyl-porphyrinato iron (III) (12):

To 9.7 mg (8.05 μmol, 1 eq) **31** were added in a Schlenk tube 17.4 mg (0.08 mmol, 10 eq) FeBr$_2$ and 22.5 μl (0.16 mmol, 20 eq) triethylamine in 3 ml toluene and degassed three times at high vacuum. The mixture was stirred overnight at reflux and after cooling filtered through celite. Then it was purified by column chromatography (silica gel, 1*25 cm, Hex:EE 8:1) to yield 10.1 mg (100%) green solid **12**.

Analysis:

Yield: 100%.

TLC(silica gel, Hex:EE 1:1)**:** R$_f$= 0.5 (UV$^+$, Vis$^+$).

MS (MALDI-TOF): M=1255 (M)$^+$.

UV-Vis (toluene): λ = 408 nm (100%, ε=11.24*10^4 M^{-1}.cm^{-1}).

ESR (10K, toluene): g$_{//}$= 5.857, g$_⊥$=2.009.

Cyclic voltammetry (DMF, 0.1M LiClO$_4$, RT): E^0= -600 mV *vs* SCE.

A.2. Synthesis of the CPO model 32 and catalase model 33:

5,15-Bis-(2'-methoxynaphthyl)-3,7,13,17-tetrabutyl-2,8,12,18-tetramethyl-porphyrinato-zinc (II) (37a and 37b):

A 90 ml acetonitrile solution of 931 mg (5 mmol, 1 eq) 2-methoxynaphthylaldehyde **36** was bubbled 15 Min. with argon and then 1.43 g (5 mmol, 1eq) **13** were added. The solution was stirred at RT. for 24 hr and 1.84 g (7.5 mmol, 1.5 eq) *o*-chloranil in 20 ml of THF were added. After 30 Min. 4.58 g (25 mmol, 5 eq) zinc acetate were added with 20 ml of methanol and the solution was refluxed for 1 hr. The solution was neutralized with 250 ml of saturated sodium hydrogenocarbonate solution and filtered through celite. The product was retained on celite and the celite was washed with dichloromethane until it was colourless. The solvent was evaporated and the crude product was purified by column chromatography (silica gel, 15*30 cm, Hex:CH$_2$Cl$_2$ 1:1, 3l then 1:2, 3l). Two fractions containing the pure atropisomers were collected, evaporated to yield resp. 960.4 mg (39.8%) **37a** and 946.5 mg (39.3%) **37b**.

Analysis:

Yield: 79.1%.

TLC (silica gel, Hex:CH$_2$Cl$_2$ 1: 1): R$_f$= 0.34 for **37b** and 0.14 for **37a** (UV$^+$, Vis$^+$).

MALDI-TOF: M=964.6 (M)$^+$.

UV-Vis (CH$_2$Cl$_2$): λ = 414 nm (100 %), 510 nm (12.6 %), 580 nm (9.3 %), 544 nm (3.9 %)

^{1}H-NMR (CDCl$_3$, 300 MHz, RT):

37b (a,b-atropisomer): δ: 10.16 (s, H$_{10,20}$, 2H); 8.32 (d, J = 9.12, H$_{4'}$, 2H); 8.04 (d, J = 8.24, H$_{5'}$, 2H); 7.71 (d, J = 9.07, H$_{8'}$, 2H); 7.33 (t, J = 7.43, H$_{6'}$, 2H); 6.91 (t, J = 7.66, H$_{7'}$, 2H); 6.61 (d, J = 8.58, H$_{3'}$, 2H); 4.0-3.85 (m, CH$_{2\alpha}$, 8H); 3.73 (s, OC$\underline{H}_3$, 6H); 2.17 (s, CH$_{3pyrrole}$, 12H); 2.12 (qui, J= 7.6, CH$_{2\beta}$, 8H); 1.71 (sext, J= 7.4, CH$_{2\gamma}$, 8H); 1.07 (t, J = 7.3, CH$_{3\delta}$, 12H).

37a (a,a-atropisomer): δ: 10.16 (s, H$_{10,20}$, 2H); 8.31 (d, J = 9.13, H$_{4'}$, 2H); 8.03 (d, J = 8.24, H$_{5'}$, 2H); 7.73 (d, J = 9.28, H$_{8'}$, 2H); 7.31 (t, J = 6.87, H$_{6'}$, 2H); 6.84 (t, J = 7.97, H$_{7'}$, 2H); 6.43 (d, J = 8.73, H$_{3'}$, 2H); 4.0-3.8 (m, CH$_{2\alpha}$, 8H); 3.79 (s, OC$\underline{H}_3$, 6H); 2.18 (s, CH$_{3pyrrole}$, 12H); 2.11 (qui, J = 7.6, CH$_{2\beta}$, 8H); 1.72 (sext, J = 7.36, CH$_{2\gamma}$, 8H); 1.06 (t, J = 7.3, CH$_{3\delta}$, 12H).

As the characterization is unambiguous with the analyses performed, ^{13}C carbon spectra have not been recorded.

a,a-5,15-Bis-(2'-methoxynaphthyl)-3,7,13,17-tetrabutyl-2,8,12,18-tetramethyl-porphyrin (38a):

289.4 mg (0.3 mmol, 1eq) **37a.** were dissolved in 100 ml dichloromethane and stirred for 30 Min. at RT. with 50 ml of concentrated HCl solution. The solution was then diluted with 250 ml water and extracted 3 times with dichloromethane. The combined organic layers were neutralized with a saturated sodium hydrogenocarbonate solution, separated, dried over sodium sulphate, filtered and concentrated to yield quantitative **38a** as a violet solid.

Analysis:

Yield: quantitative.

TLC (silica gel, Hex:CH$_2$Cl$_2$ 1:1)**:** R$_f$= 0.14 (UV$^+$, Vis$^+$).

MALDI-TOF: M= 902 (M)$^+$.

UV-Vis (CH$_2$Cl$_2$): λ = 414 nm (100%), 508 nm (8.3%), 542 nm (2.9%), 572 nm (2.9%)

^{1}H-NMR (300 MHz, CDCl$_3$, RT):

δ: 10.20 (s, H$_{10,20}$, 2H); 8.33 (d, J = 9.06, H$_{4'}$, 2H); 8.04 (d, J = 8.24, H$_{5'}$, 2H); 7.72 (d, J = 9.0, H$_{8'}$, 2H); 7.34 (t, J = 7.08, H$_{6'}$, 2H); 6.92 (t, J = 8.24, H$_{7'}$, 2H); 6.67 (d, J = 8.58, H$_{3'}$, 2H); 3.93 (t, J = 7.69, CH$_{2\alpha}$, 8H); 3.74 (s, OC$\underline{H}_3$, 6H); 2.21 (s, CH$_{3pyrrole}$, 12H); 2.13 (qui, J = 7.41, CH$_{2\beta}$, 8H); 1.69 (sext, J = 7.35, C$\underline{H}_{2\gamma}$, 8H); 1.05 (t, J = 7.41, CH$_{3\delta}$, 12H); -2.05 (br, N$\underline{H}_{porphyrin}$, 2H).

The characterization was unambiguous therefore no ^{13}C NMR spectra has been recorded.

a,b-5,15-Bis-(2'-methoxynaphthyl)-3,7,13,17-tetrabutyl-2,8,12,18-tetramethyl-porphyrin (38b):

289.4 mg (0.3 mmol, 1 eq) **37b** were dissolved in 100 ml dichloromethane and stirred for 30 Min. at RT. with 50 ml of concentrated HCl solution. The solution was then diluted with 250 ml water and extracted 3 times with dichloromethane. The combined organic layers were neutralized with a saturated sodium hydrogenocarbonate solution, separated, dried over sodium sulphate, filtered and concentrated to yield quantitative **38b** as a violet solid.

Analysis:

Yield: 100%.

TLC(silica gel, Hex:CH$_2$Cl$_2$ 1:1)**:** R$_f$= 0.34 (UV$^+$, Vis$^+$).

MALDI-TOF: M=902 (M)$^+$.

UV-Vis (CH$_2$Cl$_2$): λ = 412 nm (100%), 508 nm (18.2%), 576 nm (15.2%), 542 nm (13.7%)

^{1}H-NMR (300 MHz, CDCl$_3$, RT): δ: 10.24 (s, H-$_{10,20}$, 2 H); 8.29 (d, J = 9.06, H$_{4'}$, 2H); 8.05 (d, J= 8.24, H$_{5'}$, 2H); 7.66 (d, J= 9.22, H$_{8'}$, 2H); 7.37 (t, J = 7.96, H$_{6'}$, 2H); 6.98 (t, J = 6.98, H$_{7'}$, 2H); 6.8 (d, J = 8.51, H$_{3'}$, 2H); 3.96 (t, J = 6.59, CH$_{2\alpha}$, 8H); 3.68 (s, OC$\underline{H}_3$, 6H); 2.23 (s, CH$_{3pyrrole}$, 12H); 2.16 (qui, J = 7.2, CH$_{2\beta}$, 8H); 1.72 (sext, J = 7.2, CH$_{2\gamma}$, 8H); 1.08 (t, J = 7.2, CH$_{3\delta}$, 12H); -2.01 (br, N$\underline{H}$$_{porphyrin}$, 2H).

The characterization is unambiguous therefore no ^{13}C NMR spectra has been recorded.

a,a-5,15-Bis-(2'-hydroxy-naphthyl)-3,7,13,17-tetrabutyl-2,8,12,18-tetramethyl-porphyrin (39):

271 mg (0.3 mmol, 1 eq) **38a** were dissolved in 50 ml dry dichloromethane and cooled to 0°C. 867 ml (9 mmol, 30 eq) BBr$_3$ were added, the solution was warmed up to RT. and stirred overnight. The solution was quenched with water, extracted with dichloromethane. The combined organic layers were washed twice with saturated sodium hydrogenocarbonate solution, separated, dried over sodium sulphate, filtered and concentrated. The residue was purified by column chromatography (silica gel, 6*25 cm, Hex:EE 4:1+ 0.1% Et$_3$N) to yield 244.3 mg (93%) violet solid **39**.

Analysis:

Yield: 93%.

TLC (silica gel, Hex:EE 4: 1)**:** R$_f$= 0.1 (UV$^+$, Vis$^+$).

MALDI-TOF: M=880 (M+5)$^+$.

UV-Vis (CH$_2$Cl$_2$): λ = 414 nm (100%), 510 nm (12.6%), 580 nm (9.3%), 544 nm (3.9%)

^{1}H-NMR (300 MHz, CDCl$_3$, RT): the signal attribution was made with help of COSY, NOESY and ROESY spectra. δ: 10.3 (s, H$_{10,20}$, 2H); 8.28 (d, J = 8.79, H$_{4'}$, 2H); 8.06 (d, J= 8.24, H$_{5'}$, 2H); 7.64 (d, J = 8.92, H$_{8'}$, 2H); 7.38 (t, J = 6.99, H$_{6'}$, 2H); 7.02 (t, J = 6.93, H$_{7'}$, 2H); 6.76 (d, J = 8.3, H$_{3'}$, 2H); 5.1 (br, O$\underline{H}$, 2H); 4.02-3.9 (m, CH$_{2\alpha}$, 8H); 2.31 (s, CH$_{3pyrrole}$, 12H); 2.14 (qui, J = 7.21, CH$_{2\beta}$, 8H); 1.7 (sext, J = 7.48, C$\underline{H}_{2\gamma}$, 8H); 1.06 (t, J = 7.24, CH$_{3\delta}$, 12H); -2.1 (br, N$\underline{H}$$_{porphyrin}$, 2H).

The characterization is unambiguous therefore no ^{13}C NMR spectra has been recorded.

5,15-{(6-naphthyl-[4-tert-butyl-2-S-N,N-dimethylthiocarbamoyl-1,3-phenylen)-bis-(trimethylenoxy)-di-2,1-phenylen]}-3,7,17,27-tetrabutyl-2,8,12,18-tetramethyl-porphyrin (40):

244.3 mg (0.28 mmol, 1 eq) of **39** were dissolved in 230 ml abs. DMF and 3.09 g (9.5 mmol, 34 eq) of cesium carbonate were added. The mixture was stirred at 80°C for 30 Min. and 213.4 mg (0.42 mmol, 1.5 eq) of **13** in 20 ml abs. DMF were added over 3 hr. The red mixture was then cooled to RT., diluted with 300 ml 10% HCl and extracted 3 times with TBME. The combined organic layers were washed twice with a saturated sodium hydrogenocarbonate solution, separated, dried over sodium sulphate, filtered and concentrated. The residue was purified by column chromatography (Hex: EE, 3.5:1+ 0.1% Et_3N) to yield 234.8 mg (70.5%) red powder **40**.

Analysis:

Yield: 70.5%.

TLC(silica gel, Hex:EE 7:2)**:** R_f= 0.14 (UV$^+$, Vis$^+$).

MALDI-TOF: M=1194 (M)$^+$.

UV-Vis (CDCl$_3$): λ = 418 nm (100%), 510 nm (7%), 544 nm (1.2%), 590 nm (0.3%).

^{1}H-NMR (600 MHz, CDCl$_3$, 280K): the signal attribution was made with help of COSY, NOESY and ROESY and TOCSY spectra. δ: 10.1(s, H$_{20}$, 1H); 9.7 (s, H$_{10}$, 1H); 8.31 (d, J = 8.9, H$_{4'}$, 2H); 8.12 (d, J = 8.6, H$_{5'}$, 2H); 8.0 (d, J = 8.6, H$_{8'}$, 2H); 7.54 (t, J = 7.2, H$_{6'}$, 2H); 7.53 (d, J = 8.9, H$_{3'}$, 2H); 7.39 (t, J = 7.2, H$_{7'}$, 2H); 6.31 (s, H$_{3'',5''}$, 2H); 4.05 and 3.62 (m and t, J = 8.5, CH$_{2\alpha'}$, 2*2H); 3.94 and 3.84 and 3.48 (t and 2*m, J = 8.1, CH$_{2\alpha}$, 4H and 2*2H); 2.23 and 2.15 (2*s, CH$_{3pyrrole}$, 2*6H); 2.18 (qui, J= 7.9, CH$_{2\beta,}$, 4H), 1.9 and 1.85 (2*m, CH$_{2\beta,}$, 2*4H); 1.8 (br, N(C$\underline{H}$$_3$)$_2$, 3H); 1.8 and 1.7 (sext, J = 7.3 , CH$_{2\gamma}$, 2*4H); 1.13 (t, J = 7.5Hz, CH$_{3\delta,}$, 12H); 1.09 (s, H$_{2'''}$, 9H); 0.6 and 0.55 (m, CH$_{2\beta'}$, 2*2H); 0.01 (t, J = 8.5 , CH$_{2\gamma'}$, 4H); -0.98 (br, N(C$\underline{H}$$_3$)$_2$, 3H); -1.9 (br, N$\underline{H}$$_{porphyrin}$, 2H).

To get a better resolution for NMR the thiocarbamate protecting group (i.e. (CH$_3$)$_2$N-C=O) was replaced by a thiothiocarbamate protecting group (i.e. ((CH$_3$)$_2$N-C=S)

Analysis:

TLC (silica gel, Hex:EE 7:2+1% Et$_3$N)**:** R_f=0.15 (UV$^+$, Vis$^+$).

MS (MALDI-TOF): M=1214 (M+5)$^+$.

UV-Vis (CDCl$_3$): λ = 418 nm (100%), 510 (6.3%); 544 (3.4%).

^{1}H-NMR (600 MHz, CDCl$_3$, RT): 10.12 (s, H$_{20}$, H); 9.65 (s, H$_{10}$, 1H); 8.3 (d, J = 9, H$_{4'}$, 2H); 8.13 (d, J = 8.5, H$_{5'}$, 2H); 8.0 (d, J = 8.0, H$_{8'}$, 2H); 7.54 (d, J = 9.0, H$_{3'}$, 2H); 7.53 (t, J = 8.0, H$_{6'}$, 2H); (td, ^1J = 7.7, ^2J = 0.9, H$_{7'}$, 2H); 6.37 (s, H$_{3'', 5''}$, 2H); 4.05-3.98 (m, CH$_{2\alpha'}$, 2H); 3.94 (t, J = 8.0, CH$_{2\alpha}$, 4H); 3.84-3.79 (m, CH$_{2\alpha}$, 2H); 3.78-3.74 (m, CH$_{2\alpha}$, 2H); 3.58-3.5 (m, H$_{\alpha'}$, 2H); 2.4 (s, NC$\underline{H}_3$, 3H); 2.23 (s, CH$_{3pyrrole}$ attached to C$_{3,17}$, 6H); 2.21-2.16 (m, H$_\beta$, 4H); 2.15 (s, CH$_{3pyrrole}$ attached to C$_{7,13}$, 6H); 2.02-1.89 (2*m, H$_\beta$, 4H); 1.85-1.75 (m, H$_\gamma$, 4H); 1.71 (sext, J =7.3, Hγ, 4H); 1.17 (s, H$_{2'''}$, 9H); 1.14 (t, J = 7.3, H$_\delta$, 6H); 1.13 (t, J = 7.3, H$_\delta$, 6H); 0.85-0.78 (m, H$_{\beta'}$, 2H); 0.75-0.64 (m, H$_{\beta'}$, 2H); 0.49 (td, ^1J = 13.5, ^2J = 4.0, H$_{\gamma'}$, 2H); 0.09 (td, ^1J = 13.5, ^2J = 4.3, Hγ', 2H); -0.6 (s, NC$\underline{H}_3$, 3H); -1.9 (br, N$\underline{H}_{porphyrin}$, 2H).

^{13}C-NMR (150 MHz, CDCl$_3$, RT): 197.5: $\underline{C}$=S; 157.64: C$_{2'}$; 151.06: C$_{4''}$; 145.82: C$_{4,6,14,16}$; 144.37: C$_{1''}$; 142.93: C$_{9,11}$; 142.89: C$_{1,19}$; 141.12: C$_{2,18}$; 140.82: C$_{8,12}$; 137.39: C$_{4'a}$; 135.84: C$_{3,17}$; 135.3: C$_{7,13}$; 130.47: C$_{4'}$ 129.05 C$_{1a'}$; 127.67: C$_{5'}$; 127.1: C$_{7'}$; 126.62: C$_{8'}$; 126.31: C$_{2'',6''}$; 126.24: C$_{1'}$; 123.81: C$_{6'}$; 122.51: C$_{3'',5''}$; 116.41: C$_{3'}$, 111.36: C$_{5,15}$; 96.1: C$_{10}$; 95.61: C$_{20}$; 71.02: C$_{\alpha''}$; 44.44: N$\underline{C}$H$_3$; 38.4: N$\underline{C}$H$_3$; 35.74: C$_{\beta'}$, 35.09: C$_{\beta'}$; 34.24: C$_{1''}$; 31.22: C$_{2''}$; 30.11: C$_{\gamma''}$; 28.92: C$_{\beta''}$; 26.54: C$_\alpha$; 26.14: C$_{\alpha'}$; 23.42: C$_\gamma$; 23.36: Cγ; 14.25: C$_{\delta,\delta}$; 13.8: CH$_{3pyrrol}$ attached to C$_{3,18}$; 13.47: CH$_{3pyrrol}$ attached to C$_{7,13}$.

5,15-{(6-naphthyl-[4-tert-butyl-2-sulfhydryl-1,3-phenylen)-bis-(trimethylenoxy)-di-2,1-phenylen]}-3,7,17,27-tetrabutyl-2,8,12,18-tetramethyl-porphyrin (41):

71.1 mg (59.8 mmol, 1 eq) **40** were dissolved in 25 ml of previously degassed dioxane and the solution was bubbled with argon for 30 Min. 1.76 ml (0.598 mmol, 100 eq) of a 25% KOMe solution in methanol were added and the solution was heated to 100°C under an argon stream. After 5 ml of the green solution were evaporated, the stream was stopped and the solution was stirred at 100°C for a further 20 Min. After cooling the reaction was quenched under argon with 150 ml of a saturated ammonium chloride solution and extracted twice with 50 ml of dichloromethane. The organic layers were dried over sodium sulphate, filtered and concentrated. The residue was purified by column chromatography (silica gel, 5*25 cm, Hex:EE 8:1+0.1% Et$_3$N) to yield 65 mg (97%) red solid **41**.

Analysis:

Yield: quantitative.

TLC (silica gel, Hex:EE 8:1)**:** R$_f$= 0.6 (UV$^+$, Vis$^+$).

MALDI-TOF: M=1168 (M)$^+$.

UV-Vis (CDCl$_3$): λ = 416 nm (100%), 510 nm (7.7%), 576 nm (1.2%), 544 nm (2.1%)

^{1}H-NMR (600 MHz, CDCl$_3$, RT): the signal attribution was made with help of COSY, NOESY and ROESY and TOCSY spectra.

δ: 10.1 (s, H$_{10,20}$, 2H); 8.31 (d, J = 9, H$_{4'}$, 2H); 8.14 (d, J = 8, H$_{5'}$, 2H); 8.05 (d, J = 8, H$_{8'}$, 2H); 7.54 (d, J = 9, H$_{3'}$, 2H); 7.52 (t, J = 8, H$_{6'}$, 2H); 7.38 (t, J = 7.2, H$_{7'}$, 2H); 6.13 (s, H$_{3'',5''}$, 2H); 4.05 (m, CH$_{2\alpha}$, 4H), 3.88 (t, J = 7.4, CH$_{2\alpha}$, 4H); 3.75 (t, J = 7.9, CH$_{2\alpha'}$, 4H); 2.19 (s: CH$_{3pyrrole}$, 12H); 2.08 (qui, J = 7.5, CH$_{2\beta}$, 8H); 1.66 (sext, J = 7.6, CH$_{2\gamma}$, 8H); 1.02 (t, J = 7.2, C$\underline{H}_{3\delta}$, 12 H); 0.88 (s, H$_{2'''}$, 9H); 0.5 (m, CH$_{2\beta',\gamma}$, 8H); -2.03 (br, N$\underline{H}_{porphyrin}$, 2H); -3.01 (s, S$\underline{H}$, 1H).

^{13}C-NMR (150 MHz, CDCl$_3$, RT): 157.8: C$_{2'}$; 147.3: C$_{1''}$; 146.7: C$_{4,6,14,16}$;; 143.7: C$_{1,9,11,19}$; 141.8: C$_{2,8,12,18}$; 140.5: C$_{2'',6''}$; 138.3: C$_{4'a}$; 136.3: C$_{3,7,13,17}$; 131.0: C$_{4'}$ 130.1 C$_{1a'}$; 128.3: C$_{5'}$; 127.7: C$_{7'}$; 127.2: C$_{8'}$; 125.6: C$_{2'',6''}$; 124.81: C$_{6'}$; 121.7: C$_{3'',5''}$; 118.3: C$_{3'}$, 112.2: C$_{5,15}$; 97.3: C$_{10}$; 72.0: C$_{\alpha''}$; 36.2: C$_{\beta}$; 34.9: C$_{1'''}$; 31.9: C$_{2'''}$; 28.5: C$_{\beta'}$; 27.2: C$_{\alpha}$; 24.4: C$_{\gamma}$; 24.0: C$_{\gamma}$; 14.90: C$_{\delta}$; 14.3: CH$_{3pyrrole}$.

5,15-{(6-naphthyl-[4-tert-butyl-2-N,N-thiolato-1,3-phenylen)-bis-(trimethylenoxy)-di-2,1-phenylen]}-3,7,17,27-tetrabutyl-2,8,12,18-tetramethyl-porphyrinato iron (III) (32):

To 11.2 mg (10 µmol, 1 eq) **5** were added in a Schlenk tube 21.57 mg (0.1 mmol, 10 eq) FeBr$_2$ and 27.9 µl (0.2 mmol, 20 eq) triethylamine and 3 ml of toluene. The mixture was degassed three times in the high vacuum and refluxed for one hour. Subsequently the reaction was filtered over celite and concentrated. The residue was further purified through column chromatography silica gel, 2*15 cm, Hex:EE 8:1,) under argon to yield **32** as a brown solid.

Analysis:

Yield: 89%.

TLC (silica gel, Hex:EE 4:1)**:** R$_f$= 0.65 (UV$^+$, Vis$^+$).

MS (MALDI-TOF): M=1174 (M)$^+$.

UV-Vis (toluene): λ = 406 nm (100%), 486 (%); 578 (%); 582 (%).

ESR(10K, toluene): g$_{//}$= 5.809 and and g$_\perp$=3.098 (br) for five coordination state and g$_{//}$= 8.347 and g$_\perp$=2.006 for six coordination state.

Cyclic voltammetry: E^0=-660 mV vs SCE in DMF at RT.

5,15-{(6-naphthyl-[4-tert-butyl-2-N,N-dimethyloxythiocarbamoyl-1,3-phenylen)-bis-(trimethylenoxy)-di-2,1-phenylen]}-3,7,17,27-tetrabutyl-2,8,12,18-tetramethyl-porphyrin (42):

To a solution of 44 mg (50 µmol, 1 eq) **39** in 45 ml abs. DMF was added under argon 556.9 mg (1.71 mmol, 34 eq) cesium carbonate and the suspension was stirred at 80 °C (oil bath temperature) for 30 Min. Then 30.8 mg (60 µmol, 1.2 eq) **16** in 5 ml abs. DMF were added within 3 hours. After cooling the reaction mixture was diluted with 50 ml 4N HCl and extracted four times with 25 ml TBME. The combined organic layers were then washed twice with an aqueous saturated $NaHCO_3$ solution, dried over Na_2SO_4, filtered and evaporated. The crude product was purified by column chromatography (silica gel, 3*20 cm, Hex:EE 4:1+0.1% Et_3N) to yield 30.9 mg (51.5%) red solid **42**.

Analysis:

Yield: 51.5%.

TLC (silica gel, Hex:EE 7:1).**:** R_f=0.44 (UV$^+$, Vis$^+$).

MS (MALDI-TOF): M=1194 (M)$^+$.

UV-Vis (CDCl$_3$): λ = 416 nm (100%), 510 (9.7%); 578 (4.7%); 542 (4.3%).

^{1}H-NMR (300 MHz, CDCl$_3$, RT): the signals were attributed by COSY, TOCSY, NOESY experiments. δ: 10.12 (s, H_{20}, 1H); 9.7 (s, H_{10}, 1H); 8.3 (d, J =9.1, $H_{4'}$, 2H); 8.13 (d, J = 8.0, $H_{5'}$, 2H); 7.93 (d, J = 8.0, $H_{8'}$, 2H); 7.56 (d, J = 8.0, $H_{3'}$, 2H); 7.54 (t, J = 8.0, $H_{6'}$, 2H); 7.35 (td, ^1J = 8.0, ^2J = 0.76, $H_{7'}$, 2H); 6.24 (s, $H_{3'',5''}$, 2H); 4.1-3.8 (m, $H_{\alpha,\alpha'}$, 12H); 2.22 (s, $CH_{3pyrrole}$ attached to $C_{3,17}$, 6H); 2.2 (s, $N(CH_3)_2$, 3H); 2.17 (s, $CH_{3pyrrole}$ attached to $C_{7,13}$, 6H); 2.08 (qui, J = 7.4, H_β, 8H); 1.75 (sext, J = 7.4, H_γ, 8H); 1.28 (s, $H_{2'''}$, 9H); 1.11 (t, J = 7.4, H_δ, 8H); 1-0.78 (m, $H_{\beta'}$, 2H); 0.72-0.5 (m, $H_{\beta'}$, 2H); 0.3 (m, $H_{\gamma'}$, 2H); 0.02 (m, $H_{\gamma'}$, 2H); -1.73 (s, $N(CH_3)_2$, 3H); -2.2 (s, $N\underline{H}_{porphyrin}$, 2H).

^{13}C-NMR (75 MHz, CDCl$_3$, RT): the signals were attributed by HMBC and HMQC experiments. 184.8: C=S; 158.2: $C_{2'}$; 146.79: $C_{4''}$; 146.55: $C_{4,16}$; 146.28: $C_{6,14,1''}$; 143.32: $C_{1,9,11,19}$; 141.62: $C_{2,18}$; 141.43: $C_{8,12}$; 137.77: $C_{4'a}$; 136.09: $C_{3,17}$; 135.63: $C_{7,13}$; 131.04: $C_{4'}$; 129.72: $C_{1'a}$; 128.19: $C_{5'}$; 128.13: $C_{7'}$; 127.54: $C_{8'}$; 127.39: $C_{2'',6''}$; 127.14: $C_{1'}$; 124.43: $C_{6'}$; 121.79: $C_{3'',5''}$; 117.91: $C_{3'}$; 111.63: $C_{5,15}$; 97.08: C_{10}; 96.21: C_{20}; 71.82: $C_{\alpha''}$; 42.24: N$\underline{C}H_3$; 36.17: N$\underline{C}H_3$; 35.64: C_β; 34.6: $C_{\beta'}$; 34.35: $C_{1'''}$; 32.09: $C_{2'''}$; 30.12: $C_{\gamma'}$; 28.56: $C_{\beta''}$; 26.96: C_α; 26.72: $C_{\alpha'}$; 23.81: C_γ; 23.77: $C_{\gamma'}$; 14.67: C_δ; 14.42: $C_{\delta'}$; 14.15: $\underline{C}H_3$ attached to $C_{3,17}$; 13.94: $\underline{C}H_3$ attached to $C_{7.,13}$.

5,15-{(6-naphthyl-[4-tert-butyl-2-hydroxy-1,3-phenylen)-bis-(trimethylenoxy)-di-2,1-phenylen]}-3,7,17,27-tetrabutyl-2,8,12,18-tetramethyl-porphyrin (43):

To a solution of 15 mg (12.6 μmol, 1 eq) **42** in 5 ml abs. dioxane was added 36.5 mg (0.38 mmol, 30 eq) potassium methoxide and the suspension was stirred at 90°C (oil bath temperature) for 3 hours. After cooling the mixture was diluted with saturated ammonium chloride solution and extracted three times with TBME. Then the combined organic layers were dried over sodium sulphate, filtered and evaporated. The residue was purified by column chromatography (silica gel, 2*15 cm, Hex:EE 8:1+0.1% Et$_3$N) to yield 5.7 mg (41%) red solid **43**.

Analysis:

Yield: 41%.

TLC(silica gel, Hex:EE 7:1)**:** R$_f$=0.44 (UV$^+$, Vis$^+$).

MS (MALDI-TOF): M=1105 (M)$^+$.

UV-Vis (CDCl$_3$): λ = 416 nm (100%), 512 (7.3%); 570 (2.8%); 546 (2.7%).

^{1}H-NMR (500 MHz, CDCl$_3$, RT): the signals were attributed by COSY and NOESY experiments. δ:10.17 (s, H$_{10,20}$, 2H); 8.32 (d, J = 9.07, H$_{4'}$; 2H); 8.14 (d, J = 7.5, H$_{5'}$, 2H); 7.79 (d, J = 7.5, H$_{8'}$, 2H); 7.63 (d, J = 8.85, H$_{3'}$, 2H); 7.53 (t, J = 7.5, H$_{6'}$, 2H); 7.32 (td, ^1J = 7.5, ^2J = 0.9, H$_{7'}$, 2H); 5.95 (s, H$_{3'',5''}$, 2H); 3.92 (m, H$_\alpha$, 4H); 3.89 (t, J = 7.2, H$_{\alpha'}$,4H); 3.84 (m, H$_\alpha$, 4H); 2.21 (s, CH$_{3pyrrole}$, 12H); 2.1 (qui, J = 7.4; H$_\beta$, 8H); 1.68 (sext; J = 7.5, H$_\gamma$, 8H); 1.04 (t, J = 7.3, H$_\delta$, 12H); 0.79 (s, H$_{2'''}$, 9H); 0.65 (m, H$_{\beta'}$, 4H); -0.4 (m, H$_{\gamma'}$, 4H); -2.19 (br, O$\underline{H}$, N$\underline{H}$$_{porphyrin}$, 3H).

^{13}C-NMR (125 MHz, CDCl$_3$, RT): the signals were attributed by HMQC and HMBC experiments. 157.8. C$_{2'}$; 147.3: C$_{1'}$; 146.7: C$_{4,6,14,16}$; 143.7: C$_{1,9,11,19}$; 141.8: C$_{2,8,12,18}$; 140.5: C$_{2'',6''}$; 138.3: C$_{4'a}$; 136.3: C$_{3,7,13,17}$; 131: C$_{4'}$, 130.1: C$_{1'a}$; 128.4: C$_{1'}$; 128.3: C$_{5'}$; 127.8: C$_{7'}$; 127.2: C$_{8'}$; 125.6: C$_{2'',6''}$; 124.8: C$_{6'}$; 121.7: C$_{3'',5''}$; 118.3: C$_{3'}$, 112.2: C$_{5,15}$; 97.3: C$_{10,20}$; 72.0: C$_{\alpha''}$; 36.2: C$_{\beta,\beta'}$; 34.9: C$_{1'''}$;31.9: C$_{2''}$; 28.5: C$_{\beta\forall'}$; 27.2: C$_{\alpha,\alpha'}$; 24.4: C$_{\gamma'}$; 24.0: C$_{\gamma,\gamma'}$; 14.9: C$_{\delta,\gamma}$; 14.3: CH$_{3pyrrole}$.

5,15-{(6-naphthyl-[4-tert-butyl-2-hydroxy-1,3-phenylen)-bis-(trimethylenoxy)-di-2,1-phenylen]}-3,7,17,27-tetrabutyl-2,8,12,18-tetramethyl-porphyrinato iron (III) (33):

To 5.7 mg (5.15 μmol, 1 eq) **40** were added in a Schlenk tube 11.2 mg (0.05 mmol, 10 eq) **iron (II) dibromide** and 14.4 μl (0.10 mmol, 20 eq) **triethylamine** in 2 ml toluene. The mixture was degassed three times at high vacuum and stirred overnight at reflux and after

cooling filtered through celite. Then it was purified by column chromatography (silica gel, Hex:EE 8:1, 1*25 cm) to yield 10.1 mg (100%) green solid.

Analysis:

Yield: 100%.

TLC (silica gel, Hex: EE 4:1)**:** R_f= 0.5 (UV$^+$, Vis$^+$).

MS (MALDI-TOF): M=1158 (M)$^+$.

UV-Vis (toluene): λ = 410 nm (100%, ϵ= $14*10^4$ M^{-1}cm^{-1})

ESR (10K, toluene): $g_{//}$=5.831 and $g_\perp$=2.008.

Cyclic voltammetry: E^0= -710 mV vs SCE in DMF at RT.

A.3. Synthesis of the tailed models 34 and 35:

a,b-[5-(6'-pivaloylamino-2'-methoxyphenyl)-15-(6'-pivaloylamino-2'-hydroxy-phenyl)-3,7,13,17-tetrabutyl-2,8,12,18-tetramethyl-porphyrin] (48):

50 mg (51.36 μmol, 1 eq) **17b** were dissolved in 10 ml abs. DMF under a dry and inert atmosphere. 251 mg (0.77 mmol, 15 eq) cesium carbonate were added and the suspension was stirred at 70°C (oil bath temperature) for 30 min. After cooling at RT 2.88 μl (46.23 μmol, 0.9 eq) methyliodide were added and the reaction mixture was stirred for 2.5 hr at RT. The reaction was quenched with 20 ml 10% aqueous HCl solution and the aqueous phase extracted three times with 20 ml CH_2Cl_2. The combined organic layers were dried over Na_2SO_4, filtered and concentrated. The crude product was purified by column chromatography (silica gel, 3*25 cm, Hex: EE 6:1 +1% Et$_3$N) to yield 18.1 mg (35.6%) **48** as a violet powder.

Analysis:

Yield: 35.6%.

TLC (silica gel, Hex: EE 4:1+1% Et$_3$N)**:** R_f=0.24 (UV$^+$, Vis$^+$).

MS (MALDI-TOF): M=987 (M)$^+$.

UV-Vis (CDCl$_3$): λ = 408 nm (100%), 512 (7.3%); 570 (2.8%); 546 (2.7%).

^{1}H-NMR (600 MHz, CDCl$_3$, RT): the spectrum was interpreted with support of NOESY, COSY and TOCSY spectra. δ: 10.29 (s, H$_{10,}$20, 2H); 8.49 (d, J = 8.54, H$_{5'}$(Ar with OMe), 1H); 8.42 (d, J = 8.47 Hz, H$_{5'}$ (Ar with OH), 1H); 7.84 (t, J = 8.57, H$_{4'}$ (Ar with OMe), 1H); 7.75 (t, J = 8.47, H$_{4'}$ (Ar with OH t, 1H); 7.18 (d, J = 8.44Hz, H$_{3'}$ (Ar with OH) 1H); 7.16 (d, J = 8.57, H$_{4'}$ (Ar with OMe), 1H); 6.96 (s, N<u>H</u>Piv (Ar with OMe), 1H); 6.94 (s,

N$\underline{H}$Piv (Ar with OH), 1H); 4.09-3.95 (m, CH$_{2\alpha}$, 8H); 3.64 (s, OC$\underline{H}$3, 3H); 2.70 (s, CH$_{3pyrrole}$ (on C$_{3,7}$), 6H); 2.62 (s, CH$_{3pyrrole}$ (on C$_{13}$,17), 6H); 2.26-2.16 (m, CH$_{2\beta}$, 8H); 1.78-1.71 (m, CH$_{2\gamma}$, 8H); 1.12-1.09 (m, CH$_{3\delta}$, 12H):; -0.02 (s, NHC(O)C(C$\underline{H}_3$)$_3$ (Ar with OH), 9H); -0.05 (s, NHC(O)C(C$\underline{H}_3$)$_3$ (Ar with OMe), 9H); -2.04 (s, N$\underline{H}_{porphyrin}$, 2H).

^{13}**C-NMR (150 MHz, CDCl$_3$, RT):** 176.92: C=O (Ar with OMe); 176.82: C=O (Ar with OH), 159.47: C$_{2'}$ (Ar with OMe); 155.85: C$_{2'}$ (Ar with OH); 145.83: C$_{1,9}$; 145.63: C$_{4,6}$; 144.79: C$_{2,8}$; 144.45:C$_{14,68}$; 142.73: C$_{1,9}$; 142.6: C$_{11,19}$; 140.29: C$_{1'}$ (Ar with OH); 139.81: C$_{1'}$ (Ar with OH); 136.64: C$_{3,7}$ (Ar with OMe); 136.19: C$_{13,17}$ (Ar with OH); 131.59: C$_{4'}$ (Ar with OH); 131.33: C$_{4'}$ (Ar with OMe); 120.0: C$_{6'}$ (Ar with OMe); 118.3: C$_{6'}$ (Ar with OH); 114.1: C$_{5'}$ (Ar with OMe); 113.3: C$_{5'}$ (Ar with OH); 108.51: C$_{3'}$ (Ar with OH); 102.95: C$_{10,20}$; 98.02: C$_{5,15}$; 56.17: OMe; 39.45 and 39.46: $\underline{C}$(CH$_3$)$_3$; 35.81: C$_\beta$; 26.71 and 26.66: C$_\alpha$ and C($\underline{C}$H$_3$)$_3$; 23.55 and 23.53: C$_\gamma$; 14.53 and 14.58: C$_\delta$; 13.76: CH$_{3pyrrole}$.

a,b-[5-(6'-pivaloylamino-2'-methoxy-phenyl)-15-(6'-pivaloylamino-2'-oxy-(2''-propan-1''-S-N,N-dimethythiocarbamoyl-4''tert.butyl-phenylen)-phenyl)-3,7,13,17-tetrabutyl-2,8,12,18-tetramethyl-porphyrin] (49):

To 228 mg (0.231 mmol, 1eq) **41** in 200 ml abs.DMF were added under a dry and inert atmosphere 1.28g (3.92 mmol, 17 eq) cesium carbonate. The reaction mixture was stirred at 70°C (oil bath temperature) for 30 Min. 129.4 mg (0.346 mmol, 1.5 eq) **28** dissolved in 15 ml abs. DMF were added within 10 Min. The reaction mixture was stirred for further 45 Min at 70°C. After cooling at RT the reaction was quenched in 500 ml 10% aqueous HCl solution. The product was extracted three times with 100 ml diethylether and once with 50 ml CH$_2$Cl$_2$ from the aqueous phase. The combined organic layers were dried over Na$_2$SO$_4$, filtered and concentrated. The crude product was purified by column chromatography (silica gel, 8*20 cm, Hex:EE 3:1+1% Et$_3$N) to yield 252 mg (86.4%) **49** as a violet powder.

Analysis:

Yield: 86.4%.

TLC (silica gel, Hex:EE 5:1 + 1% Et$_3$N).**:** R$_f$=0.1 (UV$^+$, Vis$^+$).

MS (MALDI-TOF): M=1263 (M)$^+$.

UV-Vis (CH$_2$Cl$_2$): λ = 410 nm (100%), 508 (9%); 540 (4.2%); 576 (4.4%) ; 660 (2.7%).

^{1}**H-NMR** (600 MHz, CDCl$_3$, RT): the spectrum was interpreted with support of NOESY, COSY and TOCSY spectra. δ: 10.20 (s, 2H): H$_{10,20}$; 8.5 (d, J = 8.49, H$_{5'}$ (Ar with OMe), 1H); 8.43 (d, J = 8.44, H$_{5'}$ (Ar with bridge), 1H); 7.82 (t, J = 8.58, H$_{4'}$ (Ar with OMe), 1H); 7.77 (t, J = 8.57, H$_{4'}$ (Ar with bridge), 1H); 7.13 (d, J = 7.84, H$_{3'}$ (Ar with OMe),

1H); 7.12 (d, J = 7.98, H$_{3'}$ (Ar with bridge), 1H); 7.11 (s, N$\underline{H}$Piv (Ar with OMe), 1H); 6.96 (s, H$_{5'',6''}$, 2H); 6.81 (s, N$\underline{H}$Piv (Ar with bridge), 1H); 6.67 (s, H$_{3''}$, 1H); 4.02 (t, J = 7.64, CH$_{2\alpha}$', 2H); 4.06-3.99 (m, CH$_{2\alpha}$ (butyl chain on C$_{2,8}$), 4H); 3.92-3.91 (m, CH$_{2\alpha}$ (butyl chain on C$_{12,18}$), 4H); 3.61 (s, OC$\underline{H}_3$, 3H); 2.63 (s, CH$_{3pyrrole}$ (on C$_{13,17}$), 6H); 2.61 (s, CH$_{3pyrrole}$ (on C$_{3,7}$), 6H); 2.47 (s, N(C$\underline{H}_3$)$_2$, 3H); 2.27 (t, J = 7.6, CH$_{2\gamma}$', 2H); 2.16 (qui, J = 7.5, CH$_{2\beta}$ (butyl chain on C$_{2,8}$), 4H); 2.12 (qui, J =7.5, CH$_{2\beta}$ (butyl chain on C$_{12,18}$), 4H); 1.73 (sext, J =7.6, CH$_{2\gamma}$ (butyl chain on C$_{2,8}$), 4H); 1.70 (sext, J =7.6, CH$_{2\gamma}$ (butyl chain on C$_{12,18}$), 4H); 1.6 (s, N(C$\underline{H}_3$)$_2$, 3H); 1.49 (qui, J =7.79, CH$_{2\beta}$', 2H); 1.07 (t, J =7.79, CH$_{3\delta}$ (butyl chain on C$_{2,8}$), 6H); 1.04 (t, J = 7.4, CH$_{3\delta}$ (butyl chain on C$_{12,18}$), 6H); 0.88 (s, H$_{2''}$', 9H); -0.02 (s, C(O)C(C$\underline{H}_3$)$_3$ (Ar with OMe), 9H); -0.15 (s, C(O)C(C$\underline{H}_3$)$_3$ (Ar with bridge), 9H); -2.2 (s, N$\underline{H}_{porphyrin}$, 2H).

^{13}C-NMR (150 MHz, CDCl$_3$, RT): 176.94: C=O (Ar with OMe; 176.89: C=O (Ar with bridge); 159.64: C$_{2'}$ (Ar with OMe); 158.79: C$_{2'}$ (Ar with bridge); 152.88: C$_{4'''}$; 145.67: C$_{4,6}$; 145.39: C$_{14,16}$; 145.02: C$_{1'''}$; 144.048: C$_{1,9,11,19}$; 142.25 and 142.22: C$_{2,7,11,17}$; 140.56: C$_{1'}$ (Ar with bridge); 140.38: C$_{1'}$ (Ar with OMe); 137.53: C$_{6'''}$; 136.1: C$_{3'}$ (Ar with bridge) and 135.98: C$_{3'}$ (Ar with OMe); 131.14: C$_{4'}$ (Ar with bridge); 131.01: C$_{4'}$ (Ar with OMe); 126.98: C$_{3'''}$; 124.32: C$_{5'''}$; 123.94:C$_{5'''}$; 120.44: C$_{6'}$ (Ar with bridge); 113.68: C$_{6'}$ (Ar with OMe); 113.87: C$_{5'}$ (Ar with bridge); 113.68: C$_{5'}$ (Ar with OMe); 107.8: C$_{3'}$ (Ar with bridge); 107.2: C$_{3'}$ (Ar with OMe); 97.53: C$_{5,15}$; 68.17: C$_{\alpha'}$; 56.14: OCH$_3$; 39.46 and 39.35: $\underline{C}$(CH$_3$)$_3$; 35.84 and 35.8: C$_\beta$; 34.55: $\underline{C}$(CH$_3$)$_3$ from bridge; 31.53 and 31.43: N(CH$_3$)$_2$ and C$_{\gamma'}$; 31.16: C($\underline{C}$H$_3$)$_3$ from bridge; 30.09: C$_{\gamma'}$; 26.71: C$_\alpha$ and C($\underline{C}$H$_3$)$_3$ from amide; 26.58: C($\underline{C}$H$_3$)$_3$ from amide; 23.59 and 23.51: C$_\gamma$; 14.52 and 14.49: C$_\delta$; 13.8 and 13.73: CH$_{3pyrrole}$.

a,b-[5-(6'-pivaloylamino-2'-methoxy-phenyl)-15-(6'-pivaloylamino-2'-oxy-(2''-propan-1''-S-N,N-dimethythiocarbamoyl-4''tert.butyl-phenylen)-phenyl)-3,7,13,17-tetrabutyl-2,8,12,18-tetramethyl-porphyrin] (55):

67 mg (0.68 mmol, 1 eq) **48** were dissolved in 30 ml abs. DMF under a dry, inert atmosphere. 751.7 mg (2.31 mmol, 34 eq) cesium carbonate were added and the reaction mixture was stirred to 70°C (oil bath temperature) for 30 Min. 23.24 mg (0.81 mmol, 1.2 eq) **51** dissolved in 5 ml abs. DMF were added and the reaction was stirred for one hour at 70°C. The reaction was quenched after cooling at RT with 100 ml 10% aqueous HCl solution. The product was extracted by three times 50 ml TBDME. The combined organic layers were dried over Na$_2$SO$_4$, filtered and concentrated. The crude product was purified

by column chromatography (silica gel, 5*25 cm, Hex:EE 5:1 + 1% Et$_3$N) to yield 51.8 mg (65%) **55** as a violet powder.

Analysis:

Yield: 65%.

TLC (silica gel, Hex:EE 5:1+1% Et$_3$N).**:** R$_f$=0.25 (UV$^+$, Vis$^+$).

MS (MALDI-TOF): M=1175 (M-2)$^+$.

UV-Vis (CH$_2$Cl$_2$): λ = 408 nm (100%), 508 (8.8%); 542 (4.2%); 576 (3.9%) ; 628 (2%).

^{1}H-NMR (600 MHz, CDCl$_3$, RT): the spectrum was interpreted with support of NOESY, COSY and TOCSY spectra. δ: 10.29 (s, 2H): H$_{10,20}$; 8.5 (d, J = 8.53, H$_{5'}$ (Ar with OMe), 1H); 8.44 (d, J = 8.53, H$_{5'}$ (Ar with bridge), 1H); 7.81 (t, J = 8.58, H$_{4'}$ (Ar with OMe), 1H); 7.78 (t, J = 8.56, H$_{4'}$ (Ar with bridge), 1H); 7.13 (d, J = 8.58, H$_{3'}$ (Ar with OMe), 1H); 7.12 (d, J = 8.44, H$_{3'}$ (Ar with bridge), 1H); 7.09 (s, N$\underline{H}$Piv (Ar with OMe), 1H); 6.85 (s, N$\underline{H}$Piv (Ar with bridge), 1H); 4.07-4.01 (m, CH$_{2\alpha}$ (on C$_{2,8}$), 2H); 3.98 (t, J = 7.14 Hz, CH$_{2\alpha'}$, 2H); 4.0-3.92 (m, CH$_{2\alpha}$ (on C$_{2,8,12,18}$), 6H); 3.60 (s, OCH$_3$, 3H); 3.39 (s, N(C$\underline{H}_3$)$_2$, 3H); 3.01 (s, N(C$\underline{H}_3$)$_2$, 3H); 2.61 (s, CH$_{3pyrrole}$ (on C$_{3,7}$), 6H); 2.60 (s, CH$_{3pyrrole}$ (on C$_{13,17}$), 6H); 2.45 (t, J = 7.5, CH$_{2\varepsilon}$, 2H); 2.24-2.14 (m, CH$_{2\beta}$, 8H); 1.77-1.70 (m, CH$_{2\gamma}$, 8H); 1.19 (qui, J = 7.03, CH$_{2\beta}$, 2H); 1.10 (t, J = 7.37, CH$_{3\delta}$ (on C$_{12,18}$), 6H); 1.09 (t, J = 7.4, CH$_{3\delta}$ (on C$_{2,8}$), 6H); 1.01 (qui, J = 7.63, CH$_{2\delta'}$, 2H); 0.66 (qui, J = 7.69, CH$_{2\gamma'}$, 2H); -0.02 (s, C(O)C(C$\underline{H}_3$)$_3$ (Ar with bridge), 9H); -0.01 (s, C(O)C(C$\underline{H}_3$)$_3$ (Ar with OMe), 9H); -2.22 (s, N$\underline{H}_{porphyrin}$, 2H).

^{13}C-NMR (150 MHz, CDCl$_3$, RT): 197.2: C=S; 176.70: C=O (Ar with OMe); 176.54: C=O (Ar with bridge); 159.27: C$_{2'}$ (Ar with OMe); 158.5: C$_{2'}$ (Ar with bridge); 145.30: C$_{5'}$ (Ar with OMe); 145.06: C$_{5'}$ (Ar with bridge); 144.08 and 144.01: C$_{4,6,14,16}$; 142.25 and 142.24: C$_{1,9,11,19}$; 140.46 and 140.41: C$_{3,7,13,17}$; 136.14 and 136.03: C$_{1'}$; 131.12 and 131.05: C$_{4'}$; 120.58 and 120.34: C$_{6'}$; 113.88 and 113.73: C$_{5'}$, 108.15: C$_{3'}$ (Ar with OMe); 107.79 and 107.27: C$_{5,15}$; 107.14: C$_{3'}$ (Ar with bridge); 97.56: C$_{10,20}$; 68.45: C$_{\alpha'}$; 56.13: OCH$_3$; 45.38: N(CH$_3$)$_2$; 39.5 and 39.39: $\underline{C}$(CH$_3$)$_3$; 37.03: C$_{\varepsilon'}$; 35.90 and 35.84: C$_\beta$; 28.49: C$_{\beta'}$; 28.12: C$_{\delta'}$; 26.71: C($\underline{C}$H$_3$)$_3$; 26.71 and 26.60: C$_\alpha$; 25.0: C$_{\gamma'}$; 23.59 and 23.57: C$_\gamma$; 14.55: C$_\delta$; 13.76 and 13.74: CH$_{3pyrrole}$.

Part B: Synthesis of the different bridge moieties.

B.1. Bridge 15.

The synthesis of bridge **15** was done from **23** by A. Pfiffner according to a literature procedure [62]. Therefore the synthesis of **15** is not reported.

B.2. Bridge 16.

The synthesis of **29** has been done by Dr. O. Forrer and was a generous gift from her. Therefore the synthesis is not reported here.

O-(2,6-dimesyloxypropyl-4-tert-butyl-1-phenyl)-N,N-dimethylthiocarbamoyl (16):

To a solution of 111.6 mg (0.31 mmol, 1 eq) **29** in 10 ml dry CH_2Cl_2 under argon was added at 0°C 105.6 µl (0.757 mmol, 2.4 eq) triethylamine and after 30 Min. 58.9 µl (0.757 mmol, 2.4 eq) methanesulfonyl chloride. The solution was warmed to RT. and stirred for two hours. Then it was diluted with 10 ml CH_2Cl_2 and washed with 10 ml 4N HCl. The aquous phase was extracted further twice with CH_2Cl_2 and the combined organic layers were washed with brine, dried over sodium sulfate, filtered and evaporated. The residue was chromatographed (SiO_2, 3*20 cm, Hex:EE 1:1) to yield 62.7 mg (39%) colorless oil.

Analysis:

Yield: 39%.

TLC: R_f=0.68 (Hex: EE 1: 2, 254$^+$).

MS: M=510 (M)$^+$

^{1}**H-NMR** (300 MHz, CDCl$_3$, RT):

δ: 7.16 (s, H$_{3, 5}$, 2 H); 4.58 (t, J=2.54 Hz, H$_{1''}$, 2 H); 3.83 and 3.5 (2*m, H$_{3''}$, 2*2 H); 3.75 and 3.4 (2*m, H$_\gamma$, 2*4 H); 3.05 (br, N(C$\underline{H}_3$)$_2$, 6 H); 2.83 (m, H$_\alpha$, 4 H); 1.93-1.8 (m, H$_{\beta,6''}$, 8 H); 1.7-1.45 (m, H$_{4'',5''}$, 8 H); 1.28 (s, H$_{2'}$, 9 H).

B.3. Bridge 47.

4-tert-butyl-1-allyoxy-phenyl (24):

The synthesis was done according to [70]. All spectroscopic characterizations are identical to the data reported.

2-allyl-4-tert-butyl-1-phenol (25):

The synthesis was done according to [70]. All spectroscopic characterization are identical to the data reported

2-allyl-4-tert-butyl-1-N,N,-dimethylthiocarbamoyloxy-phenyl (44):

2 g (10.51 mmol, 1 eq.) **25** in 5 ml abs. DMF were added to the suspension and the solution was stirred further for 10 Min at RT until no hydrogen more evolved. To the brown solution was added 1.06 g (15.76 mmol, 2.1 eq.) N, N-dimethylthiocarbamoyl chloride at RT. The reaction mixture was then stirred at 70°C (oil bath temperature) for 3.5 hr. After cooling to RT the solution was diluted with 100 ml aquous 10% NaOH solution and extracted three times with 30 ml diethylether. The combined organic layers were then washed three times with 50 ml of water, dried over Na_2SO_4, filtered over active charcoal and concentrated. The crude product was distilled under high vacuum in a Kugelrohr apparatus to yield 1.66 g (57%) **44** as a colorless oil.

Analysis:

Yield: 57%

TLC (silica gel, Hex:EE 5:1): R_f=0.4 (254^+)

MS (EI; 70eV): 277 M^+ (8.6%); 205 $[M-72]^+$ (22.6%); 88 [M-169] (100%); 72 [M-205] (80%); 57 $[M-220]^+$ (20%).

^{1}H-NMR (CDCl$_3$, 400 MHz): 7.3-7.2 (m, $H_{3,5}$, 2H); 7.0 (d, J= 8.33 Hz, H_6, 1H); 6.1-5.9 (m, H_β, 1H); 5.2-5.1 (m, H_γ, 2H); 3.45 (s, N(CH$_3$)$_2$, 3H); 3.35 (s, N(CH$_3$)$_2$, 3H); 3.44 (d, J= 7.8 Hz, H_α, 2H); 1.3 (s C(CH$_3$)$_3$, 9H).

^{13}C-NMR (CDCl$_3$, 101 MHz): 188: C=S; 150.24: C_1; 149.3: C_4; 136.85: C_5; 131.96: C_2; 127.59: C_6; 124.59: C_3; 122.98: C_β; 116.30: C_γ; 43.66: N(CH$_3$)$_2$; 38.9: N(CH$_3$)$_2$; 35.4: C_α; 34.92: $\underline{C}$(CH$_3$)$_3$; 31.85: C($\underline{C}$H$_3$)$_3$.

S-(2-allyl-4-tert-butyl-1-phenyl)-N,N-dimethylcarbmoyl (45):

1.39 g (5.01 mmol, 1eq.) **44** were preheated at 120°C and pyrrolyzed in a quartz tube heated at 540°C under 3.10^{-2} mbar vacuum over 30 Min. The product collected on the cooling finger was then diluted with diethylether and transferred in a ballon. After evaporation of the solvent the crude product was purified by column chromatography (silica gel, 3*25cm, Hex:EE 5:1) to yield 988.3 mg (71%) **45** as an orange oil.

Analysis:

Yield: 71%

TLC (silica gel, Hex:EE 5:1): R_f=0.27 (254$^+$)

MS (EI; 70eV): 277 M$^+$ (7.3%); 237 [M-40]$^+$ (15%); 205 [M-72]$^+$ (17%); 72 [M-205]$^+$ (100%); 57 [M-220]$^+$ (27%).

^{1}**H-NMR (CDCl$_3$, 400 MHz):** 7.4 (d, J= 8.05 Hz, H$_6$, 1H); 7.3-7.2 (m, H$_{3,5}$, 2H); 6.1-5.9 (m, H$_\beta$, 1H); 5.1-5.0 (m, H$_\gamma$, 2H); 3.5 (d, J= 7.5Hz, H$_\alpha$, 2H); 3.15 (s (br), N(CH$_3$)$_2$, 3H); 3.05 (s (br), N(CH$_3$)$_2$, 3H); 1.3 (s, C(CH$_3$)$_3$, 9H)

^{13}**C-NMR (CDCl$_3$, 101 MHz):** the C=O signal has not been detected; 153.5: C$_1$; 144.2: C$_4$; 137.6: C$_{5,2}$; 127.4: C$_3$; 124.48: C$_\beta$; 116.27: C$_\gamma$; 39.23: N(CH$_3$)$_2$; 3734: C$_\alpha$; 35.16: $\underline{C}$(CH$_3$)$_2$; 31.62: C($\underline{CH_3}$)$_2$.

S-(2-oxypropyl-4-tert-butyl-1-phenyl)-N,N-dimethylcarbamoyl (46):

832.3 mg (3 mmol, 1 eq.) **45** were dissolved in 5 ml dry THF under dry and inert atmosphere. To the solution were added at 0°C 540 µl (3.24 mmol, 1.8 eq.) BH$_3$-Me$_2$S complex. The solution was stirred for 3 hr at RT. Then 2.5 ml (7.5 mmol, 2.5 eq) aquous 3M NaOH solution and 2.4 ml (7.5 mmol, 2.5 eq.) 30% aquous H$_2$O$_2$ solution were dropped slowly to keep the temperature below 10°C. The solution was then stirred for 1 hr at RT. The reaction mixture was diluted with 20 ml brine and extracted three times with 20 ml diethylether. The combined organic layers were washed once more with 25 ml brine, dried over Na$_2$SO$_4$, filtered and concentrated. The crude product was dried at high vacuum to yield 797.1 mg (90%) **46** as a colorless oil.

Analysis:

Yield: 90%

TLC (silica gel, Hex:EE 5:1): R_f=0.27 (254$^+$, Cer$^+$)

^{1}**H-NMR (DMSO, 400 MHz):** 7.34-7.28 (m, H$_{6, 3}$, 2H); 7.25-7.22 (m, H$_3$, 1H); 4.42 (t, J= 5.3 Hz, CH$_{2\gamma}$,2H); 3.4 (qui, J=5.3 Hz, CH$_{2\beta}$, 2H); 3.05 (s, (br), N(CH$_3$)$_2$, 3H); 2.95 (s (br), N(CH$_3$)$_2$, 3H); 2.7 (t, J= 5.3 Hz, CH$_{2\alpha}$, 2H); 1.25 (s, C(CH$_3$)$_3$, 9H).

^{13}**C-NMR (DMSO, 101 MHz):** 166.21: C=O; 153.2: C$_1$; 146.85: C$_4$; 138.08: C$_5$; 127.37: C$_2$; 125.17: C$_3$; 124.25: C$_6$; 61.2: C$_\gamma$; 37.48: N(CH$_3$)$_2$; 35.24: N(CH$_3$)2; 34.81: C$_\alpha$; 31.85: C(CH$_3$)$_2$; 31.54: C$_\beta$.

S-(2-mesyloxypropyl-4-tert-butyl-1-phenyl)-N,N-dimethylthiocarbamoyl (47):

500 mg (1.69 mmol, 1 eq.) **46** were dissolved in 5 ml dried CH$_2$Cl$_2$ under a dry and inert atmosphere and cooled to 0°C. To the solution were added 283 µl (2.03 mmol, 1.2 eq.) triethylamine and the reaction mixture was stirred for 30 Min. 157.8 µl (2.03 mmol, 1.2

eq.) mesitylchloride were then added and the solution was stirred for 1 hr at RT. The solution was diluted with 10 ml CH$_2$Cl$_2$ and shaked with 10 ml aquous 10% HCl solution. The aquous layer was extracted twice with 5 ml CH$_2$Cl$_2$. The combined organic layers were then washed with twice 10 ml brine, dried over Na$_2$SO$_4$, filtered and concentrated. The crude product was purified by column chromatography (silica gel, 3*25 cm, 500 ml CH$_2$Cl$_2$ pure then CH$_2$Cl$_2$:MeOH 99:1) to yield 487 mg (77%) product which crystallized after one week at 5°C.

Analysis:

Yield: 77%

TLC (silica gel, Hex:EE 5:1): R$_f$=0.27 (254$^+$)

^{1}H-NMR (DMSO, 400 MHz): 7.4-7.2 (m, H$_{3,5,6}$, 3H); 4.18 (t, J=6.0 Hz, H$_\gamma$, 2H); 3.15 (s, SO$_2$(CH3), 3H); 3.17 (s (br), N(CH$_3$)$_2$, 3H); 2.9 (s (br), N(CH$_3$)$_2$, 3H); 2.75 (t, J= 6.0Hz, H$_\alpha$, 2H); 1.9 (qui, J= 6Hz, H$_\beta$, 2H); 1.27 (s, C(CH$_3$)$_3$, 9H).

^{13}C-NMR (DMSO, 101 MHz): 165.21: C=O; 152.58: C$_1$; 144.60: C$_4$; 137.38: C$_5$; 126.70: C$_2$; 124.39: C$_3$; 123.80: C$_6$; 69.76: C$_\gamma$; 36.56: N(CH$_3$)$_2$; 36.5: $\underline{C}$(CH$_3$)$_3$; 34.63: N(CH$_3$)$_2$; 34.63: C$_\alpha$; 30.90: C($_C$H$_3$)$_2$; 29.96: C$_\beta$. (the C mesylate signal is propably masked by the DMSO solvent peaks)

B.4. Bridge 54.
d-thio valeric acid (51):

9.3 g (50 mmol, 1 eq.) δ-bromo valeric acid **50** were dissolved in 50 ml abs. ethanol. 3.8 g (50 mmol, 1 eq.) thiourea were added and the reaction mixture was refluxed for 3 hr. 35 ml (140 mmol, 2.8 eq.) 4N aquous NaOH solution were added and the solution was refluxed for further 2 hours. After cooling at RT the ethanol was removed under vacuum. The aquous solution was extracted once with 10 ml diethylether. The aquous phase was then acidified to pH=4.5 with 6 N HCl and extracted three times with 20 ml diethylether. The combined ether phases were dried over Na$_2$SO$_4$, filtered and concentrated. 5.95 g (89%) **34** as a colorless oil were obtained. The crude product was used without further purification.

Analysis:

Yield: 89%

TLC (silica gel, Hex:EE 5:1): R$_f$=0.27 (bromocresol green$^+$)

^{1}H-NMR (CDCl$_3$, 400 MHz): 12.00 (s (br), COO$\underline{H}$, 1H); 2.44 (t, J = 7.1, H5, 2H); 2.21 (s, S$\underline{H}$, 1H); 2.19 (t, J = 7.5, H$_2$, 2H); 1.6-1.5 (m, H$_{3,4}$, 4H).

^{13}C-NMR (CDCl$_3$, 101 MHz): 174.68: $\underline{C}$OOH; 33.46: C$_5$; 24.07: C$_2$; 23.8: C$_3$; 23.63: C$_4$.

159

d-S-N,N-dimethylthiocarbamoyl-valeric acid (52):

500 mg (3.37 mmol, 1 eq) **51** were dissolved in 5 ml abs. pyridine under a dry inert atmosphere. 692 mg (1.5 mmol, 1.5 eq.) N,N-dimethythiocarbamoyl chloride were added to the solution. The reaction was stirred at 50°C for 2.0 hr. After cooling at RT the solution was poured in 10 ml water. The aquous phase extrated three times with 20 ml CH_2Cl_2. The combined organic layers were washed with brine, dried over Na_2SO_4, filtered and concentrated. The crude product was purified by distillation at high vaccuum (5.10^{-2} mbar, 210°C) to yield 474 mg (57%) **35** as a colorless oil.

Analysis:

Yield: 57%

TLC (silica gel, Hex:EE 5:1): R_f=0.27 (254^+)

UV-Vis ($CHCl_3$): λ (nm): 277 (100%)

MS (EI): 221 (M^+) (28%), 121 $(M-100)^+$ (70%), 88 $(M-133)^+$ (100%)

^{1}H-NMR ($CDCl_3$, 400 MHz): 11.97 (s (br), COO$\underline{H}$, 1H); 3.43 (s, N(C$\underline{H}_3$)2, 3H); 3.32 (s, N(C$\underline{H}_3$)2, 3H); 3.19 (t, J = 7.1, H_5, 2H); 2.22 (t, J = 7.3, H_2, 2H); 1.6-1.5 (m, $H_{3,4}$, 4H).

^{13}C-NMR ($CDCl_3$, 101 MHz): 197: C(S); 175.07: $\underline{C}$(O)OH; 37.16: C_5; 34.06: N($\underline{C}H_3)_2$; 28.79: C_2; 24.64: $C_{3,4}$.

d-S-N,N-dimethylthiocarbamoyl-pentan-1-ol (53):

To 11.5 mg (0.504 mmol, 1 eq.) **52** were added 604.5 µl (0.604 mmol, 1.2 eq.) 1M BH_3.THF complex. After the end of gas evolution a yellow solution formed which was stirred for further 1 hr at RT. The solution was diluted with 5 ml diethylether and the resulting suspension was taken in 10 ml aquous 10% HCl solution. After separation of the organic layer the aquous phase was extracted three times with 5 ml diethylether. The combined organic layer were washed with 15 ml brine, then with water. After drying over Na_2SO_4 and filtration the solvent was evaporated. The crude product was purified by column chromatography (silica gel, 2*25 cm, CH_2Cl_2:MeOH 95:5) to yield 82.3 mg (79%) of a colorless oil.

Analysis:

Yield: 79%

TLC (silica gel, Hex:EE 5:1): R_f=0.27 (254^+)

MS (EI): 207 (M^+) (8%); 174 $(M-33)^+$ (6%), 121 $(M-86)^+$ (68%); 88 $(M-119)^+$ (100%)

¹H-NMR (CDCl₃, 400 MHz): 5.29 (s (br), O<u>H</u>, 1H); 3.66 (t, *J* = 6.45, H₁, 2H); 3.54 and 3.36 (s, N(CH₃)₂, 6H); 3.28 (t, *J* = 7.45, H₅, 2H); 1.73 (qui, *J* = 7.45, H₂, 2H); 1.61 (m, H₄, 2H); 1.49 (m, H₃, 2H).

¹³C-NMR (CDCl₃, 101 MHz): 197.97: C(S); 63.13: C₁; 37.16: C₅; 35.64 and 31.82: N(<u>C</u>H₃)₂; 37.9: C₅; 28.92: C₄; 25.52: C₃.

d-S-N,N-dimethylthiocarbamoyl-1-mesityloxy-pentane (54):

80 mg (0.385 mmol, 1 eq.) **53** were dissolved in dry CH₂Cl₂ under a dry and inert atmosphere. After cooling at 0°C 64.5 µl (0.463 mmol, 1.2 eq.) triethylamine were added and the solution was stirred for 15 Min. 36 µl (0.463 mmol, 1.2 eq) mesitylchloride were added and the solution was stirred 3 hr at RT. The reaction mixture was diluted with 5 ml CH₂Cl₂ and extracted with 5 ml of a 10% aquous HCl solution. The aquous phase was then extracted three times with 5 ml CH₂Cl₂ each. The combined organic layers were dried over Na₂SO₄, filtered and concentrated. The crude product was dried at high vacuum to yield 109.3 mg (99%) yellow oil **37** which crystallized after a week at 5°C.

Analysis:

Yield: 99%

TLC (silica gel, Hex:EE 5:1): R_f=0.27 (254⁺)

¹H-NMR (CDCl₃, 400 MHz): 4.24 (t, *J* = 6.44, H₁, 2H); 3.55 and 3.37 (s, N(C<u>H</u>₃)₂, 3H); 3.29 (t, *J* = 7.32, H₅, 2H); 3.00 (s, OSO₂C<u>H</u>₃, 3H);1.85-1.75 (m, H₂,₃,₄, 6H).

¹³C-NMR (CDCl₃, 101 MHz): 197.97: C(S); 70.18: OSO₂<u>C</u>H₃; 37.81: C₁ and N(<u>C</u>H₃)₂; 37.46: C₅ and N(<u>C</u>H₃)₂; 29.06: C₂; 28.65: C₄; 25.14: C₃.

Part C: Spectroscopic characterisation of iron complexes.

Most of the results are to be found in the part *Results and Discussion* and are therefore not repeated here. Only experimental conditions are described or precised.

C.1. UV-Vis spectroscopy

All UV-Vis experiments have been recorded using a Helwett-Packard diode array spectrometer (see general remarks). The experiments have been saved on the UV-Vis computer, and additionally copied on a CD-ROM to allow future consultancy. For each file the solvent has been added in the commentary of the first spectra and for each spectra recorded in a file the added species and the time after initial measurement have been precised.

Two kinds of experiments have been performed. The first experiment has been the determination of the absorption coefficient ε for models **11** and **12**. The second experiments are either quantitative or qualitative experiments to form complexes with the iron complexes.

a) Determination of the absorption coefficient

As porphyrin have a very large absorption coefficient ranging from 10^4-10^6 M^{-1} for their most intense absorption band a stock solution of the porphyrin to be studied has been prepared, having a concentration of 10^{-3} M.

For the CPO model **11** the solution was prepared under argon to avoid oxidation of the compound. As a precaution the solution was kept under light exclusion for the same reason. After each probe prelevement for UV-Vis measurement the solution was flushed with argon.

For the catalase model **12** the solution has been prepared without any special precaution regarding the obtention of an inert atmosphere.

For each prepared concentration three probes have been measured to judge the reproducibility of the determination. When one result was obviously out of the measured range of the other two experiments (20% deviation) a fourth measurement has been performed. From the set of measures a linear regression has been performed.

To refine the curve a graphic containing the data has been drawn. From this graphic the range of linearity i.e. the domain where the Beer-Lambert law applies- has been determined. From the set of measurements which were retained a novel linear regression

was done. If the obtained value of the linear regression coefficient was over 0.998 the obtained value of the slope was determined to be the absorption coefficient. If this was not the case, each set of three measurements plotted was examined and a "manual" trace was done to examine whether one value fits to the trace and was retained or if the average of the measured absorption had to be taken as value for determining the slope. From these new data the coefficient was recalculated.

In both cases the variation of the absorption coefficient calculated has been less than 10% and whatever the calculation the regression coefficient was found to be above 0.997.

The precision of the determination of the coefficient is estimated to be ±20%.

b) Qualitative experiments

To observe the changes which occurred by addition of a ligand, the ligand has first been added to the solution in a large excess to determine whether an effect was observed or not. When an effect has been observed a quantitative experiment has been performed to determine the minimum of equivalents required to get the effect.

When the addition of a large excess resulted in the destruction of the porphyrin the added quantity was reduced at each trial by the half until either a change has been observed in the spectra or no change appeared in the spectra. In this case the time after addition has been recorded.

c) Quantitative experiments

A 2 ml solution having an absorbance of 1-1.5 has been prepared for quantitative experiments. The absorbance of the solution at "resting state" was measured to determine the quantity of porphyrin present in the solution. Then an exact equivalent quantity of a ligand was added and the change upon time of the spectra were recorded.

C.2. EPR spectroscopy

The EPR sample have been prepared so that an initial porphyrin concentration of $5 \ 10^{-3}$ M has been obtained. This concentration represents the best compromise between a detectable EPR trace and the requirement of conserving an "isolated" magnetic state for each molecule.

For the experiments a first record of a spectra was taken in Basel at 110 K including a resting state spectra and the spectra resulting upon addition of a ligand. From the same batch of porphyrin the experiment was repeated at 5 to 15K at the ETH of Zürich for the complex species.

The results are found in the part *Results and Discussion*.

C.3. NMR spectroscopy

The NMR experiments were conducted under the same concentration conditions as for EPR. The spectra for high spin species were recorded in three parts to cover the full range of chemical shifts concerned.

The results are found in the *Part Results and discussion*.

C.4. UV-Vis studies on the resting state

For the resting state the influence of the solvent on the Soret has been determined using porphyrin solution having an absorbance of 1-1.6 AU.

The results are shown in the next table:

Compound:	Solvent	Soret Band (nm)
CPO Model 11	methylene chloride	406
	toluene	406
	acetonitrile	406
	DMSO	406
Catalase model 12	methylene chloride	408
	toluene	408
	acetonitrile	406
	DMSO	408

Then the influence of the addition of acid to the porphyrin solution was examined in toluene. The results are summarized in the next table. When two absorption maxima are found due to broadening of the band the most intense maxima is underlined.

acid	compound	Soret band (nm) after addition	Soret band initial (nm)
HBr	**11**	402	406
	12	394	408
	32	402	408
	33	400	408
HCl	**11**	388 + <u>412</u>	406
	12	<u>388</u>+ 412	408
	32	390+ <u>416</u>	408
	33	<u>388</u> + 412	408

C.5. HOCl and ClO⁻ complexes

The characterization of these complexes is found in part *Results and Discussion*.

1. Oxo complexes

The characterization of these complexes is found in the part *Results and Discussion*.

2. Peroxy complexes

The characterization of this complex of CPO model **11** is found in the part *Results and Discussion*.

ANNEXES

Abbreviations.

Å: Ångstrom

AcOH: acetic acid

Ala: Alanine

$AlCl_3$. aluminium chloride

Arg: Arginine

Asn: Aspargine

Asp: aspartic acid

AU: absorption unit

BBr_3: bortribromide

BCl_3: bortrichloride

$BH_3.Me_2S$: borhydride dimethylsulfide complex

BH_4: tetrahydrobiopterin

^{13}C: carbon 13 isotope

CaM: calmodulin

$CDCl_3$: deutero chloroform

°C: grade Celcius

CH_2Cl_2: dichloromethane

Cl^-: chloride ion

COSY: correlation spectroscopy

CPO: Chloroperoxidase from *Caldariomyces fumago*

CV: cyclic voltammetry

CW: continuous wave

Cys: cystein

D: dimensional

d: doublet (in NMR spectroscopy)

d_n: n deuterium atoms (in NMR solvent)

δ: chemical shift (in NMR spectroscopy)

Δ: reflux

dB: decibel

DMF: dimethyl formamide

DMSO: dimethyl sulfoxide

ε: absorption coefficent

e^-: electron

EE: ethyl acetate

EI: electron impact

ENDOR: electron nuclear double resonance spectroscopy

ESEEM: electron spin echo enveloppe modulation spectroscopy

EPR: electron paramagnetic resonance

Eq.:equation

eq or eq.: equivalent

ESR: electron spin resonance

Et_3N: triethyl amine

Et_2O: diethylether

eV: electron volt

EXFAS: extended X-ray absorption fine structure

FAB: fast atom bombardement

FAD: flavin adenine dinucleotide (oxidized form)

$FADH_2$: flavin adenine dinucleotide (reduced form)

$FeBr_2$: iron dibormide

$FeCl_3$: iron (III) chloride

FID: Free induction decay

FMN: flavin mononucleotide

FT: Fourier transformation

g: ESR g value

GHz: Gigahertz

Gly: glycine

Glu: glutamic acid

h: Plank's constant

ħ: reduced Plank's constant

H^+: proton

^1H: proton

HBr: hydrobromic acid

HCl: hydrochloric acid

HETCOR: heteronuclear correlation spectroscopy

Hex. hexane

His: histidine

HMBC: heteronuclear multiple bond correlation spectroscopy

HMQC: heteronuclear multiple-quantum coherence correlation spectroscopy

H_2O_2: hydrogen peroxide

HOCl: hypochlorite acid

HOMO: highest occupied molecular orbital

HPLC: high performance liquid chromatography

hr: hour

HRP: horseradish peroxidase

Hz: Hertz

Ile: isoleucine

J: coupling constant (in NMR spectra)

K: grade Kelvin

KOMe: potassium methylate

$LiAlH_4$: lithium aluminium hydride

LiBR: lithium bormide

$LiClO_4$. lithium perchlorate

λ: wavelength

LUMO: lowest unoccupied molecular orbital

M: mole

m: multiplet (in NMR spectra)

m: meta

m: middle

M^{-1}: per mole

MALDI-TOF: matrix assisted desorption time of flight spectroscopy

*m*CPBA: *meta*-chlorperbenzoic acid
Me: methyl

MeCN: acetonitrile

mg: milligramm

Min: minutes

ml: milliliter

mM: millimole

Me_3OBF_4. trimethyloxy tetrafluoroboride

MeOH: methanol

MO: molecular orbital

MS: mass spectroscopy

Ms: mesyl

MSCl: mesylchloride

MTHF: 2-methyltetrahydrofuran

mV: millivolt

mW: milliwatt

MW: molecular weight

N: normality

^{15}N: nitrogen isotope 15

NMR: nuclear magnetic resonance spectroscopy

NAD$^+$: nicotineamide adenine dinucleotide (oxidized form)

NADP$^+$: nicotinamide adenine dinucleotide phosphate (oxidized form)

NADH: nicotineamide adenine dinucleotide (reduced form)

NADPH: nicotinamide adenine dinucleotide phosphate (reduced form)

NaH: natrium hydride

NaOH: natrium hydroxide

NHA: N-hydroxyarginine

nm: nanometer

NO or ˙NO: nitirc oxide

NOE: nuclear overhauser enhancement

NOS: Nitric oxide synthase

NOESY: nuclear overhausen spectroscopy

O$_2$: oxygen

O$_2$˙$^-$: superoxide ion

o: ortho

$^-$OCl: hypochlorite

p: para

P450: cytochrome P450

Phe: phenylalanine

Piv: pivaloyl

ppm: part per million

Pro: proline

Q: quadrupole splitting parameter (in Mössbauer spectroscopy)

qua: quadruplet (in NMR spectroscopy)

qui: quintuplet (in NMR spectroscopy)

R$_f$: retention factor (chromatography)

RF: radio frequency

ROESY: reversed Overhouser enhancement spectroscopy

RT: room temperature (295K)

Rt: retention time (in HPLC)

s: singulet (in NMR spectroscopy)

s: strong

s: second

s^{-1}: per second

Ser. serine

sext. sextuplet (in NMR spectroscopy)

SCE: standard calomel electrode

SOD: super oxide dismutase

t: triplet (in NMR spectroscopy)

TBME: tertbutylmethylether

tert: tertiary

Thr. threonine

TLC: thin layer chromatography

TMS: tetramethylsilane

TpivPP: tetra-[*ortho*-(pivaloylamino)phenyl porphyrin

TPP: tetraphenylporphyrin

TO: turnover

TOCSY: total correlated spectroscopy

Tyr: tyrosine

UV-Vis: ultra-violet visible

Val: valine

V/V: volume to volume

vol: volume

w. weak

Xaa: amino acid undefined

Xhy: amino acid with hydrophobic character

References.

[1]: a) J.C. Kendrew, P.J Pauling,. *Proc.Roy.Soc (London)*, **1956**, *237A*, 255-276, b) H. Scouloudi, Nature, **1959**, 183, 374-376, c) H. Scouloudi, *Proc.Roy.Soc. (London)*, **1960**, *A258*, 181-201.

[2]: W. Küster, Hoppe-Seyler's, *Z.Physiol.Chem*, **1912**, *82*, 433-463.

[3]: H. Fischer, K. Zeile, *Ann.Chem.*, **1929**, *468*, 58-98.

[4]: M. Sono, M.P. Roach, E.D. Coulter, J.H. Dawson, *Chem.Rev.*, **1996**, *96*, 2841-2887.

[5]: D.R. Morris, L.P. Hager, *J.biol.Chem.*, **1966**, *241*, 1763-1768.

[6]: M. Feelish, J.S. Stamler in *Methods in Nitric Oxide research*, Wiley &Sons, **1996**.

[7]: J.A. Peterson, S.E. Graham, *Structure*, **1998**, *6*, 1079-1086.

[8]: M. Sundaramoorthy, J.M. Mauro, A.M. Sullivan, J. Terner, *Acta Cryst.*, **1995**, *D51*, 842-844.

[9]: P.L. Feldman, O.W. Griffith, D.J. Stuehr, *C&EN News*, **1993**, *Dec 20*, 26-38.

[10]: M. Sundaramoorthy, J. Terner, T. L. Poulos, *Structure*, **1995**, *3*, 1367-1377.

[11]: T.L. Poulos, B.C. Finzel, I.C. Gunsalus, G.C. Wagner, J. Kraut, *J.Biol.Chem*, **1985**, *260*, 16122-16130.

[12]: C.A. Hasemann, K.G. Ravichandran, J.A. Peterson, J. Deisenhofer, *J.Mol.Biol.*, **1994**, *236*, 1169-1185.

[13]: K.G. Ravichandran, S.S. Boddu Palli, C.A. Hasemann, J.A. Peterson, J. Deisenhofer, *Science*, **1993**, *61*, 731-736.

[14]: J.R. Cupp-Vickery, T.L. Poulos, *Struct.Biol.*, **1995**, *2*, 144-153.

[15]: S.Y. Park, H.Shimizu, S-I. Adachi, A. Nakagawa, I. Tanaka, K. Nakahara, H. Shoun, E. Obayashi, H. Nakamura, T. Lizuka, Y. Shiro, *Natural Stuctural Biology*, **1997**, *4*, 827-832.

[16]: B.R. Crane, A.S. Arvai, D.K. Gosh, C. Wu, E.D. Getzoff, D.J. Stuehr, J.A. Tainer, *Science*, **1998**, *279*, 2121-2126.

[17]: P.R. Ortiz de Montellano, in *Cytochrome P450. Structure, Mechanism and Biochemistry.*, 2nd ed., Plenum, New York, **1995**, pp 537-574.

[18]: I. Schlichting, J. Berendzen, K. Chu, A.M. Stock, S.A., Maves, D.E. Benson, R.M. Sweet, D. Ring, G.A. Petsko, S.G. Sligar, *Science*, **2000**, *287*, 1615-1622.

[19]: R. Raag, T.L. Poulos, *Biochemistry*, **1989**, *28*, 917-922.

[20]: H.A. Wagenknecht, *Dissertation*, Universität Basel, **1998**.

[21]: S. Nagano, M. Tanaka, Y. Watanabe, I. Morishima, *Biophys.Biochem.Res.Commun.*, **1995**, *207, 417-423.*

[22]: M.R.N. Murthy, T.J. Reid, A. Sicignano, N. Tanaka, G. Rossman, *J.Mol.Biol.*, **1981**, *152*, 465-499.

[23]: P-F. Chen, A-H. Tsai, V. berka, K.K. Wu, *J.Biol.Chem.*, **1997**, *272*, 6114-6118.

[24]: a) M. Humberg, I. Björkhem, *J.Biol.Chem.*, **1971**, *246*, 7411-7416 b) S. Shapiro, J.U. Piper, E. Caspi, *J.Am.Chem.Soc*, **1986**, *104*, 2301-2305.

[25]: J.T. Groves, *J.Chem.Edu.*, **1985**, *62*, 928-931.

[26]: S. Shaik, M. Filatov, D. Schröder, H. Schwarz, *Chem.Eur.J.*, **1998**, *4*, 193-199.

[27]: N. Harris, S. Cohen, M. Filatov, F. Ogliaro, S. Shaik, *Angew.Chem.*, **2000**, *112*, 2070-2074.

[28]: M. Newcomb, R. Shen, S.-Y. Choi, P.H. Toy, P.F. Hollenberg, A.D.N. Vaz, M.J. Coon, *J.Am.Chem. Soc.*, **2000**, *122*, 2677-2686.

[29]: M.A. Marletta, *J.Biol.Chem.*, **1993**, *268*, 12231-12234.

[30]: A.R. Hurshman, C. Krebs, D.E. Edmondson, B.H. Huynh, M.A. Marletta, *Biochem.*, **1999**, *38*, 15689-15696.

[31]: C.C.-Y. Wang, H.M. Douglas, J.T. Groves, *J.Am.Chem.Soc*, **1999**, *121*, 12094-12103.

[32]: R.D. Libby, A.L. Shedd, A.K. Phipps, T.M. Beachy, S.M. Gertsberger, *J.Mol.Biol.*, **1992**, *267*, 1769-1775.

[33]: M.T. Green, *J.Am.Chem.Soc.*, **1999**, *121*, 7939-7940.

[34]: T.L.Poulos, J. Kraut, *J.Am.Chem.Soc.*, **1980**, *255*, 8199-8205.

[35]: A. Deisseroth, A.L. Dounce, *Phys.Review*, **1970**, *50*, 319-375.

[36]: M.R.N. Murthy, T.J. Reid, A. Sicignano, N. Tanaka, G. Rossmann, *J.Mol.Biol.*, **1981**, *152*, 465-499.

[37]: B.K.Vainshtein, W.R. Melik-Adamyan, V.V. Barynin, A.A. Vagin, A.I.Grebenko, V.V. Borisov, K.S. Bartels, I. Fita, M.G. Rossmann, *J.Mol.Biol.*, **1986**, *188*, 49-cc.

[38]: E.F. Yusifov, A.I. Grebenko, V.V. Barynin, A.A. Vagin, W.R. Melik-Adamyan, *Sov.Phys.Crystallogr.*, **1989**, *34*, 1451-1456.

[39]: R.J.M. Corral, H.M. Rodman, J. Margolis, B.R. Landau, *J.Biol.Chem.*, **1974**, *249*, 3181-3182.

[40]: D.Keilin, E.F. Hartree, *Proc.Roy.Soc.*, **1937**, *Ser. B*, 173.

[41]: J.B. Sommer, A.L. Dounce, *Science*, **1937**, *85*, 366-367.

[42]: A.G. Malmon, *Biochim.Biophys.Acta*, **1957**, *26*, 233-240.

[43]: M. Weissbluth in *Structure and Bonding*, Springer Verlag, Berlin, *Vol 2*, pp 8-10.

[44]: A. L. Blach, *Coord.Chem.Rev.*, **2000**, *202-202*, 349-377.

[45]: I. Fita, M.G. Rossann, *J.Mol.Biol.*, **1985**, *185*, 21-37.

[46]: J. Everse, K.E. Everse, M.B: Grisham, in *Peroxidase in Chemistry and Biology*, CRC Press, Boca Raton, **1991**, Vol 1.

[47]: G.R. Schonbaum, B. Chance in *The enzymes*, PD Boyer ed., **1976**, *Vol 13*, pp 408-463.

[48]: B. Chance, *J.Biol.Chem.*, **1949**, *180*, 947-959.

[49]: B.Chance, *J.Biol:chem.*, **1952**, *194*, 471-481.

[50]: L.L. Ingraham in *Biochemical mechanisms*, Wiley, New York, **1962**, p 71.

[51]: D. Dolphin, A. Forman, D.C. Borg, J.Fayer, R.H. Felton, *Proc.Natl.Sci.U.S.*, **1971**, 614-618.

[52]: G.A. Hamilton, *Adv.Enzymol.*, **1969**, *32*, 55-96.

[53]: R.C. Jarnagin, J.H. Wang, *J.Am.Chem.Soc.,* **1958**, *80*, 6477-6481.

[54]: A.W. Wagenknecht, W.D. Woggon, *Chem.Biol.*, **1997**, *4*, 367-372.

[55]: for a review on heme models see: F.A. Walker**,** Iron porphyrin chemmistry in *Encyclopedia of inorganic chemistry*, B.R. King Ed., **1987** and references therein.

[56]: W.D. Woggon, *Topic in Current Chemistry*, **1996**, *184*, 40-96.

[57]: B. Stäubli, Dissertation, Zürich, **1989**.

[58]: B.Boitrel, A. Lecas, Z. Renko, E.Rose, *New.J.Chem*, **1989**, *13*, 73-.99

[59]: Y. Naruta, F. Tani, N. Ishibara, K. Maruyama, *J.Am.Chem.Soc.*, **1991**, *113*, 6865-6872.

[60]: B. Garcia, C-H. Lee, A. Blaskó. T.C. Bruice, *J.Am.Chem.Soc.*, **1991**, *113*, 8118-8126.

[61]: A. Robert, B. Loock, M. Momenteau, B. Meunier, *Inorg.Chem.*, **1991**, *30*, 706-711.

[62]: T. Leifels, W-D. Woggon, in preparation.

[63]: E. Baciocchi, T. Boshi, L. Cassioli, C. Galli, L. Jaquinod, A. Lapi, R. Paolesse, K.M. Smith, P. Tagliatesta, *Eur.J.Org.Chem*, **1999**, 3281-3286.

[64]: C. Claude, H.A. Wagenknecht, W-D. Woggon, *Helv.Chem.Acta*, **1998**, *81*, 1506-1520.

[65]: A. Blaskó, B. Garcia, T.C. Bruice, *J.Org.Chem.*, **1993**, *58*, 5738-5747.

[66]: R. Belal, M. Momenteau, B. Meunier, *J.Chem.Soc., Chem.Commun.*, **1989**, 409-411.

[67]: H. Aissaoui, Dissertation, Basel, **1999**.

[68]: H. Aissaoui, S. Ghirlanda, C. Gmür, W-D. Woggon, *Journal of molecular catalysis A Chemical*, **1996**, *113*, 393-402.

[69]: A.W. Wagenknecht, W-D. Woggon, *Angew. Chem.*, **1997**, *109*, 404-407.

[70]: B. Saübli, H. Fretz, U. Piantini, W-D. Woggon, *Helv.Chim.Acta*, **1987**, *70*, 1173-1193.

[71]: L.K. Gottwald, E.F. Ullman, *Tetrahedron Lett.*, **1969**, *36*, 3071-3074.

[72]: H.Ogoshi, H. Sugimoto, T. Nishiguchi, T. Watanabe, Y. Matsuda, Z-I. Yoshida, *Chemistry Letters*, **1978**, 29-32.

[73]: R.Young, C.K. Chang, *J.Am.Chem. Soc.*, **1985**, *107*, 898-909.

[74]: J.P. Collman, R.R. Gagne, C.A. Reed, T.R. Halbert, G. Lang, W.T. Robinson, *J.Am.Chem.Soc.*, **1975**, *97*, 1427-1439.

[75]: M.J. Gunter, L.N. Mander, *J.Org.Chem.*, **1981**, *46*, 4792-4795.

[76]: R. Boitrel, E. Camilleri, Y. Fleche, A. Lecas, E. Rose, *Terahedron Lett.*, **1989**, *30*, 29323-2926.

[77]: Y. Aoyama, K. Saita, H. Toi, H. Ogoshi, *Tetrahedron Lett.*, **1987**, *28*, 4853-4856.

[78]: M.A. Lisicki, P.K. Mishra, A.A. Bohthner-By, J.S. Lindsey, *J.Phys.Chem.*, **1988**, *92*, 3400-3403.

[79]: J.A. Shelnutt, X-Z. Song, J-G. Ma, S-L. Jia, W. Jentzen, C.J. Medforth, *Chem.Soc. Rev.*, **1998**, *27*, 31-41.

[80]: C.G. Kalodimos, I.O. Gerothanassis, *J.Am.Chem.Soc.*, **1998**, *120*, 6407-6408.

[81]: a) *see* ref 15, b) R.A. Freitag, J.A. Mercer-Smith, D.G. Whitten, *J.Am.Chem.Soc.*, **1981**, *103*, 1226-1230.

[82]: O. Forrer, Dissertation, Basel, **1999.**

[83]: L. Mu, postdoctoral work, Basel, **2000**.

[84]: G. Scherer, Dissertation, Freiburg im Breisgau, **1990**.

[85]: J.P. Collman, R.C. Gagne, C.A. Reed, T.R. Halbert, G. Lang, W.T. Robinson, *J.Am. Chem.Soc.*, **1975**, *97*, 1427-1439.

[86]: J.A. Shelnutt, C.J. Medforth, M.D. Berber, K.M. Barkigia, K.M. Smith, *J.Am.Chem.Soc.*, **1991**, *113*, 4077-4087.

[87]: the optimization was done using the molecular modelling software Chemdraw 3D and the force field program MM2.

[88]: S.H. Pine in *Organic Chemistry*, Mc Graw Hill international editions, 5th Ed.,**1987**, 365

[89]: A.M.F. Ueberwasser, Dissertation, Zürich, **1995**.

174

[90]: T. Inaba, I. Umezawa, M. Yuasa, T. Inoue, S. Mihashi, H. Itokawa, K. Ogura, *J.Org.Chem*, **1987**, *52*, 2957-2958.

[91]: A.B.J. Parusel, T. Wondimagegn, A. Gosh, *J.Am.Chem.Soc.*, **2000**, *122*, 6371-6374.

[92]: a) S.G. DiMagno, A.K. Wertsching, C.R. Koss, *J.Am.Chem.Soc.*, **1995**, *117*, 8279; b) *ibid.,***1994**, *116*, 8344; c) S.G. DiMagno, R.A. Williams, M.J. Therein, *J.Org.Chem.*, **1994**, *59*, 6943.

[93]: S.H. Pine in *Orgenic Chemistry*, Mc Graw Hill International Editions, 5th Edition, **281** and **295**.

[94]: J.T. Green in *Protective goup in organic chemistry*, Academic Press New York.

[94]: H. Aissaoui, personal communication.

[96]: J.L. Soret, *Compt.Rend.*, **1883**, *97*, 1267.

[97]: L.K. Hanson, W.A. Eaton, S.G. Sligar, I.C. Gunsalus, M. Gouterman, C.R. Connell, *J.Am.Chem.Soc.*, **1976**, *98*, 2672-2674.

[98]: J.P. Collman, T.N. Sorrell, B.M. Hoffman, *J.Am.Chem.Soc.*, **1975**, *97*, 913-914.

[99]: I. Bertini, C. Luchina, in *NMR of Paramagnetic Molecules in Biological Systems*, Physical Bioinorganic Chemistry series,A.B.P. Lever and H.B. Gray eds, **1986**.

[100]: R.U. Cheng, L. Latos-Grazynski, A.L. Balch, *Inorg.Chem.*, **1982**, *21*, 2412-2418.

[101]: D.L. Budd, G.N. La Mar, K.C. Langry, K.M. Smith, R. Nayyir-Mazhir, *J.Am.Chem.Soc.*, **1979**, *101*, 6091-6096.

[102]: G.N. La Mar, D.L. Budd, K.M. Smith, K.C. Langry, *J.Am.Chem.Soc.*, **1980**, *102*, 1822-1827.

[103]: R.D. Arasasingham, A.L. Balch, C.R. Cornman, J.S. de Ropp, K. Egushi, G.N. La Mar, *Inorg.Chem.*, **1990**, *29*, 1847-1850.

[104]: L. Bianci, I. Bertini, S. Marconi, R. Pierattelli, S.G. Sligar, *J.Am.Chem.Soc.*, **1994**, *116*, 4866-4873.

[105]: For review see: H.M. Schwarz, J.R. Bolton, D.G. Borg in *Biological Applications of Electron Spin Resonance*, Wiley&sons Eds., **1972**, Chapter one.

[106]: For review see: J. Hütterman, R. Kappl, in *Metal Ions in Biological Systems*, H. Sigel Ed., **1987**, *Vol 22*, 1-80.

[107]: P.F. Hollenberg, L.P. Hager, W.E. Blumberg, J. Peisach, , *J.Biol.Chem.*, **1980**, *255*, 4801-4807.

[108]: H. Aissaoui, R. Bachmann, A. Schweiger, W-D. Woggon, 3rd European ESR Meeting, Leipzig, **1997**, 24-29 August.

[109]: H. Aissaoui, R. Bachmann, unpublished results.

[110]: J.D. Liscomb, *Biochemistry*, **1980**, *19*, 3590-3599.

[111]: A-L. Tsai, V Berka, P-F. Chen, G. Palmer, *J.Biol.Chem.*, **1996**, *271*, 32563-32571.

[112]: T.L. Poulos, B.C. Finzel, A.J. Howard, *Biochemistry*, **1986**, *25*, 5314-5322.

[113]: J.R. Pilbrow in *Transition Ion in Electron paramagnetic Paramagnetic* Resonanc, Clarendon Press, Oxford, ISBN 0-19-855214-9, 129.

[114]: S. Stoll, A. Schweiger, in preparation.

[115]: G. Feher, in *Electron Paramagnetic Resonance with Application to Selected Problems in Biology"*, Gordon& Breach Science publishers, **1970**, *chapter II*, 48-77.

[116]: H. Rein, O. Ristau, F. Hackenbergger, F. Jung, *Biochim.Biophys.Acta*, **1968**, *167*, 538-546.

[117]: Measurement taken from the structures found in the Cambridge crystallographic database.

[118]: L. Mu, W-D. Woggon, in preparation.

[119]: S. Yoshioka, S. Takahashi, K. Ishimori, I. Morishima, *J.Inorg.Biochem.*, **2000**, *81*, 141-151.

[120]: T. Ueno, N. Nishikawa, S. Moroyama, S. Adachi, K. Lee, T. Okumura, N. Ueyama, A. Nakamura, *Inorg.Chem.*, **1999**, *38*, 1199-1210.

[121]: N. Ueyama, N. Nishikawa, Y. Yamada, T. Okumura, T. Nakamura, *J.Am.Chem.Soc.*, **1996**, *118*, 12826-12827.

[122]: N. Ueyama, N. Nishikawa, Y. Yamada, T. Okumura, S. Oka, H. Sakurai, A. Nakamura, *Inorg.Chem.*, **1998**, *37*, 2415-2421.

[123]: R. Bachmann, personal communication

[124]: C. Brewer, *Inorg.Chim.Acta.*, **1988**, *150*, 189-192 and ref 1 to 5 therein.

[125]: L. Weber, G. Haufe, *Z.Chem.*, **1989**, *3*, 88-100.

[126]: A.W. van der Made, J.W.H. Smeetes, R.J.M. Nolte, W. Drenth, *J.Chem.Soc.Chem.Commun.*, **1983**, 1205-1206

[127]: T. Wolter, W. Meyer-Klaucke, M. Mürther, D. Mandon, H. Winkler, A.X. Trautwein, R. Weiss, *J.Inorg.Biochem.*, **2000**, *78*, 117-122

[128]: a) J.T. Groves, T.E. Nemo, *J.Am.Chem.Soc.*, **1983**, *105*, 5786-5791; b) ibid, **1979**, *101*, 6243-6248.

[129]: S. Wolowiec, L. Latos-Grazynski, *Inorg.Chem*, **1998**, *37, 2984-2988*

[130]: H. Fuji, T. Yoshimura, H. Kamada, *Inorg. Chem.*, **1997**, *36*, 6142-6143.

[131]: Blumberg, J. Peisach, B.A. Wittenberg, J.B.J. Wittenberg, *Biol. Chem.*, **1968**, *243*, 1854-1862.

[132]: D. Dolphin, A. Forman, D.G. Borg, J. Fajer, R.H. Felton, *Proc.Nat Aca.Sci*, **1971**, *69*, 614-618

[133]: T.H. Moss, A. Ehrenberg, A.J. Bearden, *Biochemistry*, **1969**, *8*, 4159-4162.

[134]: W.J. Chuang, H.E. Van Wart, *J. Biol.Chem.*, **1992**, *267*, 13295-13301.

[135]: J.E. Penner-Hahn, K.S. Eble, T:J: MacMurry, M. Renner, A.L. Blach, J.T: Groves, J.H. Dawson, K.O. Hodgson, *J.Am.Chem.Soc.*, **1986**, *108*, 7819-7825.

[136]: A.L. Bach, L. Letos-Grazynski, M.W. Rennner, *J.Am.Chem.Soc.*, **1985**, *107*, 2983-2985.

[137]: J.T. Groves, Y. Watanabe, *J.Am.Chem.Soc.*, **1986**, *108*, 7834-7836.

[138]: J.N. Burstyn, J.A. Roe, A.R. Miksztal, B.A. Shaevitz, G. Lang, J.S. Valentine, *J.Am.Chem.Soc.*, **1988**, *110*, 1382-1388.

[139]: S. Sligar, 5th Conference of Bioinorganic chemistry, Toulouse, July 17th-20th, 2000

[140]: E. McCandisch, A.R. Miksztal, M. Nappa, A.Q. Sprenger, J.S. Valentine, J.D. Stong, T.G. Spiro, *J.Am.Chem.Soc*, **1980**, *102*, 4268-4271

[141]: C.H. Welborn, D. Dolphin, B.R. James, *J.Am.Chem.Soc.,* **1981**, *103*, 2869-2871

[142]: M. Selke, J.S. Valentine, *J.Am.Chem.Soc.*, **1998**, *120*, 2652-2653.

[143]: A. Zuberbühler, S. Kaderli, C. Claude, unpublished experiments.

Acknowledgments

I would like to thank the persons without who this work would not have this final form. Particularly the collaboration with **Stefan Stoll** from Prof. Arthur Schweiger's group at the ETH Zürich was decisive in the confirmation and refinement of the results obtained in Basel.

In Basel the work done by **Dr. Gerd Scherer**, NMR departement of the chemistry departement, provided key results during the synthesis and characterization of the intermediates and final products. His competence, useful discussions and correction of the manuscript were essential for this work.

I would like to thank Prof. Th. Kaden for having been the co referent of this work.

I thank for their service and disponibility the technical staff of the university Basel: the analytical departement with Dr. Nadig for the measurement of mass spectra, the "Werkstatt": Mr. Cabrera, Kohler and Maier, for their numerous interventions on the material, the "Materialausgabe": Mr. Vogel, Böhler and Mrs. Huber for providing and ordering the products and the secretaries Mrs Mambelli-Johnson and Rieser for solving administrative problems.

I am deptful for the synthesis of key intemediates to Andreas Pfiffner and to the students who worked for me: Marc Bornand, Michael Müller, Remo Stohler, Fabian Stapf and Andrea Studer.

Thanks also to the members of Prof. Woggon's group for the good relationship during my work. Particularly appreciated and of good remember are Dr. Hamed Aissaoui for his helpful discussions, "moral" and technical support, Dr. Richard French for his computer and practical knowledges.

Finally I am deptful to the Swiss National Fundation for Science for a grant from Sept 1996 to Sept 1998 and to the Kanton Basel Stadt for an assistentship position from October 1998 until October 2000.

Lebenslauf

Name: CLAUDE

Vorname: Cécile

Geburtsdatum: 11.12.1973

Nationalität: Frankreich

Zivilstand: Ledig

Ausbildung:

11/04/2001:   Dissertationsprüfung mit dem Prädikat „cum laude"

09/1996-10/2000: Dissertationsarbeit unter der Leitung von Prof. Dr. Wolf-Dietrich Woggon, Institut für organische Chemie der Universität Basel (Schweiz) „Enzyme models of Chloroperoxidase and catalase"

09/1995-07/1996: Diplom in Feinchemikalien, Universität Rouen (Frankreich) „Synthese und Charakterisierung von Phosphorhaltigen Verbindungen und deren Anwendung in der Wittig-Horner Reaktion"

09/1993-07/1996: Spezialisierung in "Feinchemikalien und Ingenieurswesen", I.N.S.A. (Institut National des Sciences Appliquées), Rouen (Frankreich) Ingenieursdiplom in „Feinchemikalien und Ingenieurswesen"

09/1991-08/1993: Ingenieurstudien, I.N.S.A., Lyon (Frankreich) Besuch einer europäischen Ingenieursausbildung

07/1996:   Matura Typ C (Mathemathik und Physik-Chemie) mit dem Predikat „sehr gut"

Berufserfahrung:

Seit 11/2000: ZLB Bioplasma AG, Bern (Schweiz) Validierungspezialistin

10/1998-10/2000: Universität Basel, Institut für organische Chemie, Basel (Schweiz) Assistentin der Hauptfachpraktika in organischer Chemie

03/1995-07/1995: Rhône-Poulenc Agrochimie, Centre de Recherche de La Dargoire, Lyon (Frankreich). „Synthese von Imidazolinonen als potentielle Fongiziden"

Publikationen

Poster:

1. Claude, C., Mu, L., Woggon, W-D, 2000: Poster for the 5th EUROBIC Conference in Toulouse (F), (16-20th July 2000).

2. Schweiger, A., Stoll, S., Claude, C., Woggon, W-D., 2000: Poster for the 42nd Rocky Mountain Conference on analytical Chemistry in Broomfield (Colorado), (July,30th-August 3rd, 2000), abstract submitted.

3. Claude, C., Woggon, W-D., *Towards Models for Catalase and P-450 Enzymes. Phenolate versus Thiolate Ligation to Iron Porphyrins.*, **1999**, Poster for the Regio-Symposium in Lucelles (F).

Publications:

1. Woggon, W-D., Wagenknecht, H-A., Claude, C., *J.Bioinorg.Chem.*, **2000**, *78*, in press.

2. Woggon, W-D., Aissaoui, A., Bachmann, R., Claude, C., Schweiger, A., Wagenknecht, H-A., **1998,** *Second Electronic Conference on Synthetic Organic Chemistry.*

3. Wagenknecht, H-A., Claude, C., Woggon, W-D., *Helv.Chim.Acta,* **1998,** *81(8)*, 1506-1520.

180

Eidesstattliche Erklärung.

Ich erkläre, dass ich die Dissertation „Enzyme Models of Chloroperoxidase and Catalase" nur mit der darin angegebenen Hilfe verfasst und bei keiner anderen Fakultät eingereicht habe.

Basel, 19. März 2001

Cécile CLAUDE.